Applications of the Genetic Algorithms Optimisation Approach in the Design of Circular Polarised Microstrip Antennas.

Belal Aljibouri

PhD

December 2005

Applications of the Genetic Algorithms Optimisation Approach in the Design of Circular Polarised Microstrip Antennas.

Belal Aljibouri

A thesis submitted in partial fulfilment of the requirements of

the University of Northumbria at Newcastle for the degree of

Doctor of Philosophy

December 2005

ABSTRACT

This thesis presents the results of research that has been carried out in order to design circularly polarised microstrip antenna structures. In the designs considered, there are conflicting contributions to the antenna performance in terms of the two principal objectives, namely the impedance matching and circular polarisation condition. Thus it is necessary to apply an optimisation approach to determine an optimum set of design parameters. In view of the relatively large number of design parameters the multi-objective Genetic Algorithms (GA) optimisation approach is used. Equivalent circuit models embodying the control parameters of the designs have been derived, and, from which, the matching and the axial ratio objective functions have been obtained. The antenna structures considered are used in two-way microwave digital communication systems, and mobile communications. In the thesis GA have been applied to a nearly square patch antenna, a dual feed antenna, a cross-aperture-coupled antenna, and, a patch array type antenna.

A single off-set feed nearly-square circularly polarised patch antenna structure has been designed to meet both the matching and axial ratio conditions. The design achieves a maximum ratio between the patch's dimensions in order to reduce the manufacture errors. The matching objective function was obtained from the transmission line circuit analysis. The axial ratio objective function was obtained from far-field modal expansion analysis. Within parameter constraints, feasible solutions are obtained. The design objectives of this structure are very sensitive to the variation of the design of the five control

parameters. Very good agreement between the predicted, simulated and practical results is obtained. Therefore, the GA is a very good approach that can be applied to the design of this structure. Based on this work a communication letter has been published in the IEEE Transactions on Antennas and Propagation, Vol. 51, No 8, August 2003.

A dual-feed square patch antenna using complex impedance matching has been designed to meet both matching and axial ratio conditions. In this approach the size of the external feed network is reduced thereby producing a more compact overall antenna structure. This achieved by replacing conventional quarter-wave transformers by complex impedance matching. This involved eight design parameters. The final design gave an overall area reduction of 32% as compared with that of conventional design. Then this single patch design was extended to a 2x2 patch array which involved twenty parameters. The array gave an improved bandwidth of the axial ratio at 3dB from 0.04 GHz to 0.256 GHz .and the impedance matching at -10dB from 0.152 GHz to 0.625 GHz compared with that of the single patch. Good agreement between the calculated, simulated and practical was achieved. The large numbers of parameters used in the above designs illustrate the power of the GA optimisation method. As a results of this work research papers have been published in the IEE Electronics Letters (Vol. 36, No. 12, June 2000), and (Vol. 36, No. 24, Nov. 2000).

A nearly square patch antenna with a cross-slot coupled feed has been designed. An investigation has been carried out using GAs to compare the

performance of this antenna based on cavity analysis with that based on transmission line modelling. These models involve extensive mathematical computation and analysis. A multi-objective GA is developed and applied to meet the two design objectives for each of these models, the axial ratio and the impedance matching conditions. Four parameters were involved. This design improved the bandwidth of both the matching and axial ratio as compared with a single feed nearly square patch antenna. As a result of this work research papers have been published in the IEE Proceedings Microwaves, Antennas and Propagation (Vol. 147, No. 2, April 2000), and (Vol. 148, No. 3, June 2001.

The efficient GA search technique has been applied to different designs and in all cases good results have been obtained.

ACKNOWLDGMENTS

I would like to express my sincere thanks to my director of studies Professor Alistair Sambell and my second supervisor Professor Edward Korolkiewicz for their continued guidance, technical advice and encouragement throughout this project.

Also I would like to express my thanks to the staff of School of Engineering and Technology for their support throughout my PhD studies.

Special Thanks to my mother and father, whom I lost during this project, and to my family, (My wife Haifa, and my children: Aya, Abdullah, Abdurahman, and Tasneem).

Finally, I would like to thank to all my brothers and sister in Iraq, to whom I dedicated this achievement, for having the belief and confidence in me.

Contents

ABSTRACT

This thesis presents the results of research that has been carried out in order to design circularly polarised microstrip antenna structures. In the designs considered, there are conflicting contributions to the antenna performance in terms of the two principal objectives, namely the impedance matching and circular polarisation condition. Thus it is necessary to apply an optimisation approach to determine an optimum set of design parameters. In view of the relatively large number of design parameters the multi-objective Genetic Algorithms (GA) optimisation approach is used. Equivalent circuit models embodying the control parameters of the designs have been derived, and, from which, the matching and the axial ratio objective functions have been obtained. The antenna structures considered are used in two-way microwave digital communication systems, and mobile communications. In the thesis GA have been applied to a nearly square patch antenna, a dual feed antenna, a cross-aperture-coupled antenna, and, a patch array type antenna.

A single off-set feed nearly-square circularly polarised patch antenna structure has been designed to meet both the matching and axial ratio conditions. The design achieves a maximum ratio between the patch's dimensions in order to reduce the manufacture errors. The matching objective function was obtained from the transmission line circuit analysis. The axial ratio objective function was obtained from far-field modal expansion analysis. Within parameter constraints, feasible solutions are obtained. The design objectives of this structure are very sensitive to the variation of the design of the five control

parameters. Very good agreement between the predicted, simulated and practical results is obtained. Therefore, the GA is a very good approach that can be applied to the design of this structure. Based on this work a communication letter has been published in the IEEE Transactions on Antennas and Propagation, Vol. 51, No 8, August 2003.

A dual-feed square patch antenna using complex impedance matching has been designed to meet both matching and axial ratio conditions. In this approach the size of the external feed network is reduced thereby producing a more compact overall antenna structure. This achieved by replacing conventional quarter-wave transformers by complex impedance matching. This involved eight design parameters. The final design gave an overall area reduction of 32% as compared with that of conventional design. Then this single patch design was extended to a 2x2 patch array which involved twenty parameters. The array gave an improved bandwidth of the axial ratio at 3dB from 0.04 GHz to 0.256 GHz .and the impedance matching at -10dB from 0.152 GHz to 0.625 GHz compared with that of the single patch. Good agreement between the calculated, simulated and practical was achieved. The large numbers of parameters used in the above designs illustrate the power of the GA optimisation method. As a results of this work research papers have been published in the IEE Electronics Letters (Vol. 36, No. 12, June 2000), and (Vol. 36, No. 24, Nov. 2000).

A nearly square patch antenna with a cross-slot coupled feed has been designed. An investigation has been carried out using GAs to compare the

performance of this antenna based on cavity analysis with that based on transmission line modelling. These models involve extensive mathematical computation and analysis. A multi-objective GA is developed and applied to meet the two design objectives for each of these models, the axial ratio and the impedance matching conditions. Four parameters were involved. This design improved the bandwidth of both the matching and axial ratio as compared with a single feed nearly square patch antenna. As a result of this work research papers have been published in the IEE Proceedings Microwaves, Antennas and Propagation (Vol. 147, No. 2, April 2000), and (Vol. 148, No. 3, June 2001.

The efficient GA search technique has been applied to different designs and in all cases good results have been obtained.

ACKNOWLDGMENTS

I would like to express my sincere thanks to my director of studies Professor Alistair Sambell and my second supervisor Professor Edward Korolkiewicz for their continued guidance, technical advice and encouragement throughout this project.

Also I would like to express my thanks to the staff of School of Engineering and Technology for their support throughout my PhD studies.

Special Thanks to my mother and father, whom I lost during this project, and to my family, (My wife Haifa, and my children: Aya, Abdullah, Abdurahman, and Tasneem).

Finally, I would like to thank to all my brothers and sister in Iraq, to whom I dedicated this achievement, for having the belief and confidence in me.

Chapter One

Introduction and Overview of the Thesis

1.1 Introduction

Microstrip patch antennas posses several advantages over conventional microwave antennas and have received considerable research attention. Some of the principal advantages are light weight, low profile, low cost, and compatibility with integrated circuits, and also they are mechanically and operationally robust. Further, the structure is conformable to planar and non-planar structures. However, microstrip patch antennas also possess disadvantages, such as narrow bandwidth, lower gain, and low power-handling capability.

Microstrip patch antennas are used for the radiating elements of various commercial microwave communications systems such as in highway traffic control, satellite communication for the mobile phone, direct broadcast, remote sensing, and global positioning communication. Microstrip patch antennas are also commonly used in military vehicles, aircraft, and missiles.

The design parameters of antenna structures may be determined by trial and error simulation which is costly, time consuming, and slow, especially as often there is no unique set of design parameters satisfying the required performance characteristics. A systematic approach based upon modelling analysis which will produce a good choice of practical design parameter candidates is required. These candidates will satisfy objective functions derived from the modelling analysis within given tolerance values. The mathematical model

representing the design problem may be of a very high dimension and may have non-differentiable functions in the analysis.

In the design of microstrip patch antennas there are a considerable number of physical and electromagnetic parameters involved. Traditional optimisation techniques which search for the best solutions, such as conjugate gradient and Quasi-Newton methods are in the class of local techniques [10]. These methods quickly converge to a minimum once a starting point is known close to that minimum, but are highly dependent on the initial estimate of the solution. These methods also have the disadvantage of homing in to local minima, and may therefore miss the required global minima. They also require gradient calculations and are limited to problems involving relatively few parameters [11,12]. On the other hand global optimisation methods which are largely independent of the initial starting point and place few constraints on the solution domain are more suitable. Global optimisation methods are very robust and can deal with ill-behaved functions [11-13]. These methods are much more suitable to deal with a solution space having discontinuities, and a large number of dimensions with many potential 'local optima'. The mathematical modelling of the antenna design often involves too many design parameters, such as the patch and feed network dimensions, for traditional numerical methods to handle.

In this thesis a systematic design approach is used based upon mathematical modelling of the antenna structure and using a global optimisation search technique. The design parameters involve both the antenna geometry and the microstrip feed configuration. The required design parameters in the modelling analysis are not unique and an optimal parameter solution is obtained with application of a relatively new Genetic Algorithm (GA) "global" optimisation method [13]. This method can handle a large number of parameters and also non-differentiable functions which may appear in the analyses. It is a stochastic iterative process, which is very robust in respect of the initial starting parameter estimates. In this thesis multi-objective GAs with two objective functions, the axial ratio and the reflection coefficient, are used in the design of the following microstrip patch antennas and antenna array structures:

(1) Single offset-feed circularly polarised nearly square patch antenna,

(2) Dual-feed circularly polarised square patch antenna,

(3) Cross-aperture-coupled nearly square patch antenna,

(4) 2x2 sequentially rotated circularly polarised patch array.

All the antenna designs presented will have a pre-assigned operating frequency and a substrate (Duroid 5870) with relative permittivity $\varepsilon_r = 2.33$, thickness $h = 0.79$ mm, and a loss tangent of 0.0012.

1.2 Review of the Thesis

Chapter two of this thesis describes briefly the basic structure and operation of a microstrip patch antenna. The various microstrip feed types for a single patch antenna are described. These include single, dual feeds and the slot feed. Antenna geometries and dual-feed methods to generate circular polarised radiation are presented. Two methods of modelling a microstrip patch antenna that give a clear and good physical understanding of the operation of the microstrip patch antenna are presented, namely the cavity model and the transmission line model. A review of planar microstrip patch antenna arrays is presented together with a design for nearly square patch and the feed position to produce circular polarisation radiation is presented.

In chapter three the Genetic Algorithm, GA, method of global stochastic optimisation is presented. Advantages of this approach and comparison between the GAs and the traditional local optimisation procedures are discussed. The main operators and elements of the GA procedure are given and explained in detail. A brief presentation of multi-objective optimisation is given. A step by step example of GAs is given to demonstrate the function of the genetic operators.

A sequentially multi-objective GA method is applied in chapter four to design a compact offset-feed nearly square circularly polarised microstrip

patch antenna operating at 2.45 GHz and matched to a 50Ω source impedance. The objective functions involve the design parameters which are the patch dimensions, the length and width of the matching microstrip feed line, and the feed location. For each of the five design parameters the sensitivity to small variations in the parameters is investigated. The practical, simulated, and computed results are in very good agreement.

A large number of control parameters are introduced in the design of a dual-feed circularly polarised microstrip patch antenna hence a non-dominating sorting GAs optimisation is developed and applied in chapter five to this design. In this method a set of non-dominating solutions are extracted and ranked according to their relative fitness values. This is followed by generating further sets of solutions from the fittest selected solutions. The eight design parameters are the lengths and the widths of the feed lines of the dual-feed network. The application of GAs has resulted in a reduction in the overall size of the structure of approximately 32% compared with what a conventional design technique can achieve. Very good agreement between the practical, simulated, and calculated results is obtained for this new compact and simpler feed structure. The above application is further developed to the design of a 2x2 sequentially rotated patch array which uses a single dual-feed circularly polarised microstrip patch antenna as the basic radiating element in the array. The eighteen design parameters are the dimensions, the lengths and widths of

the feed lines in the dual-feed network on each of the four radiating elements, and, the dimensions of the array feed lines. With the new approach a more compact and simpler feed structure designed by the GA optimisation has been achieved. In addition, the expected results of improving the matching, axial ratio, and VWSR bandwidths as compared with that of a single patch element. Work presented in this chapter has been published in Electronics Letters [14, 15].

In chapter six the modelling and design of a cross-aperture-coupled circularly polarised microstrip patch antenna is presented. In a cross-slot nearly square aperture feed patch antenna, since the feed network and radiating patch are on separate substrates, the properties of each substrate can be chosen to optimise, independently, the feed network and the antenna patch. The aperture coupled feed structure is known to have a number of practical advantages: it does not require an external polarizer and expensive dielectric materials [52,53]. With aperture coupling it is possible to match the feed line by varying the slot length and the length of the open-circuit stub, which is just an extension of the feed line. This eliminates the need to use an external matching network which reduces the overall size of the antenna. The isolation of the patch from the feed network by the ground plane minimises spurious feed radiation. A compact structure can be realised using aperture coupling and with the aperture positioned below the centre of the patch, the symmetry ensures better circular polarisation. In addition this antenna has the advantage over the

direct microstrip feed designs in having an increased bandwidth. Results obtained using both the cavity model and the transmission line model are compared. For each of these models the multi-objective non-dominating sorting GA is developed and applied to meet the two design objectives, circularly polarised wave propagation and the 50Ω matching condition. Based upon this work two papers have been published in the IEE Proceedings Microwaves, Antennas and Propagation [16,17]

Chapter seven presents the outcomes of the research carried out and suggestions for further work. A general review of each chapter in the thesis has been presented.

It is shown that the novel approach based on the applications of the GA optimisation approach has been applied successfully to the design of various types of circularly polarised microstrip patch antennas. The capability of the GA optimisation approach for the design of multi-objective antenna designs has been demonstrated. Suggestions are given for further work, such as including more objective functions in the design of the present structures and to investigate new antenna forms.

1.3 Summary of Published Work

The following publications are based upon work presented in this thesis:

I. B. Aljibouri, E. G. Lim, H. Evans and A. Sambell, 'Multiobjective genetic algorithm approach for a dual-feed circular polarised path antenna design', Electronics Letters, 8th June 2000, Vol. 36, No. 12, pp 1005-1006.

II. H. Evans, P. Gale, B. Aljibouri, E. G. Lim, E. Korolkiewicz, and A, Sambell, 'Application of simulated annealing to design of serial feed sequentially rotated 2x2 array'', Electronics Letters, 23th November 2000, Vol. 36, No. 24., pp 1987-1988.

III. B. Aljibouri, T. Vlasits, E. Korolkiewicz, S. Scott and A, Sambell, 'Transmission line modelling of the cross-aperture-coupled circular polarised microstrip antenna', IEE Proceedings Microwaves, Antennas and Propagation Vol. 147, No. 2 April 2000, pp 82-86.

IV. B. Aljibouri, E. G. Lim , H. Evans, T. Vlasits, E. Korolkiewicz and A, Sambell, 'Cavity model of cross-slot-coupled circularly polarised microstrip patch antenna', IEE Proceedings Microwaves, Antennas and Propagation Vol. 148, No. 3, June 2001.pp.147-152.

V. E. N Lim, E. Korolkiewicz, S. Scott, B Aljibouri, and Shi-Chang Gao 'Efficient impedance coupling formulas for rectangular segment in planner microstrip circuits', IEEE Transaction on Antennas and Propagation, Vol. 51, No 8, August 2003, pp 2137-2140

In addition the author has also contributed to the following publication:

VI. E. N Lim, E. Korolkiewicz, S. Scott, and B Aljibouri, 'An efficient formula for the input impedance of a microstrip right-angled isosceles triangular patch antenna', IEEE Antennas and Wireless Propagation Letters, Vol. 1, pp. 18-21, 2002.

Chapter Two

Review of Microstrip Patch Antennas and Arrays

2.1 Introduction

The concept of microstrip antennas was first proposed in the USA by Dechamps in 1953 [1], while Gutton and Baissiont issued a patent in France in 1955 [2]. In the 1970s, by exploiting the availability of good substrates with low loss tangents, Howell fabricated the first practical antenna [3]. This was followed by extensive research and development of microstrip antennas and arrays because of the advantages of light weight, low volume, low cost, conformal configuration, compatibility with integrated circuits and both mechanical and operational robustness. A variety of forms of microstrip antenna structures can be designed to produce different radiation patterns and polarisations. For example, placing elements such as a pin or varactor diode between the patch and the ground plane can lead to variation of the antenna's resonant frequency [3,4], and polarisation [3,5]. Also by changing the bias voltages on the diodes the impedance can be controlled [6]. Moreover, microstrip patch antennas are easy to integrate with associated circuit elements and can be used to produce either linear or circularly polarised radiation. These advantages make microstrip patch antennas very useful for various applications, such as in highway communication, mobile communication, and security applications. They are easy to deploy on military aircraft and missiles. Also, for narrow-band applications the antenna itself can be used as a filter for unwanted frequency components [18]. Many applications in communication

systems, such as tolling communication, require circularly polarised waves and microstrip patch antennas are most suitable for this application.

In this chapter the basic principles of microstrip antennas, the radiation mechanism, alternative antenna feed methods, and technique for generating circular polarisation are introduced.

2.2 Operation of the Microstrip Patch Antenna

A microstrip patch antenna consists of a conducting patch separated from a ground plane by a dielectric substrate. There are many different configurations of the patch antenna the most common being the rectangular, triangular, and circular shapes. Figure 2.2.1 illustrates a basic structure for a centre fed rectangular microstrip patch antenna, in which the length, a, is usually about half the dielectric wavelength and defines the frequency of operation. The width 'b' of the patch determines the input impedance of the antenna.

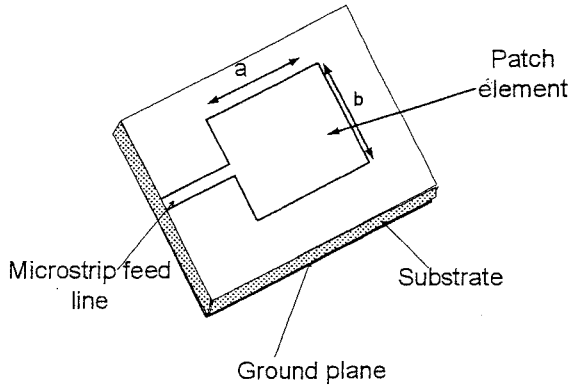

Figure 2.2.1 Basic structure of a rectangular microstrip patch antenna.

The radiation mechanism of the patch antenna can be viewed in several ways. A useful way, to illustrate the radiation mechanism, is to consider the radiation as being due to fringing electromagnetic fields which are excited between the radiating edges of the patch and the ground plane. This is shown in Figure 2.2.2 with a rectangular patch fed by a microstrip line and the fringing fields at the two edges of the patch. The electric fields at each edge of the patch can be resolved with respect to the ground plane into normal and tangential components. At the far field the normal components cancel out, and tangential components are in phase, so combine to radiate electromagnetic power normal to the surface of the structure[19,20].

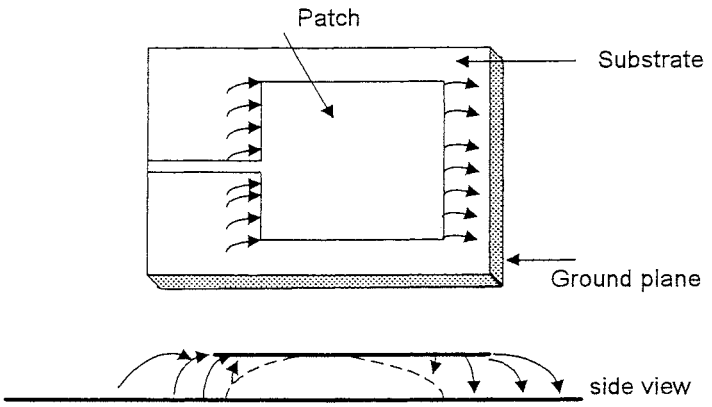

Figure 2.2.2. Fringing fields of a microstrip patch antenna

2.3 Microstrip Antenna Modelling

The modelling design analysis of the antenna is important as it reduces the need for the costly cut-and-try cycle process. In designing the microstrip patch element for a given application it is crucial to understand the physical mechanisms that govern the operation. An appropriate model will satisfy the following criteria:

- It is capable of calculating all the necessary control parameters which affect important antenna characteristics such as impedance and polarisation.
- Can produce usable results.
- Offers a good physical insight into the operation.
- It is simple and convenient for engineers to use.

There are a number of methods of modelling microstrip patch antennas which involve different levels of mathematical complexity and give different levels of accuracy. Two simple methods which give some physical insight into the operation of a patch antenna are the transmission line model, and, the cavity model [20]. Full-wave modelling techniques have also been developed such as the spectral-domain moment method, finite-difference-time domain method and finite-element method [21-26].

2.3.1 Full-Wave Analysis

The full-wave approach is the most general and accurate method of rigorously simulating the behaviour of the microstrip antenna. No assumptions are made in regard to the form of the electromagnetic field structure. Given the values of the geometric and electrical parameters of the antenna design the associated Maxwell equations, together with properly posed boundary conditions, are solved for the operational characteristics of interest.

Maxwell's equations are either taken in differential, or integral equation form. In the integral equation, or, mixed integral equation approach the metallic patches are replaced by electric surface current distributions, and the slots by magnetic surface currents. The electric and magnetic fields are related to their source functions by the associated Green's functions. Applications of the boundary conditions on the conducting surfaces give an equation for determining the electric current distributions. The method of moments (MoM) is commonly used to obtain the approximate current distribution which can

then be used to derive all other operational characteristics of interest. The finite element method (FEM) is used in the differential equation formulation of the problem, and the boundary element method (BEM) is used in the integral equation formulation, while the finite difference time domain (FDTD) is purely numerical. The FDTD method [26] is of considerable current interest and employs the two simultaneous first order Maxwell curl equations for the electric and magnetic fields. Discretization of these equations gives recurrence equations in the scalar components of the electric and magnetic fields. On the finite difference grid the electric field is staggered one-half cell with respect to the corresponding magnetic field. In the same way, on the time grid, the electric and magnetic fields are displaced by half a time step with respect to one another. The electric fields are initialised and then both magnetic and electric fields are advanced in time by an explicit leap-frog updating to obtain the steady-solution. The full wave modelling is suitable for analysing a given design but not for direct application to the problem of finding the design parameters.

The full-wave method is employed in the simulation software, Ensemble^{Tm}5.1 which has been used in this thesis.

2.3.2 Cavity Model Analysis.

Microstrip patch antennas are narrow-band resonant antennas and can be treated as lossy cavities. In the cavity model [6,8,9] the patch dimensions are

extended to account for the fringe field and the space between the extended patch and ground plane can be assumed to be a resonant cavity bounded by perfect magnetic walls on which the normal electric field component vanishes. The fields under the patch can be determined by considering the dominant resonant modes, and resonant frequencies, and the input impedance can then be derived [9]. The resonant frequencies of the TM_{mn} modes are given by

$$f_{mn} = \frac{1}{2\pi\sqrt{\mu_0 \varepsilon_{eff}}}\sqrt{\left(\frac{m\pi}{a}\right)^2 + \left(\frac{n\pi}{b}\right)^2} \qquad (2.3.2.1)$$

where m and n are the modes along a, and b respectively, μ_o is the free-space permeability, and ε_{eff} is the mutual effective dielectric constant [23].

$$\varepsilon_{eff} = \sqrt{\varepsilon_{eff}(b)\varepsilon_{eff}(a)}$$

where

$$\varepsilon_{eff}(a) = \frac{\varepsilon_r + 1}{2} + \frac{\varepsilon_r + 1}{2}\left(1 + 12\frac{h}{a}\right)^{-1/2}, \text{and,}$$

$$\varepsilon_{eff}(b) = \frac{\varepsilon_r + 1}{2} + \frac{\varepsilon_r + 1}{2}\left(1 + 12\frac{h}{b}\right)^{-1/2}.$$

The equivalent circuit network for the rectangular microstrip antenna is shown in Figure 2.3.1. Each mode is represented by a parallel R-L-C tuned circuit. In circular polarisation there are two dominant modes TM_{10} and TM_{01} being the fundamental modes [21].

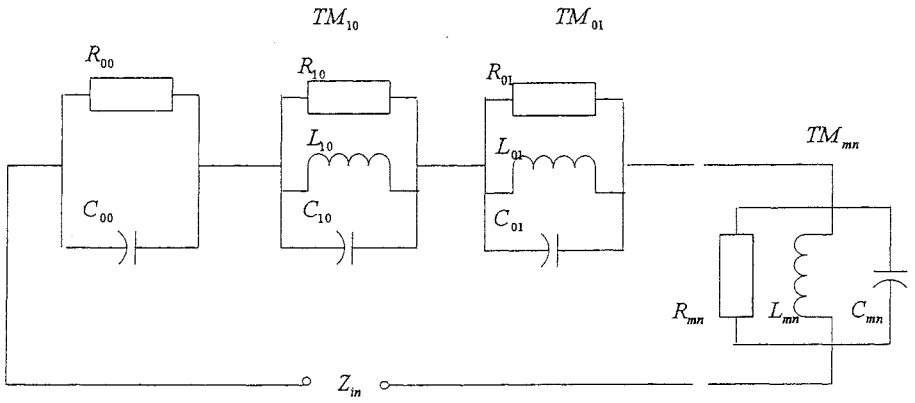

Figure 2.3.1 Equivalent network for microstrip patch antenna

The electric-field and magnetic-surface-current distributions on the side walls for the TM_{10} and TM_{01} modes are illustrated in Figure 2.3.2 For the TM_{10} mode, the magnetic currents along 'b' are constant and in phase while those along 'a' vary sinusoidally and are out of phase. For this reason , the 'b' edge is known as the radiating edge since it contributes predominantly to the radiation. The 'a' edge is known as the non-radiating edge. Similarly, for the TM_{01} mode, the magnetic currents are constant and in phase along 'a' and are out of phase and vary sinusoidally along 'b'. The 'a' edge is thus the radiating edge for the TM_{01} mode.

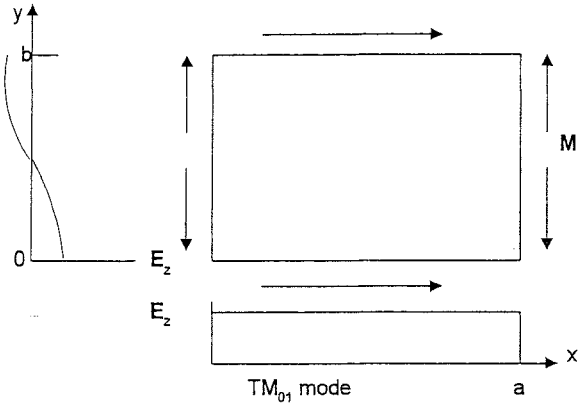

(a)

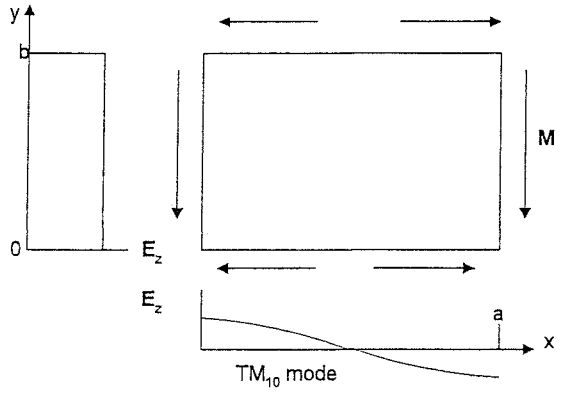

(b)

Figure 2.3.2 Electric field and magnetic-surface-current distributions for a rectangular microstrip patch antenna, a) TM_{01} mode, b) TM_{10} mode

2.3.3 Transmission Line Model Analysis

The rectangular and square patches have a physical shape such that with a centre feed position it is possible to use the transmission line model for these antennas. Although limited, this model is commonly used in the design of

patch antennas. The simple transmission line model [8-9] was first employed by Munson [7] to analyse a rectangular microstrip patch antenna. Modifications to the basic transmission line model have improved its accuracy and versatility by taking into account the mutual coupling between the radiating edges, the surface roughness of the copper, and, the width of the microstrip feed line [22].

The patch antenna can be considered as a wide microstrip transmission line and therefore a low characteristic impedance microstrip line. The area between the edges of the patch and the ground plane at the two ends can be viewed as radiating apertures, or, as slot antennas as shown in Figure 2.3.3a. Thus the low-impedance line can be regarded as being loaded at the two ends by high-impedance loads. Mutual coupling between the two slots also exists, and, the voltages and the currents at the ends of the transmission line are coupled through a two-port network representing the propagation field out of the patch. Figure 2.3.3b represents the equivalent circuit of the transmission line.

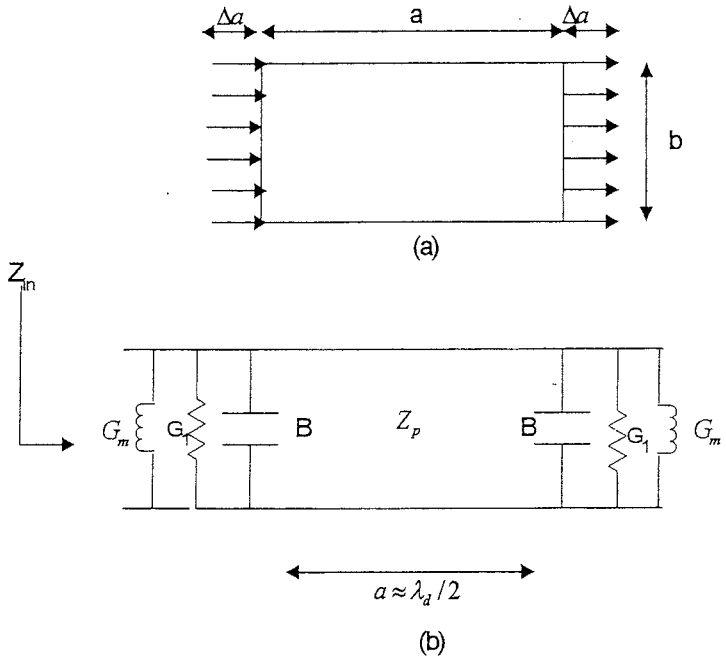

Figure.2.3.3 (a) Transmission line model of the rectangular antenna (b) the equivalent circuit for (a)

Z_p is the characteristic impedance of the microstrip line, B is the susceptance of the radiating slot, G_1 is the self-conductance of the radiating slot, and, G_m is the mutual conductance of the patch which represents the mutual effects between the slots [20].

The mutual coupling conductance G_m between the radiating edges is given by [20]

$$G_m = \frac{1}{120\pi^2}\int_0^{\pi}\left[\frac{\sin(\frac{k_o b}{2}\cos(\theta))}{\cos(\theta)}\right]^2 J_o(k_o a\sin(\theta))\sin^3(\theta)d\theta \qquad (2.3.1)$$

and the radiation conductance G_1 is given by [20]

$$G_1 = \frac{1}{120\pi^2}\int_0^{\pi}\left[\frac{\sin(\frac{k_o b}{2}\cos(\theta))}{\cos(\theta)}\right]^2 \sin^3(\theta)d\theta \qquad (2.3.2)$$

and the susceptance B is given by [20].

2.4 Generation of Circular Polarisation

2.4.1 Wave Polarisation (Axial Ratio)

Consider a plane wave propagating in a positive z-direction, as shown in Figure 2.4.1(a), with the electric field at all times orientated in the y-direction. This type of wave is termed linearly polarised in the y-direction. As a function of time and position, the electric field of such a wave (travelling in the positive z-direction) is given by [28]

$$E_y = E_2 \sin(\omega t - \beta z). \qquad (2.4.1.1)$$

Similarly, a linearly polarised wave in x-direction is given by

$$E_x = E_1 \sin(\omega t - \beta z). \qquad (2.4.1.2)$$

where βz is the phase shift varying with distance in the z-direction, and E_1 and E_2 are the amplitudes of the fields in the x and y directions respectively.

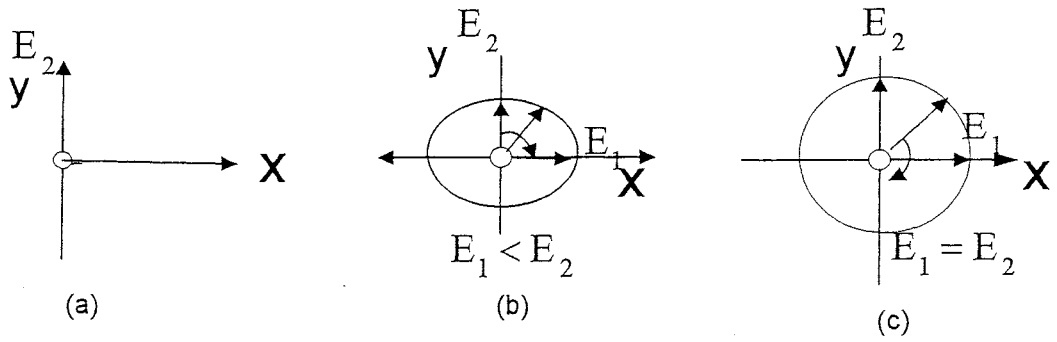

Figure 2.4.1 Polarisation states of electromagnetics waves

(a)Linear Polarisation
(b) Elliptical polarisation
(c) Circular polarisation

Generally, the electric field of a wave travelling in the z-direction could have two unequal linearly polarised components, in the x and y directions and so produces elliptical polarisation (see Figure 2.4.1b).

In these cases the polarisation is called elliptical polarisation $(E_1 \neq E_2)$, and the The electric fields in the x and y directions are given by

$$E_x = E_1 \sin(\omega t - \beta z) \qquad (2.4.1.3)$$

and

$$E_y = E_2 \sin(\omega t - \beta z + \theta) \qquad (2.4.1.4)$$

where θ is the time-phase angle by which E_x leads E_y. If $E_1 = E_2$,and the phase difference $\theta = \pm 90^\circ$, the wave is said to be circularly polarised, as shown in Figure 2.4.1c. When $\theta = +90^\circ$, the wave is called left-hand circularly polarised, and, when $\theta = -90^o$, it is called right-hand circularly polarised. In

these cases the circularly polarised wave field consists of two orthogonal linearly polarised components of equal magnitude as shown in Figure 2.4.2.

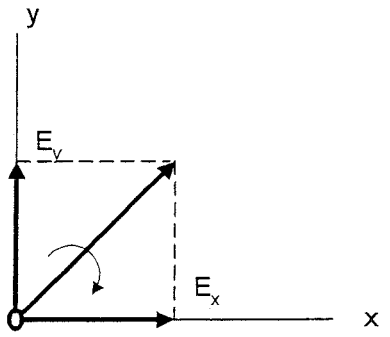

Figure 2.4.2 Orthogonal currents radiating circular polarisation.

In practice the two electrical modes will not be exactly equal, nor will the phase shift be exactly 90°.

The quality of circular polarisation is measured by the axial ratio (AR). This represents the ratio of the maximum to the minimum signal strength of the electric field vector, and is given by [28].

$$AR = 10\log\frac{E_1^2 + E_2^2 + \left[E_1^4 + E_2^4 + 2E_1^2E_2^2\cos(2\theta)\right]^{\frac{1}{2}}}{E_1^2 + E_2^2 - \left[E_1^4 + E_2^4 + 2E_1^2E_2^2\cos(2\theta)\right]^{\frac{1}{2}}}. \qquad (2.4.1.5)$$

2.4.2 Feed Structures for Circularly Polarised Microstrip Patch Antennas

For linear polarisation the antenna design usually requires only the TM_{01} or TM_{10} mode, while for circular polarisation radiation the patch must produce two orthogonal fields with equal amplitude but with 90° phase difference.

In the antenna design for circular polarisation two types of feed are used, the dual-feed with an external polarizer, and, the single feed type without an external polarizer.

2.4.2.1 Single-Feed Antennas

The advantages of this structure are the simplicity and small size which is particularly important when it is difficult to incorporate dual feeds with a power divider network within the structure. The disadvantage is that they usually have a narrower axial ratio bandwidth compared with the dual-feed antenna [26]. There are a number of different approaches to antenna design for generating circular polarisation with a single feed. By adjusting the dimension of the patch one mode is made to resonate just above the required operating frequency and the other mode to resonate below the operating frequency with a 90° phase difference.

Some of the single feed circular polarisation structures can be designed by modifying a square patch antenna as shown in Figure 2.4.3.

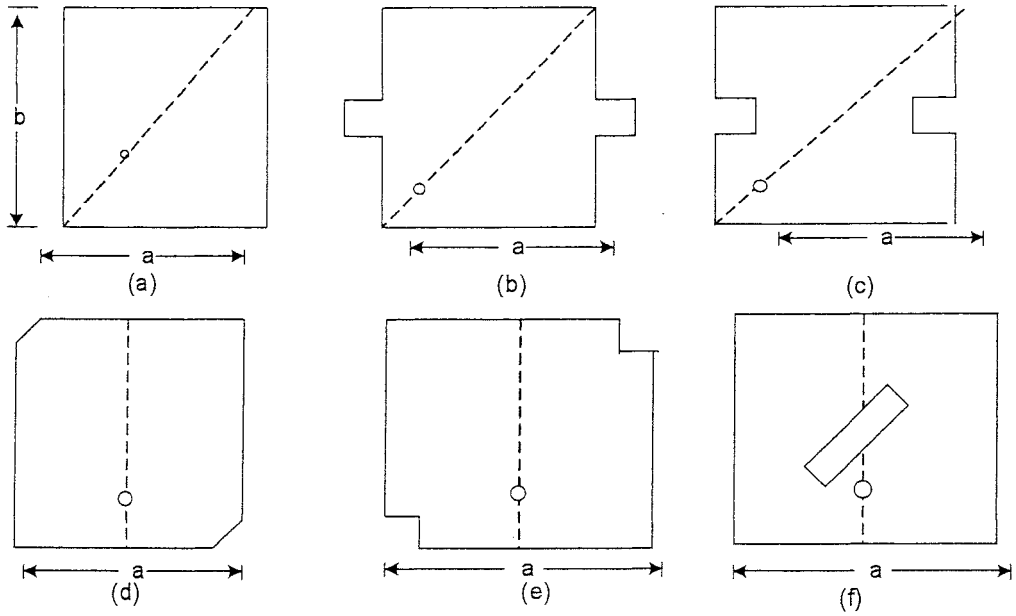

Figure 2.4.3 Various single feed modified square parch antennas.(a) Nearly square, (b) Square with two stubs, (c) Square with two notches, (d) Square with two corners chopped, (e) Square with two square notches at the corners, and (f) Square with diagonal slot

2.4.2.2 Dual-Feed Antennas

A dual feed can excite two orthogonal modes simultaneously with equal magnitude and a $\pm 90^{\circ}$ phase difference. There are several microstrip feed circuits which can generate circular polarisation such as the quadrature hybrid, the ring hybrid, and, T-junction splitter [22,28].

Two basic structures for the dual-feed circularly polarised patch using an external power divider are shown in Figure 2.4.4. In the case of the dual feed, the 90°-degree phase shift is generated by an external polarizer such as in the

feed network shown in Figure 2.4.4a. At the operating frequency the input feed is divided equally into two antennas input feeds and one of the feed paths is a quarter wavelength longer than the other feed path. Alternatively, a hybrid coupler (Figure 2.4.4b) which splits the power source and produces the required 90° phase shift between the fields can be used.

In chapter five a new approach is investigated to minimise the area of the antenna by removing a quarter wave condition on the power splitter feed network.

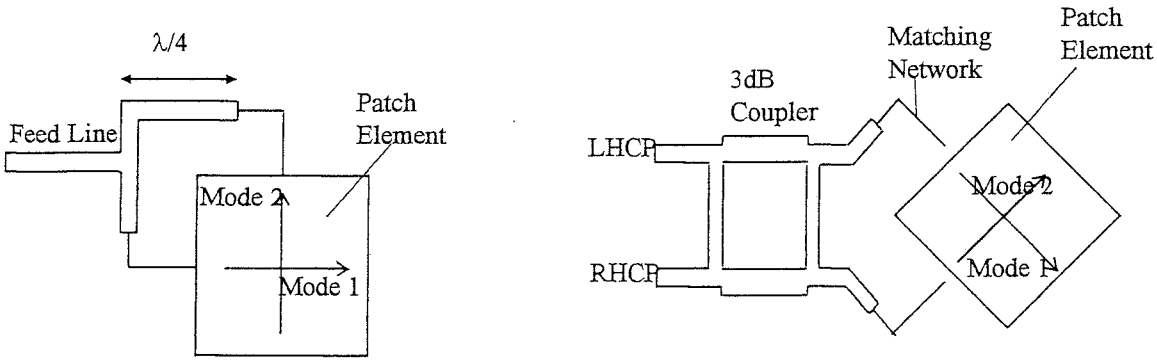

Figure 2.4.4 Dual feed circularly polarised patch antenna arrangements.

a) A Power splitter Feed b) A 3dB coupler

2.4.3 Traditional Design of a Dual-Feed Circularly Polarised Microstrip Antenna.

For a circularly polarised square microstrip patch antenna element with purely resistive matching of the feed network two conventional design methods are described and the results show the shortcomings of the conventional approach. The antenna, which is shown in Figure 2.4.5 is

designed to operate at 5.8 GHz. The dual feed square patch antenna is treated as two transmission lines excited simultaneously from a single feed source, with $Z_{in} = 50\Omega$. Each feed is terminated with a load, $Z_L = 320\Omega$. The two transmission lines effectively act as a single offset feed which generates the two orthogonal modes required for circular polarisation. In order to maintain a 90°-phase difference it is usual to make the length of one of the network feed lines a quarter-wave length longer than the other feed line.

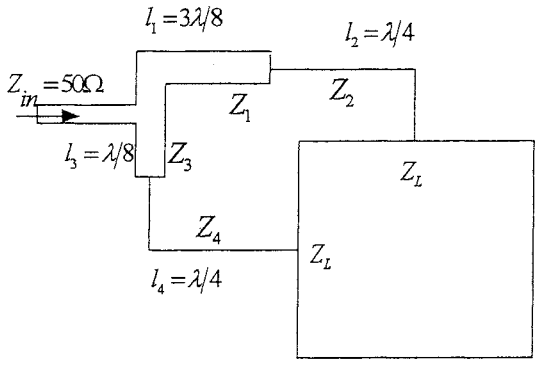

Figure 2.4.5 Dual-feed circular polarised square patch antenna with $\lambda/4$ length difference between the two ports.

The power splitter is normally designed to obtain the specified 50Ω input impedance at the feed source. Since $Z_L = 320\Omega$, this will require $Z_2 = Z_4 = 180\Omega$. The shortcoming in this approach is that the impedance value is very difficult to realise in practice using microstrip technology.

In the second approach, it is possible to make Z_{in} less than the specified input impedance 50Ω, to ensure that the impedances Z_2 and Z_4 can be realised. This is done by transforming Z_{in} to 50Ω using a further quarter wave transformer at the input between the power source and the feed network. It is also necessary to set the lines adjacent to the patch to the maximum practical impedance of 140Ω. The input impedance of the feed structure is then 33.3Ω. Further, in order to match a required input source, a quarter wave section must be inserted between the feed network and the source. However this means that overall size of the antenna structure will be relatively large, producing spurious radiation.

In chapter five a new approach using GA optimisation is presented to design a circularly polarised dual-feed microstrip patch antenna. The new approach reduces the area of the antenna and overcomes the high impedance problem of the feed network, and, reduces spurious radiation.

2.4.4 Aperture Coupled Antennas

Circularly polarised aperture coupled antennas can also use either single or dual feed configurations. This type of feed structure does not require a physical connection between the patch antenna and the feed line which facilitates the use of different substrate materials for the feed network and for the antenna. The aperture coupling consists of two substrates bonded together and separated by a ground plane. On the bottom side of the lower substrate is a

microstrip feed line which excites the patch through a slot on the ground plane separating the two substrates (see Figure 2.4.6). This structure permits independent optimisation of the feed mechanism and the radiating element [19]. Usually material with high dielectric constant is used for the bottom feed substrate, and thick low dielectric constant material for the top antenna substrate. The use of a thick, low permittivity substrate increases the bandwidth of a microstrip patch antenna [19]. In addition, this feed structure can be designed in order to improve bandwidth by adjusting the shape and the length of the coupling aperture, width of the feed line, and the length of the stub. The ground plane between the substrates also isolates the feed from the radiation element and minimises interference of spurious radiation for pattern formation and polarisation purity. Controlling the width of the feed and the length of the slot allows matching between the feed line and the patch element. This eliminates the need of any external-matching network, and external polarizer, which would increase both the size of the antenna and also its complexity. A dual feed aperture coupled antenna may use two separate slots [29], or the structure may use a crossed slot [16,17]. In both of these cases the patches are square, which assists in achieving good axial ratio. Circular polarisation can be achieved using a single-feed aperture coupled antenna (Figure 2.4.6).

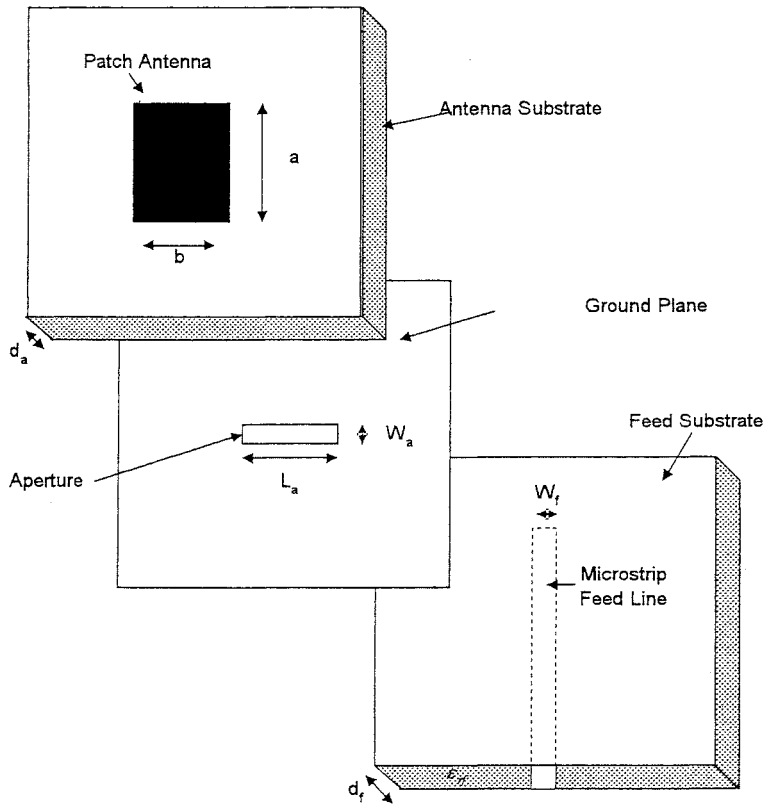

Figure 2.4.6 Aperture-coupled microstrip patch antenna.

In the single feed aperture design the patch is orientated at an angle to the linear polarisation position [31]. The inclined slot causes two orthogonal modes to be excited on the patch in the x and y directions. The phase shift can be achieved by using, for example, a nearly square patch. In such a structure the circular polarisation is very sensitive to the tolerance of the patch dimensions. It is important, therefore, that the dimensions of the patch are determined accurately. Using two slots in a cross configuration (chapter six) can improve the quality of circular polarisation [16], and also the manufacture

tolerance is increased. Applications of both the transmission line model and the cavity model to a cross-slot-aperture-coupled-circularly-polarised microstrip patch antenna are presented in chapter six.

2.5 Microstrip Patch Antenna Arrays

In many microstrip patch antenna applications, system requirements can be met with a single patch element. However, it is well known that microstrip patch antennas are limited in bandwidth and purity of polarisation. The antenna's bandwidth can be constrained by the input impedance characteristic, polarisation purity and gain parameters. In some cases, systems require higher gain, robust performance, and wider bandwidth while maintaining a low profile structure, low manufacture coast, and low weight. This calls for the development of a microstrip patch antenna array in which a large number of radiating elements are to be deployed in the array

The possible feed systems are, the parallel, the series, the hybrid parallel/series, and the sequentially rotated feed system. To design an array system with good circular polarisation over a wide bandwidth several authors [26,32] have described array systems in which every adjacent four elements are placed in a rectangular lattice sequentially arrayed in both phase and orientation. In the conventional form the feed system for this structure is a purely resistive hybrid type [22] and incorporates quarter wave transformers. A new design approach is presented (Chapter five) in which the quarter wave

transformer network is replaced by an impedance network which is not purely resistive.

2.5.1 Parallel Feed

The parallel feed which also called the corporate feed is illustrated in Figure 2.5.1 which shows the patch elements are fed by parallel transmission lines power divider. The transmission feed line is divided into two branches and each branch is divided again until it reaches each patch element. In a broadside-radiating array all the divided lines are have the same length.

The parallel-fed patch can be divided into two categories: a one-dimensional feed network, and, a two-dimensional feed network. A simple one-dimensional parallel feed patch antenna linear array is illustrated in Fig. 2.5.1a, where the structure involves of a two-way power divider branching network.

The main advantages of this type are; first that the array can be readily designed for even numbers of elements, which are not powers of two, and, for odd element numbers Secondly the structure can provide a tapered aperture distribution which would otherwise necessitate large power-divider ratios in the branching network.

Fig 2.5.1b shows a two-dimensional parallel feed with four elements aside. This sort of structure can be spread out to larger arrays with 2^N elements per side. Any attempt to modify the feed to deal with other even numbers can result in the need for large power-divider ratios [22].

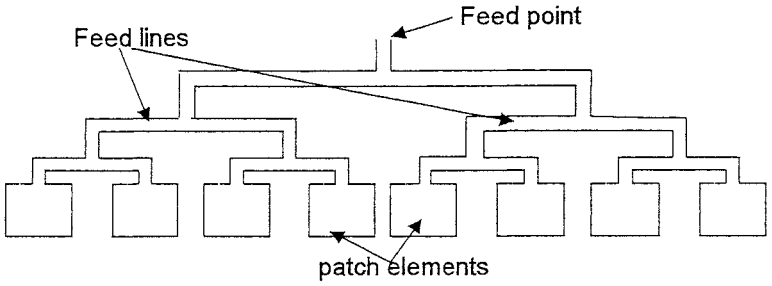

(a)

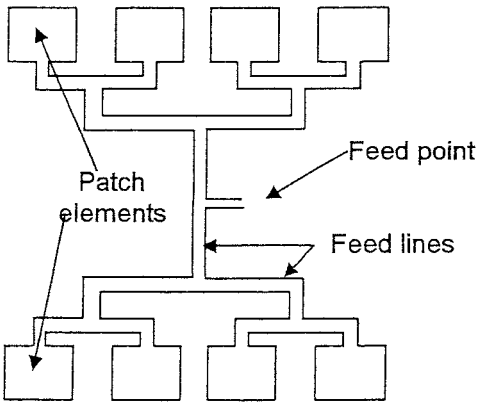

(b)

Fig. 2.5.1 Parallel fed patch array a) 1-dimensional, b) 2-dimensional

2.5.2 Series Feed

In a series feed patch array structure [3,34], the patch elements are arranged linearly and fed in series by a single transmission line. Multiple linear arrays can then be fed either in series or in parallel to build a two-dimensional planar array. Two different configurations of the series feed method are shown in Figure 2.5.2; the in-line feed using two-port patches and the out line feed using one-port patches. The in-line feed [35 36] has the feed transmission line

and the patch elements arranged in the same line. The out-of-line feed [20] has the feed line arranged parallel to the elements. The in-line feed array occupies the smallest real estate with the lowest insertion loss but generally has the least polarisation control and the narrowest bandwidth [20]. It has the narrowest bandwidth because the line passes through the patches. Thus, the phase between the adjacent elements is a function of line length and the patches' input impedances. Because the patches are weighted differently with different input impedances, the phase will be different for different elements and will change more dramatically as frequency changes due to the narrow-band characteristic of the patches.

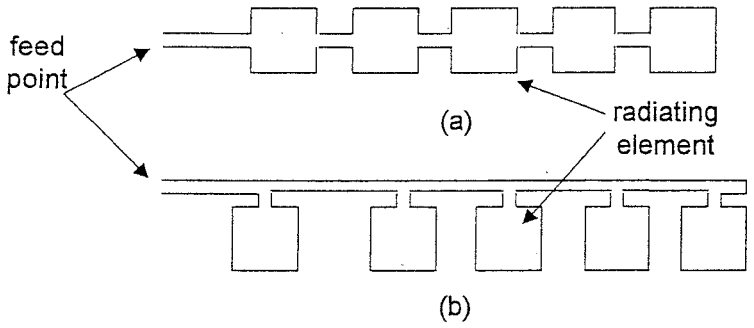

Figure 2.5.2 Series fed patch array a) on-line feed, b) off-line-feed.

2.5.3 Hybrid Series/Parallel Feed

A combination of both the series-feed and parallel-feed forms is called a hybrid series/parallel-fed array. An example of a hybrid series/parallel-fed

array is illustrated in Figure 2.5.3, where a combination of series and parallel feed lines is utilised.

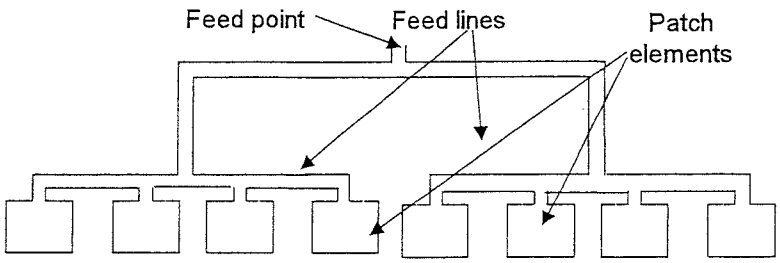

Figure 2.5.3 Hybrid fed patch array

For a circularly polarised array, a new array structure has been developed [43,44] in which every adjacent four elements are placed in a rectangular lattice sequentially arranged in both phase and orientation in order to obtain good circular polarisation over a wide bandwidth.

2.5.4 Sequentially Rotated Patch Arrays

In general the conventional rotated patch array structure consists of groups of 2x2 sequentially rotated radiating elements. The feed system required is a purely resistive hybrid type. Every adjacent four elements in a group are placed in sequential arrangement in both phase and direction, which improves the circular polarisation and radiation pattern symmetry over a wide frequency bandwidth [25].

A new design approach for the sequentially rotated array is developed in this thesis for a 2x2 radiating element patch in which the quarter wave

transformers network is replaced by an impedance network, which is not purely resistive.

2.6 Summary

In this chapter microstrip patch antennas and patch antenna arrays have been described. Basic descriptions of the radiation mechanism and circular polarisation generation techniques have been presented. Microstrip patch antenna feed configurations have been discussed, such as single, dual-feed and the slot feed. Circular polarisation and the single feed antenna patch designs to produce circular polarisation have been reviewed. Methods of modelling a microstrip patch antenna, including the transmission line modelling and cavity modelling of microstrip patch antennas have been introduced. An antenna array approach using sequentially rotated patch radiating elements is briefly introduced. General discussion of patch arrays has been discussed, this including the feed structures of the arrays.

Chapter Three

Genetic Algorithm Optimisation

3.1 Introduction

Optimisation methods seek to determine values of design parameters, which enable key functions, called objective functions, to reach optimum numerical values within prescribed limits. The objective functions are expressions, the values of which determine the performance characteristics of the device. In the calculation the design parameters are constrained to lie within pre-assigned practical limits which together define the parameter domain. Since there are usually competing requirements between the objective functions optimisation results in sets of feasible solutions, the best of which is the optimum solution: although there may not be an absolute best candidate. In matched circular polarised antenna design problems the objective functions involve the axial ratio and the reflection coefficient [Chapters 4,5,6]. Traditional methods such as variable metric and conjugate gradient [11] use direction derivatives with respect to each parameter and at each step proceed point by point in the parameter domain from an initial estimate of the solution. Thus they have a tendency to lock into local solutions and so miss the global solution. Also, convergence depends on having good starting values for the parameters. Problems involving the axial ratio and antenna impedance matching have many local minima [34]. The traditional approach becomes analytically unmanageable with an increasing number of parameters and in the present work 4,5,8, and 22 design parameters are involved.

A more recent "global" search optimisation method that can handle a large number of design parameters is the Genetic Algorithm (GA) [13, 14]. The method was first introduced by John Holland [33] in connection

with evolution and natural selection. This method does not require differentiability, or good starting values of parameters, since at each stage trial solutions, or candidates, are generated across the entire parameter domain. This offers an opportunity for parallel computation. A typical application of GAs involves the construction of a seed population of randomly selected candidates for solution, followed by the application of three operators, 'selection', 'crossover', and 'mutation'. Within the GA approach there is a choice as to which technique may be used in the application of these operators. For example a binary string form of a solution, or the decimal form of a solution may be adopted. The binary string is most commonly used and is deployed as a vehicle for the generation of successive candidates. Alternatively the use of the decimal form has been reported in [34,40]. There are no hard and fast rules for choosing some technique over another and currently there is no rigorous proof of convergence. However, there is a considerable body of successful applications ranging from image processing to protein structures, and also in antenna design [34,36]. In matched circular polarisation design the objective functions are taken to be the reflection coefficient and the (axial ratio-1) so that each function then has a minimum value of zero. The optimisation then is a minimisation problem.

The strategy of the GA search method is initially to construct a random collection of seed trial solutions across the parameter domain. Each parameter in a trial solution is encoded as a binary string and these strings are sequentially co-joined into a continuous seamless binary string

(concatenation) called a "chromosome". The set of the trial solutions constitute the initial "population".

Mimicking natural selection, new populations are propagated by selecting particular segments of two chromosomes to interchange positions in the chromosome strings thus creating two new chromosome candidates for the trial solutions. This process is called "crossover" which has been linked to the transfer of genes in natural evolution [37]. Additionally new candidates can be also be generated by "mutation" where a single binary digit is switched within a single chromosome. As each new population is constructed the chromosomes are employed to produce real values of the parameters which are then used in a "fitness function" test to select candidates for retention or rejection from the solution space. Good candidates are retained while others are discarded in such way that the population size remains constant. The cycle is repeated for a predefined number of iterations, or, until a quality test is satisfied.

The mechanics in the GA procedures are permeated at every stage with random selections of one kind or another. This characteristic prevents localisation in the search domain and ensures great diversification in the search populations.

First addressed are problems involving only one objective function. The procedures used in constructing the initial seed population and in the operations of the four operators are described in section 3.2. In section 3.3 the outline of the GA is presented. In section 3.4 the GA is illustrated by an application to a maximisation problem. Section 3.5 introduces problems involving two objective functions. A summary is given in section 3.6.

3.2 Procedures and Operations in the GA Approach

The following subsections describe the representation and initialisation of the seed population, the fitness function, and the selection, crossover and mutation operators.

3.2.1 Representation and Initialisation of a Seed Population.

The seed population consists of N trial solutions

$$X_j = X(a_{1j}, a_{2j}, \ldots, a_{nj}),\ j = 1, N$$

where $a_{ij},\ i = 1, n$ are the 'n' design parameters in the j^{th} trial solution.

In a trial solution the parameters may be represented as a decimal number, or a binary equivalent number. Initially the arithmetic length used for a parameter is chosen, which then fixes the string length of the binary representation of each parameter. Thus if the latter is of length m then concatenating the strings of all n parameters in a trial solution, into a single seamless binary string, results in a binary string of total length $m \times n$. Such a binary string is called a chromosome, or, a trial solution chromosome. The values of a_{ij} are obtained within the parameter search domain (L_i, U_i) by the formula [13] (Appendix A)

$$a_{ij} = L_i + \frac{V_{ij}}{2^m - 1}(U_i - L_i), \quad \text{for } i = 1, m,\ j = 1, N$$

In this way the N random seed trial solutions, $X_j,\ j = 1, N$ are constructed. The seed trial solutions are immediately tested for an acceptable solution(s) and if not accepted the seed population moves on into the GA iterative cycle.

3.2.2 The Relative Fitness Functions

The relative fitness uses the objective function to provide a measure of how individuals have fared in a sample population. The relative fitness function value of an individual candidate decides if the candidate proceeds to the next generation. Several measures of the relative fitness have been proposed which employ the values of the objective function of each member in the population. The fitness value may be obtained by linear transformation, dynamic linear scaling, power law scaling, and, logarithmic scaling. The most commonly used is the relative fitness given by [13]

$$F_J = \frac{f(X_j)}{\sum_{j=1}^{N} f(X_j)}, \tag{3.1}$$

where $f(X_j)$ is the value of the objective function for the solution X_j. According to its relative fitness value each individual has a probability of being a member of the next generation.

3.2.3 The Selection Operator

This operator selects the relatively better solutions from the current population and deletes the remaining. The better solutions are then employed in the crossover and mutation processes to generate new offspring to maintain the population size. The selection guides a GA's search in the direction of promising regions in the search space. Many selection methods, such as the Roulette wheel selection method, Tournament selection, and, Rank-based selection method have been proposed [34].

The simplest and most used selection method is the Roulette Wheel method, since it assigns a correct simple proportional representation of the best solutions to be members of the next generation. Each trial solution string is assigned to a sector on a roulette wheel Figure 3.1(a), the size of the sector being proportional to the fitness value of the solution. The roulette wheel is spun as many times as the population size, and, each time a chromosome is selected by the roulette wheel pointer [12,13,34]. Because the solutions are located in sectors proportional to their fitness values, an individual with a higher fitness value will have more chances to be selected than an individual with a low fitness value. The computational realisation of the Roulette wheel solution is best described by starting with the wheel divided into N equal unit sectors as shown in Figure 3.1(b).

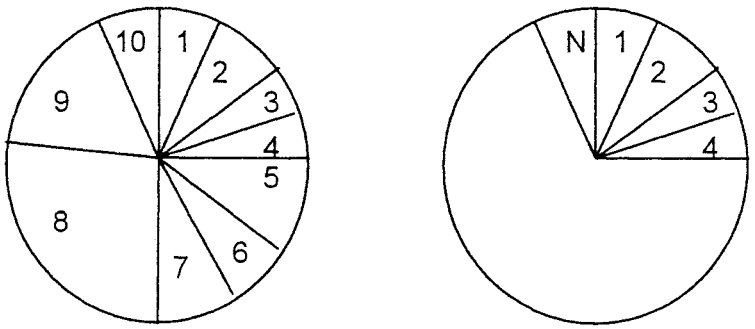

Figure 3.1 (a) Roulette Wheel selection (b) N-Unit sectors

For a maximisation Each of the N trial solutions is allocated a number of these sectors in direct proportion to its relative merit in the population as given by its relative fitness value $F(X_j)$. The trial solution is then awarded S_j unit sectors where

$$S_j = Int\{F(X_j) \times N\}$$

where Int is the integer round off of $F(X_j) \times N$.

Computationally, S_j copies of X_j are placed in the population, but each with a different name (subscript) and so the size of the population is not changed. Some trial solution(s) receive no allocation of unit sectors and so are rejected. The surviving trial solutions are then eligible to be selected for a parental role in the crossover procedure.

Diagrammatically, the S_j unit sectors of the successful candidate copies may be co-joined to produce the conventional wheel sector configuration as shown in Figure 3.2(a). However, this is not necessary since the random pointer selection picks out the same best sectors whatever their position on the Roulette Wheel, Figure 3.2(b).

An illustration of selection is given below in table 3.1

j	$F(X_j)$	$F(X_j) \times N$	int$\{F(X_j) \times N\}$
1	0.14	0.56	1
2	0.49	1.96	2
3	0.06	0.24	0
4	0.31	1.24	1

Table 3.1 Allocation of Unit Sectors.

The trial solution X_3 is rejected while solutions X_1, X_2, X_4 are retained, with X_2 assigned two unit sectors on the roulette wheel.

If a copy of X_2 is now relabelled X_3 then the new set X_1, X_2, X_3, X_4 constitutes a full population of four solutions eligible to produce to the crossover/mutation operation for further iterations(s).

3.2.4 The Crossover Operators

Crossover is the main random search tool of the GA approach. This operator is applied to a proportion of chromosomes of the eligible solutions which have been selected to be parents of new offspring chromosomes. The proportion is called the 'crossover rate' denoted by p_c. In practice [13], $p_c \in [0.4, 0.9]$ so that somewhere between 40% and 90% of a given population are chosen as parents for the next generation.

From within the binary chromosome strings of two parents, substring segments are chosen at random to be exchanged or crossed over, between the parents, in order to create two new chromosomes [34,35,36]. The new offspring now replace, completely, the two parents in the population. A one point crossover between two parent chromosomes is illustrated below.

parents	offspring
000↑100011100	000↑001101010
111↑001101010	111↑100011100

where ↑ is the one point crossover position.

The two substring segments 000, and 111 are swapped over between the parent chromosomes to produce two new chromosomes.

In general if there are many crossover points 1,2,3,...,5 as shown below

Chromosomes 1	$\{\uparrow \uparrow \uparrow \ldots\ldots \uparrow_s\}_{end}$
Chromosomes 2	$\{\uparrow \uparrow \uparrow \ldots\ldots \uparrow_s\}_{end}$
Crossover points	$\{1 \quad 2 \quad 3 \quad \ldots\ldots s\}_{end}$

then simultaneously the binary segments between (0,1), (2,3),...(s,end) are swapped over. That is starting at the left hand end the binary segments in alternate segments are crossed over, The number of crossover points is chosen at random in the interval [1, (mxn-1)]

3.2.5 Mutation Operator

To complement the crossover process by increasing the diversification trial solutions the mutation operator is employed. Mutation consists of simply switching over one binary bit in the chromosome string of an eligible candidate which, again is chosen at random. The mutation operator is applied with a low rate p_m, typically, $p_m \in [0.01,0.1]$. The mutation operator is illustrated as follows:

Parent	Offspring
10101010	10001010
↑	↑

3.3 Outline of the GA Method

The procedural sequence is as follows:

1. Initialise and encode a random population of chromosomes.

2. Decode and evaluate each chromosome's relative fitness in the population.

3. Reproduce a new generation by stochastically selecting current chromosomes as parents according to fitness in order to generate new children.

4. Apply crossover and mutation operators to generate the new chromosomes.

5. Repeat 2-4 until an adequate solution is found (Reproduction).

A flow diagram is shown in Figure 3.2

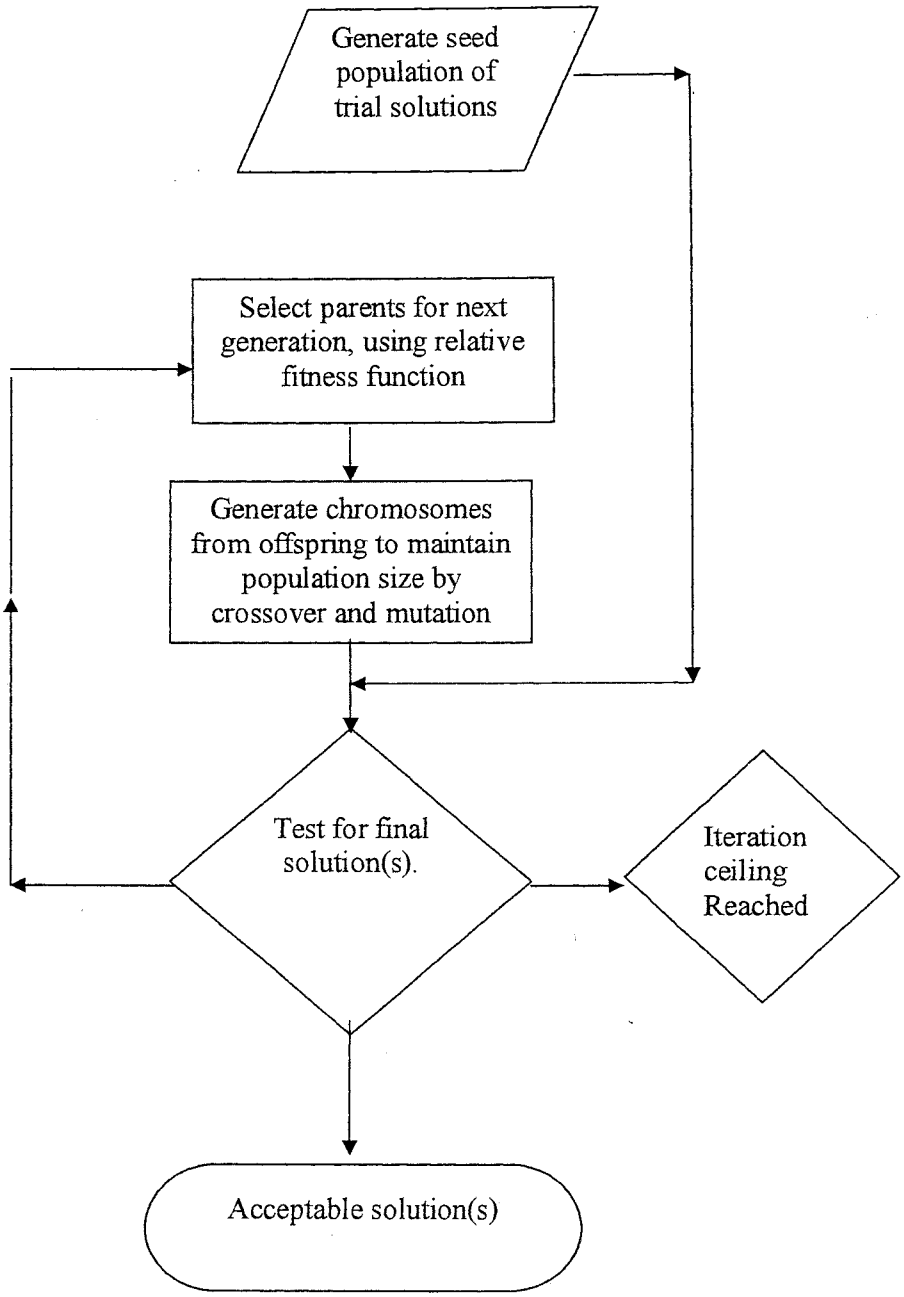

Figure 3.2 Genetic algorithms flow chart.

3.4 Genetic Algorithms Example

The problem is to find the maximum value of the function, $f(x,y)$:

$$f(x,y) = \left|\frac{\sin(\pi(x-3))}{\pi(x-3)}\right| \cdot \left|\frac{\sin(\pi(y-3))}{\pi(y-3)}\right|$$

on the parameter domain $x \in [0,8]$, $y \in [0,8]$.

The above objective function $f(x,y)$ is plotted in Figure 3.3 which has a well-defined global maximum at x=3.0, and y=3.0, and also a number of local maximam. Further the function it is not everywhere differentiable [40].

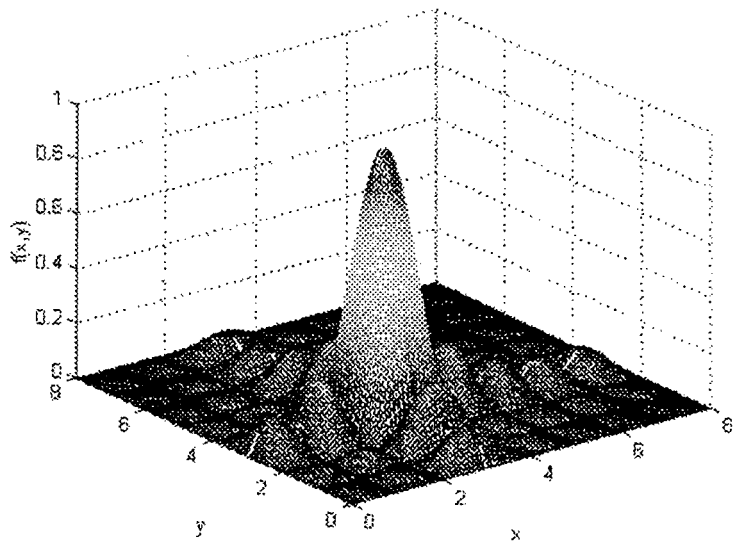

Figure.3.3 A plot of the solution surface for the 2D magnitude Sinc function.

The GA first generates a set of ten initial random values of the seed chromosome population in the search domain in their binary representation form:

$P_{c1} = [11010110100101011110]$
$P_{c2} = [00100100100111000010]$
$P_{c3} = [01011110001110010111]$
$P_{c4} = [01011110000110011111]$
$P_{c5} = [01111111001110011011]$
$P_{c6} = [01111100001100011110]$
$P_{c7} = [01101101001100011010]$
$P_{c8} = [01011101001100010111]$
$P_{c9} = [01101101000100010010]$
$P_{c10} = [01011101001100010100]$

This initial population is converted to corresponding scaled real values by the scaling formula (section 3.1)[42].

The corresponding real parameter values of this chromosome population are

$P_1 = (x_1, y_1) = [0.4962, 4.1916]$
$P_2 = (x_2, y_2) = [6.0450, 2.0176]$
$P_3 = (x_3, y_3) = [7.2727, 4.7937]$
$P_4 = (x_4, y_4) = [0.7038, 1.5861]$
$P_5 = (x_5, y_5) = [1.6774, 0.8426]$
$P_6 = (x_6, y_6) = [1.3666, 1.6168]$
$P_7 = (x_7, y_7) = [0.4418, 7.1769]$
$P_8 = (x_8, y_8) = [1.6422, 1.8260]$
$P_9 = (x_9, y_9) = [1.1046, 6.2033]$
$P_{10} = (x_{10}, y_{10}) = [4.9423, 0.2581]$

Then the objective function, $f_i(x_i, y_i)$, is evaluated, and these values are then used to evaluate the corresponding relative fitness value. For this maximisation problem the relative fitness value is equal to the value of the objective function.

The relative fitness function values of the above parameter population are as follows:

$f_1(x_1, y_1) = 0.0163$
$f_2(x_2, y_2) = 0.0142$
$f_3(x_3, y_3) = 0.0042$
$f_4(x_4, y_4) = 0.0249$
$f_5(x_5, y_5) = 0.0012$
$f_6(x_6, y_6) = 0.0054$
$f_7(x_7, y_7) = 0.0290$
$f_8(x_8, y_8) = 0.17840$
$f_9(x_9, y_9) = 0.0087$
$f_{10}(x_{10}, y_{10}) = 0.0003$

From the above function evaluations it can be concluded that the parameter set, P_8 is the best one and that the parameter set P_{10} is the worst.

The roulette wheel selection procedure is now applied as shown below:

1. Calculate the total fitness for the population:

$$F = \sum_{i=1}^{10} eval_i[P_i] = 0.2825.$$

2. Calculate the selection probability p_{si} for each parameter set

$$p_{si} = \frac{eval_i[P_i]}{F}$$

$p_{s1} = 0.576, p_{s2} = 0.502, p_{s3} = 0.148, p_{s4} = 0.881, p_{s5} = 0.420,$
$p_{s6} = 0.191, p_{s7} = 1.020, p_{s8} = 6.310, p_{s9} = 0.307, p_{s10} = 0.010$

3. Calculate the cumulative probability q_i for each chromosome:

$$q_i = \sum_{j=1}^{10} p_{sj}$$

$q_1 = 0.576, q_2 = 0.1.078, q_3 = 0.1.226, q_4 = 2.107, q_5 = 2.527$
$q_6 = 2.718, q_7 = 3.738, q_8 = 10.048, q_9 = 10.355, q_{10} = 10.365$

- Generate a random number r from the range $[0,1]\times \max(p_{si})$, i=1,2,...10.
- If $r \le q_1$ then select the first chromosome P_1; otherwise select the kth chromosome P_k, $2 \le k \le$ *population size* such that $q_{k-1} \le r \le q_k$.

The following 10 random numbers are generated

$r_1 = 1.96, r_2 = 0.813, r_3 = 0.376, r_4 = 0.843, r_5 = 5.196$
$r_6 = 7.281, r_7 = 4.638, r_8 = 3.694, r_9 = 1.338, r_{10} = 6.954$

The first number $r_1 = 1.96$ is greater than q_3 and smaller than q_4 meaning that the chromosome 4 is selected for the new population; the second number $r_2 = 0.831$ is greater than q_1 and smaller than q_2 meaning that the chromosome 2 is selected for the new population, and so on. Finally, the new population consists of the following chromosomes:

$P_{c4} = [01011110000110011111] = P'_1$
$P_{c2} = [00100100100111000010] = P'_2$
$P_{c1} = [11010110100101011110] = P'_3$
$P_2 = [00100100100111000010] = P'_4$
$P_{c8} = [01011101001100010111] = P'_5$
$P_{c8} = [01011101001100010111] = P'_6$
$P_{c8} = [01011101001100010111] = P'_7$
$P_{c7} = [01101101001100011010] = P'_8$
$P_{c4} = [01011110000110011111] = P'_9$
$P_{c8} = [01011101001100010111] = P'_{10}$

The probability of the crossover is set to be $p_c = 0.4$. This means that 4 chromosome's pairs will be selected for crossover operator. The other

remaining chromosomes will migrate to the next generation. Four random numbers are generated as follow:

3, 5, 6, and 7. This means that the chromosomes $P_3^{'}, P_5^{'}, P_6^{'}$ and $P_9^{'}$ were selected for crossover.

The one-point crossover has been used and this randomly selects one cut-point, k, and exchanges the right parts of two parents to generate offspring. We generate a random integer number *pos* from the range from 1 to 19 (because 20 is the total length of a chromosome) as a cutting point. Since the generated crossover position is 9, the four selected chromosomes are cut after bit number 9, and offspring are generated by exchanging the chromosome segments between each pair as follows:

$P'_3 = [11010110100101011110]$
$P'_5 = [01011101001100010111]$

New ↓

$P'_3 = [11010110101100010111]$
$P'_5 = [01011110000101011110]$

$P'_6 = [01011101001100010111]$
$P'_9 = [01011110000110011111]$

New ↓

$P'_6 = [01011101000110011111]$
$P'_9 = [01011110001100010111]$

Mutation alters one or more genes with a probability equal to the mutation rate. The probability of the mutation rate is set as $p_m = 0.01$, and

means that an average of 1% of the total chromosome population would undergo mutation. Since there are $10 \times 20 = 200$ bits in the entire population, 2 mutations per generation is expected. All the bits have an equal chance to be mutated. Thus a sequence of random numbers $r_i (i = 1,2,\cdots 200)$. The following random numbers are generated 84 and 186, therefore the bits number 84 and 186 were selected for mutation:

Table 3.2 Mutation bit selection

Bit position	Chromosome number.	Bit number.	Random number.
77	4	7	84
183	10	3	186

After mutation the final population is as follows:

$P'_1 = [01011110000110011111]$
$P'_2 = [01111100000110011110]$
$P'_3 = [01111111001110010111]$
$P'_4 = [01111100000110011110]$
$P'_5 = [01011110001110011011]$
$P'_6 = [01111111001110010111]$
$P'_7 = [01111100000110011110]$
$P'_8 = [01011110000110011111]$
$P'_9 = [01001111001110011011]$
$P'_{10} = [01111110001110010111]$

The corresponding real values of variables (x, y) and the fitness values are given by

$f(5.7376,1.0255) = 0.0126$
$f(1.0231,1.0238) = 0.00408$
$f(6.1658,.7884) = 0.02189$
$f(2.7767,4.9002) = 0.02344$
$f(1.1301,0.1543) = 0.01907$
$f(2.7621,1.9072) = 0.01835$
$f(2.7557,2.2571) = 0.42008$
$f(6.7244,3.3925) = 0.34680$
$f(0.8364,1.493) = 0.017030$
$f(0.18344,7.1884) = 0.32152$

This completes one iteration of the genetic algorithm. The GA application is terminated after 200 iterations, and the best chromosome is located in the 42^{ed} iteration with the values $f(2.99997,3.0005) = 1.000$. The iteration sequence is illustrated in Figure 3.4 below:

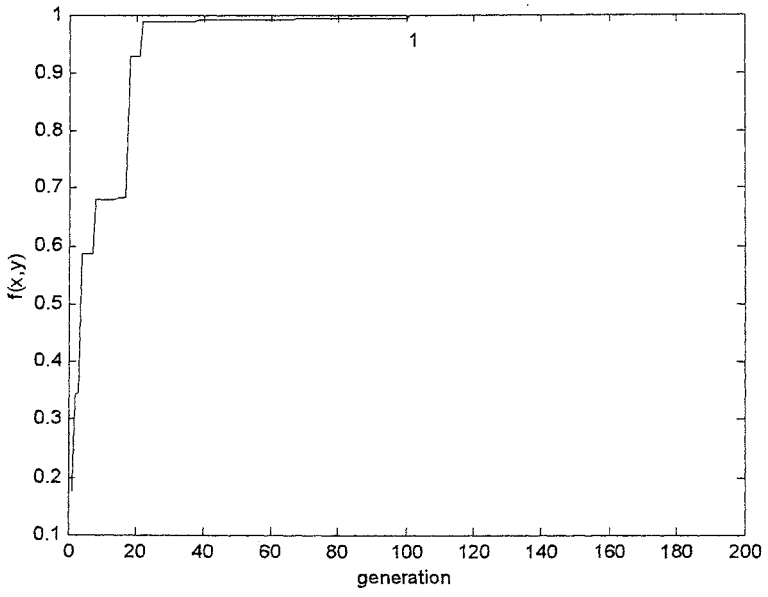

Figure 3.4 The genetic algorithm optimisation convergence to the global optimum solution (fitness=1.0)

3.5 Multi-Objective Genetic Algorithms Optimisation

Many design problems require the simultaneous optimisation of a number of objective functions. In these problems there may be no solution that is best with respect to all the objective functions. The most common procedure for solving a multi-objective function problem is by combining all the objective functions into a single objective function. Various methods such as the method of objective weighting, method of distance functions, and by a min-max formulation have been reported [12].

Typically, there exists a set of solutions that are of better quality, called pareto-optimal solutions, or non-dominated solutions. [13,39,40]. The remaining solutions are called dominated solutions. A pareto-optimal solution for a maximisation problem can be defined as follows:

Let $\mathbf{x}_1$ and $\mathbf{x}_2$ be two sets of solutions for the problem. The solution $\mathbf{x}_1$ is said to dominate the solution $\mathbf{x}_2$, (written as $\mathbf{x}_1 > \mathbf{x}_2$,) if

1. For all elements x_1^i, x_2^i in the vectors $\mathbf{x}_1, \mathbf{x}_2$: $x_1^{\,i} \geq x^i{}_2$
2. There exists a j such that $x^j{}_1 > x^j{}_2$.

However, there usually is no solution out of the non-dominated set which is absolutely better than any other, so any one of the non-dominated set is an acceptable solution.

A better procedure is the non-dominated sorting genetic algorithm [58]: this is used in the present work. The main feature of this optimisation is to classify all potential solutions into two types namely the dominated solution, and, the non-dominated solution type. For minimisation

problems a solution $\mathbf{x}$ is dominated if there exist a feasible solution $\mathbf{y}$ such that

$f_i(\mathbf{x}) \geq f_i(\mathbf{y})$ for all i.

If a solution is not dominated by any other feasible solution it is called a pareto-front solution (see Figure 3.5).

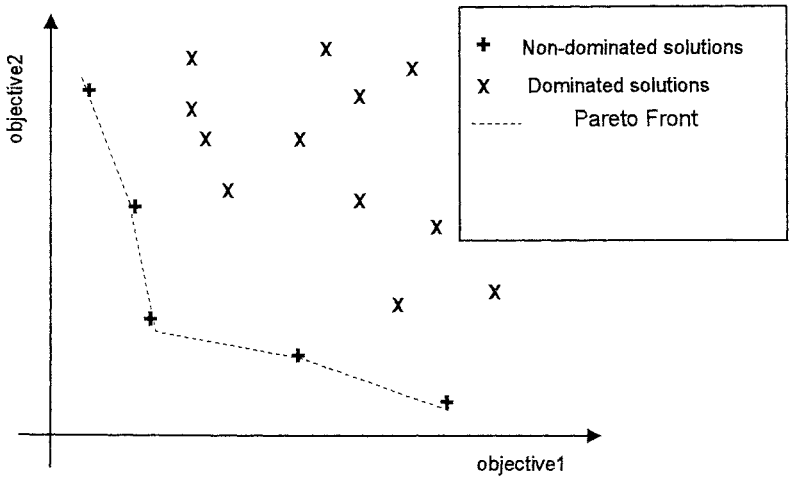

Figure 3.5 Pareto front for minimisation

The idea of this procedure is based on several types of classifications of the individuals. Before the selection is performed, the population is ranked on the basis that all nondominated solutions are sorted into one category, with respect to the fitness value (see Figure 3.6).

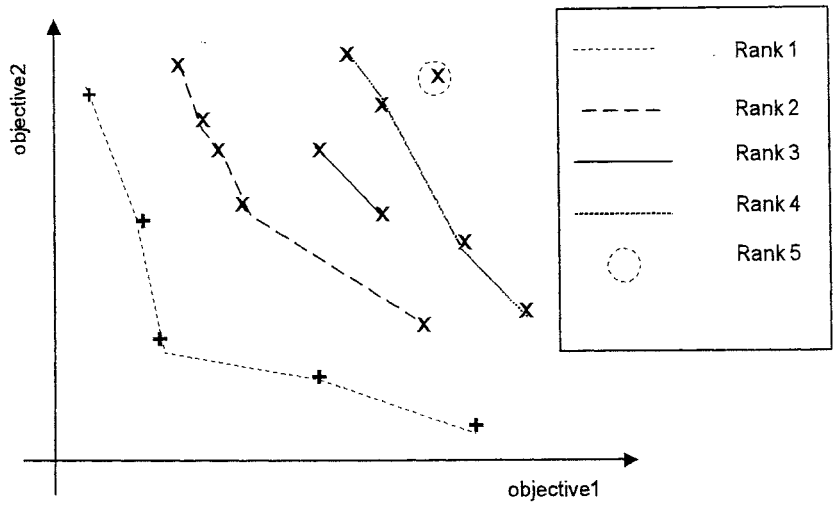

Figure 3.6 Non-dominance ranking

Population members that are not dominated by any other population members are termed non-dominated members and are given rank-1, (Pareto-front1). Then the rank1 solutions are removed from the ranking population. The non-dominated members from the remaining population are then assigned rank-2 (Pareto-front2) and are likewise removed. This process is continued until all the solutions within the present population are ranked. To ensure that the procedure converges to a rank-1 solution an additional share operator is applied, which requires a niching computation carried out using Hamming distance mapping in genotype space [39,40], then the sharing operator is applied.

The steps in the non-dominating sorting genetic algorithm may be conveniently displayed as follows:

Let $g_1 = (a_1, a_2, \cdots, a_n)$ and, $g_2 == (b_1, b_2, \cdots, b_n)$ be two chromosomes with rank-1

1. σ_{share} is a user define niche.

2. The distance between g_1 and g_2 is evaluated by using the Hamming distance function [40] given by

$$d_{Ham\min g}(g_1, g_2) = \sum_{i=1}^{n} |a_i - b_i|$$

3. Applying the niching function :

$$sh(d_{i,j}) = \begin{cases} 1 - \dfrac{d}{\sigma_{share}} & d < \sigma_{share} \\ 0 & \text{otherwise} \end{cases}$$

4. Compute niche count m_i for every chromosome:

$$m_i = \sum_{j=1}^{n} sh(d_{i,j})$$

5. Evaluate the sharing function for each chromosome by reducing the objective function value, F_i, for the chromosome as follows:

$$F_i^{share} = \frac{F_i}{m_i}$$

F_i^{share} is the share value' which is used by the selection operator instead of the original objective function value.

3.6 Summary

In this chapter an introduction to GAs has been presented. The GA approach as used in this thesis has been presented. As an illustration a step-by-step account of an application to a simple maximisation problem is given. A brief review of multi-objective GAs optimisation approach has also been outlined.

Chapter Four

Application of Multi-objective GAs Optimisation to the Design of a Nearly Square Offset-Feed Circularly Polarised Patch Antenna

4.1 Introduction

The single feed patch antenna is one of the most common structures that can be used for circular polarisation applications. Designs using a single-feed rely on generating two orthogonal linearly polarised modes, equal in magnitude and 90° out of phase. Typical types of single-feed circularly polarised patch antennas have been illustrated in chapter two, Figure 2.4.2.

For the nearly square patch antenna with a corner feed it is found that the dimensions of the patch are very close to each other resulting in sensitivity to manufacture errors. This problem would be reduced if it were possible to increase the area of the perturbation segment. It is shown in this chapter that this can be obtained by using a microstrip feed offset from the corner position and along one side of the patch. However as the offset position is increased the input impedance is reduced so that it is difficult to design a simple matching network that still maintains the compact structure of the antenna.

For matching, as complex impedances are involved it is not possible to use a quarter wave transformer. If the constraint on the quarter wave length condition is relaxed then matching of complex impedance is possible. However this form of matching cannot be realised if the offset location is close to the centre line of the antenna. Consequently, with an offset feed position, there is a trade-off between the requirements to increase the area of the perturbation segment and the need to use a simple matching network, so as to maintain the compactness of the antenna.

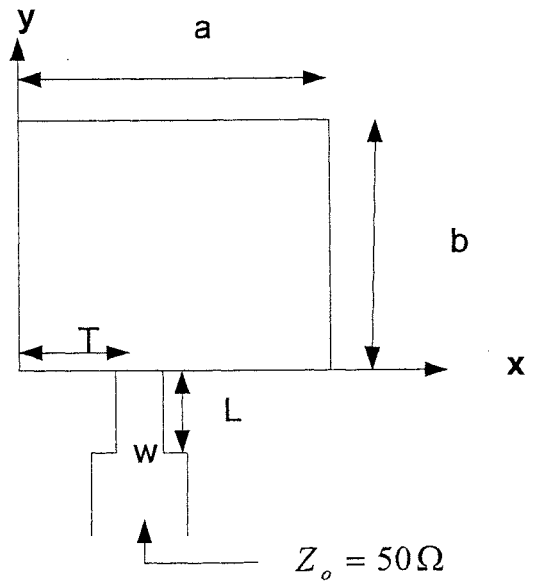

Figure 4.1.1 Nearly Square offset-feed circularly polarised patch antenna

The design of the offset feed structure is described in the following sections. Section 4.2 introduces the derivation of the axial ratio objective function. The derivation of the impedance matching objective function is presented in section 4.3. In section 4.4 the application of the GA optimisation approach to the design is presented. The results and discussion are presented in section 4.5. Sensitivity analysis of the design parameters is presented in section 4.6, and the conclusion is summarised in section 4.7.

4.2 Derivation of the Axial Ratio Objective Function.

The two orthogonal currents components E_x and E_y are given by [29]

$$E_x \propto \frac{\cos(\pi x_o/a)}{k-k_{10}}, \text{ and, } E_y \propto \frac{\cos(\pi y_o/b)}{k-k_{01}} \text{ with } k_{10} = \pi/a, \text{ and, } k_{01} = \pi/b .$$

To produce circular polarisation the following equation needs to be satisfied

$$\frac{E_y}{E_x} = A\frac{(k-k_{10})}{(k-k_{01})} = |1|\angle \pm \pi/2 \tag{4.2.1}$$

where $A = \cos\left(\frac{\pi y_0}{b}\right) \Big/ \cos\left(\frac{\pi x_0}{a}\right)$; (x_0, y_0) being the feed point location.

To a good approximation, the effective wave-number can be expressed as [8]

$$k = k_0\sqrt{\varepsilon_r} - jk_0\frac{\sqrt{\varepsilon_r}}{2Q} = k' + jk'' \tag{4.2.2}$$

where $k_0 = 2\pi f/c$, in which f is the operating frequency, and Q is the quality factor, which includes, copper, dielectric, radiation and surface wave losses of the structure. In equation (4.2.2), $k' = k_0\sqrt{\varepsilon_r}$, and, $k'' = -k'/2Q$

From equation (4.2.1) the amplitude and phase conditions for circular polarisation are given in equations (4.2.4) and (4.2.5).

$$\arg\left(\frac{E_y}{E_x}\right) = \pm\frac{\pi}{2} \tag{4.2.4}$$

and,

$$|E_y| = |E_x| \tag{4.2.5}$$

For the phase condition given by equation 4.2.4

$$\arg\left(\frac{k-k_{10}}{k-k_{01}}\right) = \frac{\pi}{2} \tag{4.2.6}$$

so that,

$$\tan^{-1}\left\{\frac{k''(k_{10}-k_{01})}{(k'-k_{10})(k'-k_{01})+k''^2}\right\} = \frac{\pi}{2}, \text{ which requires}$$

$$(k'-k_{10})(k'-k_{01})+k''^2 = 0,$$

hence,

$$k'^2 - (k_{10}+k_{01})k' + k_{10}k_{01} + k''^2 = 0 \tag{4.2.7}$$

or $$\left\{k' - \frac{(k_{10}+k_{01})}{2}\right\}^2 + k''^2 = \left\{\frac{(k_{10}-k_{01})}{2}\right\}^2 \tag{4.2.8}$$

In the k-plane this represents a circle, centre $(0, \frac{(k_{10}+k_{01})}{2})$, and, diameter, $(k_{10}-k_{01})$. A geometric representation of $k, k-k_{10}$, and, k-k_{01} is shown in Figure 4.2.1

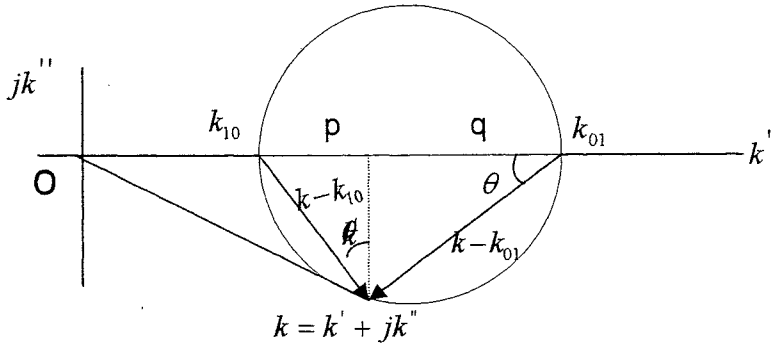

Figure 4.2.1 Geometric relations of phasors k_{10}, k_{01}, and k in the $k-$plane for CP.

The angle between the phasors $k-k_{10}$, and, k-k_{01} is 90°. Therefore k must lie on a circle with diameter $(k_{01}-k_{10})$. Also from equation 4.2.2, k must also lie on a straight line with slope equal to $(k''/k') = 1/2Q$ passing through the origin. Therefore for the solution for k' is given by the intersection of the straight line and the circle. There are three possibilities:

- no solution if $(k_{01}-k_{10}) < 2k''$.
- one solution if $(k_{01}-k_{10}) \approx 2k''$.
- two solutions if $(k_{01}-k_{10}) > 2k''$.

The magnitude condition of E_x and E_y requires that

$$A^2|k-k_{10}|^2 = |k-k_{01}|^2 \qquad (4.2.9)$$

$$A^2\{(k'-k_{10})^2 + k''^2\} = \{(k'-k_{01})^2 + k''^2\}$$

and therefore

$$k'^2 - \frac{2\left(A^2k_{10} - k_{01}\right)k'}{\left(A^2-1\right)} + k''^2 + \frac{A^2k^2{}_{10} - k^2{}_{01}}{\left(A^2-1\right)} = 0 \tag{4.2.10}$$

$$\left\{k' - \frac{\left(A^2k_{10} - k_{01}\right)}{\left(A^2-1\right)}\right\}^2 + k''^2 = \frac{\left(A^2k_{10} - k_{01}\right)^2 - A^2k^2{}_{10} + k^2{}_{01}}{\left(A^2-1\right)^2} \tag{4.2.11}$$

The analytic results of the polarisation condition just obtained are now employed to obtain an equation for A. Eliminating k''^2 between equations (4.2.9) and (4.2.11) determines k' in terms of A, k_{01} and k_{10}, as follows:

$$\left(A^2+1\right)\left(k_{10}-k_{01}\right)k' + \left(A^2k_{10} + k_{01}\right)\left(k_{01} - k_{10}\right) = 0 \tag{4.2.12}$$

whence,

$$k' = \frac{\left(A^2k_{10} + k_{01}\right)}{\left(A^2+1\right)} \tag{4.2.13}$$

and hence,

$$k'' = \frac{-k'}{2Q} = \frac{-\left(A^2k_{10} + k_{01}\right)}{2Q\left(A^2+1\right)} \tag{4.2.14}$$

From Figure 4.2.1

$$\sin(\theta) = \frac{p}{|k-k_{10}|} = \frac{|k''|}{|k-k_{01}|} \tag{4.2.15}$$

$$\cos(\theta) = \frac{q}{|k-k_{01}|} = \frac{|k''|}{|k-k_{10}|} \tag{4.2.16}$$

where the diameter of the circle is

$$p + q = k_{01} - k_{10} \tag{4.2.17}$$

Substituting (4.2.13) through (4.2.16) into (4.2.17) then gives

$$\begin{aligned} k_{01} - k_{10} &= |k''|\frac{|k-k_{10}|}{|k-k_{01}|} + |k''|\frac{|k-k_{01}|}{|k-k_{10}|} \\ &= |k''|\frac{1}{A} + |k''|A \\ &= |k''|\left(\frac{1}{A} + A\right) = |k''|\frac{\left(A^2+1\right)}{A} \\ \therefore \quad &= \frac{-\left(A^2+1\right)}{A}\cdot\frac{\left(A^2k_{10}+k_{01}\right)}{2Q\left(A^2+1\right)} = \frac{-\left(A^2k_{10}+k_{01}\right)}{2AQ} \end{aligned} \tag{4.2.18}$$

whence,

$$A^2 k_{10} + k_{01} + 2AQ(k_{01} - k_{01}) = 0$$

$$A^2 + 2AQ\left\{\frac{k_{01}}{k_{10}} - 1\right\} + \frac{k_{01}}{k_{10}} = 0 \qquad (4.2.19)$$

In terms of the patch dimensions a,b, since $k_{01} = \pi/b$, $k_{10} = \pi/a$

then,

$$A^2 + 2AQ\left\{\frac{a}{b} - 1\right\} + \frac{a}{b} = 0 \qquad (4.2.20)$$

The axial ratio objective function is then given by

$$F(A,a,b) = A^2 + 2AQ\left\{\frac{a}{b} - 1\right\} + \frac{a}{b}. \qquad (4.2.21)$$

For a nearly square patch antenna of given size the circular polarisation conditions can be met by a feed source at any point on a locus uniquely related to the patch dimension, (see Figure 4.2.2)

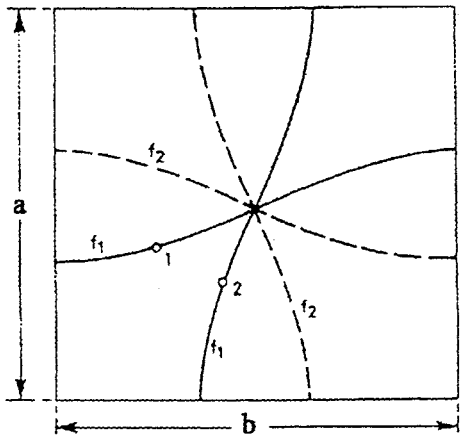

Figure 4.2.2 Feed loci for a nearly square patch antenna

o Feed Location

----------Right hand circular polarisation,

_____Left hand circular polarisation.

From equation 4.2.19 it can be shown numerically that if the feed location is moved from a diagonal position to the position (a) (Figure 4.2.2) the ratio

a/b increases. Thus the effect of manufacturing tolerances on the axial ratio is reduced.

4.3 Derivation of the Matching Objective Function for a Microstrip Feed

Matching can be more readily obtained using a microstrip feed rather than a probe feed. A rectangular patch antenna having dimensions 'a' and 'b' is shown in Figure 4.3.1, where W is the feed width of the microstrip line and T is the offset from the corner of the antenna. The matching objective function is obtained from the input impedance.

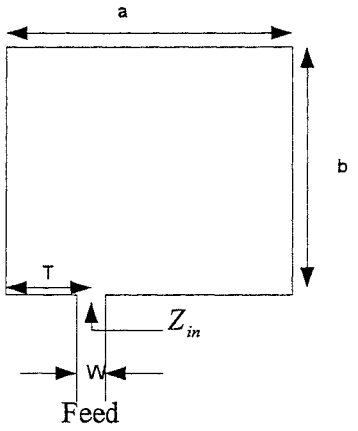

Figure 4.3.1. Input impedance of the rectangular patch

The input impedance for a rectangular patch antenna with a single microstrip feed given in equation 4.3.1 has been derived by Okoshi [27] using coplanar circuit analysis. The formula involves the evaluation of a double infinite series in terms of the resonant modes m and n, and is given by

$$Z_{in(T)} = \frac{j4\omega\mu_o h a^3 b}{W^2\pi^4}\sum_{m=0}^{\infty}\sum_{n=0}^{\infty}\frac{\varepsilon_m^2\varepsilon_n^2}{m^2\left[m^2b^2+n^2a^2-D^2\right]}\cos^2\left(\frac{m\pi T}{a}\right)\sin^2\left(\frac{m\pi W}{2a}\right) \tag{4.3.1}$$

where, $\varepsilon_m = 1\,(m = 0)$ $\varepsilon_n = 1\,(n = 0)$

$= \sqrt{2}\ (m \neq 0)$ $= \sqrt{2}\ (n \neq 0)$

h is the dielectric thickness, $D^2 = k^2a^2b^2/\pi^2$, $k^2 = \omega^2\mu\varepsilon_o\varepsilon_r(1 - j/Q)$, and, Q is the total quality loss factor, which includes copper(Q_c), dielectric(Q_d), radiation(Q_r) and surface wave(Q_{sw}) losses. The loss factors are connected by the relation

$$\frac{1}{Q} = \frac{1}{Q_c} + \frac{1}{Q_d} + \frac{1}{Q_r} + \frac{1}{Q_{sw}} \tag{4.3.2}$$

For thin substrates the losses due to the surface waves are very small and consequently can be neglected [26]. The loss factors are given as follows[26]:

$$Q_c = h\sqrt{\mu_o\pi f_r\sigma_c} \tag{4.3.3}$$

where, σ_c is the conductivity of the metal used.

$$Q_d = \frac{1}{\tan\delta} \tag{4. 4.4}$$

where tan δ is the loss tangent of the dielectric.

$$Q_r = \frac{\pi}{4GZ_p} \tag{4.3.5}$$

where, Z_p is the characteristic impedance of the patch, and $G = G_1 + G_m$ is the total conductance of the slots [20].

The mutual coupling conductance G_m between the radiating edges (see chapter two)

To obtain a more computational efficient form of the input impedance the double infinite series in equation (4.3.1) is first arranged in the four modal groups, (m = n = 0), (m ≥ 1, n = 0), (m = 0, n ≥ 1), and, (m ≥ 1, n ≥ 1). It is shown [42] that each of the single series and the inner series within the double series can telescoped to closed form to give the efficient result:

$$Z_{in(T)} = \frac{j\omega\mu h}{ab}\left[-\frac{a}{k^2}\cot(ka) + \frac{2a^2b^2}{\pi^3 W^2}\sum_{n=1}^{\infty}\frac{(\sin\theta_1 - \sin m\theta_2)^2 \coth(D\pi)}{n^2 D}\right. \qquad (4.3.6)$$

where, $A = ka/\pi$, $B = kb/\pi$, $\theta_1 = \frac{\pi}{a}(u_p - \frac{W}{z})$, $\theta_2 = \frac{\pi}{b}(u_p - \frac{W}{z})$.

From the above equation (4.3.6) numerical evaluation shows that for a centre feed at, $T = a/2$, the first term is dominant and gives the input impedance to four significant figures. Figure 4.3.3 shows the normalised $Z_{in(T)}$ with respect to the centre feed impedance of the patch as function of T.

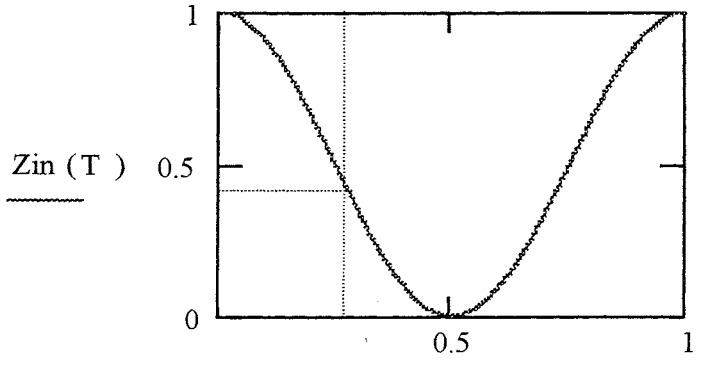

(b)

Figure .4.3.3 Normalised input impedance.

The input impedance of the composite structure of the patch elements and feed lines (Figure 4.1) and is given by Z_{in}

$$Z_{in(feed)} = Z_{feed}\frac{Z_{in(T)} + iZ_{feed}\tan(\theta_{feed})}{Z_{feed} - iZ_{in(T)}\tan(\theta_{feed})} \qquad (4.4.7)$$

where, Z_{feed} is the characteristic impedance of the feed line, θ_{feed} is the electric length, and Z_{patch} is the input impedance of the patch at x_o

The matching objective function is then given by

$$\Gamma(a,b,T,W,L) = \frac{Z_{in(feed)} - 50}{Z_{in(feed)} + 50}. \qquad (4.3.8)$$

4.4 The Application of Multi-objective GA optimisation

A sequential Multi-objective GA has been developed and applied to the design of the offset-feed nearly square patch antenna, in order to check if there are any other solutions that can be found other than the solution found by the method in the previous section. In this approach the objective functions are ranked according to their importance (priority) in the design. Then the GA optimisation applied to the top ranked objective function, being the AR in the present design. The AR is a function of the variables a, b, and T. The accepted feasible AR solutions for the AR are constrained in the interval $0 \le AR \le 1dB$. A set of feasible solutions are obtained, (a_i, b_i, T_i), $i = 1,2,\ldots,k$. These solutions are ordered according to the values of the axial ratio in a solution matrix as shown below.

$$\begin{bmatrix} AR_1 & (a_1, b_1, T_1) \\ AR_2 & (a_2, b_2, T_2) \\ . & . \\ . & . \\ . & . \\ AR_k & (a_k, b_k, T_k) \end{bmatrix}$$

The next stage is to apply the GA optimisation approach to the second objective function, the reflection coefficient Γ, which involves the five parameters of the design. The optimisation procedure in this stage is applied in the following steps. In the first step, the previous solutions for the AR objective function, (a_i, b_i, T_i), $i = 1, \ldots k$ are used in reflection coefficient objective function, Γ, and a GAs optimisation performed with respect to the parameters $(z_{fed}, \vartheta_{feed})$. Feasible solutions so obtained are ranked in the following solution matrix.

$$\begin{bmatrix} AR_1 & \Gamma_1 & (a_1, b_1, T_1, Z_{feed1}, \theta_{feed1}) \\ AR_2 & \Gamma_2 & (a_2, b_2, T_2, Z_{feed2}, \theta_{feed2}) \\ & & \\ & & \\ & & \\ AR_m & \Gamma_m & (a_m, b_m, T_i, Z_{feedm}, \theta_{feedm}) \end{bmatrix}$$

In the above matrix the first row contains the solution with best AR and an acceptable value of Γ.

In the calculation each of the parameters, Z_{feed}, θ_{feed}, T, a, and b is represented by 20 of binary bits, so each solution set is represented in terms of 100 binary bits.

The population size per iteration was 100 chromosomes and the crossover rate implemented was 0.80 (80%) with a uniform crossover operator. The

mutation rate was 0.01 (1%) and the roulette wheel selection method used as a selection operator. A limit of 500 was set for the number of iterations.

For the microstrip patch dimensions, 'a' and 'b' the tolerances are set to be within $\lambda_g/2 \pm 5\%$, where λ_g is the wavelength of the patch [23]. The offset feed position is located in the interval [0, $a/2$], and, the characteristic impedance of the feed line is within a search interval of [70Ω 140Ω], while the feed line search interval was [$\pi/8$, $\pi/2$].

The tolerance for the AR was $0 \leq AR \leq 1dB$ in order to ensure good circular polarisation, while, the tolerance for Γ was $\Gamma \leq -10dB$ in order to ensure a good impedance matching condition.

The operating frequency of the structure is 2.45 GHz and has a 50Ω input power source.

4.5 Results and Discussion

Using the two different modal models, the same values of the antenna design parameters were obtained: a=39mm, b=39.5mm x_o=9.57mm, $W_{feedline}$=0.77mm , and $\theta_{feedline}$=17mm,

In this section the calculated, simulated and practical results for the input impedance, the reflection coefficient, and, the axial ratio are shown in Figure (4.5.1). Very good agreement between calculated, simulated, and practical results are obtained

All the results were carried out over a frequency range of 2.2 -2.6 GHz. Full wave simulation results were obtained using Ensemble™ [43]. An Aneochic Chamber and Wiltron 360 network analyser were used to obtain the practical

results. The practical measurements were obtained using a sweep oscillator as a signal generator, with output of about 20 dBm. The signal goes from the generator to the Anechoic Chamber containing the designed antenna as the transmitter and also a receiving antenna which is in the form a 2x1 linear array. This array is connected to a rotating joint which spins the antenna at about 120 rpm and the signal is picked up by the receiving antenna and goes to a spectrum analyser. The analyser is set up for zero span, that is, a fixed point span so that the analyser functions as a fixed frequency power meter. An operating frequency of 2.45 GHz, is used, and the video output from the analyser transmits the power to a processing Analogue-to- Digital (A-to-D) system and hence to the pc processor.

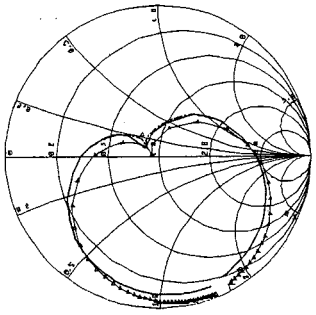

a) Input Impedance: _____ Practical, △___△Simulated,_ _ _ _ Calculated

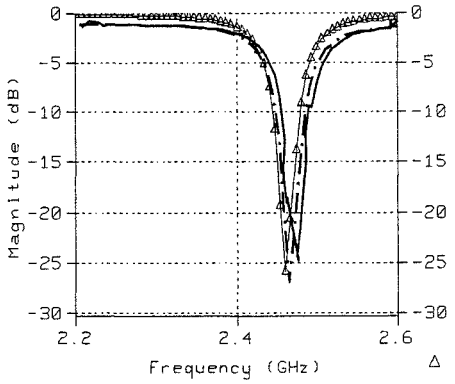

b) Reflection Coefficient ——— Practical, △——△ Simulated,- · - · - Calculated

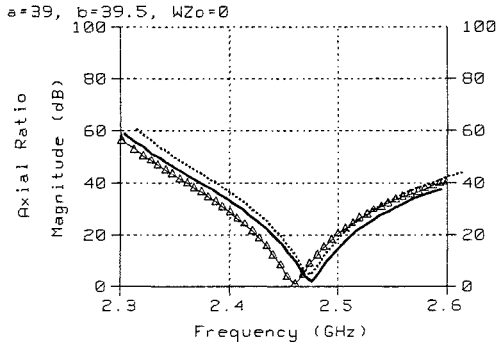

c) Axial Ratio, ——— Practical, △——△ Simulated,- · - · - Claculated

Figure 4.5.1 Offset-fed CP nearly square patch antenna.

4.6 Sensitivity of The Design Parameters

To investigate the sensitivity of AR and Z_{in} to manufacturing tolerances, the effect of variation in the different design parameters has been studied. The results are shown in Table 4.6.1.

Parameter Set					Objective Functions	
a mm	b mm	W(Zo)mm	L(Zo) mm	Offset feed mm	Axial ratio dB	Γ dB
39	39.5	0.77	17	9.57	0.47	-28
39.2	39.5	0.77	17	9.57	4.21	-10
38.8	39.5	0.77	17	9.57	4.25	-15
39	39.3	0.77	17	9.57	4.3	-11
39	39.7	0.77	17	9.57	3.97	-16
39	39.5	0.7	17	9.57	.67	-22
39	39.5	1	17	9.57	0.70	-19
39	39.5	0.77	16	9.57	0.66	-18
39	39.5	0.77	18	9.57	0.68	-21
39	39.5	0.77	17	9	3.64	-19
39	39.5	0.77	17	10.14	3.66	-23

Table 4.6.1 Sets of solutions for the offset-feed nearly square circularly polarised patch antenna.

Perturbed Parameter Values:± variations

In respect of the AR, Table 4.6.1 shows that the changes in the patch dimensions by 0.5% result in an eight-fold increase and changes in the offset

feed location by 0.9% produces a seven-fold increase. The changes in the feed line length and width have a small effect on the AR.

In respect of the Reflection Coefficient changes in the patch dimensions by 0.5% result in increasing the reflection coefficient from –22dB to –15dB, and changes in the feed line dimensions and offset feed location by 5% reduce the impedance matching by around 30%.

These results demonstrate the robustness of the GAs optimisation method in the design computations.

In order to visualise the effect which changes in the parameters have on circular polarisation and impedance matching some graphs of the Smith's Chart were produced and shown in Figures 4.6.1.

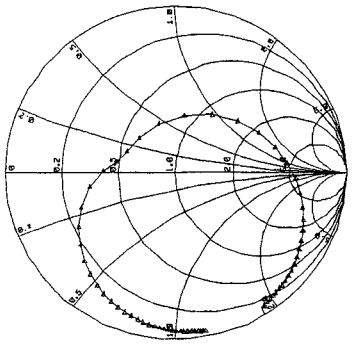

a) a=39.2mm

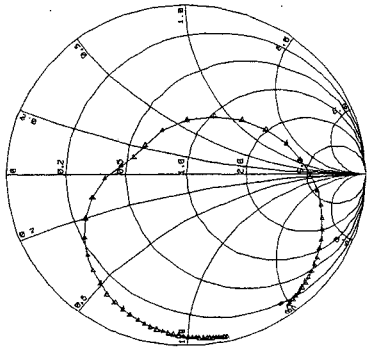

b) b=39.3mm

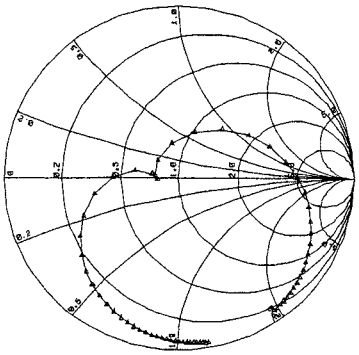

c) x_o=9mm

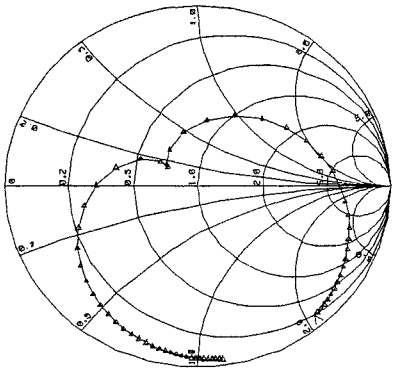

d) W_{feed}=1.00mm

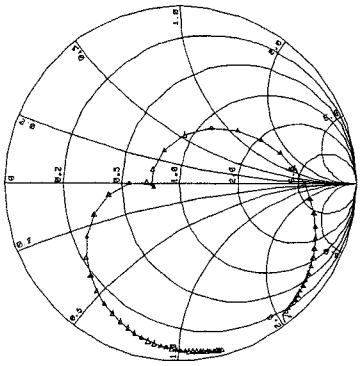

e) θ_{feed}=16.00mm

Figure 4.6.1 Input Impedance's for some altered parameters values

4.7 Summary:

The Multi-objective GA approach has been demonstrated successfully in the highly sensitive design of the offset-feed nearly square patch antenna. Very good agreement between the practical, simulated, and computed results was obtained, and the error over the frequency range was less than 1%. Using the full-wave simulation the effects of altering the control parameter values in the objective functions has been investigated. It can be seen that the input impedance and the axial ratio are very sensitive to very small variations in the patch dimensions and the feed position. Variation in the patch dimensions and the feed positions have a relatively small effect on the antenna performance compared with changes in the length and width of the feed line. It can be conclude that the GAs optimisation method is very robust and can deal with a high dimensional and sensitive design problem

Chapter Five

Multi-objective Genetic Algorithms Approach to the Design of Dual-Feed Circularly Polarised Microstrip Patch Antennas and Antenna Arrays

5.1 Introduction:

In this chapter GA optimisation is applied to both the design of a single dual-feed circularly polarised microstrip patch antenna (sections 5.1,2,3,4,5), and also to a sequentially rotated 2x2 patch array structure (sections 5.6, 7,8,9). For each of the above designs a main aim is to reduce the overall size of the antenna structure compared with structures designed by the conventional approach: that is using quarter wave transformers.

The design approach to a single patch element using an equivalent circuit model is presented in section 5.2. The application of the GA optimisation is discussed in section 5.3 followed by the results and conclusion in sections 5.4, and 5.5.

A new approach to the antenna array design is introduced in section 5.6 and the design equations presented in section 5.7. Results from applying the GA method are presented in section 5.8 and the conclusion in section 5.9.

A summary of the work in this chapter is given in section 5.10. Two papers based on this work have been published [14, 15].

5.2 Multi-objective Genetic Algorithm Implementation to the Design of the Dual-Feed CP Microstrip Antenna.

In this section the design of a dual-feed circular polarised microstrip patch antenna is based on a complex impedance matching approach [44]. This approach reduces the overall size of the antenna structure as compared with traditional design of feeding a square patch antenna at two adjacent

edges using quarter wave transformers (Figure 5.2.1) power divider feed network, and it is possible by relaxing the length condition of $\lambda/4$ transformers to obtain matching and circular polarisation objectives as shown in Figure 5.2.1(b). This matching network introduces complex impedances at the junction point a, b, and d,. As a result instead of maintaining the 90° phase shift between the two modes using an extra feed length l (Figure 5.2.1(a)) which is commonly used, the required phase shift is obtained through the reactance elements at the junction point of the feed network. Moreover, by varying the lengths of the transmission lines and the characteristic impedances of the feed network, the same current magnitude between the voltage modes at the two ports of the feed network can be realised. Matching condition is also obtained by this approach. In this new approach the design problem is characterised by the eight variables as shown in the Figure 5.2.1, the design parameters being the characteristic impedances Z_1, Z_2, Z_3, Z_4, and, the feed network lengths, $\theta_1, \theta_2, \theta_3, \theta_4$. The equivalent transmission line circuit is used to derive the impedance matching, and the axial ratio objective functions. Multi-objective GA has been applied to meet the objective functions for matching and circular polarisation.

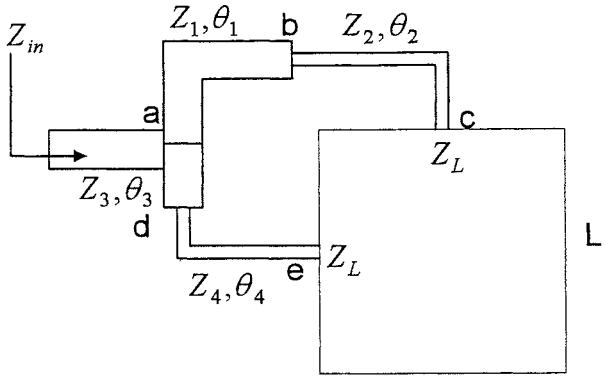

(a)

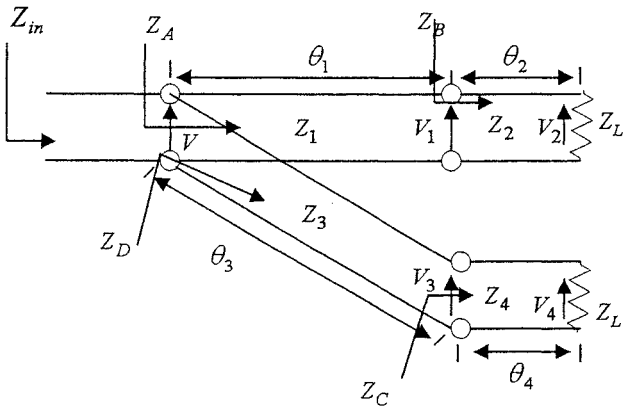

(b)

Figure 5.2.1 a) Dual-feed CP square patch antenna L=16.39mm, εr = 2.33 and h=0.79mm b) Equivalent circuit of the antenna

The impedance matching objective function is given by

$$\Gamma = \frac{Z_{in} - Z_0}{Z_{in} + Z_0} \tag{5.3.1}$$

which is zero for 100% impedance matching.

The circular polarisation objective function is obtained from transmission line analysis. Because the two feed lines act in parallel the input impedance Z_{in} is given by

$$Z_{patch}(Z_1, Z_2, Z_3, Z_4, \theta_1, \theta_2, \theta_3, \theta_4) = \frac{Z_A Z_D}{Z_A + Z_D} \tag{5.3.2}$$

where

$$Z_B = Z_2 \frac{Z_L + jZ_2 \tan(\theta_2)}{Z_2 + jZ_L \tan(\theta_2)} \tag{5.3.3}$$

$$Z_A = Z_1 \frac{Z_B + jZ_1 \tan(\theta_1)}{Z_1 + jZ_B \tan(\theta_1)} \tag{5.3.4}$$

$$Z_C = Z_4 \frac{Z_L + jZ_4 \tan(\theta_4)}{Z_4 + jZ_L \tan(\theta_4)} \tag{5.3.5}$$

$$Z_D = Z_3 \frac{Z_C + jZ_3 \tan(\theta_3)}{Z_3 + jZ_C \tan(\theta_3)} \tag{5.3.6}$$

and Γ_{in} is the input reflection coefficient at junction 'a'.

The circular polarisation objective function of the axial ratio is then given by (Appendix B)

$$AR = \frac{V_2}{V_4} = \frac{e^{-i(\theta_1+\theta_2)}[1+\Gamma_1][1+\Gamma_2]}{[1+\Gamma_1 e^{-2i\theta_1}][1+\Gamma_2 e^{-2i\theta_2}]} \times \frac{[1+\Gamma_3 e^{-2i\theta_3}][1+\Gamma_4 e^{-2i\theta_4}]}{e^{-i(\theta_3+\theta_4)}[1+\Gamma_3][1+\Gamma_4]} \tag{5.3.7}$$

where,

$$\Gamma_1 = \frac{Z_B - Z_1}{Z_B + Z_1} \tag{5.3.8}$$

$$\Gamma_2 = \frac{Z_L - Z_2}{Z_L + Z_2} \tag{5.3.9}$$

$$\Gamma_3 = \frac{Z_C - Z_3}{Z_C + Z_3} \tag{5.3.10}$$

$$\Gamma_4 = \frac{Z_L - Z_4}{Z_L + Z_4} \tag{5.3.11}$$

and where $\Gamma_1, \Gamma_2, \Gamma_3,$ and Γ_4 are the reflection coefficients at junctions b, c, d, and, e respectively.

In addition, practical ranges on the design parameters, such as the widths and the lengths of the feed lines of the feed network, have also been applied. It is desirable to ensure that the widths of the feed network lines are as narrow as possible to reduce spurious radiation, and yet be realisable. It is also necessary to guarantee that the lengths of the feed lines are sufficient to fit the feed network within the area of the microstrip patch antenna structure. This will also assist to minimise the overall size of the structure and reduce the electromagnetic coupling between the design elements.

5.3 Application of the Non-dominating Sorting Genetic Algorithm.

A multi-objective optimisation approach based on a non-dominated sorting GA procedure is a modification of a basic genetic algorithm involving only the fitness values. In the design the Duroid substrate with 2.33 relative permittivity and thickness 0.79mm has been used. The operating frequency of the structure is 5.8 GHz, and a 50Ω source impedance.

The non-dominated sorting GA described in chapter three optimises the unknown parameters of the feed network. Each solution consists of eight parameter variables, the lengths and widths of the feed network lines. Each

variable is characterised by a 10 bit binary string, and so each solution set is represented by an 80 bit binary string. For each iteration the population size for each iteration was 100 chromosomes. The crossover rate P_c implemented was 0.80 (80%)with the uniform crossover operator while the mutation rate value employed was 0.02 (2%) the share operator was σ_{share}=8. The roulette wheel selection method is used and the number of iterations was limited to 500.

To realise the microstrip feed lines a search interval (120Ω,140Ω) was used in the calculation for all the parameters Z_1, Z_2, Z_3, Z_4. The upper limit of 140Ω represents the maximum impedance that can be realised in practice. This is necessary in order to keep the characteristic impedance of the microstrip feed lines close to 140Ω so as to minimise the structure's area, and, also to reduce the couplings between feed lines and antenna. The value of 120Ω has been chosen as lower limit for the feed lines impedances in order to minimise the step discontinuities at the feed line junctions, which reduces spurious radiation. In addition, in order to fit the feed network onto the antenna geometry the lengths $\theta_1, \theta_2, \theta_3, \theta_4$ were constrained within the interval $[\pi/4\ ,\ \pi]$.

The acceptable range for $|V_2/V_4|$ was 1 ± 0.05, and, for $\arg(V_2/V_4)$ was $90^\circ \pm 4^\circ$, so as to ensure good circular polarisation, while the tolerance for Γ_{in} was ± 0.02, in order to produce a good matching condition.

5.4 Results and Discussion for the Dual-Feed Circularly Polarised Patch Antenna

Practical, calculated and simulated results for an optimised LHCP and a RHCP dual feed microstrip patch antenna with a quarter wave-length transformers feed network structure using the conventional approach are presented. The results were obtained over a frequency range of 5.6GHz-6GHz and the practical results were measured by using a Wiltron 360 network analyser. Simulation results were obtained using a full wave simulation package Ensemble™. The operating frequency of the patch antenna design was 5.8GHz and the source impedance was 50-Ω. Six sets of solutions for the optimised feed network are presented in Table 5.1.

	θ_1	Z_1	θ_2	Z_2	θ_3	Z_3	θ_4	Z_4	Z_{in}	$\lvert V_2/V_4\rvert$	$\arg(V_2/V_4)$	CP
1	2.31	135.0	1.96	132.4	0.8	135.2	1.16	134.3	50-0.5i	0.97	86	RHCP
2	1.2	137.4	0.74	137.1	2.3	135.7	1.97	138.6	49.5+0.5i	1.08	89.7	LHCP
3	1.16	133.5	0.81	127.7	2.32	138.7	2.05	132.9	49.6+0.8i	0.95	88.2	RHCP
4	1.9	134.8	2.3	138	1.16	135.48	1.0	136.1	51.05+0.06i	1.07	86.3	LHCP
5	1.01	139.3	1.01	143.3	0.67	141.7	2.28	140.1	52-0.28I	0.98	90.2	LHCP
6	1.2	136.4	0.74	137.1	2.3	135.7	1.97	138.6	49.5+0.5i	1.08	89.7	LHCP

Table 5.1 sets of solutions for the GA optimised feed network.

As can be seen in Table 5.1, for most solutions the impedances of the microstrip feed lines are very close to each other, hence the width of the feed

lines are very close to each other. Therefore, the step discontinuities between the feed lines are very small. It is thus possible to use an average value of impedance for all four feed lines, (set 2), as this value satisfies the design ranges and typical manufacturing tolerances. This also makes the design particularly attractive as the effect of the step discontinuity is eliminated and spurious radiation is reduced and manufacturing tolerance is relaxed.

The layout of a circular polarised dual-feed antenna of conventional (quarter-wave lengths) structure is shown in Figure 5.3.2a, and the layout for the new structure is shown in Figure 5.3.2b. The total length of the feed network for the GA design approach is 39.25 mm on the square patch. However, the length of the feed network in the conventional approach is 39.66mm on the square patch plus a 9.15 mm quarter wavelength transformer thus making the total length 48.71mm. This results in a microstrip patch antenna of 728.714 mm^2 for the traditional design, and, 494.65mm^2 for the new design so the area of the new design is about 32% less than that of the traditional design.

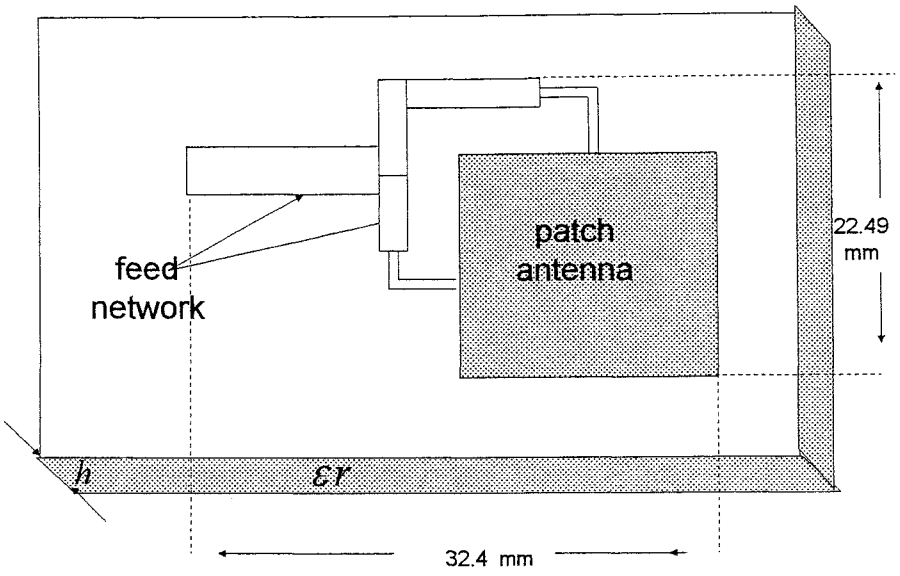

(a)

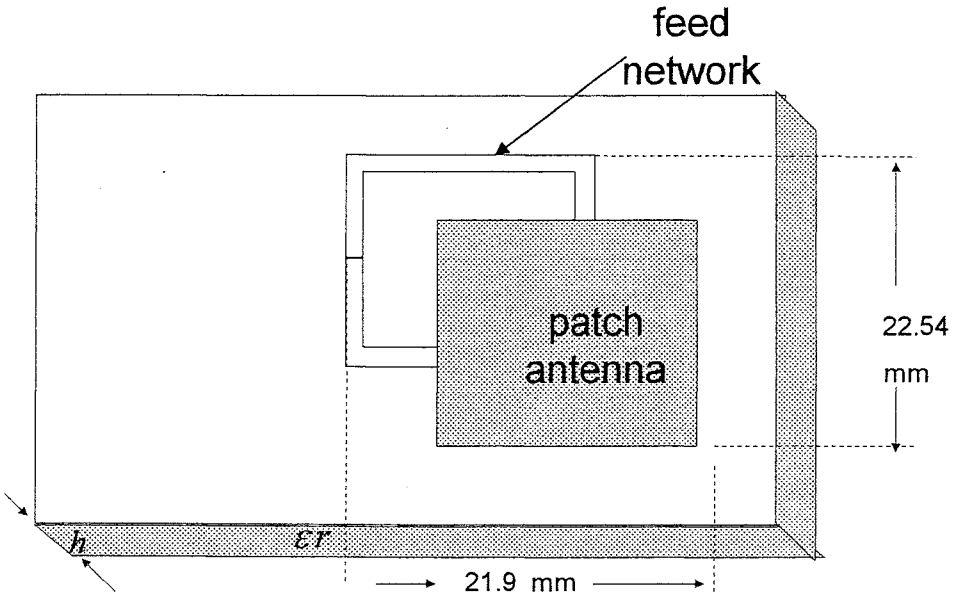

(b)

Fig. 5.3.2 Configurations of dual-feed circular polarised microstrip patch antennas a) Conventional antenna b). GA optimised antenna

Practical and calculated results for the reflection coefficient of the LHCP set of solution using a characteristic feed line impedance of 137.2Ω are shown in Figure 5.3.3. It can be seen that a reflection coefficient of –25 dB for the practical result occurs at the resonant frequency with a bandwidth range of 220 MHz and with less than a 10% loss of power transmitted (s_{11}<-10 dB). It also indicates that a good matching condition at 5.8 GHz has been obtained.

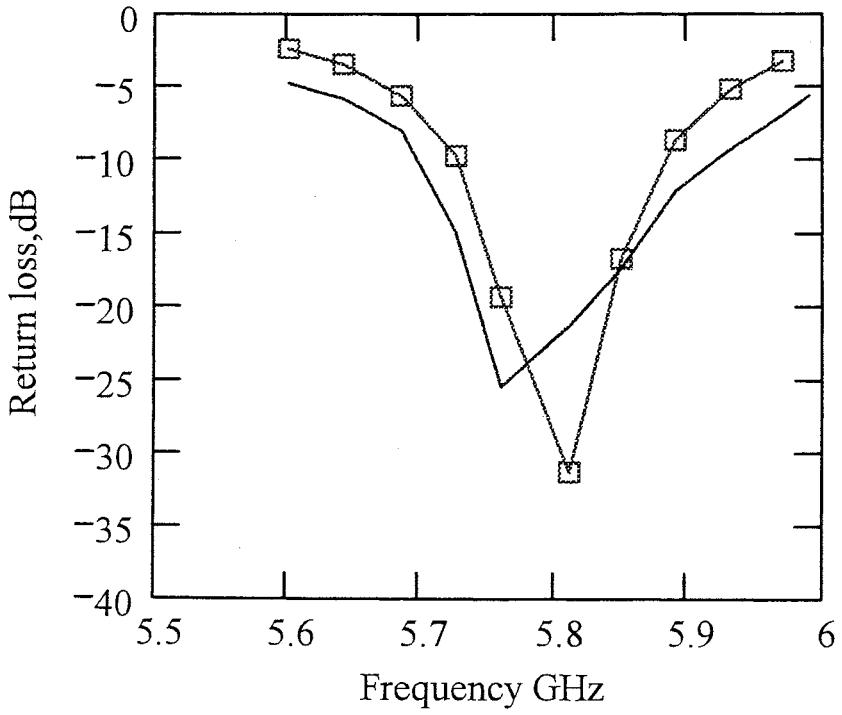

Figure 5.3.3 Reflection coefficient for the LHCP GA optimised antenna

Practical

calculated

The simulated results of the axial ratio for LHCP and RHCP are shown in figure 5.3.4. It can be seen that at the design frequency, a good axial ratio, less than 0.5 dB, very close to a pure circular polarisation, has been achieved.

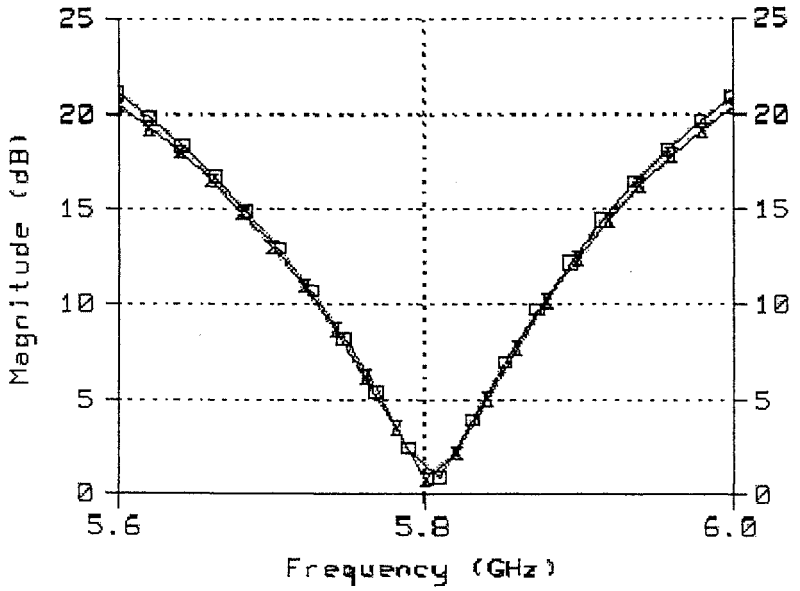

Figure 5.3.4 Axial ratio of RHCP and LHCP set 1 and set 2 antennas.

Predicted radiation patterns around 7 dBi and 90° degree for the RHCP and LHCP designs are obtained and shown in Figure5.3.5.

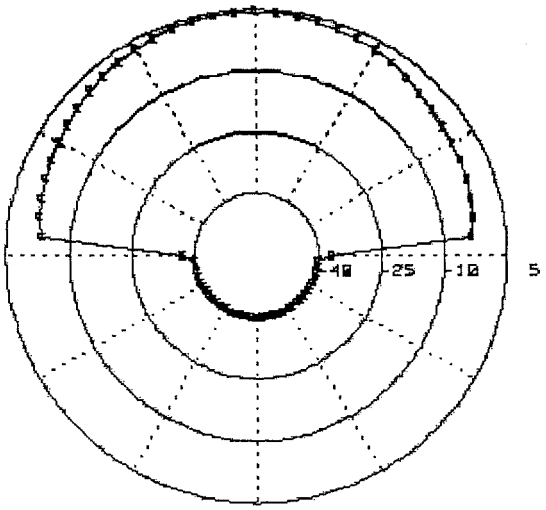

Figure 5.3.6 Radiation patterns of the LHCP and RHCP set 1 and set 2 antennas.

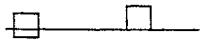
LHCP

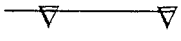
RHCP

The input impedance results from a full-wave simulation using the set 1 (RHCP) parameters and the parameters obtained from the conventional antenna design over the frequency range 5.6-6.0 GHz, are shown in Figure 5.3.6. It can be seen that the impedance loci with double resonance loop corresponding to the orthogonal modes demonstrate that good circular polarisation is obtained.

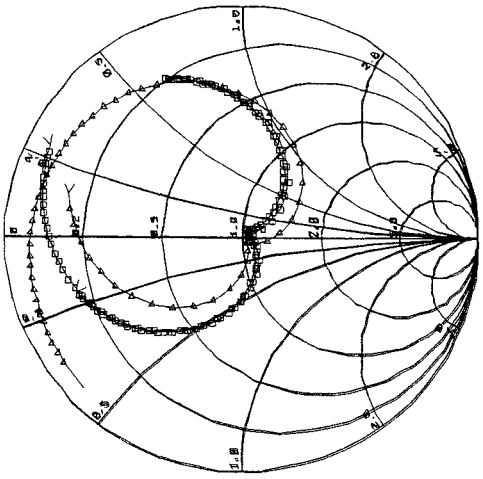

Figure 5.3.6 Input impedance of the GA RHCP and Conventional antennas

RHCP antenna

Conventional antenna

The VSWR has been measured practically and by using the full-wave simulation package and indicates that a bandwidth of 5.72% for VSWR 2:1 has been achieved as shown in Figure. 5.3.7

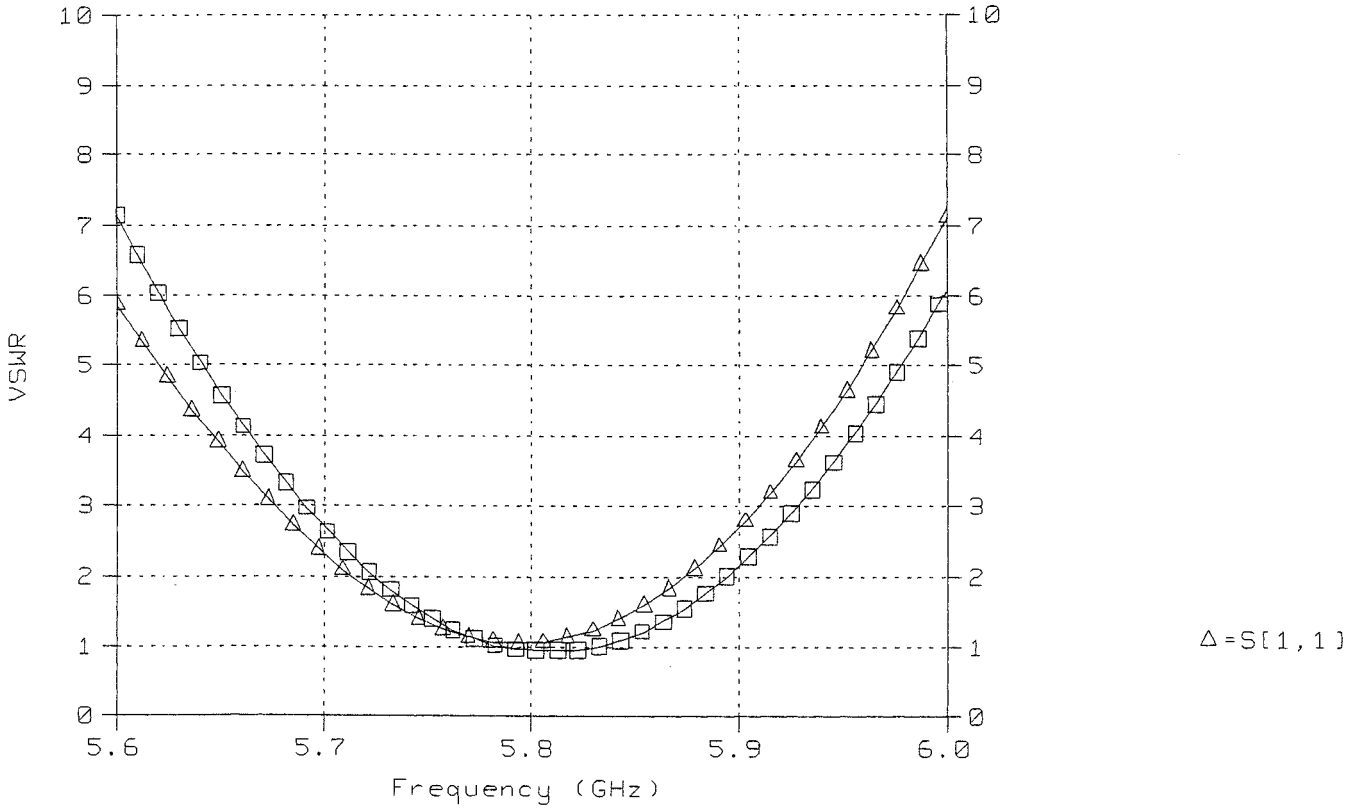

Figure 5.3.7 VSWR of set 1 RHCP and Conventional antennas.

RHCP antenna

Conventional antenna

5.5 Conclusion

In this section a novel design approach for a CP direct dual-feed antenna based on using a complex impedance feed network, optimised using the multi-objective genetic algorithm optimisation, has been developed and applied. It has been shown that the new design approach has resulted in a reduction in the overall size of the structure of approximately 32% compared with a conventional design technique. Very good agreement between the practical, simulated, and calculated results has been obtained for this new compact and simpler feed structure. Thus the GA optimisation method has proved very successful in this application.

5.6 The Sequentially Rotated Circularly Polarised Dual-Feed Microstrip Patch Antenna Array

The purpose of this section is to introduce a new approach using the multi-objective genetic algorithm optimisation approach to design a 2x2 sequentially rotated circularly polarised microstrip patch antenna array. Sequential rotation [9,22,26] is a technique that improves the bandwidth, radiation pattern symmetry and axial ratio of circularly polarised patch arrays. The layout of a 2x2 sequentially rotated circularly polarised patch array is shown Figure 5.4.1. Each radiating element of the array, which is itself is a single dual-feed circularly polarised microstrip patch antenna, is deployed such that each antenna dual feed is rotated physically with respect to its neighbour by 90°. In addition, between every two successive radiating elements there is a 90° phase difference generated by adjusting the lengths of the microstrip lines in the feed network of the array. The line lengths are designed to ensure that the input impedance at each element is well matched. For dual-feed microstrip arrays the axial ratio, and input matching do not degrade off resonance, and, hence the structure serves to widen the bandwidth [15].

Evans et al have designed a 2x2 sequentially rotated patch array using an annealing optimisation method [15]. As a radiating element the design used the dual feed circularly polarised single microstrip antenna developed in this thesis [Section. 5.3.2, 14]. The resulting design improved the purity of circular polarisation and increased the impedance bandwidth. However the design uses a quarter wave transformer for the array feed network, the line

widths of which are of necessity quite large and this introduces spurious line radiation losses, and, also a mutual coupling effect between the individual quarter wave elements. These problems are significantly reduced by using a sequentially rotated 2x2 patch array which does not involve the quarter wave line elements (Figure 5.4.1). In this new approach the non-dominating sorting genetic algorithm approach, used in the optimisation for the design of the dual-feed circularly polarised microstrip patch antenna, has been extended to design a 2x2 sequentially rotated circularly polarised microstrip patch antenna array. In order to fit the feed network onto the antenna geometry the lengths $\theta_1, \theta_2, \ldots, \theta_{11}$ were constrained within the interval [$\pi/4$, π].

The acceptable range for $|V_2/V_4|$ was 1 ± 0.05, and, for $\arg(V_2/V_4)$ was $90^\circ \pm 4^\circ$, so as to ensures good circular polarisation, while the tolerance for Γ_{in} was ± 0.05, in order to produce a good matching condition.

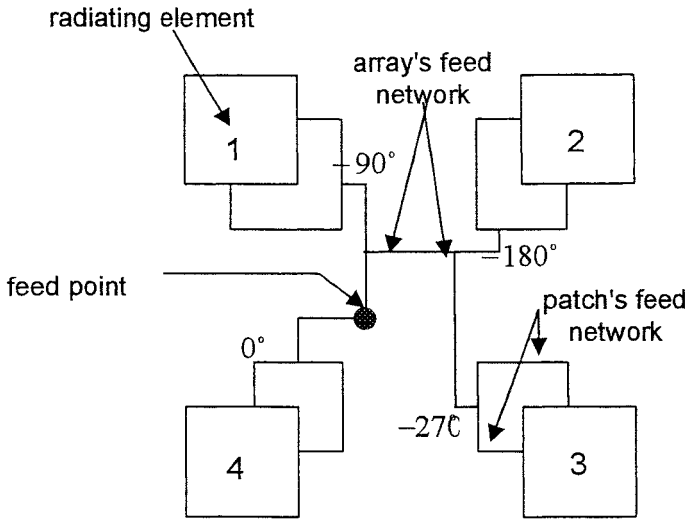

a

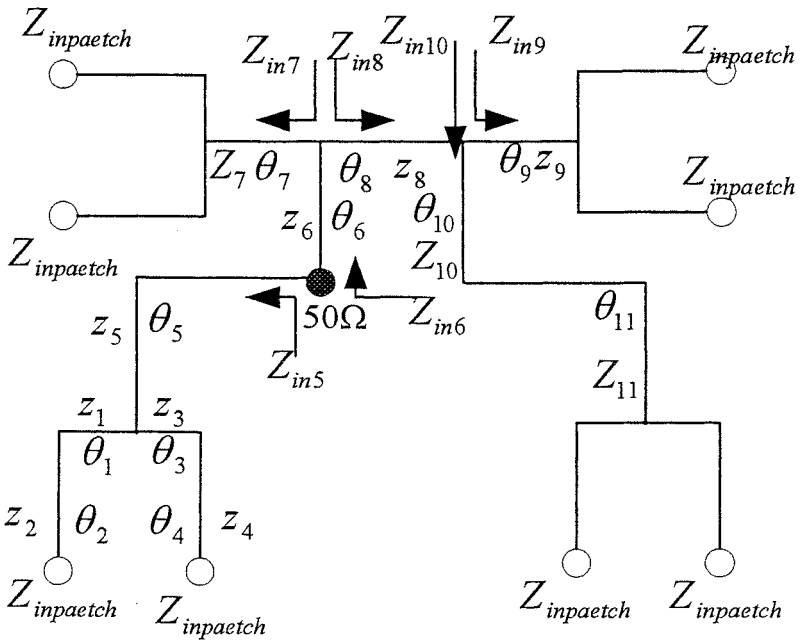

b

Figure 5.4.1) a) 2x2 sequential rotated circularly polarised patch array with hybrid feed network

b) Equivalent circuit of the array

5.7 Array Design and Optimisation

This array design is based on a combined parallel/series feed array network, the equivalent circuit of which is shown in Fig 5.4.1b. The design parameter set ($Z_1, \theta_1, Z_2, \theta_2, \ldots, Z_{11}, \theta_{11}$), of the array structure, presents a high dimensional problem. To design a 2x2 sequentially rotated patch array, the multi-objective optimisation approach discussed in section 5.4 has been extended. Identical patch elements are used in the array.

The reflection coefficient (input impedance matching) condition is

$$\Gamma_{in} = \frac{Z_{in} - Z_o}{Z_{in} + Z_o} \tag{5.8.1}$$

where Z_o is the input impedance of the source feed.

In order to maintain the correct polarisation on each radiating patch the following constraints were necessary:

$$\begin{aligned} &\theta_5 + \theta_6 + \theta_7 = 90^\circ \\ &\theta_5 + \theta_6 + \theta_8 + \theta_9 = 180^\circ \\ &\theta_5 + \theta_6 + \theta_8 + \theta_{10} + \theta_{11} = 270^\circ \end{aligned} \tag{5.8.2}$$

Also, in order to ensure that each patch element receives equal power, the following conditions were required:

$$\begin{aligned} &Z_{in5} = 3Z_{in6} \\ &Z_{in7} = 2Z_{in8} \\ &Z_{in9} = Z_{in10} \end{aligned} \tag{5.8.3}$$

The circular polarisation of the array is maintained by introducing a 90° phase shift at the input ports between any two consecutive radiating elements, thus ensuring that all the patches have identical polarisations. The input impedance of

the entire structure is required to be 50Ω and the feed of patch number 4, is in parallel with the patches numbers 1,2 and 3, which are themselves in series. In order to reduce the step and bend discontinuities, and also the coupling radiation and spurious radiation between the array elements, the values of the characteristic impedances of the feed lines have been constrained to the interval between 70Ω and 145Ω.

5.8 Results and Discussions for the Patch Array

Three sets of solutions for the feed lines of the feed network design are presented in Table 5.2.

Table 5.2 Three set of solutions of 2x2 circularly patch antenna array.

	Set No.1	Set No.2	Set No.3
Z_1	135.6	133.6	139.6
θ_1	2.31	1.631	2.11
Z_2	132	127	137
θ_2	0.8	1.8	1.28
Z_3	127.7	137.7	137.4
θ_3	2.32	1.82	1.22
Z_4	134.3	135.1	143.3
θ_4	1.16	0.916	1.16
Z_5	100.5	98.7	101
θ_5	1.57	1.56	1.58
Z_6	82.23	84.23	80.23
θ_6	1.5	1.45	1.85
Z_7	129.1	139.4	125.3
θ_7	1.7	1.26	1.17
Z_8	79.7	80.1	82.7
θ_8	1.34	1.63	1.54
Z_9	138.9	135.9	140
θ_9	1.35	1.43	1.58
Z_{10}	80.4	82.4	84.1
θ_{11}	1.45	1.05	1.6

To verify the validity of the genetic algorithms optimisation approach, practical, simulated and optimisation results for the solution set 1 were obtained and presented below. These results cover a frequency range of 5.4 GHz to 6.2 GHz. The Wiltron 360 network analyser was used for the practical results and simulation results were obtained using Ensemble™ 5.1. The operational design frequency for the array was 5.8 GHz with a 50-Ω source impedance.

Practical and calculated results for the reflection coefficient are shown in Figure 5.4.2. It can be seen that a reflection coefficient of about –35 dB has been achieved at the resonant frequency with a bandwidth range of 600 MHz and with less than 1% of transmitted power loss. It also shows that a good matching condition at 5.8GHz has been obtained.

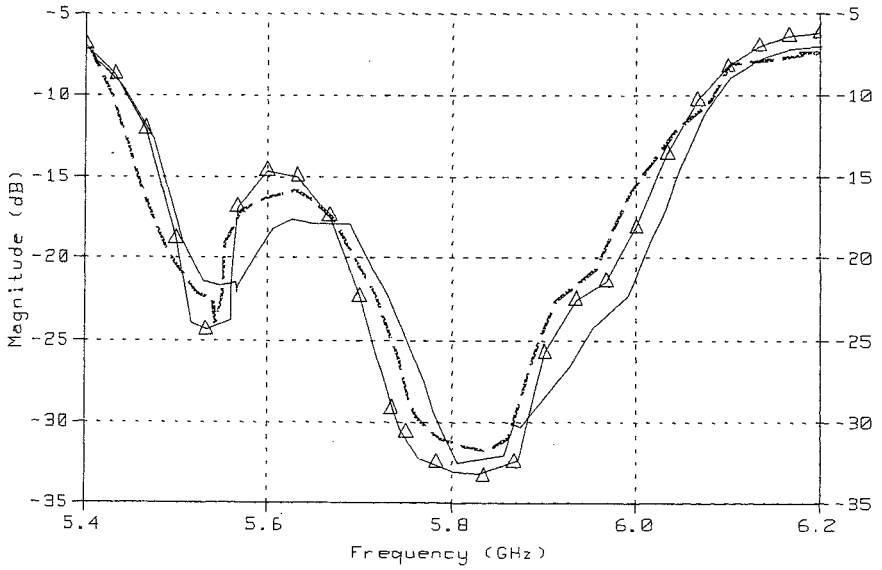

Figure 5.4.2 Reflection coefficient Results

— — — — Practical

Simulated

Calculated

Practical and simulated input impedance results are illustrated in Figure 5.4.3, which shows very good impedance matching at the operating frequency for both results. Good agreement between the two results is maintained over the complete frequency range specified, especially at the cusp in the impedance locus, which corresponds to the good circular polarisation position.

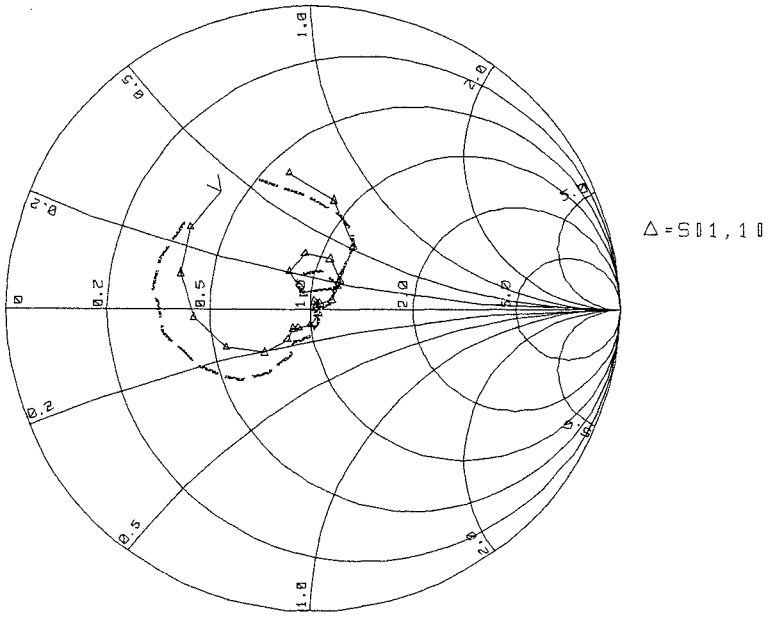

Figure. 5.4 3 Smith Chart results for the array

△———△ Simulated

— — — — Practical

Axial ratio results are presented in Figure 5.4.4. It can be seen that a good axial ratio (<0.5dB) has been achieved at the resonant design frequency, indicating a good circular polarisation achievement. It is also clear that the array has a wider bandwidth than that for the single patch.

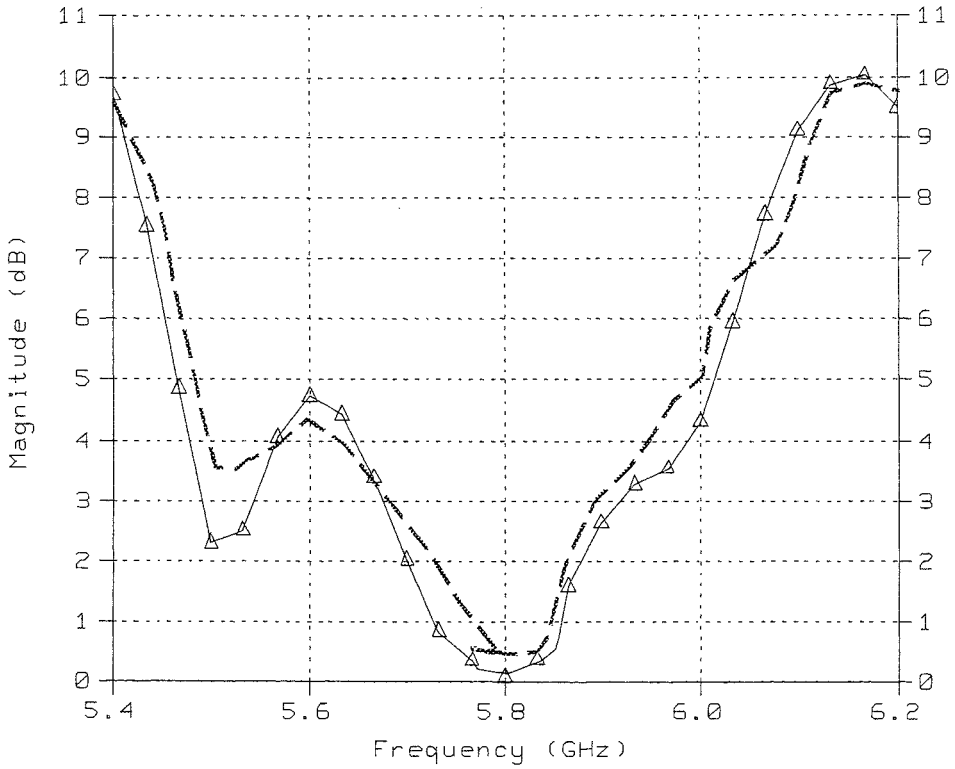

Fig. 5.4.4 Axial ratio results

------ Parctical

△ ___ △ Simulated

The VSWR has been measured practically and by using the full-wave simulation package and shows that a bandwidth of 11.72% for VSWR 2:1 has been achieved as shown in Figure 5.4.5.

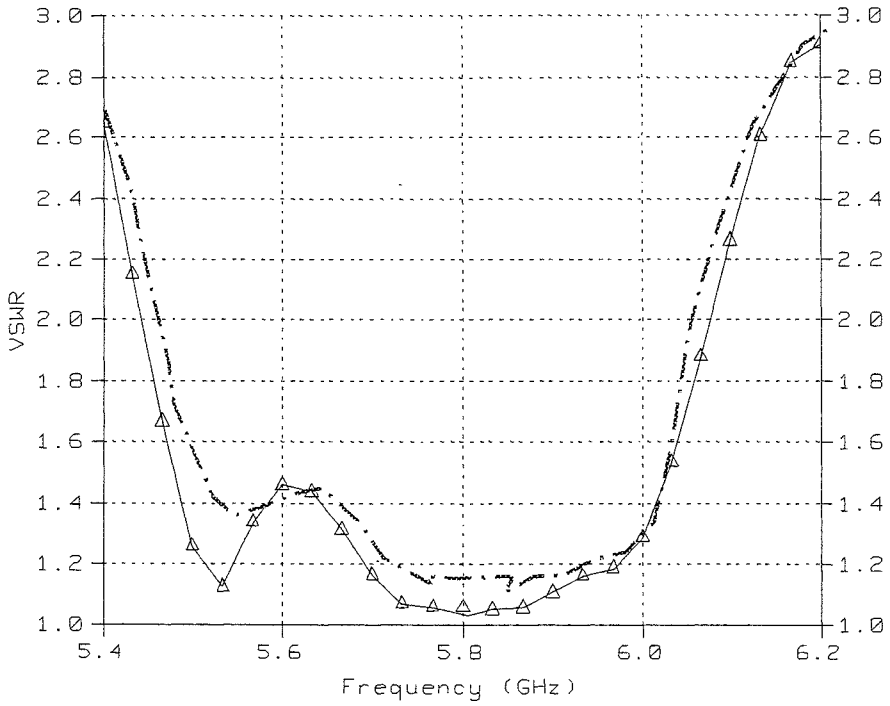

Figure. 5.4.5 VSWR of the patch array

------ practical

△——△ Simulated

5.9 Conclusion

In this section the optimisation technique based on a multi-objective GA optimisation used in section 5.3 has been extended and applied successfully to the design of a 2x2 sequentially rotated circularly polarised patch array. It has been shown that very good agreements between the practical, simulated, and calculated results have been realised. With the new approach a more compact and simpler feed structure designed by the GA optimisation has been achieved. In addition, the expectation of improving the impedance, axial ratio, and VWSR bandwidths compared with those from a single patch element has been realised. These results demonstrate the validity and integrity of the new optimisation design approach in dealing with a very high dimensional and complex design problem.

5.10 Summary

In this chapter the transmission line model has been used to obtain an equivalent circuit for a single dual-feed patch antenna from which expressions for the circular polarisation, and, the impedance matching objective functions have been derived.

In sections 5.3,4,5 the model was used in a GA optimisation design calculation and the results were in good agreement with practical and simulated results.

In sections 5.7-8 the equivalent circuit model was extended to the case of a 2x2 sequentially rotated patch array to obtain the required circular polarisation and impedance matching objective functions used in the calculation for the 2x2 design parameters. Good agreement between the optimised values, and both practical and simulated results was obtained.

Chapter Six

Application of Genetic Algorithm Optimisation to a Cross-Aperture-Coupled Circularly Polarised Microstrip Patch Antenna.

6.1 Introduction

The circularly polarised antenna designs modelled in the previous chapters were based on a planar microstrip structure in which the feed lines and antenna patches were coplanar. In contrast for a cross-slot aperture feed patch antenna, since the feed network and radiating patch are on separate substrates, the properties of each substrate can be chosen to affect, independently, the feed network and the antenna patch. This allows the feed network to be designed so as to produce minimum spurious radiation while the patch can be designed to enhance its radiation properties.

The aperture coupled feed structure is known to have a number of additional practical advantages compared with a normal patch antenna. It does not require an external polariser and expensive dielectric materials [45,46]. With aperture coupling it is possible to match the feed line by varying the slot length and the length of the open-circuit stub which is just an extension of the feed line. This eliminates the need to use an external matching network and hence reduces the overall size of the antenna. The isolation of the patch from the feed network by the ground plane minimises spurious feed radiation. A compact structure can be realised using aperture coupling and with the aperture positioned below the centre of the patch where the resulting symmetry ensures better circular polarisation [16,17,24].

As the slot length can be made greater than half the patch width the impedance matching condition is maintained over a wider bandwidth [47,48]. Theoretical and experimental investigations on the single feed microstrip line aperture fed antenna have been reported, using a single slot,

two cross-slots of unequal lengths, and also using a ring antenna [24,25,49-51]. Aperture coupled structures have been fully analysed using the spectral domain method and a full wave analysis in the real domain [24,47]. These methods can only be used to examine the effects of given design parameters on the performance of the antenna. Also the methods are numerically intensive because of the poor convergence of the reaction integrals and the necessary tabulation of Green's function values. Also the methods do not produce equivalent circuit models suitable for small scale CAD computations.

In this chapter the GA has been applied to the design of a cross-slot nearly square aperture feed patch antenna.

The application of the GA method to the cross-slot coupled antenna requires the axial ratio and matching objective functions. The objective functions depend upon the analytic modelling of the antenna structure and two modelling approaches which generate different equivalent circuit representations are available: the transmission line model and the cavity model. For these models a comparison of the results obtained using the GAs together with both practical and simulated results is given.

Both the transmission line model, and the cavity model [16,17] can readily be used to derive equivalent circuits of the antennas from which the objective functions for the GA optimisation can be constructed.

For the nearly square patch the resonant wave numbers $k_{01} = \pi/b$ and $k_{10} = \pi/a$ of the principal field modes are very close to each other. Consequently it can be assumed that the total quality loss factor Q is the

same for both modes [52]. The loss factor Q includes conduction, dielectric, radiation and surface wave losses of the structure. and the resonant wave number k_o can be replaced by an effective wave number k_e [53].

It has been shown [21] that the effect of surface waves can be normally neglected, provided $k_0 d_a \sqrt{\varepsilon_r} \leq 0.3$ where d_a is the substrate thickness, a condition normally satisfied when patch antennas are realised using substrates having low values of ε_r and/or are operating at low frequencies.

In the cross-slot design problem the analytic complexity is considerable. There are four design parameters: the patch dimensions, slot length, and the open stub length. In section 6.2 the resonant cavity model with the equivalent circuit is presented along with the results. In section 6.3 the transmission line model with equivalent circuit is presented along with the results.

6.2 Cavity Model of Circularly Polarised Cross-slot-Coupled Patch Antenna

In this section a circularly polarised cross-slot-coupled microstrip patch antenna structure shown in Figure 6.2.1a is designed using the cavity model analysis and the GA approach. In this structure the patch element with dimensions a, b is separated from the feed line by a ground plane. This ground plane contains a cross-slot aperture, and the aperture coupling controls the matching between the feed network and the patch element. An open circuit stub extends the microstrip feed line, which eliminates the need of an external matching network and ensures that the size of the structure is compact. Equal slots lengths are use to maintain the symmetry of excitation of the patch and to ensure generation of good quality circular polarisation. A cavity model equivalent circuit representing the antenna structure is shown in Figure 6.2.1b. The equivalent circuit involves RLC circuits which are connected in parallel. Using this equivalent circuit the two objective functions, the axial ratio and the matching objective functions, are derived.

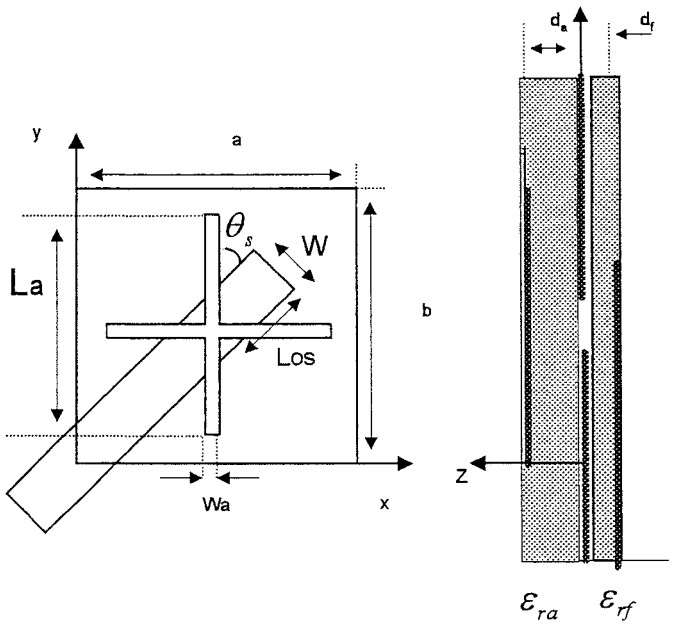

a)

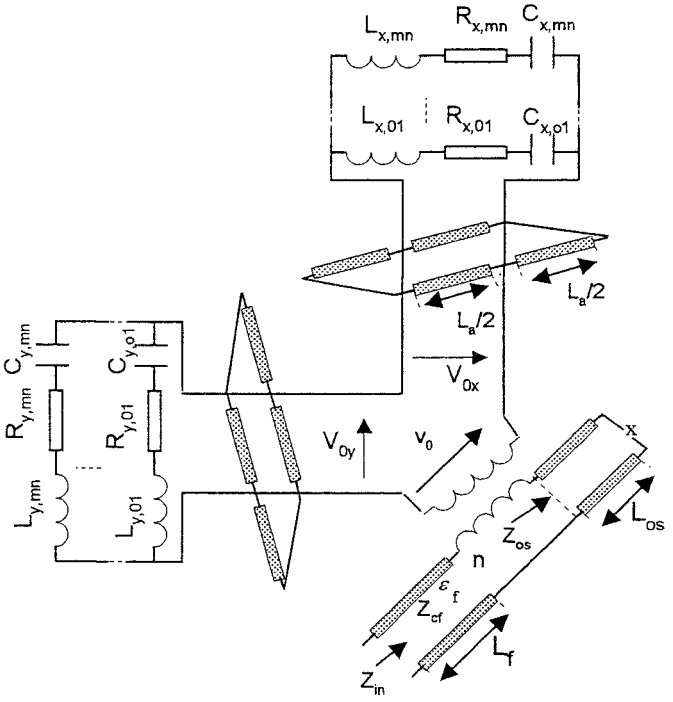

b)

Figure 6.2.1) a) Cross-aperture-coupled microstrip antenna, b) Equivalent circuit based on the cavity model

$\varepsilon_{ra} = \varepsilon_{rf} = 2.33,\ d_f = 1.575mm, d_a = 3.15,\ \theta_s = \pm 45,\ W_a = 2mm$

In section 6.2.1 the turns ratio is obtained. The field distribution analysis is introduced in section 6.2.2. Section 6.2.3 presents the derivation of the impedance matching objective function. Derivation of the axial ratio is presented in section 6.2.4. The results from the application of GAs to the cavity model and a discussion are presented in sections 6.2.5 and 6.2.6, respectively.

6.2.1 Derivation of the Turns Ratio

In this section it will be shown that the effect of a cross-slot aperture can be considered as the superposition of two inclined slots at angles of +45° and -45° with respect to the microstrip feed line Figure 6.2.2a.

The discontinuity voltage on the microstrip line due to an aperture field $\mathbf{E}$ is given by [50]

$$\Delta v = \iint \mathbf{E} \times (\hat{\mathbf{z}}) \cdot \mathbf{h}_m \, ds \tag{6.2.1}$$

where $\mathbf{E}$ is the electric field in the aperture plane, and, $\mathbf{h}_m$ is the normalised magnetic field on the feed line [54].

Assuming the slots are narrow then the electric field in the aperture plane is normal to the slot length and constant across the width of the slot. For the cross-slot aperture the total field $\mathbf{E}$ results from a combination of the two-aperture field $\mathbf{E}_{au}, \mathbf{E}_{av}$ in the directions $\mathbf{u}$ and $\mathbf{v}$ as shown in Figure.6.2.2a.

The discontinuity voltage for the cross-slot aperture is therefore given by [16]

$$\Delta v = \iint_{s_1} (\mathbf{E}_{au}) \times (\hat{\mathbf{z}}) \cdot \mathbf{h}_m ds_1 + \iint_{s_2} (\mathbf{E}_{av}) \times (\hat{\mathbf{z}}) \cdot \mathbf{h}_m ds_2 \qquad (6.2.2)$$

where s_1 and s_2 are the intersections of each slot geometry with the footprint of the microstrip line geometry (Figure 6.2.1a).

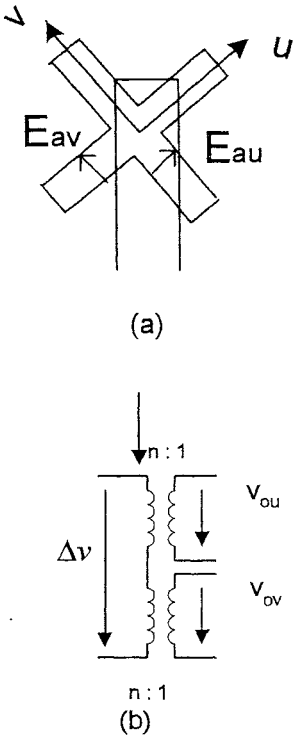

Figure 6.2.2. a) Cross-aperture to microstrip line transition, b) The equivalent circuit.

For slot in the v direction the electric field satisfying the boundary conditions in the slots is given in the form of a single piece-wise sinusoidal mode [55]

$$\mathbf{E}_{au} = \frac{V_0}{W_a} \frac{\sin\left[k_a\left(\frac{L_a}{2} - |u|\right)\right]}{\sin\left(k_a \frac{L_a}{2}\right)} \hat{\mathbf{v}} \qquad |u| \le \frac{L_a}{2} \quad , \quad |\mathrm{v}| \le \frac{W_a}{2}$$

$$= 0, \quad \text{otherwise} \tag{6.2.3}$$

where V_0 is the slot voltage developed at the centre of the two slots and k_a is the wave number of the aperture [56].

For each slot, the transition between V_0 and the discontinuity voltage nV_{ou} (or $\mathrm{nV_{ov}}$) on the microstrip line, is given by [50,54]

$$\iint_{s_1} \mathbf{E}_{au} \times \left(-\hat{\mathbf{z}}\right) \cdot \mathbf{h}_m d_{s_1} = nV_{ou} \tag{6.2.4}$$

and

$$\iint_{s_2} \mathbf{E}_{av} \times \left(-\hat{\mathbf{z}}\right) \cdot \mathbf{h}_m d_{s_2} = nV_{ov} . \tag{6.2.5}$$

Thus the total discontinuity voltage on the microstrip line is,

$$\Delta v = nV_{ou} + nV_{ov} = n\left(V_{ou} + V_{ov}\right) \tag{6.2.6}$$

The transition between a cross-aperture and a microstrip line can be modelled by the series connection of two ideal transformers each having a turns ratio n as shown in Figure.6.2.1b. The discontinuity voltage due to the cross slot is obtained from equations 6.2.2, and 6.2.6 and is given by [16]

$$\Delta v = \frac{V_0}{W_a \sqrt{2W_e d_a} \sin\left(k_a \frac{L_a}{2}\right)} I \tag{6.2.7}$$

where

$$I = \iint_{S_1} \sin\left[k_a\left(\frac{L_a}{2} - |u|\right)\right] du dv + \iint_{S_2} \sin\left[k_a\left(\frac{L_a}{2} - |v|\right)\right] du dv$$

Each of the above integrations is performed over the overlapping area of the aperture and the effective width of the microstrip line. Three mutually distinct cases arise for the domain of integration (see Figures. 6.2.3a, 6.2.3b and 6.2.3c.). However, it is clear that there is an intersection region between the two areas of integrations, which need be calculated just once. Therefore, it is convenient to calculate the field through the aperture as if there were two independent rectangular slots crossing at right angles and then to subtract the surplus contribution over the overlapping domain of the two slots.

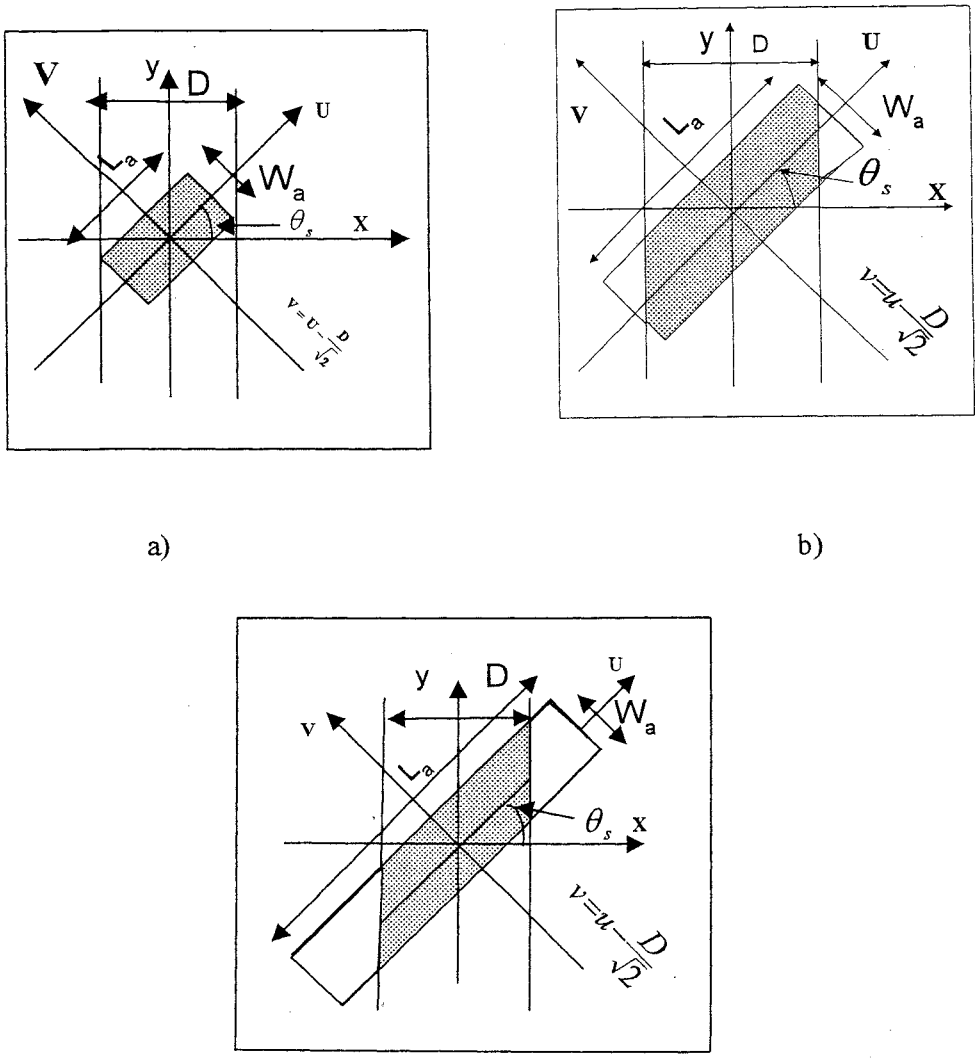

Figure. 6.2.3 Three possible aperture to microstrip line transitions

For each of the possible slot geometries, a,b,c, shown in Figure 6.2.3 the sum of the two integrals in equation 6.2.7,are evaluated in appendix C and are given below:

$$I_a = \frac{2W_a}{k_a}\left\{\cos(k_a) - \cos\left(\frac{k_a L_a}{2}\right)\right\} \tag{6.2.8}$$

$$I_b = \frac{1}{k_a}\left(\frac{L_a}{2}+\frac{W_e}{\sqrt{2}}+\frac{W_a}{2}\right)\cos\left(\frac{k_a W_a}{2}\right)+\frac{2}{k_a^{\,2}}\cos\left[k_a\left(\frac{L_a}{2}-\frac{W_e}{\sqrt{2}}\right)\right]\sin\left(\frac{k_a W_a}{2}\right)$$
$$-\frac{2}{k_a^{\,2}}\sin\left[k_a\left(\frac{L_a}{2}-\frac{W_e}{\sqrt{2}}\right)\right]\cos\left(\frac{k_a W_a}{2}\right)-\frac{2W_a}{k_a}\cos\left(\frac{k_a L_a}{2}\right) \qquad (6.2.9)$$

and

$$I_c = \frac{4}{k_a^{\,2}}\sin\left(\frac{k_a W_a}{2}\right)\cos\left[k_a\left(\frac{L_a}{2}-\frac{W_e}{\sqrt{2}}\right)\right]-\frac{2W_a}{k_a}\cos\left(\frac{k_a L_a}{2}\right) \qquad (6.2.10)$$

The square overlapping area between the two slots is shown in Figure 6.2.4 below

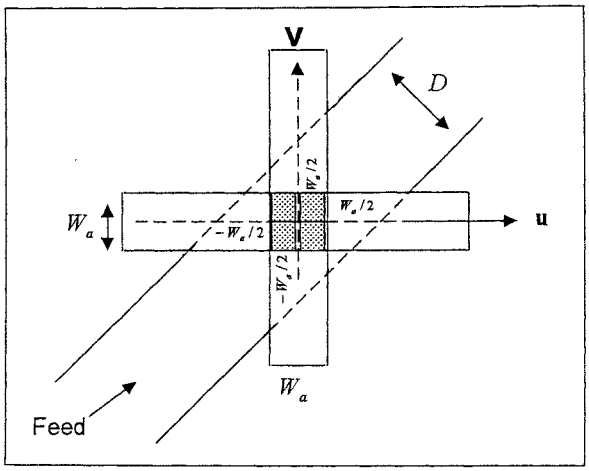

Figure.6.2 4 The over lapping area between the two slots..

The required integration over this area is given by

$$I = \frac{-2Wa}{ka}\left\{\cos\left[ka\left(\frac{La}{2}-\frac{Wa}{2}\right)\right]-\cos\left(ka\frac{La}{2}\right)\right\} \qquad (6.2.11)$$

The value of I in equation 6.2.11 needs to be subtracted from the values of I_a I_b, and I_c to obtain required expression for the Δv.

$$\Delta v = nV_o \qquad (6.2.12)$$

6.2.2 Field Distribution Analysis

It is assumed that the electric field distribution in each of the two orthogonal apertures is in the form of a single piece-wise sinusoidal mode [46].

The electric field in the aperture parallel to the **y** axis has only an **x** directed component E_{ax}, given by

$$E_{ax} = \frac{V_{0y}}{W_a} \frac{\sin\left[k_a\left(\frac{L_a}{2} - \left|y - \frac{b}{2}\right|\right)\right]}{\sin\left(k_a \frac{L_a}{2}\right)} \qquad \begin{matrix} \frac{a-W_a}{2} \le x \le \frac{a+W_a}{2} \\ \frac{b-L_a}{2} \le y \le \frac{b-L_a}{2} \\ z = 0 \end{matrix} \qquad (6.2.13)$$

$$= 0, \qquad \text{otherwise}$$

where V_{0y} is the voltage at the centre of the aperture parallel to the y axis and k_a is the wave number of the aperture which can be determined using Cohn's method [56].

Similarly the electric field in the aperture parallel to the x axis has only a y component E_{ay} given by

$$E_{ay} = \frac{V_{0x}}{W_a} \frac{\sin\left[k_a\left(\frac{L_a}{2} - \left|x - \frac{b}{2}\right|\right)\right]}{\sin\left(k_a \frac{La}{2}\right)} \qquad \begin{matrix} \frac{a-L_a}{2} \le x \le \frac{a+L_a}{2} \\ \frac{b-W_a}{2} \le y \le \frac{b-W_a}{2} \\ z=0 \end{matrix} \qquad (6.2.14)$$

$$= 0, \qquad \text{otherwise}$$

where V_{0x} is the voltage at the centre of the aperture parallel to the y axis

By the equivalence principle [20], the magnetic currents in each of the two apertures just above the ground plane are then given by

$$M_{ax} = -2E_{ay} \qquad (6.2.15)$$

and,

$$M_{ay} = 2E_{ax}. \tag{6.2.16}$$

The equivalent magnetic current density excitation is assumed to be uniformly distributed in the cavity volume above the slot [57] as shown in Figure.6.2.5 The corresponding current densities J_{mx} and J_{my} in the aperture cavities are therefore given by

$$J_{mx} = \frac{-2V_{0x}}{d_a W_a} \frac{\sin\left[k_a\left(\frac{L_a}{2} - \left|x - \frac{a}{2}\right|\right)\right]}{\sin\left(k_a \frac{L_a}{2}\right)} \qquad \begin{matrix} \frac{a-L_a}{2} \le x \le \frac{a+L_a}{2} \\ \frac{b-W_a}{2} \le y \le \frac{b+W_a}{2} \\ 0 \le z \le d_a \end{matrix} \tag{6.2.17}$$

$$= 0, \qquad \text{otherwise}$$

and,

$$J_{my} = \frac{-2V_{0y}}{d_a W_a} \frac{\sin\left[k_a\left(\frac{L_a}{2} - \left|y - \frac{b}{2}\right|\right)\right]}{\sin\left(k_a \frac{L_a}{2}\right)}; \qquad \begin{matrix} \frac{a-W_a}{2} \le x \le \frac{a+W_a}{2} \\ \frac{b-L_a}{2} \le y \le \frac{b+L_a}{2} \\ 0 \le z \le d_a \end{matrix} \tag{6.2.18}$$

$$= 0, \qquad \text{otherwise}$$

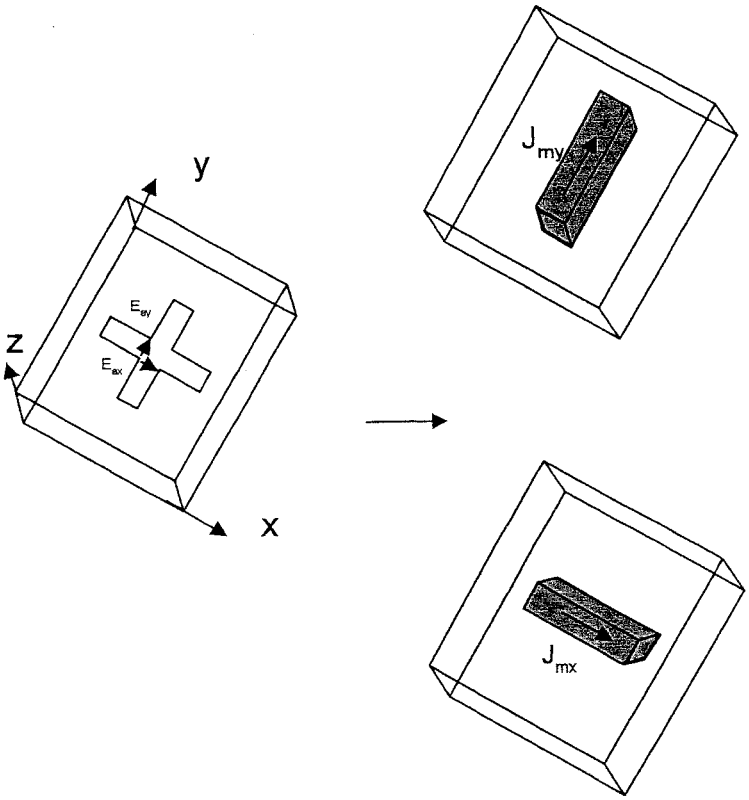

Figure.6.2.5 Equivalent magnetic currents replacing the electric fields in the apertures.

The magnetic field $\mathbf{H}$ inside the cavity volume and the magnetic current density $\mathbf{J}_m$ are related by Maxwell's equation

$$\nabla \times \nabla \times \mathbf{H} - k^2 \mathbf{H} = -j\omega\mu_0 \mathbf{J}_m . \tag{6.2.19}$$

For a thin substrate the magnetic fields H_x, H_y ,which only have x and y components, given by [17]

$$H_x = \sum_{m=0}^{\infty}\sum_{n=0}^{\infty} A_{mn} B_{x,mn} k_n \cos(k_m x)\sin(k_n y) \tag{6.2.20}$$

and,

$$H_y = \sum_{n=0}^{\infty}\sum_{n=0}^{\infty} A_{mn} B_{y,mn} k_m \sin(k_m x)\cos(k_n y). \tag{6.2.21}$$

where,

$$B_{x,mn} = \frac{-j\omega\varepsilon . A_{mn} V_{0x}}{d_a k_n \cdot (k^2 - k_{mn}^2)} \cdot \frac{4\sin c\left(k_n \frac{W_a}{2}\right)\sin\left(\frac{n\pi}{2}\right)\cos\left(\frac{m\pi}{2}\right)}{\sin\left(k_a \frac{L_a}{2}\right)} \cdot \frac{k_a\left[\cos\left(k_m \frac{L_a}{2}\right) - \cos\left(k_a \frac{L_a}{2}\right)\right]}{k_a^2 - k_m^2} \tag{6.2.22}$$

$$B_{y,mn} = \frac{-j\omega\varepsilon . A_{mn} V_{0y}}{d_a k_m \cdot (k^2 - k_{mn}^2)} \cdot \frac{4\sin c\left(k_m \frac{W_a}{2}\right)\sin\left(\frac{m\pi}{2}\right)\cos\left(\frac{n\pi}{2}\right)}{\sin\left(k_a \frac{L_a}{2}\right)} \cdot \frac{k_a\left[\cos\left(k_n \frac{L_a}{2}\right) - \cos\left(k_a \frac{L_a}{2}\right)\right]}{k_a^2 - k_n^2} \tag{6.2.23}$$

$$A_{mn} = \sqrt{\frac{\chi_m \chi_n}{ab}}, \qquad \text{where} \qquad \chi_p = \begin{cases} 1 & \text{if } p=0 \\ 2 & \text{if } p\neq 0 \end{cases}$$

and

$$k_m = \frac{m.\pi}{a}, \qquad k_n = \frac{n.\pi}{b}. \tag{6.2.24}$$

The electric field $\mathbf{E}_z$ can be determined from the Maxwell equation [17]

$$E_{z(x,y)} = \frac{1}{j\omega\varepsilon}\sum_{n=0}^{\infty}\sum_{n=0}^{\infty} A_{mn} C_{mn} \cos(k_m x)\cos(k_n y) \tag{6.2.25}$$

where,

$$C_{mn} = B_{x,mn}\, k_m^2 - B_{y,mn}\, k_n^2. \tag{6.2.26}$$

Hence, the electromagnetic fields in the cavity are now known and defined by equations 6.2.21, 6.2.22, and 6.2.25 .

The losses in the cavity can also be taken into account by replacing k by an effective wave number as given by [58]

$$k_{eff}^2 = k_0^2 \varepsilon_r \left(1 - j\delta_{eff}\right) \tag{6.2.27}$$

where $\delta_{eff} = 1/Q$ is the effective loss tangent which includes the radiation, copper, and dielectric losses. The value of δ_{eff} is given by [59]

$$\delta_{eff} = \delta + \frac{\Delta}{d_a} + \frac{d_a A \pi^4}{\omega_r \varepsilon_0 \varepsilon_{ra} s^2} \cdot \frac{1}{11520} \cdot \left[(1-B)\left(1 - \frac{A}{15} + \frac{A^2}{420}\right) + \frac{B^2}{5}\left(2 - \frac{A}{7} + \frac{A^2}{189}\right)\right] \tag{6.2.28}$$

where, δ is the loss tangent of the substrate, Δ is the skin depth and

$$s = \frac{a+b}{2}, \qquad A = \left(\frac{2s}{\lambda_0}\right)^2, \qquad B = \left(\frac{\pi \cdot s}{\lambda_0}\right), \qquad \omega_r = \frac{c}{2(s + 2\Delta l)\sqrt{\varepsilon_{el}}}$$

where

$$\varepsilon_{el} = \frac{1}{2}\left[\varepsilon_{ra} + 1 + (\varepsilon_{ra} - 1)\left(1 + \frac{12 d_a}{s}\right)^{\frac{-1}{2}}\right] \tag{6.2.29}$$

and,

$$\Delta l = \frac{d_a}{2.\pi} \cdot \frac{\frac{s}{d_a} + 0.366}{\frac{s}{d_a} + 0.556} \cdot \left[0.28 + \frac{\varepsilon_{ra} + 1}{\varepsilon_{ra}}\left(0.264 + \log\left(\frac{s}{d_a} + 0.366\right)\right)\right] \tag{6.2.30}$$

As the values of a and b are close to each other it is assumed that the value δ_{eff} is the same for wave propagation in the x and y directions.

6.2.3. Derivation of the Matching Objective Function

The admittances of the patch due to the two orthogonal apertures can be evaluated using the energy conservation theorem and are given by [20]

$$Y_{x,ant} = \frac{\iiint_V H_x J_{mx}^* dv}{\left|V_{0x}\right|^2}, \quad \text{and,} \quad Y_{y,ant} = \frac{\iiint_V H_y J_{my}^* dv}{\left|V_{0y}\right|^2} \tag{6.2.31}$$

Substituting the expression for the magnetic field from equations. 6.2.21, and 6.2.22 and the magnetic current density from equations 6.2.15 and 6.2.16, and performing the integration, the following analytic formulas are obtained for the admittance values of the antenna at the apertures [17]

$$Y_{x,ant} = \sum_{m=0}^{\infty}\sum_{n=0}^{\infty} \frac{16 \cdot j\omega\varepsilon \cdot A_{mn}^2}{d_a\left[\omega^2 - \omega_{mn}^2\right]\left(1 + j\delta_{eff}\frac{\omega^2}{\omega_{mn}^2}\right)} \left\{ \frac{\operatorname{sinc}\left(k_n \frac{W_a}{2}\right)\sin\left(\frac{n\pi}{2}\right)\cos\left(\frac{m\pi}{2}\right)}{\sin\left(k_a \frac{L_a}{2}\right)} \cdot \frac{k_a\left[\cos\left(k_m \frac{L_a}{2}\right) - \cos\left(k_a \frac{L_a}{2}\right)\right]}{k_a^2 - k_m^2} \right\}^2 \tag{6.2.32}$$

$$Y_{y,ant} = \sum_{n=0}^{\infty}\sum_{n=0}^{\infty} \frac{16 \cdot j\omega\varepsilon \cdot A_{mn}^2}{d_a\left[\omega^2 - \omega_{mn}^2\right]\left(1 + j\delta_{eff}\frac{\omega^2}{\omega_{mn}^2}\right)} \left\{ \frac{\operatorname{sinc}\left(k_m \frac{W_a}{2}\right)\sin\left(\frac{m\pi}{2}\right)\cos\left(\frac{n\pi}{2}\right)}{\sin\left(k_a \frac{L_a}{2}\right)} \cdot \frac{k_a\left[\cos\left(k_n \frac{L_a}{2}\right) - \cos\left(k_a \frac{L_a}{2}\right)\right]}{k_a^2 - k_n^2} \right\}^2 \tag{6.2.33}$$

Each term in the above two infinite series corresponds to one of the parallel connected RLC circuits as shown in Figure 6.2.1b. The equivalent circuits of the patch admittance, as seen by the slot parallel to the y axis, have the following circuit elements [17]:

$$L_{x,mn} = \frac{d_a}{16\varepsilon c^2 A_{mn}^2} \cdot \left\{ \frac{\operatorname{sinc}\left(k_n \frac{W_a}{2}\right) \sin\left(\frac{n\pi}{2}\right) \cos\left(\frac{m\pi}{2}\right)}{\sin\left(k_a \frac{L_a}{2}\right)} \cdot \frac{k_a\left[\cos\left(k_m \frac{L_a}{2}\right) - \cos\left(k_a \frac{L_a}{2}\right)\right]}{k_a^2 - k_m^2} \right\}^{-2} \quad (6.2.34)$$

$$C_{x,mn} = L_{x,mn}^{-1} \frac{\varepsilon_{ra} k_{mn}^2}{c^2}$$

$$R_{x,mn} = L_{x,mn} k_{mn} c \delta_{eff}$$

Similarly, the equivalent circuits of the patch, as seen by the slot parallel to the x axis, have circuit elements:

$$L_{y,mn} = \frac{d_a}{16\varepsilon c^2 A_{mn}^2} \cdot \left\{ \frac{\operatorname{sinc}\left(k_m \frac{W_a}{2}\right) \sin\left(\frac{m\pi}{2}\right) \cos\left(\frac{n\pi}{2}\right)}{\sin\left(k_a \frac{L_a}{2}\right)} \cdot \frac{k_a\left[\cos\left(k_n \frac{L_a}{2}\right) - \cos\left(k_a \frac{L_a}{2}\right)\right]}{k_a^2 - k_n^2} \right\}^{-2} \quad (6.2.35)$$

$$C_{y,mn} = L_{y,mn}^{-1} \frac{\varepsilon_{ra} k_{mn}^2}{c^2},$$

$$R_{y,mn} = L_{y,mn} k_{mn} c \delta_{eff}$$

Finally, combining the two patch admittances with the feed impedance gives the input impedance of the antenna structure [17]

$$Z_{in} = \frac{n^2}{Y_{x,ant} + Y_{ap}} + \frac{n^2}{Y_{y,ant} + Y_{ap}} - jZ_f \cot\left(k_f L_{os}\right) \quad (6.2.36)$$

The above is then used in the matching objective function.

6.2.4 Derivation of the Axial Ratio Objective Function

For the calculation of the axial ratio the far field components of the antenna are first determined in the boresight. This is obtained by replacing the electric field at the edges of the patch by equivalent magnetic currents as given by [21]

$$\mathbf{M} = 2d_a E_{z(x,y)}(\mathbf{z} \times \mathbf{n}) \tag{6.2.37}$$

where $\mathbf{n}$ is the outward normal unit vector to the magnetic wall at the edges of the patch.

The electric field components radiated by the patch along the edges of the patch are given by [17]

$$E_x = \frac{d_a k_0 e^{-jk_0 r}}{4\pi\omega\varepsilon r} \cdot \sum_{m=0}^{\infty} A_{m0} B_{y,m0} \tag{6.2.38}$$

$$E_y = \frac{d_a k_0 e^{-jk_0 r}}{4\pi\omega\varepsilon r} \cdot \sum_{n=0}^{\infty} A_{0n} B_{x,0n} \tag{6.2.39}$$

The expressions for $B_{x,0n}$ and $B_{y,m0}$ can be written in the following form:

$$B_{x,0n} = V_{0x} \cdot B'_{x,0n} \tag{6.2.40}$$

$$B_{y,m0} = V_{oy} \cdot B'_{y,m0} \tag{6.2.41}$$

where

$$B'_{x,0n} = \frac{j\omega\varepsilon . A_{0n}}{d_a k_n \cdot (k^2 - k_n^2)} \cdot \frac{4\text{sinc}\left(k_n \frac{W_a}{2}\right)\sin\left(\frac{n\pi}{2}\right)}{\sin\left(k_a \frac{L_a}{2}\right)} \cdot \frac{k_a\left[1 - \cos\left(k_a \frac{L_a}{2}\right)\right]}{k_a^2} \tag{6.2.42}$$

$$B'_{y,m0} = \frac{j\omega\varepsilon . A_{0n}}{d_a k_n \cdot (k^2 - k_m^2)} \cdot \frac{4\text{sinc}\left(k_m \frac{W_a}{2}\right)\sin\left(\frac{m\pi}{2}\right)}{\sin\left(k_a \frac{L_a}{2}\right)} \cdot \frac{k_a\left[1 - \cos\left(k_a \frac{L_a}{2}\right)\right]}{k_a^2} \tag{6.2.43}$$

From the equivalent circuit, the voltages V_{0x} and V_{oy} can be expressed as [17].

$$V_{0x} = V_0 \cdot \frac{(Y_{x,ant} + Y_{ap})^{-1}}{(Y_{x,ant} + Y_{ap})^{-1} + (Y_{y,ant} + Y_{ap})^{-1}} \tag{6.2.44}$$

$$V_{0y} = V_0 \cdot \frac{\left(Y_{y,ant} + Y_{ap}\right)^{-1}}{\left(Y_{x,ant} + Y_{ap}\right)^{-1} + \left(Y_{y,ant} + Y_{ap}\right)^{-1}} \tag{6.2.45}$$

Substituting these results into the expressions for the electric field components in the boresight gives the computational formulas for the field components E_x and E_y:

$$E_x = \frac{V_0 d_a k_0 e^{-jk_0 r}}{2\pi\omega\varepsilon r} \cdot \frac{\left(Y_{x,ant} + Y_{ap}\right)^{-1}}{\left(Y_{x,ant} + Y_{ap}\right)^{-1} + \left(Y_{y,ant} + Y_{ap}\right)^{-1}} \cdot \sum_{m=0}^{\infty} A_{m0} B'_{y,m0} \tag{6.2.46}$$

and

$$E_y = \frac{V_0 d_a k_0 e^{-jk_0 r}}{2\pi\omega\varepsilon r} \cdot \frac{\left(Y_{y,ant} + Y_{ap}\right)^{-1}}{\left(Y_{x,ant} + Y_{ap}\right)^{-1} + \left(Y_{y,ant} + Y_{ap}\right)^{-1}} \cdot \sum_{n=0}^{\infty} A_{0n} B'_{x,0n} \tag{6.2.47}$$

The amplitude error (A_e) and phase error (θ_e) required for the calculation of the axial ratio can be expressed as [17]

$$A_e = \frac{|E_x|}{|E_y|} = \frac{|Y_{y,ant} + Y_{ap}|}{|Y_{x,ant} + Y_{ap}|} \cdot \frac{\left|\sum_{m=0}^{\infty} A_{m0} B'_{y,m0}\right|}{\left|\sum_{n=0}^{\infty} A_{0n} B'_{x,0n}\right|} \tag{6.2.48}$$

and,

$$\theta_e = \angle\left(\frac{E_x}{E_y}\right) = \angle\left(\frac{Y_{y,ant} + Y_{ap}}{Y_{x,ant} + Y_{ap}} \cdot \frac{\sum_{m=0}^{\infty} A_{m0} B'_{y,m0}}{\sum_{n=0}^{\infty} A_{0n} B'_{x,0n}}\right). \tag{6.2.49}$$

Finally, the value of axial ratio is calculated by equation 2.5.1.5

equations.6.2.48 and 6.2.49 based on the resonant cavity model, enable the axial ratio at a given frequency to be determined in term of the design parameters.

The above results for impedance matching, and axial ratio (circular polarisation) have been used in the multi-objective GA method presented in section 6.2.5.

6.2.5 Application of Genetic Algorithms Using the Cavity Model.

As can be seen from the equations (6.2.36), (6.2.48), and (6.3.49), the objective functions are characterised by four geometrical variables, the patch dimensions, a and b, the slot dimensions L_a, and W_a, and the open stub length L_{os}. For each of the two substrates used the thicknesses d_a, and d_f.are fixed. The slot width, W_a(2 mm) ensures that the electric field is uniform across the slot width. This leaves the optimisation algorithm with four control variables, the dimensions of the patch, length of the slot, and, the length of the open stub. Interval constraints on the design parameters are applied. The dimensions of the nearly square patch element have to be less than half the modal field's wave lengths in the orthogonal directions. Accordingly, the length of the equal slots has been set at less than the min (a,b).and greater than $\sqrt{2}D + Wa$, where D is the effective width of the microstrip feed line. The length of the open stub, connected to the feed line, is geometrically confined between $W_a/\sqrt{2}$ and $1/2\sqrt{a^2+b^2}$.

The optimisation procedure involves two objective functions so a non-dominating sorting multi-objective optimisation approach as described in chapter five is applied.

The slot structure is much more complex than the dual-feed structure described in Chapter five. More computations are required and the population size is increased to 200 trial solutions per iteration, with

the number of possible iterations increased to 1000. Also the mutation rate is increased from 0.01 to 0.05 to improve the sampling diversity. The crossover rate implemented was 0.80 (%80) with a uniform crossover operator in order to create more new possible solutions for examination., and the roulette wheel selection method was used.

6.2.6 Results and Discussion

In this section practical, calculated and simulated results for the cavity model, are presented. The input impedance, reflection coefficient, and axial ratio have been calculated, simulated, and, measured over a range of frequency between 2.2 GHz and 2.6 GHz.

The practical measurements are carried out using a Wiltron 360 Network Analyser. A full-wave simulation package, Ensemble 5.1^{TM} was used to obtain the simulated results.

Three sets of optimised solutions for the cavity model are presented in Table 6.2.1.

	a mm	B mm	$L_a$mm	L_{os}mm	Zin Ω	IARI dB
1	30.9	33.9	21.2	14.3	55.3+0.92i	0.41
2	31.2	33.9	20.2	12.5	53.3+0.69i	0.31
3	33.9	30.9	21.3	12.5	49.2+1.3i	0.89

Table 6.2.1 Three sets of optimised solutions for the cavity model.

Practical, simulated, and calculated results of the input impedance are shown in Figures (6.2.6). It can be seen that the cavity model can predict the input impedance of the cross-aperture-coupled microstrip patch antenna with good accuracy. The model gives an impedance loci with the double resonant loop corresponding to the two orthogonal modes at the resonant frequency. Good agreement is obtained over the complete frequency range specified. The important part of the impedance response is between the resonant frequencies of the TM_{10} and TM_{01} modes, and the optimum value is located at the cusp in the impedance locus. The practical measurement gave a resonant frequency within 1.5 % of the calculated results.

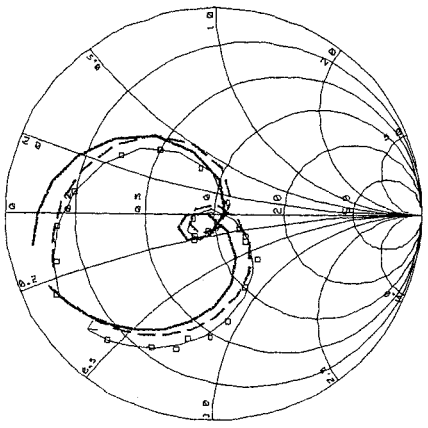

Figure 6.2.6. Input impedance for the cavity model

□—□—□ Simulated, _ _ _ _ _ Practical, _____ Calculated

The radiating power measurement, which is characterised by the reflection coefficient measurement is shown in Figure 6.2.7. It can be seen that for the practical, simulated, and calculated results that a reflection coefficient of less than –35 dB has been achieved. Good agreement between the practical, simulated, and calculated results is observed.

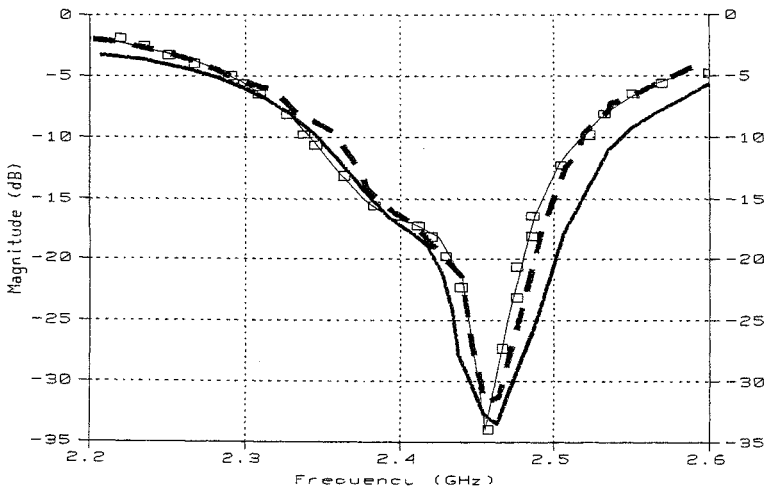

Figure 6.2.7. Reflection Coefficient for the cavity model

□—□—□ Simulated, _ _ _ _ _ Practical, _____ Calculated

Figure 6.2.8 shows the calculated axial ratio, the measured axial ratio, and the axial ratio using full-wave simulation. The agreement is good and the prediction of the frequency for the optimum axial ratio is accurate to about 1%.

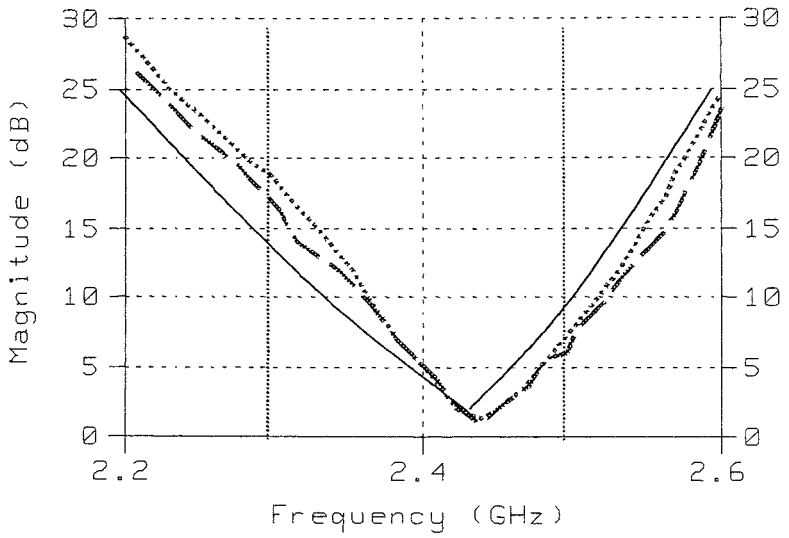

Figure 6.2.8 Axial Ratio for the cavity model

——— Simulated; - - - - Practical , ····· Calculated.

6.3 Transmission Line Model of Cross-Aperture-Coupled Circular Polarised Patch Antenna.

In this section the circular polarised antenna fed through a cross-aperture in a ground plane by means of a microstrip feed line is modelled using the transmission line model. The field linkages from the feed to slots, and slots to antenna are modelled as voltage transformers, which are employed in the synthesis of the overall transmission line model of the structure. The equivalent circuit shown in Figure 6.3.1 is used to obtain the required formulas for the input impedance and axial ratio objective functions. The matching objective function is obtained in section 6.3.1. and in section 6.3.2 the axial ratio objective function is established. The GA application to the antenna design and the results are given in sections 6.3.3, 6.3.4.

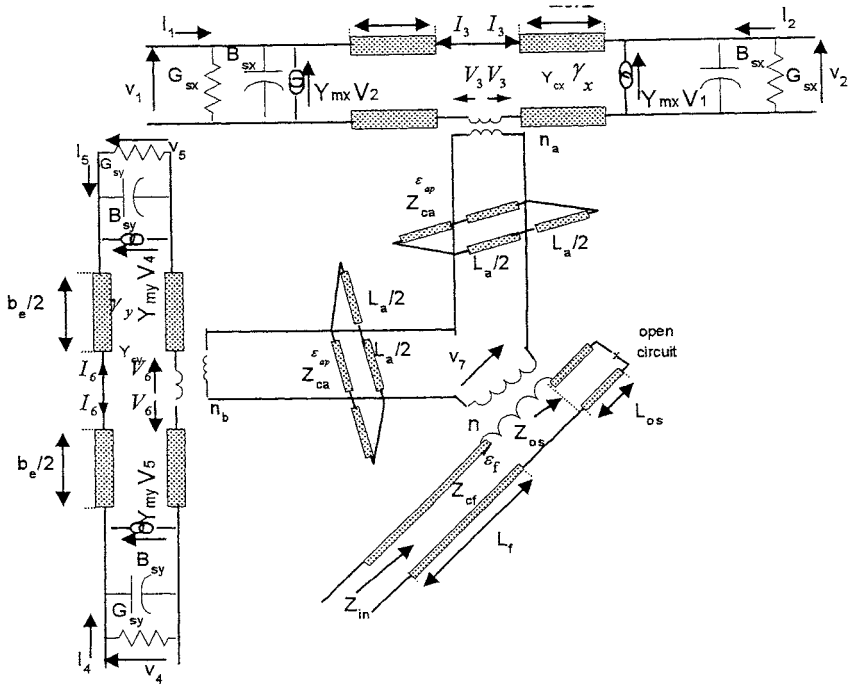

Figure 6.3.1 Equivalent circuit model of the structure shown in Figure. 6.2.1.

6.3.1 The Matching objective function

The operation of the circularly polarised patch antenna shown in Figure.6.2.1 is based on the two orthogonal apertures fields exciting the patch independently in the x and y directions. The admittance of the patch for the x direction is given by [16],

$$Y_{PX} = 1 - \frac{Y_{cx}}{\sinh\left(\gamma_x \frac{a_e}{2}\right)\cosh\left(\gamma_x \frac{a_e}{2}\right)\left[Y_{sx} + Y_{cx}\coth(\gamma_x a_e) + Y_{mx} + \frac{Y_{cx}}{\sinh(\gamma_x a_e)}\right]}. \quad (6.3.1)$$

where Z_{cx} and γ_x are the characteristic impedance and the propagation constant respectively in the x-direction (Figure 6.3.1)

Following a similar procedure, the admittance, Y_{py}, for the excitation of the patch in the y direction (see Figure. 6.3.1) is given by

$$Y_{Py} = 1 - \frac{Y_{cy}}{\sinh\left(\gamma_y \frac{b_e}{2}\right)\cosh\left(\gamma_y \frac{b_e}{2}\right)\left[Y_{sy} + Y_{cy}\coth(\gamma y b_e) + Y_{my} + \frac{Y_{cy}}{\sinh(\gamma_y b_e)}\right]} \tag{6.3.2}$$

where Z_{cy} and γ_y are the characteristic impedance and the propagation constant respectively.

The individual self-admittances (Y_{ap}) of the two orthogonal slots is determined by considering them as short circuited slot lines [50] so that

$$Y_{ap} = -\frac{2j}{Z_{ca}} \cdot \cot\left(k_a \frac{L_a}{2}\right). \tag{6.3.3}$$

The values of the total admittance for the two apertures are then

$$Y_{ta} = n_a^2 Y_{PX} + Y_{ap} \quad \text{and} \quad Y_{tb} = n_b^2 Y_{PY} + Y_{ap} \tag{6.3.4}$$

where, n_a and n_b are the turns ratios of the patch-to-slot impedance transformers which are obtained by assuming that, due to the size of the antenna, there is a uniform current distribution in the ground plane under the patch. The turns ratios are then the ratios of the fraction of the current flowing on the slots over the total current in the patch [54], and are given by

$$n_a = \frac{L_a}{a}, \text{ and, } n_b = \frac{L_a}{b}. \tag{6.3.5}$$

Since it has been established that the cross-slot can be regarded as two orthogonal slots in series connection, the input impedance of the circular

polarisation antenna on the microstrip feed line under the centre of the aperture is given by [16]

$$Z_{in} = n^2 \cdot \left(\frac{1}{Y_{ta}} + \frac{1}{Y_{tb}} \right) - jZ_{cf} \cdot \cot\left(k_f L_{os}\right) \tag{6.3.6}$$

where Z_{cf} is the characteristic impedance of the microstrip feed line, k_f is the wave number of the microstrip feed line, and, n is the turns ratio of the slot line-to-microstrip transition given by [50].

The above expression for Z_{in} is used in the matching objective function.

6.3.2 Derivation of the Axial Ratio Objective Function

The phase and amplitude formulas required to evaluate the axial ratio objective function are derived based on the equivalent circuit shown in Figure 6.3.1. The axial ratio objective function is given by equation (2.5.22) [20] where A_e, and ϕ_e, the amplitude and the phase, are obtained in terms of the voltages V_2, V_5 of two orthogonal radiating edges, and the voltages V_3, V_6 in the centres of the two orthogonal apertures and also the feed line voltage V_7. The voltages V_3, V_6 are given by [16]

$$V_3 = V_7 \frac{Y_{tb}}{Y_{ta} + Y_{tb}} \qquad \text{and} \qquad V_6 = V_7 \cdot \frac{Y_{ta}}{Y_{ta} + Y_{tb}} \tag{6.3.7}$$

where Y_{ta} and Y_{tb} are given by equation 6.3.7 The voltages V_2 and V_5 can be determined using the transmission line theory:

$$V_2 = \frac{V_3}{2} \cdot \frac{1}{\cosh\left(\gamma_{cx}\frac{a_e}{2}\right) + \frac{Y_{sx}}{Y_{cx}}\sinh\left(\gamma_x \frac{a_e}{2}\right)} \tag{6.3.8}$$

and

$$V_5 = \frac{V_6}{2} \cdot \frac{1}{\cosh\left(\gamma_{cx}\frac{b_e}{2}\right) + \frac{Y_{sx}}{Y_{cy}}\sinh\left(\gamma_y \frac{b_e}{2}\right)}. \tag{6.3.9}$$

As the radiated electric field is generated by the voltage on the edges of the patch the phase difference between the x and y components of the electricl field in the boresight direction (phase error, θ_e) is the same as the phase difference between V_2 and V_5, namely

$$\theta_e = \arg(V_5) - \arg(V_2). \tag{6.3.10}$$

The x and y directed electric field components in the far field are directly proportional to the voltages V_2 and V_5 respectively, therefore the amplitude A_e is given by: [16]

$$A_e = \frac{|V_5|}{|V_2|}. \tag{6.3.11}$$

The above expression for A_e and θ_e applied to the AR formula (2.5.22) then gives the required AR objective functions in terms of the antenna design parameters

The GA used in section 6.2.5 then is applied to this model

6.3.3 Results and Discussion

In this section practical, calculated and simulated results for the transmission line model, are presented. The input impedance, reflection coefficient, and axial ratio of the antennas have all been calculated, simulated and measured over the range of frequency between 2.2 GHz and 2.6 GHz.

The practical measurements are carried out using a Wiltron 360 Network Analyser. A full-wave simulation package, Ensemble 5.1^{TM} was used to obtain the simulated results.

Three sets of optimised solutions are presented in Table 6.3.1.

	a mm	b mm	L_a mm	L_{os} mm	Zin- Ω	IARI dB
1	31.3	34	21	12.6	50.9+0.15i	0.605
2	30.9	33.8	21.2	12.4	53+0.49i	0.255
3	31.1	34	21.4	13.9	51.3+6.6i	0.74

Table 6.3.1 Three sets of optimised solutions for the transmission line model.

Comparing Table 6.2.1 and 6.3.1 it can be seen that there is a good agreement between the cavity and transmission line models. Consequently the transmission line model which is conceptually simpler in engineering terms is perfectly adequate in engineering design work.

Practical, simulated, and calculated results of the input impedance are shown in Figure 6.3.2. It can be seen that the transmission line model can predict the input impedance of the cross-aperture-coupled microstrip patch antenna with good accuracy. The model gives impedance loci with the double resonant loop corresponding to the two orthogonal modes at the resonant frequency. This is typical for circular polarised antenna and demonstrates good circular polarisation. Good agreement is obtained over the complete frequency range specified. The important part of the impedance response is between the resonant frequencies of the TM_{10} and TM_{01} modes, and the optimum value is located at the cusp in the impedance locus. The practical measurement gave a resonant frequency within 2% of the calculated results.

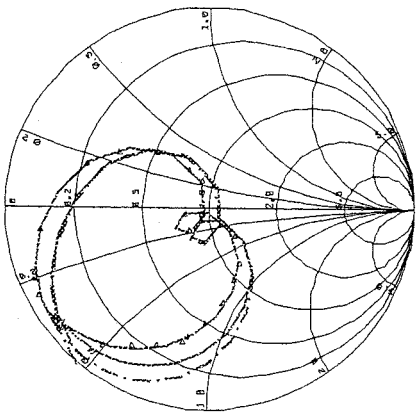

Figure 6.3.2. Input impedance for the transmission line model

—Δ— Simulated, _ _ _ _ _ Practical, _____ Calculated

The radiating power measurement, which is characterised by the reflection coefficient measurement, is shown in Figure 6.3.3. It can be seen that for the practical, simulated, and calculated results that a reflection coefficient of less than –33dB has been achieved. Good agreement between the practical, simulated, and calculated results is observed.

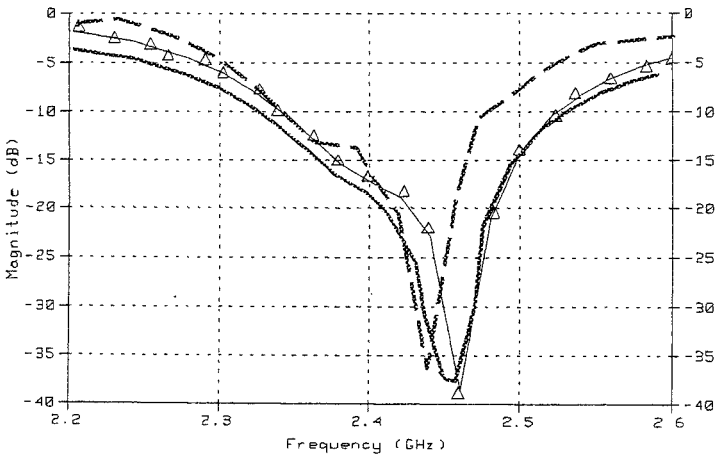

Figure 6.3.3. Reflection coefficient for the Transmission line

—△— Simulated, _ _ _ _ _ Practical, _____Calculated

The axial ratio is shown in Figure 6.3.4. This Figure shows the calculated axial ratio ,the measured axial ratio, and, the axial ratio using full-wave simulation. The agreement is generally good and the prediction of the frequency for the optimum axial ratio is accurate to about 1.5%

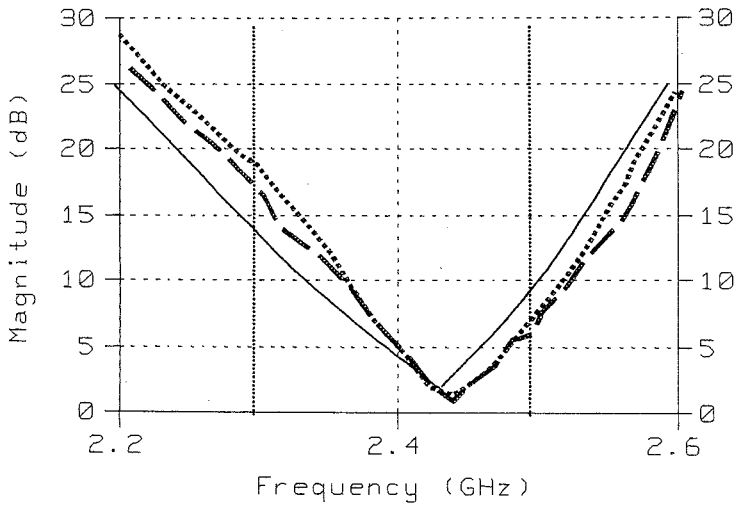

Figure.6.3.4 Axial Ratio for the transmission line model

———— Simulated, ... Practical , _ _ _ _ Calculated.

The axial ratio is shown in Figure 6.3.4. This Figure shows the calculated axial ratio ,the measured axial ratio, and, the axial ratio using full-wave simulation. The agreement is generally good and the prediction of the frequency for the optimum axial ratio is accurate to about 1.5%

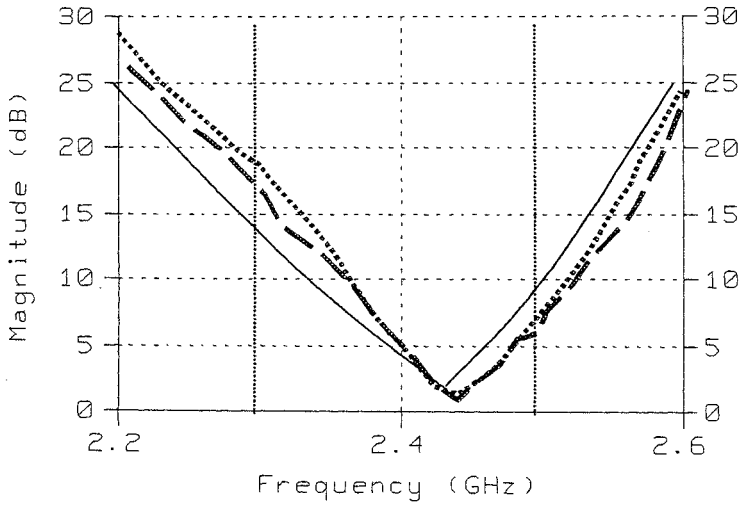

Figure.6.3.4 Axial Ratio for the transmission line model

———— Simulated, ... Practical , _ _ _ _Calculated.

6.4 Summary

The advantages of the slot fed patch antenna structure have been discussed along with two modelling approaches used to obtain the GAs objective functions.

Using the cavity model the feed-to-slot-to patch antenna connections used equivalent magnetic current sources in the slots from which the electrical field on the patch was obtained using the energy conservation theorem. Expressions for the antenna patch admittances were obtained using the equivalent circuit. Expressions for all the elements in the axial ratio and the matching objective functions were then known. The GA optimisation was used to obtain numerical results for the antenna design parameters and good agreement with both simulated (Ensemble™), and practical measurement was obtained.

Using the transmission line model the field equations connecting the feed-to-slot-to-antenna patch have been used to obtain an equivalent circuit of the operational mechanism of the antenna. From the equivalent circuit analysis, expressions were obtained for the matching and the axial ratio objective functions. These objective functions were used in the GAs optimisation to obtain solutions for the antenna design parameters. The numerical results obtained were compared with simulated (Ensemble™), and practical measurements and good agreement obtained.

There is no great difference between the results from using the transmission line model or the more complex cavity model. Therefore the simpler transmission line model turns out to be quite suitable for calculating the design parameters.

Chapter Seven

Summary of the Thesis and Further Work

7.1 Summary and Conclusion

This thesis presents the results of the research, which has been carried out in the investigation of the modelling and design optimisation for circularly polarised microstrip patch antennas and patch arrays. In this research the relatively new global GA optimisation approach has been developed and applied successfully to various type of microstrip patch antenna and patch array structures. The main objectives of the designs were to match the input impedance with 50Ω source impedance, and to achieve a good axial ratio condition for circular polarisation. A multi-objective GA optimisation approach has been developed and implemented to the design of circular polarisation microstrip patch antennas and antenna arrays.

In chapter two the basic microstrip patch antenna concepts and operational mechanism are briefly described. The main feed configurations of the microstrip patch antenna are presented. Principles of propagation for a circular polarisation wave have been introduced. Main methods for the generation of circular polarisation are presented. Full wave analysis for the antenna is briefly discussed. The cavity model and the transmission line model which give a good physical insight with good understanding of the operating mechanism of the antenna have been presented. A general introduction to planar microstrip patch antenna arrays has been introduced.

In chapter three the GA, which is a relatively new global stochastic optimisation approach, has been outlined and the advantages of this approach are discussed. The crossover, mutation and selection operators, and elements of the genetic algorithm procedure are given and explained in detail. An outline of the non-dominating sorting multi-objective genetic algorithms has been given. A step by step illustration of a GA implementation has been introduced to give a good general idea of the role of the GA operators. The objective function used in the illustration has one global maximum point and also many local maximum points.

Chapter four presents the first application of GA to the antenna design of a single offset feed circularly polarised microstrip patch antenna. The design procedure involves two objective functions and five design parameters. A sensitivity analysis has been carried out by altering the values of the control parameters in order to demonstrate the robustness of this approach. A very good agreement between the calculated, simulated and the practical results has been obtained.

In chapter five the GA has been applied to the design of a dual-feed circularly polarised square microstrip patch antenna. In this design spurious radiation from step discontinuities are eliminated and the manufacturing

tolerance is increased. This application involves a higher dimensional problem and more constraints. A non-dominating sorting genetic algorithm optimisation has been developed and applied successfully to the design of a dual-feed circularly polarised microstrip patch antenna operating at 5.8 GHz with input impedance matching to a 50Ω source impedance. In the resulting design the overall area of the combined patch antenna with the feed network is reduced by about 32%. Good agreement between the calculated, simulated and the measured results are obtained. This approach is further developed to the design of a 2x2 sequentially rotated patch array using a dual-feed circularly polarised microstrip patch antenna for each of the radiating elements in the array. This antenna design results in an even higher dimensional problem than that of the dual-feed single square patch antenna and has additional constraints. The application of the GA approach resulted in improved impedance matching, a better axial ratio, and a wider VWSR bandwidth. The comparisons between the calculated, simulated and measured results confirmed the validity and integrity of the design approach.

Chapter six introduces the analyses and modelling of a cross-aperture-coupled circular polarised microstrip patch antenna. The cavity model and the transmission-line modelling of this structure are presented. In both cases the modelling analysis is extensive and many functions and their evaluation are

involved. Nevertheless, the GA optimisation approach developed was implemented successfully for both methods. The optimisation method is based on a multiobjective nondominating sorting genetic algorithms. Calculated, simulated and practical results are in good agreement. It is been established that there is no great difference between the results from using the transmission line model or the more complex cavity model. Therefore the simpler transmission line model turns out to be quite suitable for calculating the design parameters.

It has been established that a novel approach based on the applications of the GA optimisation approach can be applied successfully to the design of various types of circularly polarised microstrip patch antennas with matching to the input impedance source of 50Ω. This shows that the GAs optimisation approach is extremely useful for the design of multi-parameter antenna designs.

7.2 Suggestions for Further Work

In this section a number of suggestions and recommendations for further research and work on the material presented in this thesis are outlined.

The power of the GA approach can be used to increase the number of the objective functions in the design analysis. In addition to the impedance

matching and axial ratio objective functions, objective functions for the bandwidth and/or directivity may also be included in the design.

The dual-feed antenna element in the 2x2 patch array can be replaced by, for example, the offset feed nearly square patch (chapter four), or by a corner deleted square patch antenna

The above structure with an aperture-coupled slot design can be investigated.

Larger sequentially rotated patch arrays, which include the sequentially rotated 2x2 dual-feed square patch array as a sub-array in the structure can also be investigated. More conditions and system specifications can be added to the investigation, such as the power divided system for each 2x2 sub-array, so that a required loop pattern can be realised. That is if the structure needs the outer sub-arrays to receive more power than the inner ones, or vice versa. The latter investigation can be extended to the offset feed nearly square circularly polarised patch element and to the cross-slot aperture coupled circularly polarised patch elements.

Other patch antenna geometries and antenna array structures can be investigated, such as the triangular antenna, and the circular antenna.

The rapid development and powerful implementations of genetic algorithms to the design and modelling of antenna structures opens a promising avenue to further development in antenna design structures without relying on trial and error approaches.

References

1. Dechamps, G. A., 'Microstrip Microwave Antennas' 1953, 3ed USAF Symposium on Antennas.

2. Gutton, H. and G. Baissinot, 'Flat Aerial for Ultra High Frequencies' ,1955, French patent No. 703 113.

3. Howell, J. W, 'Microstrip Antennas' IEEE Transactions on antennas and propagation, 1975 Vol. AP-25, No. 1, pp 90-93.

4. Derneryd, A. G., 'Linear Polarised Microstrip Antennas' IEEE Transaction Antenna & propagation V. 25 1975,

5. Derneryd, A.G. and Lind, A.G, 'Cavity Model of the Rectangular Microstrip Antenna' Proceeding of workshop on printed circuit antenna technology, 1979, 17-19 Oct New Mexico State University.

6. Lo, Y. T., D. Solomon, and W. F. Richards 'Theory and Experiments on Microstrip Antennas', IEEE Transactions on Antennas and Propagation, 1979 Vol. AP-27, No. 2 pp 137-145.

7. Munson, R .E. 'Conformal Microstrip Antennas and Microstrip Phased Arrays', IEEE Transactions on Antennas and Propagation, Jan 1974, 22, p.74-78.

8. Richards W. F., Lo, Y. T., Harrison, D. D., 'An Improved Theory for Microstrip Antennas and Applications' IEEE Transactions Antennas and Propagation, Jan. 1981, Vol. Ap-29, pp 38-46.

9. Richards, W. F., 'Antenna Handbook: Theory', Application and Design, 1988, Chap. 10, Van Nostrand Reinhold Co.

10. Davis, L. 'Handbook of Genetic Algorithms', New York, 1991.

11. Gill, P. E, Murray, W., and Wrigtht, H.M, 'Practical Optimisation', Academic Press 1981, London.

12. Steuer, R. E., 'Multiple Criteria Optimization: Theory, Computation, and Application' , John Wiley 1986, Canada.

13. Michalewicz, Z, 'Genetic Algorithms + data Structure = Evolution Programs', Springer-Verlag, 1992.

14. Aljibouri B., E. G. Lim, H. Evans and A. Sambell, 'Multi-objective Genetic Algorithm Approach for a Dual-Feed Circular Polarised Patch Antenna Design', Electronics Letters, 8th June 2000, Vol. 36, No. 12, pp 1005-1006.

15. Evans, H, Gale P., Aljibouri, B, Lim E. G., Korolkiewicz E., and Sambell, A, 'Application of Simulated Annealing to Design of Serial Feed Sequentially Rotated 2x2 Array' Electronics Letters, 25th November 2000, Vol. 36, No. 24., pp 1987-1988.

16. Aljibouri, B., Vlasits T., Korolkiewicz, ,E., Scott S. and Sambell, A, 'Transmission Line Modelling of the Cross-Aperture-Coupled Circular Polarised Microstrip Antenna' IEE Proceedings Microwaves, Antennas and Propagation April 2000, Vol. 147, No. 2, pp 82-86.

17. Aljibouri, B., Lim E. G., Evans H., Vlasits T., Korolkiewicz E. and Sambell, A, 'Cavity Model of Cross-Slot-Coupled Circularly Polarised Microstrip Patch Antenna' IEE Proceedings Microwaves, Antennas and Propagation, June 2001, Vol. 148, No. 3,.pp.147-152.

18. Pozar, D. M, 'Microwave Engineering' John Wiley & sons 1998, Chapter 8 pp 422-496 New York.

19. Pozar, D. M, 'Microstrip Antennas' Proceedings of the IEEE, 1992,. Vol. 80, No. 1, pp 79-91.

20. Balanis, C. A, 'Antenna Theory: Analysis and Design' John Wiley & sons 1997, Chapter 14 pp 761-762 New York.

21. Carver, K. R., Mink, J. W, 'Microstrip Antenna Technology', IEEE Transactions Antennas & Propagation, 1981,Vol AP-29, No.1 Jan, pp 2-24

22. James, J.R and P.S.Hall, 'Handbook of Microstrip Antennas', 1989 Vols. 1 and 2, Peter Peregrinus, London, UK.

23. Garg R, P. Bhartia, I. Bahl, and A. Ittipiboon, 'Microstrip Antenna Design Handbook', 2000 MA: Artech House.

24. Pozar, D. M, 'A Reciprocity Method of Analysis for Printed Slot and Slot-Coupled Microstrip Antennas' IEEE Transactions Antennas and Propagation, Dec. 1986, Vol. AP-34, No. 12 pp 1439-1446.

25. Bahattacharyya, A.K., Antar, Y.M.M. and Ittipiboon, A, 'Full wave Analysis for the Equivalent Circuit of an Inclined Slot on a Microstrip Ground Plane', IEE Proceeding H, 1992, 139(3), pp. 245-250.

26. K. F. Lee, and, W. Chen, 'Advances in Microstrip and Printed Antennas', 1997, John Wiley & Sons, Inc. New York

27. Okoshi, T, 'Planar Circuits for Microwave and Light Waves' New York, Springer-Verlag, 1985.

28. Balanis, C. A, 'Advanced Engineering Electromagnetics' John Wiley & sons 1989, New York.

29. Aksun, M. I., Chuang, S. L., 'On Slot-Coupled Microstrip Antennas and Their Applications to CP Operation- Theory and Experiment' IEEE Transactions Antennas and Propagation, August 1990 Vol. AP-38, No. 8 pp 1224-12.50.

30. Pozar, D. M. 'Microstrip Antenna Aperture Coupled to a Microstrip Line' Electronics Letters, 17th Jan., 1985, Vol. 21, No.2, pp 49-50.

31. Targonski S. D., Pozar D. M, 'Design of Wideband Circularly Polarised Aperture-Coupled Microstrip Antennas', IEEE Transactions on Antennas and Propagation, 1993, Vol. 41, No. 2, Feb. pp 214-220.

32. Pozar, D. M. and Schaubert D. H, 'Microstrip Antennas: The Analysis and Design of Microstrip Antennas and Arrays', IEEE Press, New York 1995

33. Holland. H, 'Adaptation in Natural and Artificial Systems', University of Michigan press,Ann Arbor, 1975.

34. Samii, Y. R, and Michielssen, E 'Electromagnetic Optimisation by Genetic Algorithms' John Wiley, 1999, new York.

35. De Jong, K. A, 'An Analysis of Behaviour of a Class of Genetic Adaptive Systems' Doctoral dissertation, University of Michigan, Ann Arbor, 1957.

36. Johnson, J .M. and Rahmat Samii, Y.. "Genetic Algorithms in Engineering Electromagnets" IEEE Antennas and Propagation Magazine Vol. 39, No. 4, 1997.P.7-25.

37. Haupt, R. L. "An Introduction to Genetic Algorithms for Electromagnetic" IEEE Antennas and Propagation Magazine Vol. 37, No. 2, 1995, P. 7-15.

38. Goldberg, D E'Genetic Algorithms in Search, Optimization and Machine Learning', 1989 Addison-Wesly, Reading, MA.

39. Srinivas, N. and Deb, K, 'Multi-objective Optimization Using Non-dominating Sorting Genetic Algorithms' Evaluation Computing, 1995, Vol. 2 pp. 221-248.

40. Samii, Y.R, and Michielssen, E., 'Electromagnetic Optimization by Genetic Algorithms' 1999, John Wiely & Sons, USA.

41. Haneishi, M., and Suzuki, 'Circular Polarization and Bandwidth', in Handbook of Microstrip Antennas, 1989, Vol 1, James, J. R. and Hall, P. S. Peter Peregrinus, London.

42. E. N Lim, E. Korolkiewicz, S. Scott, B Aljibouri, and Shi-Chang Gao 'Efficient impedance coupling formulas for rectangular segment in planner microstrip circuits', IEEE Transaction on Antennas and Propagation, Vol. 51, No 8, August 2003, pp 2137-2140

43. ANSOFT Corporation, Ensemble 5.1, 1998.

44. Day, P. L, 'Transmission Line Transformation Between Arbitrary Impedance Using the Smith Chart' IEEE Transactions Microwave Theory and Technologies, 1975, pp. 772-773.

45. Iwasaki, H., 'A Circularly Polarized Small-Size Microstrip Antenna With a Cross-Slot', IEEE Transaction on Antenna and Propagation, Oct. 1996 Vol. 44, No. 10,. pp 1399-1401.

46. Sullivan, P. L, Schaubert, D. H.: ' Analysis of an Aperture Coupling Microstrip Antenna' IEEE Transactions Antennas and Propagation, August 1986, Vol. AP-34, pp 977-984.

47. Taso C. H. Hwang Y. M., Killburg F., and Dietrich F., 'Aperture-Coupled Patch Antennas with Wide-Bandwidth and Dual Polarisation Capabilities' 1988 IEEE Antennas and Propagation Symp. Dig., pp 936-939.

48. Pues. H., Van de Capelle, A. 'Accurate Transmission Line Model for the Rectangular Microstrip Patch Antenna', IEE Proceedings, 1984, V. 31 Pt. h, No. 6, Dec., pp 334-340.

49. Das, M.K., 'Generalized Multi-port Reciprocity Analysis of Surface-to Surface Transitions Between Multiple Printed transmission Lines', IEEE Transactions on Microwave Theory and Techniques, 1993, 41 pp. 1164-1177.

50. Himdi, M., Daniel, J.P. and Terrent, C, 'Transmission Line Analysis of Aperture-Coupled Microstrip Antenna', Electronics Letters, 1989, 25(18), pp. 1229-12.50.

51. Sawamura, M., Tabata, M. and Haneishi, M., 'Radiation Properties of Ring Microstrip Antenna Fed by symmetrical Cross Slot', In: digest of the IEEE Antennas and propagation Society International Symposium, June 1995, California, pp.2074-2077.

52. Jackson, D. R., et al, 'Computer-Aided Design of Rectangular Microstrip Antennas', Chap. 5 in Advances in Microstrip and Printed Antennas by Lee, K. F. and Chen W, 1998, interscience pp 22.5-271.

53. Richards, W. F., Zincher, J. R., Clark, R. D., Long, S. A.: 'Experimental and Theoretical Investigation of the Inductance Associated with a Microstrip

Antenna Feed ', December 1985 Electromagnetics, Vol. 3, No. 3-4, July, pp 327-346.

54. Rao, J. S., Joshi, K.K, and Das, B.N, 'Analysis of Small Aperture Coupling Between Rectangular Waveguide and Microstrip Line', IEEE Transactions on Microwave Theory and Technique, 1981, 29(2), pp 150-154.

55. Sullivan, P. L, Schaubert, D. H.: ' Analysis of an Aperture Coupling Microstrip Antenna' IEEE Transactions Antennas and Propagation, August 1986, Vol. Ap-34, pp 977-984.

56. Chon, S. B. 'Slot Line on a Dielectric Substrate', IEEE Transaction on Microwave Theory and Techniques, 1969, 17(10), pp. 786-778.

57. Himdi, M., Daniel, J.P. and Terrent, C, 'Analysis of Aperture-coupled Microstrip Antenna Using Cavity Method', Electronics Letters, 1991, 27(5), pp. 455-457.

58. Barlately, L., Smith, H.K., and Mosig, J.R.: 'Printed Radiating Structures and Transitions in Multilayered Substrates' Int. J. Microwave, Milimeter-Wave Computer-Adid Engineering, 1992, 2, pp. 273-285.

59. Thouroudde, D, Himdi M, and Daniel. J.P: 'CAD-Oriented Cavity Model for Rectangular Patches', Electronics Letters 1990, 26(13), pp 842-844.

Appendix A

Scaling Factor in Random Parameter Selection

It is required to show that in the formula (Chapter 4)

$$a_{ij} = L_i + \frac{V_{ij}}{2^m - 1}(U_i - L_i) \quad \text{for } i = 1, m, \; j = 1, N$$

the scale factor $V_{ij}/(2^m - 1)$ is less than unity, and where V_{ij} is the real value of a random binary string of length 'm'..

For any binary string of length 'm' the maximum possible real value of the string occurs when each binary digit is '1' and the maximum possible real value is

$2^{m-1} + 2^{m-2} + \ldots + 2^{m-m}$.

Therefore,

$$\frac{V_{\max}}{2^n - 1} = \frac{2^{n-1} + 2^{n-2} + \ldots + 2^0}{2^{n-1} - 1} \tag{A2}$$

$$\frac{2^{n-1}\left(1 + 2^{-1} + 2^{-2} + \ldots + 2^{1-n}\right)}{2^{n-1}\left(2 - 2^{1-n}\right)} \tag{A3}$$

$$\frac{1 + 2^{-1} + 2^{-2} + \ldots + 2^{1-n}}{2 - 2^{1-n}} \tag{A4}$$

The sum of the geometric series in the above numerator is given by

$$S_n = 2 - \frac{1}{2^{n-1}} \tag{A6}$$

That is,

$$\frac{V_{\max}}{2^n - 1} = \frac{2 - \dfrac{1}{2^{n-1}}}{2 - 2^{1-n}} = 1 \tag{A7}$$

Therefore

$$\frac{(V_{ij})_{\max}}{2^n - 1} \le 1. \tag{A8}$$

Appendix B

Circular Polarisation condition for a Dual-Feed Circular Polarised Patch Antenna

The dual feed square patch antenna shown in Figure (a) below and the equivalent circuit model in Figure (b).

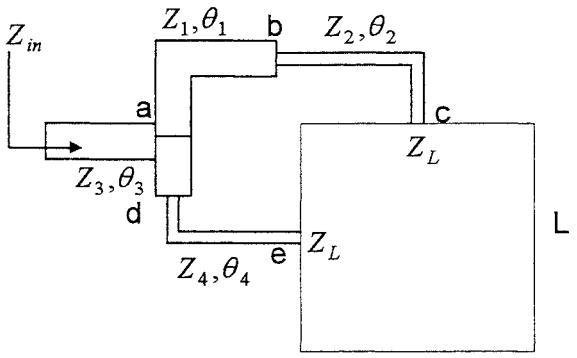

a

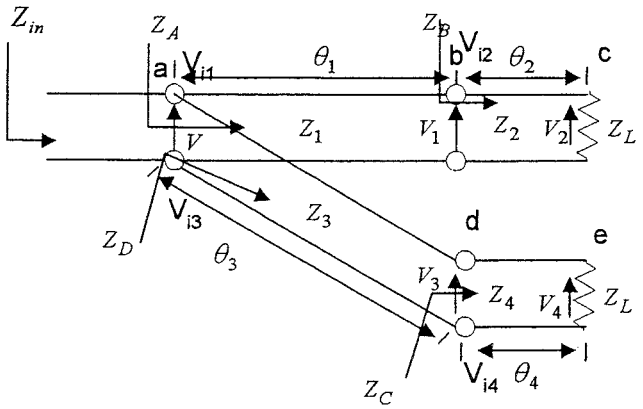

b

Figure (a) Dual-feed CP square patch antenna, (b) Equivalent circuit of the antenna

The circular polarisation objective function $V_{inpatch}$ for dual-feed square patch antenna, can be derived as follows:

The reflection coefficients at junctions b, c, d, and e in, are. $\Gamma_1, \Gamma_2, \Gamma_3, \text{and}, \Gamma_4$, respectively

$$\Gamma_1 = \frac{Z_B - Z_1}{Z_B + Z_1} \tag{B1}$$

$$\Gamma_2 = \frac{Z_L - Z_2}{Z_L + Z_2} \tag{B2}$$

$$\Gamma_3 = \frac{Z_C - Z_3}{Z_C + Z_3} \tag{B3}$$

$$\Gamma_4 = \frac{Z_L - Z_4}{Z_L + Z_4} \tag{B4}$$

For the dual feed network based on a power divider to produce circular polarisation is shown in Figure B, and its equivalent circuit is shown in Figure B.

However, at node a toward Z1 the voltages can be obtained as follow

$$V = V_{i1}[1 + \Gamma_1 e^{-2i\theta_1}] \tag{B5}$$

$$V_1 = V_{i1} e^{-i\theta_1}[1 + \Gamma_1] \tag{B6}$$

while at node b the voltages can expressed as follows:

$$V_1 = V_{i2}[1 + \Gamma_2 e^{-2i\theta_2}] \tag{B7}$$

$$V_2 = V_{i2} e^{-i\theta_2}[1 + \Gamma_2] \tag{B8}$$

Therefore

$$\frac{V_1}{V} = \frac{e^{-i\theta_1}[1 + \Gamma_1]}{[1 + \Gamma_1 e^{-2i\theta_1}]} \tag{B9}$$

and

$$\frac{V_2}{V_1} = \frac{e^{-i\theta_2}[1+\Gamma_2]}{[1+\Gamma_2 e^{-2i\theta_2}]} \tag{B10}$$

So

$$\frac{V_2}{V} = \frac{V_1}{V} \times \frac{V_2}{V_1} \tag{B12}$$

$$\frac{V_2}{V} = \frac{e^{-i\theta_1}[1+\Gamma_1]}{[1+\Gamma_1 e^{-2i\theta_1}]} \times \frac{e^{-i\theta_2}[1+\Gamma_2]}{[1+\Gamma_2 e^{-2i\theta_2}]} \tag{B13}$$

$$\frac{V_2}{V} = \frac{e^{-i\theta_1} e^{-i\theta_2}[1+\Gamma_1][1+\Gamma_2]}{[1+\Gamma_1 e^{-2i\theta_1}][1+\Gamma_2 e^{-2i\theta_2}]} \tag{B14}$$

Similarly we can obtain that

$$\frac{V_4}{V} = \frac{e^{-i\theta_3} e^{-i\theta_4}[1+\Gamma_3][1+\Gamma_4]}{[1+\Gamma_3 e^{-2i\theta_3}][1+\Gamma_4 e^{-2i\theta_4}]} \tag{B15}$$

Therefore,

$$V_{iinpatch} = \frac{e^{-i(\theta_1+\theta_2)}[1+\Gamma_1][1+\Gamma_2]}{[1+\Gamma_1 e^{-2i\theta_1}][1+\Gamma_2 e^{-2i\theta_2}]} \times \frac{[1+\Gamma_3 e^{-2i\theta_3}][1+\Gamma_4 e^{-2i\theta_4}]}{e^{-i(\theta_3+\theta_4)}[1+\Gamma_3][1+\Gamma_4]} \tag{B16}$$

Appendix C
Evaluation of the Integration on the Overlapping Area Between the Inclined Slot and the Feed Line

The integration of the overlapped area between the feed line and the aperture, Figure c, below can be evaluated as follow:

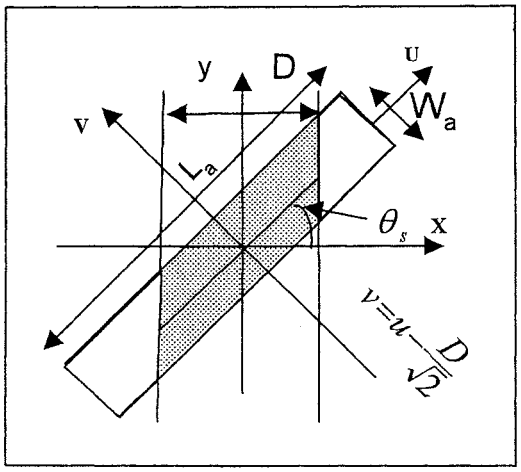

Figure c: Overlapping Area between the Inclined Slot and the Feed Line

$$I_c = 2\int_{v=\frac{-W_a}{2}}^{v=\frac{W_a}{2}}\int_{u=0}^{u=v+\frac{D}{\sqrt{2}}} \sin\left[k_a\left(\frac{L_a}{2}-|u|\right)\right]dudv \tag{C.1}$$

The first integration is

$$\int_0^{v+\frac{D}{\sqrt{2}}} \sin\left[K_a\left(\frac{L_a}{2}-u\right)\right]du = \frac{1}{k_a}\cos\left[K_a\left(\frac{L_a}{2}-u\right)\right]_0^{v+\frac{D}{\sqrt{2}}} = \frac{1}{k_a}\cos\left[k_a\left(\frac{L_a}{2}-v-\frac{D}{\sqrt{2}}\right)\right]-\frac{1}{k_a}\cos\left(\frac{k_aL_a}{2}\right) \tag{C.2}$$

Therefore the second integration can be evaluated as follows:,

$$I_c = 2\int_{\frac{-W_a}{2}}^{\frac{W_a}{2}}\left\{\frac{1}{k_a}\cos\left[k_a\left(\frac{L_a}{2}-v-\frac{D}{\sqrt{2}}\right)\right]-\frac{1}{k_a}\cos\left(\frac{k_aL_a}{2}\right)\right\}dv \tag{C.3}$$

$$= 2\int_{\frac{-W_a}{2}}^{\frac{W_a}{2}}\frac{1}{k_a}\cos\left[k_a\left(\frac{L_a}{2}-v-\frac{D}{\sqrt{2}}\right)\right]dv - 2\int_{\frac{-W_a}{2}}^{\frac{W_a}{2}}\frac{1}{k_a}\cos\left(\frac{k_aL_a}{2}\right)dv \tag{C.4}$$

$$=\frac{-2}{{k_a}^2}\sin\left[k_a\left(\frac{L_a}{2}-v-\frac{D}{\sqrt{2}}\right)\right]\Bigg|_{-\frac{W_a}{2}}^{\frac{W_a}{2}}-\frac{2W_a}{k_a}\cos\left(\frac{k_aL_a}{2}\right) \tag{C.5}$$

Hence,

$$I_c=\frac{2}{{k_a}^2}\left\{\sin\left[k_a\left(\frac{L_a}{2}+\frac{W_a}{2}-\frac{D}{\sqrt{2}}\right)\right]-\sin\left[k_a\left(\frac{L_a}{2}-\frac{W_a}{2}-\frac{D}{\sqrt{2}}\right)\right]\right\} -\frac{2W_a}{k_a}\cos\left(\frac{k_aL_a}{2}\right) \tag{C.6}$$

$$I_c=\frac{2}{{k_a}^2}\left\{\sin\left[k_a\left(\frac{L_a}{2}+\frac{W_a}{2}-\frac{D}{\sqrt{2}}\right)\right]-\sin\left[k_a\left(\frac{L_a}{2}-\frac{W_a}{2}-\frac{D}{\sqrt{2}}\right)\right]\right\} -\frac{2W_a}{k_a}\cos\left(\frac{k_aL_a}{2}\right) \tag{C.7}$$

Therefore:

$$I_c=\frac{4}{{k_a}^2}\sin\left(\frac{k_aW_a}{2}\right)\cos\left[k_a\left(\frac{L_a}{2}-\frac{D}{\sqrt{2}}\right)\right]-\frac{2W_a}{k_a}\cos\left(\frac{k_aL_a}{2}\right) \tag{C.8}$$

Appendix D
Derivation of Mode Coefficients $(B_{x,mn}, B_{y,mn})$

The cavity model's mode coefficients, $(B_{x,mn}, B_{y,mn})$, (Chapter six) can be derived as follow:

$$B_{x,mn} = \frac{j\omega\varepsilon}{(k^2 - k^2{}_{mn})} \int_0^a \int_0^b J_{mx} \Psi_{x,mn} dxdy \tag{D1}$$

where

$$\Psi_{x,mn} = A_{mn}.k_n.\cos(k_m x).\sin(k_n y) \tag{D2}$$

and

$$J_{mx} = \frac{-2V_{0x}}{d_a W_a} \frac{\sin\left[k_a\left(\frac{L_a}{2} - \left|x - \frac{a}{2}\right|\right)\right]}{\sin\left(k_a \frac{L_a}{2}\right)} \qquad \begin{matrix} \frac{a-L_a}{2} \le x \le \frac{a+L_a}{2} \\ \frac{b-W_a}{2} \le y \le \frac{b+W_a}{2} \\ 0 \le z \le d_a \end{matrix} \tag{D3}$$

$$= 0, \qquad \text{otherwise}$$

Substituting D1 and D2 into D3 gives

$$B_{x,mn} = \frac{-2j\omega A_{mn} V_{ox}}{d_a k_n (k^2 - k^2{}_{mn}) W_a} \cdot \int_{\frac{a-L_a}{2}}^{\frac{a+L_a}{2}} \int_{\frac{b-W_a}{2}}^{\frac{b+W_a}{2}} \frac{\sin\left[k_a\left(\frac{L_a}{2} - \left|x - \frac{a}{2}\right|\right)\right]}{\sin\left(k_a \frac{L_a}{2}\right)} \cos(k_m x)\sin(k_n y) dxdy \tag{D4}$$

The integration with respect to the x and y variables can be separated, which gives

$$B_{x,mn} = \frac{-2j\omega A_{mn} V_{ox}}{d_a k_n (k^2 - k^2{}_{mn}) W_a} \cdot \frac{1}{\sin\left(k_a \frac{L_a}{2}\right)} \cdot$$

$$\underbrace{\int_0^a \sin(k_n y)dy}_{I_1}.\underbrace{\int_0^b \sin\left[k_a\left(\frac{L_a}{2}-\left|x-\frac{a}{2}\right|\right)\right]\cos(k_m x)dx}_{I_2} \tag{D5}$$

where the value of the first integral I_1 is

$$I_1 = \frac{1}{k_n}\left[\cos\left(k_n\frac{b}{2}+k_n\frac{W_a}{2}\right)-\cos\left(k_n\frac{b}{2}-k_n\frac{W_a}{2}\right)\right] \tag{D6}$$

That is

$$I_1 = \frac{2}{k_n}\sin\left(k_n\frac{W_a}{2}\right)\sin\left(\frac{n\pi}{2}\right) \tag{D7}$$

Replacing x by $x+a/2$ in the second integral gives

$$I_2 = \int_{-\frac{L_a}{2}}^{\frac{L}{2}} \sin\left[k_a\left(\frac{L_a}{2}-|x|\right)\right]\cos\left[k_m\left(\frac{a}{2}+x\right)\right]dx$$

$$= \int_0^{\frac{L_a}{2}} \sin\left[k_a\left(\frac{L_a}{2}-x\right)\right]\cos\left[k_m\left(\frac{a}{2}+x\right)\right]dx$$

$$+ \int_{-\frac{L_a}{2}}^{0} \sin\left[k_a\left(\frac{L_a}{2}+x\right)\right]\cos\left[k_m\left(\frac{a}{2}+x\right)\right]dx$$

$$= \int_0^{\frac{L_a}{2}} \sin\left[k_a\left(\frac{L_a}{2}-x\right)\right]\cos\left[k_m\left(\frac{a}{2}+x\right)\right]dx$$

$$+ \int_0^{\frac{L_a}{2}} \sin\left[k_a\left(\frac{L_a}{2}-x\right)\right]\cos\left[k_m\left(\frac{a}{2}-x\right)\right]dx$$

$$= \int_0^{\frac{L_a}{2}} \sin\left[k_a\left(\frac{L_a}{2}-x\right)\right]\left\{\cos\left[k_m\left(\frac{a}{2}+x\right)\right]+\cos\left[k_m\left(\frac{a}{2}-x\right)\right]\right\}dx$$

$$= 2\cos\left(k_m\frac{a}{2}\right)\int_0^{\frac{L_a}{2}} \sin\left[k_a\left(\frac{L_a}{2}-x\right)\right]\cos(k_m x)dx$$

$$= 2\cos\left(k_m\frac{a}{2}\right).$$

$$\int_0^{\frac{L_a}{2}}\left\{\sin\left[k_a\frac{L_a}{2}+(k_m-k_a)x\right]+\sin\left[k_a\frac{L_a}{2}-(k_m+k_a)x\right]\right\}dx \qquad \text{(D8)}$$

So the second integral's value is

$$I_2 = \frac{2k_a\cos\left(k_m\frac{a}{2}\right)}{{k_a}^2-{k^2}_m}\left[\cos\left(k_m\frac{L_a}{2}\right)-\cos\left(k_a\frac{L_a}{2}\right)\right] \qquad \text{(D9)}$$

Therefore, the mode coefficients $(B_{x,mn})$ are given by

$$B_{x,mn} = \frac{-j\omega\varepsilon.A_{mn}V_{0x}}{d_a k_n\cdot\left(k^2-k_{mn}^2\right)}\cdot\frac{4\sin c\left(k_n\frac{W_a}{2}\right)\sin\left(\frac{n\pi}{2}\right)\cos\left(\frac{m\pi}{2}\right)}{\sin\left(k_a\frac{L_a}{2}\right)}\cdot\frac{k_a\left[\cos\left(k_m\frac{L_a}{2}\right)-\cos\left(k_a\frac{L_a}{2}\right)\right]}{k_a^2-k_m^2} \qquad \text{(D10)}$$

Similarly, the mode coefficients $(B_{y,mn})$ are given by

$$B_{y,mn} = \frac{-j\omega\varepsilon.A_{mn}V_{0y}}{d_a k_m\cdot\left(k^2-k_{mn}^2\right)}\cdot\frac{4\sin c\left(k_m\frac{W_a}{2}\right)\sin\left(\frac{m\pi}{2}\right)\cos\left(\frac{n\pi}{2}\right)}{\sin\left(k_a\frac{L_a}{2}\right)}\cdot\frac{k_a\left[\cos\left(k_n\frac{L_a}{2}\right)-\cos\left(k_a\frac{L_a}{2}\right)\right]}{k_a^2-k_n^2} \qquad \text{(D11)}$$

Appendix E

Derivation of the Admittance of the Aperture Patch Antenna, $(Y_{x,ant}, Y_{y,ant})$, Using the cavity model

The admittance of the patch antenna using the cavity model (Chapter six) involves, $Y_{x,ant}$, and $Y_{y,ant}$, which are admittance of the patch at the x, and y direction respectively.

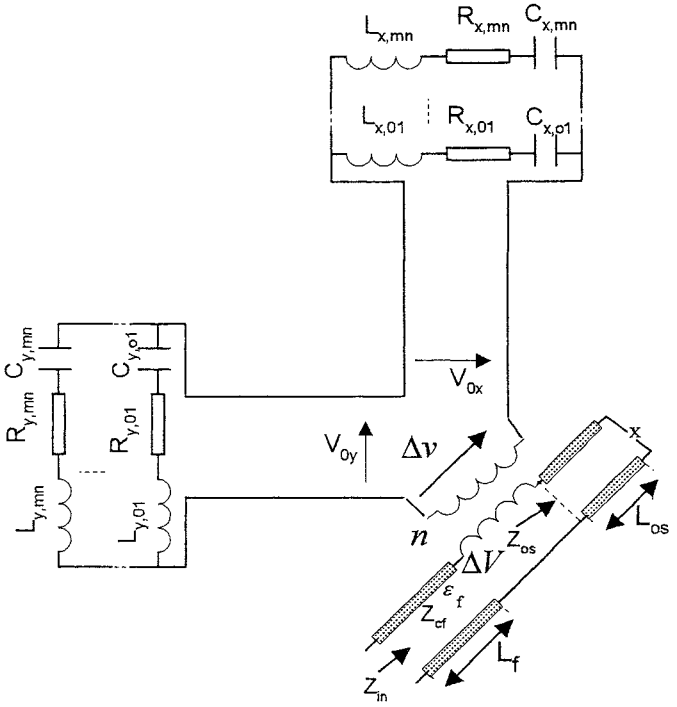

Equivalent circuit based on the cavity model

These admittance can be derived as follow:

$$Y_{x,ant} = \frac{\iiint_V H_x J_{mx}^* dv}{\left|V_{0x}\right|^2} \tag{E1}$$

where

$$H_x = \sum_{m=0}^{\infty}\sum_{n=0}^{\infty} A_{mn} B_{x,mn} k_n \cos(k_m x)\sin(k_n y)$$

and

$$J_{mx} = \frac{-2V_{0x}}{d_a W_a} \frac{\sin\left[k_a\left(\frac{L_a}{2} - \left|x - \frac{a}{2}\right|\right)\right]}{\sin\left(k_a \frac{L_a}{2}\right)} \qquad \begin{matrix} \frac{a-L_a}{2} \le x \le \frac{a+L_a}{2} \\ \frac{b-W_a}{2} \le y \le \frac{b+W_a}{2} \\ 0 \le z \le d_a \end{matrix} \qquad \text{(E3)}$$

$$= 0, \qquad \text{otherwise}$$

Substituting E1 and E2 into E3 gives

$$Y_{x,ant} = \frac{-2V_{0x}}{d_a W_a |V_{0x}|^2 \sin\left(k_a \frac{L_a}{2}\right)}.$$

$$\int_{\frac{a-L_a}{2}}^{\frac{a+L_a}{2}} \int_{\frac{b-W_a}{2}}^{\frac{b+W_a}{2}} \int_0^{d_a} \sum_m \sum_n A_{mn} B_{x,mn}{}^* k_n \cos(k_m x) \sin(k_n y) \cdot \sin\left[k_a\left(\frac{L_a}{2} - \left|x - \frac{a}{2}\right|\right)\right] dx dy dz \qquad \text{(E4)}$$

Performing the integration with respect to variable z and changing the order of summation and integration gives

$$Y_{x,ant} = \frac{-2V_{0x} A_{mn} B^*_{x,mn} k_n}{W_a |V_{0x}|^2 \sin\left(k_a \frac{L_a}{2}\right)}.$$

$$\int_0^a \int_0^b \cos(k_m x) \sin(k_n y) \cdot \sin\left[k_a\left(\frac{L_a}{2} - \left|x - \frac{a}{2}\right|\right)\right] dx dy$$

$$= \sum_m \sum_n \frac{-2V_{0x} A_{mn} B^*_{x,mn} k_n}{W_a |V_{0x}|^2 \sin\left(k_a \frac{L_a}{2}\right)} \underbrace{\int_0^a \sin(k_n y) dy}_{I_1} \cdot \underbrace{\int_0^b \sin\left[k_a\left(\frac{L_a}{2} - \left|x - \frac{a}{2}\right|\right)\right] \cos(k_m x) dx}_{I_2} \qquad \text{(E5)}$$

The value of integrals I_1 and I_2 have been evaluated in Appendix D and are given by

$$I_1 = \frac{2}{k_n}\sin\left(k_n\frac{W_a}{2}\right)\sin\left(\frac{n\pi}{2}\right) \tag{E6}$$

$$I_2 = \frac{2k_a\cos\left(\frac{m\pi}{2}\right)}{k_a^2 - k_m^2}\left[\cos\left(k_m\frac{L_a}{2}\right)\right] \tag{E7}$$

Substituting I_1, I_2 and the expression for $B_{x,mn}$ which is given by

$$B_{x,mn} = \frac{-j\omega\varepsilon\cdot A_{mn}V_{0x}}{d_a k_n\cdot\left(k^2 - k_{mn}^2\right)}\cdot\frac{4\sin c\left(k_n\frac{W_a}{2}\right)\sin\left(\frac{n\pi}{2}\right)\cos\left(\frac{m\pi}{2}\right)}{\sin\left(k_a\frac{L_a}{2}\right)}\cdot\frac{k_a\left[\cos\left(k_m\frac{L_a}{2}\right)-\cos\left(k_a\frac{L_a}{2}\right)\right]}{k_a^2 - k_m^2} \tag{E8}$$

into (E6), the expression for the input impedance is given by

$$Y_{x,ant} = \sum_m\sum_n \frac{16\cdot j\omega\varepsilon\cdot A_{mn}^2}{d_a\left(\left(k^*\right)^2 - k_{mn}^2\right)}\cdot \left\{\frac{\sin c\left(k_n\frac{W_a}{2}\right)\sin\left(\frac{n\pi}{2}\right)\cos\left(\frac{m\pi}{2}\right)}{\sin\left(k_a\frac{L_a}{2}\right)}\cdot\frac{k_a\left[\cos\left(k_m\frac{L_a}{2}\right)-\cos\left(k_a\frac{L_a}{2}\right)\right]}{k_a^2 - k_m^2}\right\}^2 \tag{E10}$$

Similarly, the input impedance $Y_{y,ant}$ is given by

$$Y_{y,ant} = \sum_m \sum_n \frac{16 \cdot j\omega\varepsilon \cdot A_{mn}^2}{d_a\left[\omega^2 - \omega_{mn}^2\left(1 + j\delta_{eff}\frac{\omega^2}{\omega_{mn}^2}\right)\right]} \cdot \left\{\frac{\sin c\left(k_m \frac{W_a}{2}\right)\sin\left(\frac{m\pi}{2}\right)\cos\left(\frac{n\pi}{2}\right)}{\sin\left(k_a \frac{L_a}{2}\right)} \cdot \frac{k_a\left[\cos\left(k_n \frac{L_a}{2}\right) - \cos\left(k_a \frac{L_a}{2}\right)\right]}{k_a^2 - k_n^2}\right\}^2$$

(E11)

Appendix F

Derivation of the Patch Admittance at the Aperture Using Transmission Line Model

The transmission line equivalent circuit for the patch admittance in the x-direction is shown below

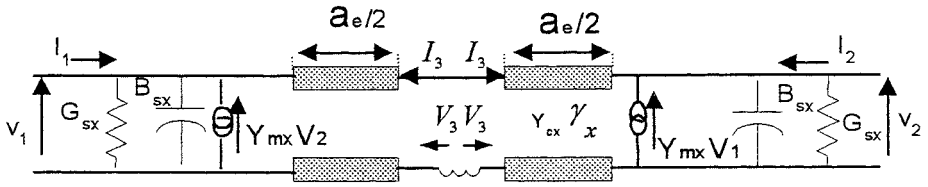

Equivalent circuit of the patch antenna for the x direction.

In order to obtain the value of the input impedance, the admittance matrix must first be determined.

The elements of the admittance matrix can be determined as given by

$$Y_{px,mn} = \frac{I_m}{V_n} \Big| \quad V_{m'} = 0 \quad m' \neq m \tag{F.1}$$

With

$$Y_{sx} = G_{sx} + jB_{sx}$$

And taking into account the symmetry of the network, the elements of the admittance matrix are as follows

$$
\begin{aligned}
Y_{px,11} &= Y_{px,22} = Y_{sx} + Y_{cx}\coth(\gamma a_e) \\
Y_{px,33} &= \frac{Y_{cx}}{2}\coth\left(\gamma\frac{a_e}{2}\right) \\
Y_{px,12} &= Y_{px,21} = -Y_{mx} - \frac{Y_{cx}}{2\sinh(\gamma a_e)} \\
Y_{px,13} &= Y_{px,31} = -Y_{px,23} = -Y_{px,32} = \frac{Y_{cx}}{2\sinh\left(\gamma\frac{a_e}{2}\right)}
\end{aligned}
\tag{F.3}
$$

Hence the admittance matrix of the transmission line network shown in Figure F1 is given by

$$
Y_{px} = \begin{bmatrix}
Y_{sx} + Y_{cx}\coth(\gamma a_e) & -Y_{mx} - \dfrac{Y_{cx}}{\sinh(\gamma a_e)} & \dfrac{Y_{cx}}{2\sinh\left(\gamma\frac{a_e}{2}\right)} \\
-Y_{mx} - \dfrac{Y_{cx}}{\sinh(\gamma a_e)} & Y_{sx} + Y_{cx}\coth(\gamma a_e) & \dfrac{-Y_{cx}}{2\sinh\left(\gamma\frac{a_e}{2}\right)} \\
\dfrac{Y_{cx}}{2\sinh\left(\gamma\frac{a_e}{2}\right)} & \dfrac{-Y_{cx}}{2\sinh\left(\gamma\frac{a_e}{2}\right)} & \dfrac{Y_{cx}}{2}\coth\left(\gamma\frac{a_e}{2}\right)
\end{bmatrix}
\tag{F.4}
$$

The admittance relates the currents and voltages at the three ports of the network as given by

$$
\begin{bmatrix} I_1 \\ I_2 \\ I_3 \end{bmatrix} = \begin{bmatrix} Y_{px,11} & Y_{px,12} & Y_{px,13} \\ Y_{px,21} & Y_{px,22} & Y_{px,23} \\ Y_{px,31} & Y_{px,32} & Y_{px,33} \end{bmatrix} \cdot \begin{bmatrix} V_1 \\ V_2 \\ V_3 \end{bmatrix}
\tag{F.5}
$$

The input admittance at port 3 is defined as

$$Y_{PX} = \frac{I_3}{V_3} \qquad I_1 = I_2 = 0 \tag{F.6}$$

Substituting this condition into (F.5) and multiplying the equation with the inverse of the admittance matrix gives

$$\begin{bmatrix} V_1 \\ V_2 \\ V_3 \end{bmatrix} = \left[Y_{px}\right]^{-1} \cdot \begin{bmatrix} 0 \\ 0 \\ I_3 \end{bmatrix} \tag{F.7}$$

Hence

$$\frac{I_3}{V_3} = \frac{\left|\left[Y_{px}\right]\right|}{Y^c_{px,33}} \tag{F.8}$$

Where $\left|\left[Y_{px}\right]\right|$ is the determinant of the matrix $\left[Y_{px}\right]$ and

$Y^c_{px,33}$ is the cofactor of element $Y_{px,33}$

$$\left|\left[Y_{px}\right]\right| = Y_{px,33}\left(Y^2_{px,11} - Y^2_{px,12}\right) - 2Y^2_{px,13}\left(Y_{px,11} + Y_{px,12}\right) \tag{F.9}$$

$$Y^c_{px,33} = Y_{px,33}\left(Y^2_{px,11} - Y^2_{px,12}\right) \tag{F.10}$$

Therefore

$$Y_{PX} = 1 - 2\frac{Y^2_{px,13}\left(Y_{px,11} + Y_{px,12}\right)}{Y_{px,33}\left(Y^2_{px,11} - Y^2_{px,12}\right)}$$

$$=1-2\frac{Y_{px,13}^{2}}{Y_{px,33}\left(Y_{px,11}-Y_{px,12}\right)} \tag{F.11}$$

Hence, the input impedance of the transmission line network, which is the patch impedance at the aperture is given by

$$Y_{PX}=1-\frac{Y_{cx}}{\sinh\left(\gamma\frac{a_e}{2}\right)\cosh\left(\gamma\frac{a_e}{2}\right)\left[Y_{sx}+Y_{cx}\coth(\gamma a_e)+Y_{mx}+\frac{Y_{cx}}{\sinh(\gamma a_e)}\right]} \tag{F.12}$$

Similarly

$$Y_{PY}=1-\frac{Y_{cy}}{\sinh\left(\gamma\frac{b_e}{2}\right)\cosh\left(\gamma\frac{b_e}{2}\right)\left[Y_{sy}+Y_{cy}\coth(\gamma a_e)+Y_{my}+\frac{Y_{cy}}{\sinh(\gamma b_e)}\right]} \tag{F.13}$$

Appendix G :
Genetic Algorithms Computer Programmers

```
%XXXXXXXXXXXXXXXXXXXXXXXXXXXX
%  nearly square offset-fed microstrip patch antenna
%XXXXXXXXXXXXXXXXXXXXXXXXXXXXX
% Design variables
f=2.45*10^9; % Operating frequency
Q=83;       % Quality factor
mu=4*10^-7*pi;
er=2.33;    % Relative permittivity
e0=8.85*10^-12;
w=2*pi*f;
h=0.00079; %Substrate thickness
ww=0.000672; %
ke=sqrt(w^2*mu*e0*er*(1-i*(1/Q)));
nv=3; % Number of variables
np=50; % Number of population
np2=np/2;
maxit=100;  % number of maximum iterations
len=[20 20 20]; % Vector of chromosome
Tlen=sum(len);
%XXXXXXXXXXXXXXXXXXXXXXXXXXXXXXXXXXXXXXXXXXX
% Generation of initial population in a matrix Chromosomes of 50 row by row chromosomes (len) in binary form
Ch=round(rand([np,Tlen]));
%XXXXXXXXXXXXXXXXXXXXXXXXXXXXXXXXXXXXXXXXXXX
var=zeros(np*maxit,nv);eval=zeros(np*maxit,1); % spare reservation for each matrix, Var of Eval
```

```
% XXXXXXXXXXXXXXXXXXXXXXXXXXXXXXXXXXXXXXXXXXXXXXXX
% Parameters design bounds
lob=[0.040 0.041 0.01]; % Lower bounds
upb=[0.041 0.042 0.05]; % Upper bounds
% XXXXXXXXXXXXXXXXXXXXXXXXXXXXXXXXXXXXXXXXXXXXXXXX
% XXXXXXXXXXXXXXXXXXXXXXXXXXXXXXXXXXXXXXXXXXXXXXXXXXXXXXXXXXXXXXXXXXXXXXXXXXXXXXX
% Converting the binary representations to the real values, a, b, T.
%XXXXXXXXXXXXXXXXXXXXXXXXXXXXXXXXXXXXXXXXXXXXXXXXXXXXXXXXXXXXXXXXXXXXXXXXXXXXXXX
rang=upb-lob;
num=2.^(len)-1;
lop=cumsum([1 len]);
upp=cumsum([len]);
 for it=1:maxit
iteration=it;
  for j=1:np
  phe=zeros([np nv]);
  end
for ii=1:nv
   index=lop(ii):upp(ii);
   sx=[];
    for j=len(ii)-1:-1:0
      sx=[sx 2^j];
     end

sx=sx';
Chindex=Ch(:,index);
 phe(:,ii)=Chindex*sx;
```

```
 phen(:,ii)=lob(ii)+(rang(ii)/num(ii)).*phe(:,ii);
 Phen=phen;
end
a=Phen(:,1);
b=Phen(:,2);
T=Phen(:,3); % Binary conversion of initial values to real values ends producing the " INITIAL POPULATION"
 %XXXXXXXXXXXXXXXXXXXXXXXXXXXXXXXXXXXXXXXXXXXXXXXXXXXXXXXXXXXXXXXXXXXXXX
 % Evaluation of  Objective function formulas for 50 sampled solutions
 %XXXXXXXXXXXXXXXXXXXXXXXXXXXXXXXXXXXXXXXXXXXXXXXXXXXXXXXXXXXXXXXXXXXXXX
A=(ke*a/pi)';
B=(ke*b/pi)';
th1=((pi*T)./a)';
th2=((pi*ww)./(2*a))';
R10=(i*w*mu*h./(a.*b))'.*(8*a.^4/(pi^4*ww^2))'.*((cos(th1).*sin(th2)).^2./(1-A.^2));
R01=(i*w*mu*h./(a.*b))'.*(2*b.^2/pi^2)'.*(1./(1-B.^2));
C10=Q./(R10*w);
L10=R10/(Q*w);
C01=Q./(R01*w);
L01=R01/(Q*w);
Y10=(1./R10)+i*(w*C10-1./(w*L10));
Y01=(1./R01)+i*(w*C01-1./(w*L01));
phase=(angle(Y10./Y01)*(180/pi))';
magnitude=abs(Y10./Y01);
objval=abs(magnitude-1)';
%XXXXXXXXXXXXXXXXXXXXXXXXXXXXXXXXXXXXXX
% Axial ratio objective function obtained
%XXXXXXXXXXXXXXXXXXXXXXXXXXXXXXXXXXXXXX
```

```
if it==1
   var(1:np,:)=phen(1:np,:);
   eval_mag(1:np,:)=objval(1:np,:);
   eval_phase(1:np,:)=abs(phase(1:np,:));
 else
  var(1+np*(it-1):np*it,:)=phen(1:np,:);
  eval_mag(1+np*(it-1):np*it,:)=objval(1:np,:);
  eval_phase(1+np*(it-1):np*it,:)=abs(phase(1:np,:));
end
% Fifty sample solutions obtained.
%%%%%%%%%%%%%%%%%%%%%%%%%%%%%%%%%%%%%%%%%%%%%%%%%%%%%%%%%%%%%%%%
% ranking the objective function values
[objval,ind]=sort(objval);
% sorting chromosomes according to fitting and discard the half bottomof the population
Ch=Ch(ind(1:np),:);
% XXXXXXXXXXXXXXXXXXXX
% Cross over operator
% XXXXXXXXXXXXXXXXXXXX
%select random crossover points
cross=round((Tlen-1)*rand(np2,1));

crs=cross;
for k=1:2:np2
  Ch(np2+k,1:cross)=Ch(k,1:cross);
  Ch(np2+k,cross+1:Tlen)=Ch(k+1,cross+1:Tlen);
  Ch(np2+k+1,1:cross)=Ch(k+1,1:cross);
  Ch(np2+k+1,cross+1:Tlen)=Ch(k,cross+1:Tlen);
```

```
end
% Initial population of 50 chromosomes completed.
% XXXXXXXXXXXXXXXXXXXXX
% Mutation operator applied to 0.05 member of initial population
% XXXXXXXXXXXXXXXXXXXX
ix=ceil(np*rand);
iy=ceil(Tlen*rand);
Ch(ix,iy)=1-Ch(ix,iy);
ixx=ceil(np*rand);
iyy=ceil(Tlen*rand);
Ch(ixx,iyy)=1-Ch(ixx,iyy);
ixy=ceil(np*rand);
iyx=ceil(Tlen*rand);
Ch(ixy,iyx)=1-Ch(ixy,iyx);
%end
%%%%%%%%%%%%%%%%%%%%%%%%%%%%%%%%%%%%%%%%%%%%%%%%%%%%%%%%%%%%%
noit=it;
end

%XXXXXXXXXXXXXXXXXXXXXXXXXXXXXXXXXXXXXX
% First population using both CROSSOVER and MUTATION completed.
%XXXXXXXXXXXXXXXXXXXXXXXXXXXXXXXXXXXXXXX
%[eval index]=sort(eval);
match=zeros(np*maxit,1);
%XXXXXXXXXXXXXXXXXXXXXXXXXXXXXXXXXXXXXXXXXXXXXXXXXXXXXX
% checking the matched solutions according to the most suitable solutions
%
```

```
for in=1:np*maxit
  if ((eval_mag(in)) > 0 & eval_mag(in)< 0.2 )
    if (eval_phase(in)<95 & eval_phase(in)>85)
       match(in,:)=eval_mag(in,:);
    end
  end
end
[match index]=sort(match);
match(np*maxit)
var(index(np*maxit),:)
```

```
%XXXXXXXXXXXXXXXXXXXXXXXX
% dual-feed square patch.m file
%XXXXXXXXXXXXXXXXXXXXXXXX
nv=8;    % number of variables
np=100;   % number of populations
maxit=500;  % number of maximum iterations
%XXXXXXXXXXXXXXXXXXXXXXXXXXXXXXXXXXXXXXXXXX
% Lengths of the parameters
len=[20 20 20 20 20 20 20 20];
Tlen=sum(len);
%XXXXXXXXXXXXXXXXXXXXXXXXXXXXXXXXXXXXXXXXXX
% % Generation of initial population in a matrix Chromosomes of 50 row by row chromosomes (len) in binary form
Ch=round(rand([np,Tlen]));
%XXXXXXXXXXXXXXXXXXXXXXXXXXXXXXXXXXXXXXXXXX

%XXXXXXXXXXXXXXXXXXXXXXXXXXXXXXXXXXXXXXXXXX
% Bounds of the design parameters
lob=[120 120 120 120 0.70 0.70 0.70 0.70]; % Lower bounds
upb=[140 140 140 140 2.5 2.5 2.5 2.5];     % Upper bounds
% XXXXXXXXXXXXXXXXXXXXXXXXXXXXXXXXXXXXXXXXXX
% Converting the binary representations to the real values
%XXXXXXXXXXXXXXXXXXXXXXXXXXXXXXXXXXXXXXXXXX
rang=upb-lob;
num=2.^(len)-1;
lop=cumsum([1 len]);
upp=cumsum([len]);
var=zeros(np*maxit,nv);
```

```
cvar=zeros(np*maxit,1);
eval=zeros(np*maxit,1);
for it=1:maxit
  iteration=it;
  for j=1:np
  phe=zeros([np nv]);
  end
 for ii=1:nv
   index=lop(ii):upp(ii);
   sx=[];
    for j=len(ii)-1:-1:0
      sx=[sx 2^j];
     end

sx=sx';
Chindex=Ch(:,index);
 phe(:,ii)=Chindex*sx;
 phen(:,ii)=lob(ii)+(rang(ii)/num(ii)).*phe(:,ii);
 Phen=phen;
end
c=320;
 x1=Phen(:,1);
 x2=Phen(:,2);
 x3=Phen(:,3);
 x4=Phen(:,4);
 x5=Phen(:,5);
 x6=Phen(:,6);
```

```
x7=Phen(:,7);
x8=Phen(:,8);
% Binary conversion of initial values to real values ends producing the " INITIAL POPULATION"
%XXXXXXXXXXXXXXXXXXXXXXXXXXXXXXXXXXXXXXXXXXXXXXXXXXXXXXXXXXXXXXXXXX
%% Evaluation of  Objective functions formulas for 100 sampled solutions
%XXXXXXXXXXXXXXXXXXXXXXXXXXXXXXXXXXXXXXXXXXXXXXXXXXXXXXXXXXXXXXXXXXx
r1=x2.*((c+i*x2.*tan(x6))./(x2+i*c*tan(x6)));
r11=x1.*((r1+i*x1.*tan(x5))./(x1+i*r1.*tan(x5)));
r3=x4.*((c+i*x4.*tan(x8))./(x4+i*c*tan(x8)));
r33=x3.*((r3+i*x3.*tan(x7))./(x3+i*r3.*tan(x7)));
YIN=1./r11+1./r33;
RIN=1./YIN;
objval=RIN; % Input impedance objective Functioin
ro1=(r1-x1)./(r1+x1);
ro2=(c-x2)./(c+x2);
ro3=(r3-x3)./(r3+x3);
ro4=(c-x4)./(c+x4);
vv=(exp(i.*(x7+x8)).*(1+ro1).*(1+ro2).*(1+ro3.*exp(-2*i*x7)).*(1+ro4.*exp(-2*i*x8)));
vvv=(exp(i.*(x5+x6)).*(1+ro3).*(1+ro4).*(1+ro1.*exp(-2*i*x5)).*(1+ro2.*exp(-2*i*x6)));
v=vv./vvv; % Axial ratio evaluations
if it==1
  var(1:np,:)=phen(1:np,:);
  eval(1:np,:)=objval(1:np,:);
  cvar(1:np,:)=v(1:np,:);
else
  var(1+np*(it-1):np*it,:)=phen(1:np,:);
  eval(1+np*(it-1):np*it,:)=objval(1:np,:);
```

```
  cvar(1+np*(it-1):np*it,:)=v(1:np,:);
end
% sorting the input impedance objective function values
[objval,ind]=sort(objval);
% sorting the CP objective function values
[cvar,ind]=sort(cvar);
segma=8; % is the sharing distance between the chromosomes of the same ranking
% calculating the hamming distance of genotype chromosomes structures
for nn=1:10
   for mm=1:10
      for nm=1:10
      dhammingCh(nm)=sum(abs(Ch(nn)-Ch(mm));
      if segma<dhamming
         shar(nm)=0
      else
         shar(nm)=1-(dhamming(nm)/segma)
      end
   end
end
% calculate the niche for each chromosome
for ii=1:100
   M(Ch(ii))=sum(shar(ii))
end
% calculate the sharing function for each chromosomes
for jj=1:100
Fshare(jj)=objval(jj)/M(jj)
end
```

```
%XXXXXXXXXXXXXXXXXXXXXXXXXXXXXXXXXXXXXXXXXXXX
% Roulette Wheel Selection Procedure
%XXXXXXXXXXXXXXXXXXXXXXXXXXXXXXXXXXXXXXXXXXXX
pro=objval/Fit;
qpro=cumsum(pro);
rrwn=rand(np,1);
sel=zeros(np,Tlen);
for ik=1:np
  for j=2:np
    if rrwn(ik)<qpro(1)
       sel(ik,:)=Ch(1,:);
      elseif rrwn(ik)<qpro(j-1) & rrwn(ik) <= qpro(j)
        sel(ik,:)=Ch(j,:);
     end
    end
  end
  Chc=Ch;
% XXXXXXXXXXXXXXXXXXXX
% Cross over operator
% XXXXXXXXXXXXXXXXXXXX
% Random crossover operators with half of population
bit=ceil(Tlen*rand(1,159));
for ij=2:2:np/2
  sel(ij-1,[bit])=Ch(ij,[bit]);
  sel(ij,[bit])=Chc(ij-1,[bit]);
end
```

```
% XXXXXXXXXXXXXXXXXXXXXXX
% Mutation operator applied to 0.01 member of initial population
% XXXXXXXXXXXXXXXXXXXXXX
pm=0.1;
rm=rand(np,Tlen);
for il=1:np*Tlen
  if rm(il)<pm
    sel(il)=1-sel(il);
  end
end
Ch=sel;
noit=it
end
%XXXXXXXXXXXXXXXXXXXXXXXXXXXXXXXXXXXXXXXXX
% First population using both CROSSOVER and MUTATION completed.
%XXXXXXXXXXXXXXXXXXXXXXXXXXXXXXXXXXXXXXXXX

match=zeros(np*maxit,1);
%XXXXXXXXXXXXXXXXXXXXXXXXXXXXXXXXXXXXXXXXXXXXXXXXXXXXXXXXXXXXXXXXXXXXX
% Checking the matched solutions according to to the most suitsble solutions
for in=1:maxit
  if real(eval(in))<52 & real(eval(in))>48 & abs(imag(eval(in)))<2.5
    if abs(real(cvar(in)))<0.1
      if ((0.95<imag(cvar(in)) & imag(cvar(in))<1.2) | (-1.2<imag(cvar(in)) & imag(cvar(in))<-0.95))
        match(in)=eval(in);
        match1(in)=match(in);
      end
```

```
    end
  end
end
[match index]=sort(match);


%XXXXXXXXXXXXXXXXXXXXXXXXXXXXXXXXXXXXXXXXXXXXXXXXXXXX
%  Transmission line model for cross-aperture coupled patch antenna
XXXXXXXXXXXXXXXXXXXXXXXXXXXXXXXXXXXXXXXXXXXXXXXXXXXXXXXXXXXXXXXXXXXXXXXXXXXXXXX
% The Design Parameters

mu=4*pi*10^(-7);
f=2.45*10^9; %Operate frequency
epso=8.86*10^(-12);
c=3*10^8; % speed of the light
Zo=sqrt(mu/epso);
da=3.15*10^(-3); % patch substrate thickness
epsa=1.5;
Zca=90; % characteristic impedance of the feed line
lamo=c/f; % free space wave-length
Wa=2*10^-3; % width of the slot
epsra=2.33; % relative permittivity of patch substrate
epsrf=2.33; % relative permittivity of feed substrate
df=1.6*10^(-3); % thickness of the feed substrate
Wf=4.6*10^(-3);  % width of the feed line
D=Wf;
lama=c/(f*sqrt(epsa)); % wave length
```

```
ko=(2*pi)/lamo; % wave number
delta=1/30; % quality factor
keff=sqrt((ko^2)*epsra*(1-i*tan(delta))); % effective wave number
epsef=(epsrf+1)/2+((epsrf-1)/2)*(1+12*(df/Wf))^-0.5;
lamf=c/(f*sqrt(epsef));
nv=4;   % number of variables
np=100;  % number of populations
maxit=1000;  % number of maximum iterations
len=[5 5 5 5];
Tlen=sum(len);
%XXXXXXXXXXXXXXXXXXXXXXXXXXXXXXXXXXXXXXXXXX
% Generation of initial population in a matrix Chromosomes of 50 row by row chromosomes (len) in binary form
Ch=round(rand([np,Tlen]));
% Paramete design bounds
lob=[33.*10^-3 34.5*10^-3 20*10^-3 9*10^-3]; % Lower bounds
upb=[33.*10^-3 34.5*10^-3 20*10^-3 9*10^-3]; % Upper bounds

% XXXXXXXXXXXXXXXXXXXXXXXXXXXXXXXXXXXXXXXXXX
% XXXXXXXXXXXXXXXXXXXXXXXXXXXXXXXXXXXXXXXXXX
% Converting the binary representations to the real values a,b, La, Los
rang=upb-lob;
num=2.^(len)-1;
lop=cumsum([1 len]);
upp=cumsum([len]);
var=zeros(np*maxit,nv);
eval=zeros(np*maxit,1);
eval1=zeros(np*maxit,1);
```

```
eval2=zeros(np*maxit,1);
for it=1:maxit
  iteration=it;
  for j=1:np
  phe=zeros([np nv]);
  end
 for ii=1:nv
   index=lop(ii):upp(ii);
   sx=[];
    for j=len(ii)-1:-1:0
      sx=[sx 2^j];
     end

sx=sx';
Chindex=Ch(:,index);
 phe(:,ii)=Chindex*sx;
 phen(:,ii)=lob(ii)+(rang(ii)/num(ii)).*phe(:,ii);
 Phen=phen;
end
% Binary conversion of initial values to real values ends producing the " INITIAL POPULATION"
 %XXXXXXXXXXXXXXXXXXXXXXXXXXXXXXXXXXXXXXXXXXXXXXXXXXXXXXXXXXXXXXXXXXXXXXX
 %%%%%%%%%%%%%%%%%%%%%%%%%%%%%%%%%%%%%%%%%%%%%%%%%%%%%%%%%%%%%%%%%%%%%%%%%
 % Evaluation of  Objective function formulas for 50 sampled solutions
 %XXXXXXXXXXXXXXXXXXXXXXXXXXXXXXXXXXXXXXXXXXXXXXXXXXXXXXXXXXXXXXXXXXXXXXX
a=Phen(:,1);
a=a+da
b=Phen(:,2);
```

```
b=b+da
 La=Phen(:,3);
 Los=Phen(:,4);
 %%%%%%%%%%%%%%%%%%%%%%%%%%%%%%%%%%%%%%%%%%%%%%%%%%%%%%%%%%%%%%%%%%
 % % Evaluation of  Objective functions formulas for 100 sampled solutions
 %XXXXXXXXXXXXXXXXXXXXXXXXXXXXXXXXXXXXXXXXXXXXXX
 eo(1)=1
 eo(2)=0
 eo=eo'
 for mm=1:2
   for nn=1:2
     km(mm)=(mm-1)*pi./a
     kn(nn)=(nn-1)*pi./b
     kmn=sqrt(km(mm).^2+kn(nn).^2)
     Amn=sqrt((eo(mm)*eo(nn))./(a.*b))
   end
 end
 Lae=La-Wf;

epsef=(epsrf+1)/2+((epsrf-1)/2)*(1+12*(df/Wf))^-0.5;
lamf=c/(f*sqrt(epsef));
lama=c/(f*sqrt(epsa));
Zcf=(120*pi)/(sqrt(epsef)*(Wf/df+1.393+0.66*log(Wf/df+1.444)));
Zcan=(da*Zo)./(((a+b)/2)*sqrt(epsra));
Zr=1./((pi*(a+b)/2)/(lamo*Zo)*(0.9+i*(1-0.636*log(((2*pi)/lamo)*da))));
Zp1=2*Zcan.*((Zr+i*Zcan.*tan(2*pi*(f/c)*sqrt(epsra)*(b/2)))./(Zcan+i*Zr.*tan(2*pi*(f/c)*sqrt(epsra)*(b/2))));
Zp2=2*Zcan.*((Zr+i*Zcan.*tan(2*pi*(f/c)*sqrt(epsra)*(a/2)))./(Zcan+i*Zr.*tan(2*pi*(f/c)*sqrt(epsra)*(a/2))));
```

```
%Los=(Los+df);
n1=(2*La)./((a+b)+2.3*da);
ka=2*pi/lama;
D=(120*pi*da)/(Zcf*sqrt(epsef));
%x1=sin(ka*Wa/2)*cot(ka*La/2)*(4/(ka^2*Wa*sqrt(2*D*da)));
x2=sin(ka*Wa/2)*(2*sqrt(2)/(ka*sqrt(Wa*2*da)));
%x3=cot(ka*La/2)*(2/(ka*sqrt(2*D*da)));
%n=x1+x2-x3;
n=x2;
%n=1.011;
%n=x2+x1-x3;
Yap=-2*i*cot(2*pi*Lae/(2*lama))./Zca;
Zap=1./Yap;
Yp1=1./Zp1;
Yp2=1./Zp2;
Zos=-i*Zcf*cot(2*pi*Los/lamf);
% Input impedance objective Functioin
Zin=n.^2.*(1./(n1.^2.*Yp1+Yap)+1./(n1.^2.*Yp2+Yap))+Zos;
Beta=2*pi*(f/c)*sqrt(epsra);
Z10=1./(n1.^2.*Yp1+Yap);
Z01=1./(n1.^2.*Yp2+Yap);
V10=(Z10./(Z10+Z01)).*(1./n1);
V01=(Z01./(Z10+Z01)).*(1./n1);
Vs10=V10./(cosh(i*Beta*b/2)+Zcan.*sinh(i*Beta*b/2)./Zr);
Vs01=V01./(cosh(i*Beta*a/2)+Zcan.*sinh(i*Beta*a/2)./Zr);
for ff=1:np
```

```
  Exm(ff)=norm(Vs10(ff))';
  Eym(ff)=norm(Vs01(ff))';
end
Exm=Exm';
Eym=Eym';
for u=1:np
  phi(u)=atan2(imag(V10(u)),real(V10(u)))-atan2(imag(V01(u)),real(V01(u)));
end
phi=phi';
OB=sqrt(0.5*(Exm.^2+Eym.^2-sqrt(Exm.^4+Eym.^4+2*Exm.^2.*Eym.^2.*cos(2*phi))));
OA=sqrt(0.5*(Exm.^2+Eym.^2+sqrt(Exm.^4+Eym.^4+2*Exm.^2.*Eym.^2.*cos(2*phi))));
AR=OA'./OB';
AR=AR';
% Axial ratio evolutions
AxdB=20*log10(AR);
%AxdB=AxdB';
objval=abs(50-real(Zin))+abs(imag(Zin));
%XXXXXXXXXXXXXXXXXXXXXXXXXXXXXXXXXXXXXXXX
if it==1
  var(1:np,:)=phen(1:np,:);
  eval(1:np,:)=objval(1:np,:);
  eval1(1:np,:)=Zin(1:np,:);
  eval2(1:np,:)=AxdB(1:np,:);
else
  if mod(it,2)==0
    AxdB=AxdB';
  end
```

```
  var(1+np*(it-1):np*it,:)=phen(1:np,:);
  eval(1+np*(it-1):np*it,:)=objval(1:np,:);
  eval1(1+np*(it-1):np*it,:)=Zin(1:np,:);
  eval2(1+np*(it-1):np*it,:)=AxdB(1:np,:);
end
% sorting the input impedance objective function values
[objval,ind]=sort(objval);
% sorting the CP objective function values
[AxdB,ind]=sort(AxdB);
segma=8; % is the sharing distance between the chromosomes of the same ranking
% calculating the hamming distance of genotype chromosomes structures
for nn=1:10
  for mm=1:10
    for nm=1:10
    dhammingCh(nm)=sum(abs(Ch(nn)-Ch(mm));
    if segma<dhamming
      shar(nm)=0
    else
      shar(nm)=1-(dhamming(nm)/segma)
    end
  end
end
% calculate the niche for each chromosome
for ii=1:100
  M(Ch(ii))=sum(shar(ii))
end
```

```
% calculate the sharing function for each chromosomes
for jj=1:100
Fshare(jj)=objval(jj)/M(jj)
end
Fit=sum(objval);
pro=objval/Fit;
qpro=cumsum(pro);
rrwn=rand(np,1);
sel=zeros(np,Tlen);
for ik=1:np
  for j=2:np
    if rrwn(ik)<qpro(1)
       sel(ik,:)=Ch(1,:);
      elseif rrwn(ik)<qpro(j-1) & rrwn(ik) <= qpro(j)
        sel(ik,:)=Ch(j,:);
     end
   end
 end
 Chc=Ch;
 % XXXXXXXXXXXXXXXXXXX
% Cross over operator
% XXXXXXXXXXXXXXXXXXX
bit=ceil(Tlen*rand(1,19));
for ij=2:2:np/2
  sel(ij-1,[bit])=Ch(ij,[bit]);
  sel(ij,[bit])=Chc(ij-1,[bit]);
end
```

```
% XXXXXXXXXXXXXXXXXXXXXX
% Mutation operator applied to 0.01 member of initial population
% XXXXXXXXXXXXXXXXXXXXXX
pm=0.01;
rm=rand(np,Tlen);
for il=1:np*Tlen
  if rm(il)<pm
    sel(il)=1-sel(il);
  end
end
Ch=sel;
noit=it
end
%XXXXXXXXXXXXXXXXXXXXXXXXXXXXXXXXXXXXXXXXXXXXXXXXXX
% First population using both CROSSOVER and MUTATION completed.
%XXXXXXXXXXXXXXXXXXXXXXXXXXXXXXXXXXXXXXXXXXXXXXXXXX
match=zeros(np*maxit,1);
for in=1:np*maxit
  if abs(real(eval(in)))< 5
    if eval2(in)<=.8
      match(in,:)=eval1(in,:);
    end
  end
end
[solution index]=sort(match);
match(index(np*maxit))
%XXXXXXXXXXXXXXXXXXXXXXXXXXXXXXXXXXXXXXXXXXXXXXXXXX
```

```
%XXXXXXXXXXXXXXXXXXXXXXXXXXXXXXXXXXXXXXXXXXXXXXXXXXXXXXXXXXXXXXXXXXXXXXXXXXXXXXX
%  Cavity model for cross-aperture coupled patch antenna
% XXXXXXXXXXXXXXXXXXXXXXXXXXXXXXXXXXXXXXXXXXXXXXXXXXXXXXXXXXXXXXXXXXXXXXXXXXXXXXX
% The Design Parameters

mu=4*pi*10^(-7);
f=2.45*10^9;
epso=8.86*10^(-12);
c=3*10^8;
Zo=sqrt(mu/epso);
da=3.15*10^(-3);
epsa=1.5;Zca=90;
lamo=c/f;
Wa=2*10^-3;
epsra=2.33;
epsrf=2.33;
df=1.6*10^(-3);
Wf=4.6*10^(-3);
D=Wf;
lama=c/(f*sqrt(epsa));
ko=(2*pi)/lamo;
delta=1/30;
keff=sqrt((ko^2)*epsra*(1-i*tan(delta)));
epsef=(epsrf+1)/2+((epsrf-1)/2)*(1+12*(df/Wf))^-0.5;
lamf=c/(f*sqrt(epsef));
%n=1.01*ones(100,1);
```

```
nv=4;    % number of variables
np=100;   % number of populations
maxit=500;  % number of maximum iterations
%XXXXXXXXXXXXXXXXXXXXXXXXXXXXXXXXXXXXXXXXXXXXXXX
% Lengths of the parameters
len=[5 5 5 5];
Tlen=sum(len);
%XXXXXXXXXXXXXXXXXXXXXXXXXXXXXXXXXXXXXXXXXXXXXXX
% Generation of initial population
Ch=round(rand([np,Tlen]));
%XXXXXXXXXXXXXXXXXXXXXXXXXXXXXXXXXXXXXXXXXXXXXXX
% Bounds of the design parameters
lob=[30.*10^-3 30.5*10^-3 15*10^-3 7*10^-3]; % Lower bounds of the parameters
upb=[39.*10^-3 39.5*10^-3 25*10^-3 11*10^-3]; % Upper bounds of the Parameters
% XXXXXXXXXXXXXXXXXXXXXXXXXXXXXXXXXXXXXXXXXXXXXXX
% Converting the binary representations to the real values
rang=upb-lob;
num=2.^(len)-1;
lop=cumsum([1 len]);
upp=cumsum([len]);
var=zeros(np*maxit,nv);
eval=zeros(np*maxit,1);
eval1=zeros(np*maxit,1);
eval2=zeros(np*maxit,1);
for it=1:maxit
  iteration=it;
```

```
  for j=1:np
  phe=zeros([np nv]);
  end
 for ii=1:nv
   index=lop(ii):upp(ii);
   sx=[];
    for j=len(ii)-1:-1:0
      sx=[sx 2^j];
    end

sx=sx';
Chindex=Ch(:,index);
 phe(:,ii)=Chindex*sx;
 phen(:,ii)=lob(ii)+(rang(ii)/num(ii)).*phe(:,ii);
 Phen=phen;
end
a=Phen(:,1);
a=a+da
b=Phen(:,2);
b=b+da
 La=Phen(:,3);
 Los=Phen(:,4);
 %XXXXXXXXXXXXXXXXXXXXXXXXXXXXXXXXXXXXXXXXXXXXXXXXXXXXXXXXXXXXXXXXXXXXXXX
% Derivations of the Objective Functions
 %XXXXXXXXXXXXXXXXXXXXXXXXXXXXXXXXXXXXXXXXXXXXXXXXXXXXXXXXXXXXXXXXXXXXXXXx
 eo(1)=1
 eo(2)=0
```

```
eo=eo'
function [Jmx Jmy I1x I2x I1y I2y]=cav(x,y)
Jmx=(2/(da*Wa))*sin(ka*((La/2)-abs(x-a/2))*cos(km*x);
%XXXXXXXXXXXXXXXXXXXXXXXXXXXXXXXXXXXXXXXXXXXXXXXXXXXXXXXXXXXXXXXXXX%
function PSIy=Akm(x,y)
global ka La b da Wa
for mm=1:10
  for nn=1:10
    km(mm)=(mm-1)*pi./a
    kn(nn)=(nn-1)*pi./b
    kmn(mm,nn)=sqrt(km(mm).^2+kn(nn).^2)
    Amn(mm,nn)=sqrt((eo(mm)*eo(nn))./(a.*b))
    PSIy(mm,nn)=Amn(mm,nn)*km(mm)*sin(km(mm)*x)*cos(kn(nn)*y)
  end
end
%XXXXXXXXXXXXXXXXXXXXXXXXXXXXXXXXXXXXXXXXXXXXXXXXXXXXXXXXXXXXXXXXXXXXXXXXXXXXX
function PSIx=Akn(x,y)
global ka La b da Wa
for mm=1:10
  for nn=1:10
    km(mm)=(mm-1)*pi./a
    kn(nn)=(nn-1)*pi./b
    kmn(mm,nn)=sqrt(km(mm).^2+kn(nn).^2)
    Amn(mm,nn)=sqrt((eo(mm)*eo(nn))./(a.*b))
    PSIx(mm,nn)=Amn(mm,nn)*kn(nn)*cos(km(mm)*x)*sin(kn(nn)*y)
  end
end
```

```
%XXXXXXXXXXXXXXXXXXXXXXXXXXXXXXXXXXXXXXXXXXXXXXXXXXXXXXXXXXXXXXXXXXXXXXXXXXX
function I2=SINY(x)
global ka La b da Wa
I2=sin(ka*((La/2)-abs(x-a/2))*cos(km*x)
%XXXXXXXXXXXXXXXXXXXXXXXXXXXXXXXXXXXXXXXXXXXXXXXXXXXXXXXXXXXXXXXXXXXXXXXX
function I3=SINY(x)
global ka La b da Wa
I3=sin(km*x)
%XXXXXXXXXXXXXXXXXXXXXXXXXXXXXXXXXXXXXXXXXXXXXXXXXXXXXXXXXXXXXXXXXXXXXXXX
function I1=SINY(y)
global ka La b da Wa
I1=sin(kn*y)
%XXXXXXXXXXXXXXXXXXXXXXXXXXXXXXXXXXXXXXXXXXXXXXXXXXXXX
function J1=SINX(x)
global ka La a da Wa
ka=60;
La=0.18;
a=0.30;
Wa=0.02;
da=0.015
J1=(200./(da*Wa))*(sin(ka*((La/2)-abs(x-a/2))))./sin(ka*La/2))
%XXXXXXXXXXXXXXXXXXXXXXXXXXXXXXXXXXXXXXXXXXXXXXXXXXXXXXXXXXXXXXXXXXX
function J2=SINY(y)
global ka La b da Wa
J2=(2/(da*Wa))*(sin(ka*((La/2)-abs(y-b/2)))/sin(ka*La/2))
%XXXXXXXXXXXXXXXXXXXXXXXXXXXXXXXXXXXXXXXXXXXXXXXXXXXXXXXXXXXXXXXXXXXXXXXX
function F=integ(Theta)
```

```
global b lam0
F=(sin(((b.*pi)/lam0)*cos(Theta))./cos(Theta)).^2.*(sin(Theta)).^3;
%XXXXXXXXXXXXXXXXXXXXXXXXXXXXXXXXXXXXXXXXXXXXXXXXXXXXXXXXXXXXXXXXXXXXX
global b lam0
lam0=122.449;
Ls=[43.6745 43.7964];
for i=1:length(Ls)
  b=Ls(i);
  takaml(i)=quad('integ',0,pi,[],[])
end
%XXXXXXXXXXXXXXXXXXXXXXXXXXXXXXXXXXXXXXXXXXXXX
%%%%%%%%%%%%%%%%%%%%%%%%%%%%%%%%%%%%%%%%%%%%%%%%%%%%%%%%%%%%%%%%%%%%%%%%%%%%%%
%%%%%%%%%%%%%%
% Sorting the values for all above calculations
if it==1
  var(1:np,:)=phen(1:np,:);
  eval(1:np,:)=objval(1:np,:);
  eval1(1:np,:)=Zin(1:np,:);
  eval2(1:np,:)=AxdB(1:np,:);
else
  if mod(it,2)==0
    AxdB=AxdB';
  end

  var(1+np*(it-1):np*it,:)=phen(1:np,:);
  eval(1+np*(it-1):np*it,:)=objval(1:np,:);
  eval1(1+np*(it-1):np*it,:)=Zin(1:np,:);
```

```
end
%XXXXXXXXXXXXXXXXXXXXXXXXXXXXXXXXXXXXXXXXXXXXXXXXXXXXXXXXXXXXXXXXXXXXXXX
% Mutation operators
pm=0.01;
rm=rand(np,Tlen);
for il=1:np*Tlen
  if rm(il)<pm
    sel(il)=1-sel(il);
  end
end
Ch=sel;
%XXXXXXXXXXXXXXXXXXXXXXXXXXXXXXXXXXXXXXXXXXXXXXXXXXXXXXXXXXXXXXXXXXXXXXX
noit=it
end
%XXXXXXXXXXXXXXXXXXXXXXXXXXXXXXXXXXXXXXXXXXXXXXXXXXXXXXXXXXXXXXXXXXXXXXX
% Checking the matched solutions according to the most suitable solutions
% input impedance plus or minus 5,
% Axial ratio between Zero and 0.8 dB
match=zeros(np*maxit,1);
for in=1:np*maxit
  if abs(real(eval(in)))< 5
    if eval2(in)<=.8
      match(in,:)=eval1(in,:);
    end
  end
end
[solution index]=sort(match);
```

```
match(index(np*maxit))
%XXXXXXXXXXXXXXXXXXXXXXXXXXXXXXXXXXXXXXXXXXXXXXXXX
%XXXXXXXXXXXXXXXXXXXXXXXXXXXXXXXXXXXXXXXXXXXXXXXXXXX


function [Jmx Jmy I1x I2x I1y I2y]=cav(x,y)
Jmx=(2/(da*Wa))*sin(ka*((La/2)-abs(x-a/2))*cos(km*x);
%XXXXXXXXXXXXXXXXXXXXXXXXXXXXXXXXXXXXXXXXXXXXXXXXXXXXXXXXXXXXX%
function PSIy=Akm(x,y)
global ka La b da Wa
for mm=1:10
   for nn=1:10
     km(mm)=(mm-1)*pi./a
     kn(nn)=(nn-1)*pi./b
     kmn(mm,nn)=sqrt(km(mm).^2+kn(nn).^2)
     Amn(mm,nn)=sqrt((eo(mm)*eo(nn))./(a.*b))
     PSIy(mm,nn)=Amn(mm,nn)*km(mm)*sin(km(mm)*x)*cos(kn(nn)*y)
   end
end
%XXXXXXXXXXXXXXXXXXXXXXXXXXXXXXXXXXXXXXXXXXXXXXXXXXXXXXXXXXXXXXXXXXXXXXXX
function PSIx=Akn(x,y)
global ka La b da Wa
for mm=1:10
   for nn=1:10
     km(mm)=(mm-1)*pi./a
     kn(nn)=(nn-1)*pi./b
     kmn(mm,nn)=sqrt(km(mm).^2+kn(nn).^2)
```

```
  eval2(1+np*(it-1):np*it,:)=AxdB(1:np,:);
end
 % Calculations of the fitness functions
Fit=sum(objval);
pro=objval/Fit;
%XXXXXXXXXXXXXXXXXXXXXXXXXXXXXXXXXXXXXXXX
% Roulette Wheel Selection Procedures

qpro=cumsum(pro);
rrwn=rand(np,1);
sel=zeros(np,Tlen);
for ik=1:np
  for j=2:np
    if rrwn(ik)<qpro(1)
       sel(ik,:)=Ch(1,:);
      elseif rrwn(ik)<qpro(j-1) & rrwn(ik) <= qpro(j)
        sel(ik,:)=Ch(j,:);
     end
    end
 end
 Chc=Ch;
 %XXXXXXXXXXXXXXXXXXXXXXXXXXXXXXXXXXXXXXXXXXXXXXXXXXXXXXXXXXXXXXXX
% Random crossover operators with half of population
bit=ceil(Tlen*rand(1,19));
for ij=2:2:np/2
  sel(ij-1,[bit])=Ch(ij,[bit]);
  sel(ij,[bit])=Chc(ij-1,[bit]);
```

```
end
%XXXXXXXXXXXXXXXXXXXXXXXXXXXXXXXXXXXXXXXXXXXXXXXXXXXXXXXXXXXXXXXX
% Mutation operators
pm=0.01;
rm=rand(np,Tlen);
for il=1:np*Tlen
  if rm(il)<pm
    sel(il)=1-sel(il);
  end
end
Ch=sel;
%XXXXXXXXXXXXXXXXXXXXXXXXXXXXXXXXXXXXXXXXXXXXXXXXXXXXXXXXXXXXXXXX
noit=it
end
%XXXXXXXXXXXXXXXXXXXXXXXXXXXXXXXXXXXXXXXXXXXXXXXXXXXXXXXXXXXXXXXX
% Checking the matched solutions according to the most suitable solutions
% input impedance plus or minus 5,
% Axial ratio between Zero and 0.8 dB
match=zeros(np*maxit,1);
for in=1:np*maxit
  if abs(real(eval(in)))< 5
    if eval2(in)<=.8
      match(in,:)=eval1(in,:);
    end
  end
end
[solution index]=sort(match);
```

```
match(index(np*maxit))
%XXXXXXXXXXXXXXXXXXXXXXXXXXXXXXXXXXXXXXXXXXXXXXX
%XXXXXXXXXXXXXXXXXXXXXXXXXXXXXXXXXXXXXXXXXXXXXXXXX


function [Jmx Jmy I1x I2x I1y I2y]=cav(x,y)
Jmx=(2/(da*Wa))*sin(ka*((La/2)-abs(x-a/2))*cos(km*x);
%XXXXXXXXXXXXXXXXXXXXXXXXXXXXXXXXXXXXXXXXXXXXXXXXXXXXXXXXX%
function PSIy=Akm(x,y)
global ka La b da Wa
for mm=1:10
   for nn=1:10
     km(mm)=(mm-1)*pi./a
     kn(nn)=(nn-1)*pi./b
     kmn(mm,nn)=sqrt(km(mm).^2+kn(nn).^2)
     Amn(mm,nn)=sqrt((eo(mm)*eo(nn))./(a.*b))
     PSIy(mm,nn)=Amn(mm,nn)*km(mm)*sin(km(mm)*x)*cos(kn(nn)*y)
   end
end
%XXXXXXXXXXXXXXXXXXXXXXXXXXXXXXXXXXXXXXXXXXXXXXXXXXXXXXXXXXXXXXXXXXXX
function PSIx=Akn(x,y)
global ka La b da Wa
for mm=1:10
   for nn=1:10
     km(mm)=(mm-1)*pi./a
     kn(nn)=(nn-1)*pi./b
     kmn(mm,nn)=sqrt(km(mm).^2+kn(nn).^2)
```

```
    Amn(mm,nn)=sqrt((eo(mm)*eo(nn))./(a.*b))
    PSIx(mm,nn)=Amn(mm,nn)*kn(nn)*cos(km(mm)*x)*sin(kn(nn)*y)
  end
end
%XXXXXXXXXXXXXXXXXXXXXXXXXXXXXXXXXXXXXXXXXXXXXXXXXXXXXXXXXXXXXXXXXXXXX
function I2=SINY(x)
global ka La b da Wa
I2=sin(ka*((La/2)-abs(x-a/2))*cos(km*x)
%XXXXXXXXXXXXXXXXXXXXXXXXXXXXXXXXXXXXXXXXXXXXXXXXXXXXXXXXXXXXXXXXXXX
function I3=SINY(x)
global ka La b da Wa
I3=sin(km*x)
%XXXXXXXXXXXXXXXXXXXXXXXXXXXXXXXXXXXXXXXXXXXXXXXXXXXXXXXXXXXXXXXXXXX
function I1=SINY(y)
global ka La b da Wa
I1=sin(kn*y)
%XXXXXXXXXXXXXXXXXXXXXXXXXXXXXXXXXXXXXXXXXXXXXXXXXX
function J1=SINX(x)
global ka La a da Wa
ka=60;
La=0.18;
a=0.30;
Wa=0.02;
da=0.015
J1=(200./(da*Wa))*(sin(ka*((La/2)-abs(x-a/2)))./sin(ka*La/2))
%XXXXXXXXXXXXXXXXXXXXXXXXXXXXXXXXXXXXXXXXXXXXXXXXXXXXXXXXXXXXXXXX
function J2=SINY(y)
```

```
global ka La b da Wa
J2=(2/(da*Wa))*(sin(ka*((La/2)-abs(y-b/2)))/sin(ka*La/2))
%XXXXXXXXXXXXXXXXXXXXXXXXXXXXXXXXXXXXXXXXXXXXXXXXXXXXXXXXXXXXXXXXXXXX
function F=integ(Theta)
global b lam0
F=(sin(((b.*pi)/lam0)*cos(Theta))./cos(Theta)).^2.*(sin(Theta)).^3;
%XXXXXXXXXXXXXXXXXXXXXXXXXXXXXXXXXXXXXXXXXXXXXXXXXXXXXXXXXXXXXXXXXXX
global b lam0
lam0=122.449;
Ls=[43.6745 43.7964];
for i=1:length(Ls)
  b=Ls(i);
  takaml(i)=quad('integ',0,pi,[],[])
end
%XXXXXXXXXXXXXXXXXXXXXXXXXXXXXXXXXXXXXXXXXXXX
```

Transmission-line modelling of the cross-aperture-coupled circular polarised microstrip antenna

B.Al-Jibouri, T.Vlasits, E.Korolkiewicz, S.Scott and A.Sambell

Abstract: A circular polarised antenna fed through a cross-aperture in a ground plane by means of a microstrip feed line is modelled, and an original analysis using a transmission-line method is presented. The field linkages from the feed to the slots and the slots to the antenna are modelled as voltage transformers, which are employed in the synthesis of the overall transmission-line model of the structure. This analysis allows for an efficient computational procedure to predict the input impedance of the structure. The application of a full wave simulation package and the experimental results obtained for the structure support the theory presented.

1 Introduction

In Europe, the USA and the far-east, increasing interest is being expressed in developing road pricing, in order to reduce traffic on motorways and city congestion, using a two-way, high-speed digital data communication system between a road-side unit (RSU) and an on-board unit (OBU), which can be conveniently placed behind the windscreen of a vehicle [1]. The OBU antenna needs to be small in size with a low profile, inexpensive to manufacture and be mechanically and operationally robust. Further, circular polarisation needs to be used so that the OBU can be placed behind the windscreen of a vehicle in any orientation [2]. Circular polarisation and the other requirements can be met by using a nearly square patch antenna with a cross-slot feed in the ground plane. The advantage of a slot feed is that it does not require an external polariser and expensive dielectric materials [3, 4]. With aperture coupling, it is possible to match the feed line by varying the slot length and the length of the open-circuit stub which is an extension to the feed line. This eliminates the need for an external matching network and ensures that the size of the OBU is small.

In this paper, a transmission-line model of a single-feed microstrip line coupled to a nearly square patch antenna, through an equal length cross-slot in the ground plane, is developed. Equal slots lengths are used to maintain the symmetry of excitation of the patch and to ensure generation of circular polarisation having a good axial ratio. As the slot length can be greater than half the patch width, the matching condition is maintained over a wider bandwidth [5, 6]. Theoretical and experimental investigations on the single-feed microstrip line antenna have been reported using a single slot, two cross-slots of unequal lengths and a ring antenna [7–10].

IEE Proceedings online no. 20000069

DOI: 10.1049/ip-map:20000069

Paper first received 25th March and in revised form 22nd October 1999

The authors are with the School of Engineering, University of Northumbria at Newcastle, Ellison Building, Ellison Place, Newcastle upon Tyne, NE1 8ST, UK

Some of the authors of this paper have reported on the modelling of a cross-aperture coupled patch antenna using a transmission-line model [11]. An original analysis of a single-feed cross-slot aperture-coupled circular polarised antenna is presented here. The transmission-line model is derived and results are obtained for both mismatched and matched conditions. For a matched antenna, the resulting axial ratio as a function of frequency is examined.

2 Derivation of the transmission-line model of a cross-slot aperture-fed antenna

The general mode of excitation of a single-feed antenna can be separated into two modes by perturbing the antenna patch with a slot or some other form of a truncated segment [12, 13]. In this paper, circular polarisation is obtained using a nearly square patch of dimensions a and b as shown in Fig. 1.

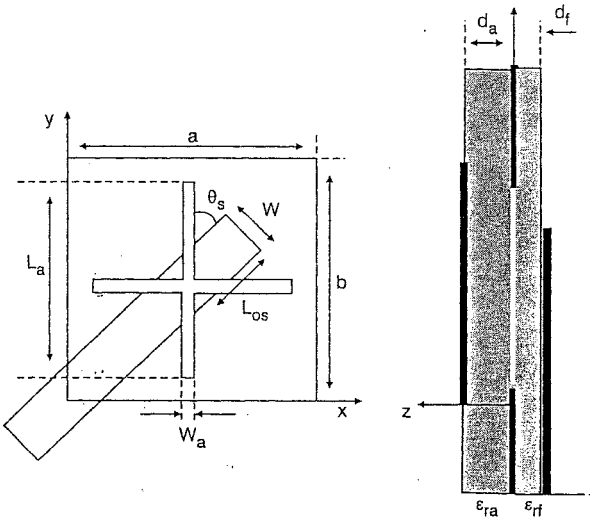

Fig. 1 *Design parameters of the cross-aperture-coupled microstrip antenna, a = 32.1mm, b = 34.5mm, W = 4.724mm, L_{os} = 9mm, L_a = 18mm, W_a = 2mm, ε_{ra} = 2.33, ε_{rf} = 2.33, d_a = 3.15mm, d_f = 1.575mm and θ_s = ±45°*

Since the patch dimensions a and b are nearly equal, the resonant wave numbers $k_{01} = \pi/b$ and $k_{10} = \pi/a$ of the modes are close. Consequently, it can be assumed that the total quality loss factor Q is the same for both modes [14],

and the resonant wave number k_o can be replaced by an effective wave number k_e [15], where

$$k_e \approx k_o\sqrt{\varepsilon_r}[1 - j/Q] \quad (1)$$

with the condition that $Q > 1$. The loss factor Q includes conduction, dielectric, radiation and surface wave losses of the structure. For thin substrates, the losses due to the surface waves are very small and so can be neglected [16]. The radiation loss is inversely proportional to the thickness of the substrate and it is usually the dominant term [17].

For circular polarisation the dimensions a and b of the patch are related [18] by

$$b = a\left[1 + \frac{1}{Q}\right] \quad (2)$$

The self-admittances of the patch radiating slots are $Y_{sx} = G_{sx} + jB_{sx}$ and $Y_{sy} = G_{sy} + jB_{sy}$, whereas Y_{mx} and Y_{my} are the coupling coefficients between the radiating edges. Accurate expressions for the self-admittance Y_s and the mutual admittances Y_m have been derived [19, 20]. It has been shown [21] that the effect of surface waves can be neglected provided $k_0 d_a\sqrt{\varepsilon_r} \leq 0.3$, where d_a is the substrate thickness, a condition normally satisfied when patch antennas are realised using substrates having low values of ε_r and/or are operating at low frequencies.

The modelling of the transformer slots to patch coupling assumes that only the dominant modes of the electric and magnetic fields are present, so that the transformer ratios n_a and n_b are equal to the fraction of current flowing through the slot over the total intensity [22], hence

$$n_a = L_a/a \quad \text{and} \quad n_b = L_a/b \quad (3)$$

The two short-circuit transmission lines of length $L_a/2$ in Fig. 2 represent the stored energy near the slots. The modelling of the transformer feed to slot coupling is restricted to a small aperture with a narrow width compared with the slot length [23, 24].

The discontinuity voltage on the microstrip line due to an aperture field $\boldsymbol{E}$ is given by [25]

$$\Delta v = \iint \boldsymbol{E} \times (\hat{z}) \cdot \boldsymbol{h}_m ds \quad (4)$$

where $\boldsymbol{E}$ is the electric field in the aperture plane, and $\boldsymbol{h}_m$ is the normalised magnetic field of the field feed line having a uniform distribution given by [23]

$$\boldsymbol{h}_m = \frac{1}{\sqrt{W_e d_a}} \cdot \hat{y} \qquad |y| \leq \frac{W_e}{2}$$
$$= 0 \qquad \text{otherwise} \quad (5)$$

where W_e is the effective width of the microstrip line [26] and d_a is the thickness of the substrate.

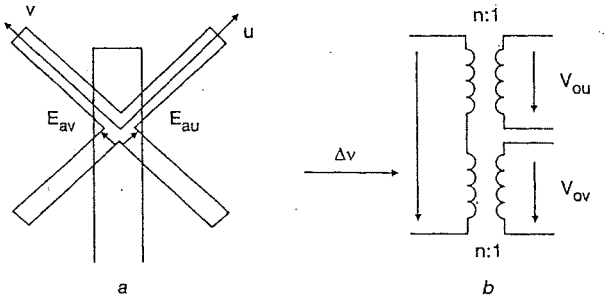

Fig.3 *Equivalent circuit of the cross-aperture to microstrip line transition*

For the cross-slot aperture the total field $\boldsymbol{E}$ results from a combination of the two-aperture fields $\boldsymbol{E}_{au}$, $\boldsymbol{E}_{av}$ in the directions $\boldsymbol{u}$ and $\boldsymbol{v}$ as shown in Fig. 3*a*. The discontinuity voltage for the cross-slot aperture is therefore given by

$$\Delta v = \iint_{s_1} (\boldsymbol{E}_{au}) \times (\hat{z}) \cdot \boldsymbol{h}_m ds_1 + \iint_{s_2} (\boldsymbol{E}_{av}) \times (\hat{z}) \cdot \boldsymbol{h}_m ds_2 \quad (6)$$

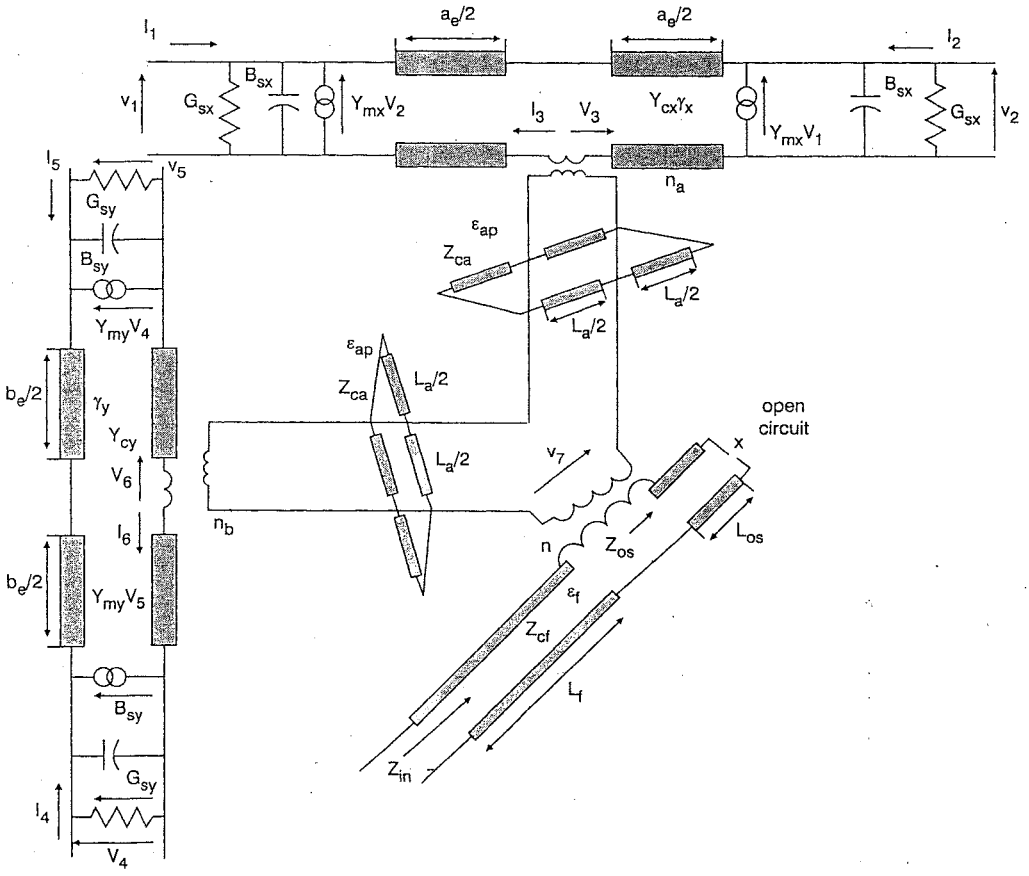

Fig.2 *The transmission-line equivalent circuit*

where s_1 and s_2 are the intersections of each slot geometry with the footprint of the microstrip line. Assuming the slots are narrow the electric field in the aperture plane is normal to the slot length and constant across the width of the slot. The field satisfying the boundary conditions in the slots is given by [4]

$$E_{au} = \frac{V_0}{W_a} \frac{\sin\left[k_a\left(\frac{L_a}{2} - |u|\right)\right]}{\sin\left(k_a \frac{L_a}{2}\right)} \hat{v} \qquad |u| \le \frac{L_a}{2} \quad |v| \le \frac{W_a}{2}$$
$$= 0 \qquad \text{otherwise} \tag{7}$$

V_0 is the slot voltage developed at the centre of the slot parallel to the u axis, and, k_a is the wave number of the aperture [27]. For each slot, the relationship between V_0 and the discontinuity voltage nV_{ou} (or nV_{ov}) on the microstrip line is represented by a transformer with a turns ratio n and is given by [23]

$$\iint_{s_1} \boldsymbol{E}_{au} \times (-\hat{z}) \cdot \boldsymbol{h}_m ds_1 = nV_{ou} \tag{8}$$

and

$$\iint_{s_2} \boldsymbol{E}_{av} \times (-\hat{z}) \cdot \boldsymbol{h}_m ds_2 = nV_{ov} \tag{9}$$

Thus the resulting discontinuity voltage is given by

$$\Delta v = nV_{ou} + nV_{ov} = n\left(V_{ou} + V_{ov}\right) \tag{10}$$

Consequently, the transition between a cross-aperture and a microstrip line can be modelled by the series connection of two ideal transformers having a turns ratio n, as shown in Fig. 3*b*. The discontinuity voltage due to the cross slot is obtained from eqns. 4 and 7 and is given by

$$\Delta v = \frac{V_0}{W_a\sqrt{2W_e d_a}\sin\left(k_a \frac{L_a}{2}\right)} \times \left[\iint_{s_1} \sin\left[k_a\left(\frac{L_a}{2} - |u|\right)\right] dudv + \iint_{s_2} \sin\left[k_a\left(\frac{L_a}{2} - |v|\right)\right] dudv\right] \tag{11}$$

The integration above is performed over the overlapping area of the aperture and the effective width of the microstrip line. Three mutually distinct cases arise for the forms of the domains of integration, see Figs. 4*a*, *b* and *c*.

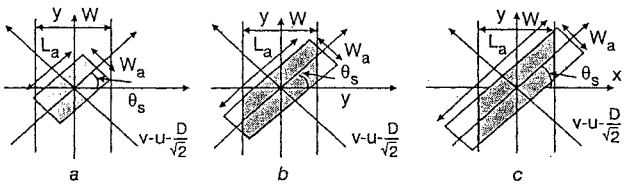

Fig. 4 *Aperture to microstrip line transition*

The values of the above integral for the cases, *a*, *b* and *c* are given by

$$I_a = \frac{2W_a}{k_a}\left\{1 - \cos\left(\frac{k_a L_a}{2}\right)\right\} \tag{12}$$

$$I_b = \frac{1}{k_a}\left(\frac{L_a}{2} + \frac{W_e}{\sqrt{2}} + \frac{W_a}{2}\right)\cos\left(\frac{k_a W_a}{2}\right) + \frac{2}{k_a^2}\cos\left[k_a\left(\frac{L_a}{2} - \frac{W_e}{\sqrt{2}}\right)\right]\sin\left(\frac{k_a W_a}{2}\right) - \frac{2}{k_a^2}\sin\left[k_a\left(\frac{L_a}{2} - \frac{W_e}{\sqrt{2}}\right)\right]\cos\left(\frac{k_a W_a}{2}\right) - \frac{2W_a}{k_a}\cos\left(\frac{k_a L_a}{2}\right) \tag{13}$$

and

$$I_c = \frac{4}{k_a^2}\sin\left(\frac{k_a W_a}{2}\right)\cos\left[k_a\left(\frac{L_a}{2} - \frac{W_e}{\sqrt{2}}\right)\right] - \frac{2W_a}{k_a}\cos\left(\frac{k_a L_a}{2}\right) \tag{14}$$

3 The input impedance of the antenna at the apertures

The operation of the circularly polarised patch antenna shown in Fig. 1 is based on the two orthogonal apertures fields exciting the patch independently in the x and y directions. Two sets of the characteristic impedance Z_{cx} and Z_{cy} and the propagation constants γ_x and γ_y need to be evaluated.

The admittance matrix $[Y_x]$ connecting the currents and voltages at the three ports of the transmission-line model in the x direction (Fig. 2) is

$$[Y_x] = \begin{bmatrix} Y_{sx}+Y_{cx}\coth\left(\gamma_x\frac{a_e}{2}\right) & -Y_{mx} & \frac{-Y_{cx}}{\sinh\left(\gamma_x\frac{a_e}{2}\right)} \\ -Y_{mx} & Y_{sx}+Y_{cx}\coth\left(\gamma_x\frac{a_e}{2}\right) & \frac{-Y_{cx}}{\sinh\left(\gamma_x\frac{a_e}{2}\right)} \\ \frac{-Y_{cx}}{\sinh\left(\gamma_x\frac{a_e}{2}\right)} & \frac{-Y_{cx}}{\sinh\left(\gamma_x\frac{a_e}{2}\right)} & 2Y_{cx}\coth\left(\gamma_x\frac{a_e}{2}\right) \end{bmatrix} \tag{15}$$

It then follows that the input admittance Y_{in_x} of the transmission line is given by

$$Y_{in_x} = 2Y_{cx}\left[\coth\left(\frac{\gamma_x a_e}{2}\right) - \frac{Y_{cx}}{\sinh^2\left(\frac{\gamma_x a_e}{2}\right)\left[Y_{sx} + Y_{cx}\coth\left(\frac{\gamma_x a_e}{2}\right) - Y_m\right]}\right] \tag{16}$$

Similarly, the input admittance, Y_{in_y}, for the patch excitation in the y direction (Fig. 2) can be derived. The self-admittance Y_{ap} of the two slots, considered as short circuited slot lines is given by

$$Y_{ap} = -\frac{2j}{Z_{ca}} \cdot \cot\left(k_a \frac{L_a}{2}\right) \tag{17}$$

The expressions for the total admittances of the two apertures are

$$Y_{ta} = n_a^2 Y_{in_x} + Y_{ap} \quad \text{and} \quad Y_{tb} = n_b^2 Y_{in_y} + Y_{ap} \tag{18}$$

As the cross-slot can be modelled by two transformers connected in series, the input impedance 'seen' by the microstrip feed line under the centre of the aperture is given by

$$Z_{in} = n^2 \cdot \left(\frac{1}{Y_{ta}} + \frac{1}{Y_{tb}}\right) - jZ_{cf} \cdot \cot\left(k_f L_{os}\right) \tag{19}$$

4 Determination of the axial ratio

Single-feed circular polarised patches typically provide good performance, but only in a limited frequency band contained between the resonant frequencies of the two orthogonal modes. The value of the best axial ratio within this band and the frequency where it occurs is strongly influenced by the dimensions of the patch. Therefore it is important for the theoretical model to predict the values of the axial ratio as a function of frequency so that the dimensions of the antenna can be accurately determined.

The axial ratio is calculated in terms of the voltages V_2, V_5 of the two radiating edges, the voltages V_3, V_6 at the centre of the two apertures, and, also the feed line voltage V_7.

The voltages V_3, V_6 are determined by

$$V_3 = V_7 \frac{Y_{tb}}{Y_{ta} + Y_{tb}} \quad \text{and} \quad V_6 = V_7 \frac{T_{ta}}{Y_{ta} + Y_{tb}} \tag{20}$$

where Y_{ta} and Y_{tb} are given by eqn. 18. The voltages V_2 and V_5 are related to voltages V_3 and V_6. These relations can be obtained using the transmission-line theory and are given by

$$V_2 = V_3 \frac{1}{\cosh\left(\gamma_x \frac{a_e}{2}\right) + \frac{Y_{sx}}{Y_{cx}} \sinh\left(\gamma_x \frac{a_e}{2}\right)} \tag{21}$$

and

$$V_5 = V_6 \frac{1}{\cosh\left(\gamma_y \frac{b_e}{2}\right) + \frac{Y_{sx}}{Y_{cy}} \sinh\left(\gamma_y \frac{b_e}{2}\right)} \tag{22}$$

The phase difference between the x and y components of the field in the boresight direction (phase error, ϕ_e) is the same as the phase difference between V_2 and V_5, namely

$$\phi_e = \arg(V_5) - \arg(V_2) \tag{23}$$

The x and y directed field components in the far field are directly proportional to the voltages V_2 and V_5, respectively, therefore the amplitude error A_e is given by

$$A_e = \frac{|V_5|}{|V_2|} \tag{24}$$

The axial ratio achieved in the design is obtained from the amplitude and phase error as given by [17]

$$AR = \sqrt{\frac{1 + A_e^2 + [1 + A_e^4 + 2A_e^2 \cos(2\phi_e)]^{\frac{1}{2}}}{1 + A_e^2 - [1 + A_e^4 + 2A_e^2 \cos(2\phi_e)]^{\frac{1}{2}}}} \tag{25}$$

which can be evaluated using eqns. 20–25 at a given frequency.

5 Comparison between measured and calculated results

To compare the results predicted by the transmission-line model with practical results, three unmatched antennas were fabricated having different slot lengths. A feed line of fixed length 51mm, as measured from the centre of the slots, was used. The measured and computed input impedance of the antennas as a function of frequency over a range of 2–3GHz, in 0.2GHz steps, are shown in Fig. 5. Good agreement is obtained over the complete frequency range specified. In the design of circular polarised antennas for optimum axial ratio, the important part of the impedance response is between the resonant frequencies of the TM_{10} and TM_{01} modes, and the optimum value is located at the cusp in the impedance locus. As can be seen for the cases *b* and *c* of Fig. 5, the position of the cusp is within 2% of that predicted by the transmission-line model. The largest error of some 5% occurs for case *a*, where the slot lengths are small, and is due to the assumption that the excitation modes on the antenna are perfectly orthogonal, whereas in the fabricated antenna this is only approximated. The structure generates orthogonal modes, the amplitude of which will be a maximum when the aspect ratio of the slots is large. It is therefore expected that the computed and practical results will have the best agreement for those slots.

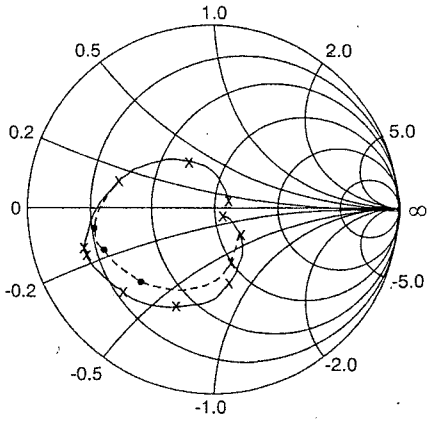

Fig. 6 *Input impedance of a matched cross-aperture coupled antenna of frequency range = 2.25–2.7GHz; steps = 50MHz*
—○— calculated, —×— measured

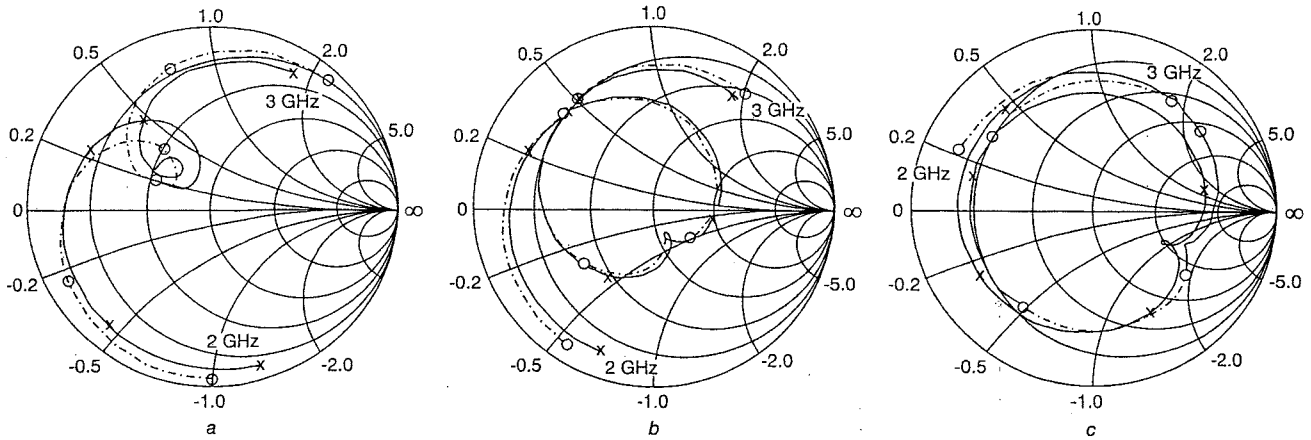

Fig. 5 *Measured and calculated input impedances for mismatched aperture-coupled antennas, a = 32.1mm, b = 34.5mm, L_{os} = 9mm, W = 4.724mm, W_a = 2mm, ε_{ra} = 2.33, ε_{rf} = 2.33, d_a = 31.5mm, d_f = 1.575mm*
(a) L_a = 15mm
(b) L_a = 20mm
(c) L_a = 25mm
—○— calculated, —×— measured

The input impedance of the matched antenna in Fig. 1 as a function of frequency, based on the transmission-line model, is shown in Fig. 6 together with the measured result. There is good agreement between the predicted and measured results.

Fig. 7 shows the calculated axial ratio using the transmission-line model compared with that obtained experimentally and using a full wave simulation package [29]. The agreement is generally good and the results show a minimum axial ratio at 2.4GHz, compared with 2.45GHz for the measurement result. However, part of this error is due to the difficulty of measuring the axial ratio accurately.

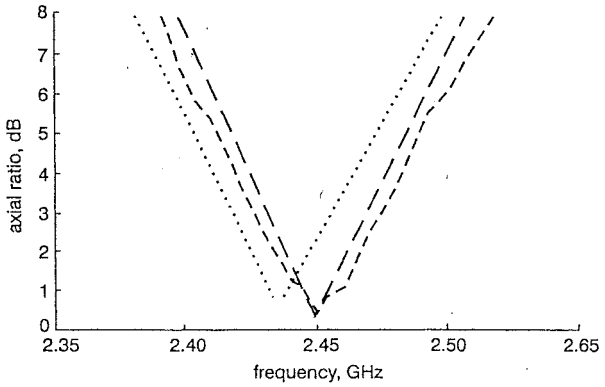

Fig. 7 *Axial ratio of the cross-aperture-coupled antenna shown in Figs. 1 and 2*
- - - - measured result
— — — full-wave simulation
····· transmission-line method

6 Conclusion

In this paper, an original analysis of a cross-aperture-coupled circularly polarised antenna based on the transmission-line method has been presented. In order to apply the transmission-line method, the transition between a cross-slot aperture and a microstrip line has been investigated, and it is found that the cross-aperture can be regarded as the series connection of two orthogonal slots, which excite the patch in the x and y directions independently. This allowed the representation of the patch by transmission-line networks. The input impedance and the axial ratio of the cross-aperture-coupled circular polarised antenna have been derived. The model is computationally efficient for optimising the dimensions of the antenna for circular polarisation and input matching.

This paper has shown that the transmission-line model of the cross-slot circular polarised antenna agrees with the simulated results based on the full-wave analysis and the experimental results. It also confirms that the effect of the surface wave can be neglected if thin substrates are used. The advantage of the transmission-line model is that it allows for good understanding of the coupling mechanism between the antenna and the slots and between the slots and the microstrip line. The derived equations allow for direct computation on a PC and then the transmission-line model is readily simulated using P-Spice.

7 References

1 CHAN, T.K., and KOROLKIEWICZ, E.: 'Design of microwave transponder for automatic debiting systems'. Proceedings of the 24th European Microwave conference, Cannes, France, Sept. 1994, pp. 1025–1029
2 VLASITS, T., KOROLKIEWICZ, E., and SAMBELL, A.: 'A 5.8 GHz microwave link for automatic debiting applications', *Microw. J.*, 1995, **38**, (7), pp. 80–87
3 IWASAKI, H.: 'A circularly polarized small-size microstrip antenna with a cross-slot', *IEEE Trans. Antennas Propag.*, 1996, **44**, (10), pp. 399–1401
4 SULLIVAN, P.L., and SCHAUBERT, D.H.: 'Analysis of an aperture coupled microstrip antenna', *IEEE Trans. Antennas Propag.*, 1986, **34**, (8), pp. 977–984
5 TARGONSKI, S.D., and POZAR, D.M.: 'Design of wideband circularly polarised aperture-coupled microstrip antennas', *IEEE Trans. Antennas Propag.*, 1993, **41**, (2), pp. 214–220
6 TASO, C.H., HWANG, Y.M., KILLBURG, F., and DIETRICH, F.: 'Aperture-coupled patch antennas with wide bandwidth and dual polarisation capabilities'. Digest of the 1988 IEEE Antennas and Propagation symposium, 1988, pp. 936–939
7 HIMDI, M., DANIEL, J.P., and TERRENT, C.: 'Transmission line analysis of aperture-coupled microstrip antenna', *Electron. Lett.*, 1989, **25**, (18), pp. 1229–1230
8 BAHATTACHARYYA, A.K., ANTAR, Y.M.M., and ITTIPIBOON, A.: 'Full wave analysis for the equivalent circuit of an inclined slot on a microstrip ground plane', *IEE Proc. H, Microw. Antennas Propag.*, 1992, **139**, (3), pp. 245–250
9 DAS, M.K.: 'Generalised multiport reciprocity analysis of surface-to surface transitions between multiple printed transmission lines', *IEEE Trans. Microw. Theory Tech.*, 1993, **41**, (6/7), pp. 1164–1177
10 SAWAMURA, M., TABATA, M., and HANEISHI, M.: 'Radiation properties of ring microstrip antenna fed by symmetrical cross slot'. Digest of the IEEE Antennas and Propagation Society international symposium, California, 1995, Vol. 4, pp. 2074–2077
11 VLASITS, T., KOROLKIEWICZ, E., and SAMBELL, A.: 'Analysis of cross-aperture coupled patch antenna using transmission line model', *Electron. Lett.*, 1996, **32**, (21), pp. 1934–1935
12 HANESHI, M., and YOSHIDA, S.: 'A design of circularly polarized rectangular microstrip antenna by one-point feed', *Electron. Commun. Jpn.*, 1981, **64-B**, (4) pp. 46–54
13 HALL, P.S., and DAHELE J.S.: 'Dual and circularly polarized microstrip antennas' *in* LEE, K.F. and CHEN W. (Eds.): 'Advances in microstrip and printed antennas' (Wiley Interscience, 1997), Chap. 4, pp. 163–222
14 JACKSON, D.R., LONG, S.A., WILLIAMS, J.T., and DAVIS, V.B.: 'Computer-aided design of rectangular microstrip antennas' *in* LEE, K.F. and CHEN W. (Eds.): 'Advances in microstrip and printed antennas' (Wiley Interscience, 1997), Chap. 5, pp. 223–271
15 RICHARDS, W.F., ZINCHER, J.R., CLORK, R.D., and LONG, S.A.: 'Experimental and theoretical investigation of the inductance associated with a microstrip antenna feed', *Electromagnetics*, 1985, **3**, (3/4), pp. 327–346
16 CARVER, K.R., and MINK, J.W.: 'Microstrip antenna technology', *IEEE Trans. Antennas Propag.*, 1988, **AP-29**, pp. 2–24
17 BALAINS, C.A.: 'Antenna theory: analysis and design' (John Wiley & Sons, 1997), Chap. 14, pp. 761–762
18 RICHARDS, W.F.: 'Antenna handbook: theory, application and design' (Van Nostrand Reinhold Co., 1988), Chap. 10
19 PUES, H., and VAN DE CAPELLE, A.: 'Accurate transmission line model for the rectangular microstrip patch antenna', *IEE Proc. H, Microw. Antennas Propag.*, 1984, **31**, (6), pp. 334–340
20 LIVE, E.: 'Improved formulas for input impedance of coax-fed microstrip patch antennas', *IEE Proc. H, Microw. Antennas Propag.*, 1982, **129**, (4), pp. 161–164
21 JAMES, J.R., and HENDERSON, A.: 'High-frequency behaviour of microstrip open-circuit terminations', *IEE. J. Microw., Opt.*, 1974, **3**, (5), pp. 205–218
22 HIMDI, M., DANIEL, J.P., and TERRET, C.: 'Analysis of aperture coupled microstrip antenna using cavity method', *Electron. Lett.*, 1989, **27**, (5), pp. 391–392
23 RAO, J.S., JOSHI, K.K., and DAS, B.N.: 'Analysis of small aperture coupling between rectangular waveguide and microstrip line', *IEEE Trans. Microw. Theory Tech.*, 1988, **29**, (2), pp. 150–154
24 AKHAVAN, H.G., and MIRSHEKARSYAHKAL, D.: 'Approximation model for microstrip fed slot antenna', *Electron. Lett.*, **30**, (23), pp. 1902–1903
25 ANTAR, Y.M.M., BHATTECHARYYA, A.K., and ITTIPIBOON, A.: 'Microstrip line-slot line transition analysis using the spectral domain technique', *IEEE Trans. Microw. Theory Tech.*, 1992, **40**, (3), pp. 515–523
26 VAN DE CAPELLE: 'Transmission line model for rectangular microstrip antennas' *in* 'Handbook of microstrip antennas' (Peter Peregrinus Ltd., 1989), Chap. 10
27 COHN, S.B.: 'Slot line on a dielectric substrate', *IEEE Trans. Microw. Theory Tech.*, 1969, **17**, (10), pp. 786–778
28 MOSIG, J.R, HALL, R.C., and GARDIOL, F.E.: 'Numerical analysis of microstrip patch antennas' *in* 'Handbook of microstrip antennas' (Peter Peregrinus Ltd, 1989), Chap. 8
29 Boulder Microwaves Technologies, Ensemble, Product information brochure, 1995

Cavity model of circularly polarised cross-aperture-coupled microstrip antenna

B.Al-Jibouri, H.Evans, E.Korolkiewicz, E.G.Lim, A.Sambell and T.Viasits

Abstract: A cavity model is used to analyse an aperture-fed nearly square circularly polarised patch antenna. The form of the aperture is that of a symmetric cross-slot that couples the excitation between a single microstrip feed line and the patch antenna. Using equivalent magnetic current sources at the slots, the modal electric and magnetic fields under the patch are obtained, and hence analytical expressions for the patch admittances at the aperture are derived and used to obtain an equivalent circuit of the circular polarised antenna. Good agreement is obtained between the circuit modelling and practical results.

1 Introduction

An aperture-coupled feed structure is known to have a number of practical advantages. Since the feed network and radiating patch are on separate substrates, both the thickness and dielectric properties of each substrate can be independently chosen to meet requirements of the feed network to the radiation patch. The isolation of the patch from the feed network by the ground plane minimises spurious feed radiation. A compact structure can be realised using aperture coupling, and as the aperture is positioned below the centre of the patch, the symmetry ensures good circular polarisation [1, 2].

Aperture-coupled structures have been fully analysed using spectral domain [3, 4] and spatial solution [5] methods. These analyses can be used to examine the effects of the design parameters on the performance of the antenna with good accuracy. However, these approaches are numerically intensive and, because of the poor convergence of the reaction integrals and tabulation of Green's functions, can be time consuming and require expensive computations. In addition, these methods of analysis do not produce equivalent circuit models which are suitable for small-scale CAD computations.

Although not as rigorous as the above full-wave analyses, the cavity model [6, 7] can readily be used to derive equivalent circuit models of the antennas for implementation of small-scale CAD. It has been shown that in the cavity model the antenna substrate thickness must be much less than the free-space wavelength [8], a condition normally satisfied in the design of microstrip patch antenna structures.

In this paper the cavity model has been used to model a circularly polarised nearly square patch antenna, excited using a microstrip feed line via a symmetrical cross-slot [1, 2, 9]. In contrast to a single slot structure the cross-slot structure allows the use of slot length greater than half the patch width; hence the matching condition is maintained over a wider bandwidth. In addition, the equal cross slots provide symmetry of excitation of the patch and ensure generation of circular polarisation with good axial ratio [2, 10]. An equivalent circuit model has been derived and used to determine the input impedance of the antenna and further, based on the derived equivalent circuit the conditions for producing a good axial ratio are also examined. It is shown that there is a close agreement between the practical results and those predicted by the cavity model approach.

IEE Proceedings online no. 20010498

DOI: 10.1049/ip-map:20010498

Paper first received 13th September 2000 and in revised form 23rd April 2001

The authors are with the School of Engineering, University of Northumbria at Newcastle, Ellison Building, Ellison Place, Newcastle upon Tyne, NE1 8ST, UK

2 Field distribution

The structure of the antenna using a symmetrical cross-slot is shown in Fig. 1, where it is assumed that the electric field distribution in each of the two orthogonal apertures is in the form of a single piece-wise sinusoidal mode [3]. The electric field in the aperture parallel to the y axis has only an x-directed component E_{ax}, given by

$$E_{ax} = \frac{V_{0y}}{W_a}\frac{\sin\left[k_a\left(\frac{L_a}{2}-\left|y-\frac{b}{2}\right|\right)\right]}{\sin\left(k_a\frac{L_a}{2}\right)} \quad \begin{matrix}\frac{a-W_a}{2} \le x \le \frac{a+W_a}{2} \\ \frac{b-L_a}{2} \le y \le \frac{b-L_a}{2} \\ z = 0\end{matrix}$$
$$= 0, \qquad \text{otherwise} \tag{1}$$

where V_{0y} is the voltage at the centre of the aperture parallel to the y axis and k_a is the wave number of the aperture determined by Cohn's method [11]. Similarly, the electric field in the aperture parallel to the x axis has only a y component E_{ay} given by

$$E_{ay} = \frac{V_{0x}}{W_a}\frac{\sin\left[k_a\left(\frac{L_a}{2}-\left|x-\frac{b}{2}\right|\right)\right]}{\sin\left(k_a\frac{L_a}{2}\right)} \quad \begin{matrix}\frac{a-L_a}{2} \le x \le \frac{a+L_a}{2} \\ \frac{b-W_a}{2} \le y \le \frac{b-W_a}{2} \\ z = 0\end{matrix}$$
$$= 0, \qquad \text{otherwise} \tag{2}$$

where V_{0x} is the voltage at the middle of the aperture parallel to the x axis.

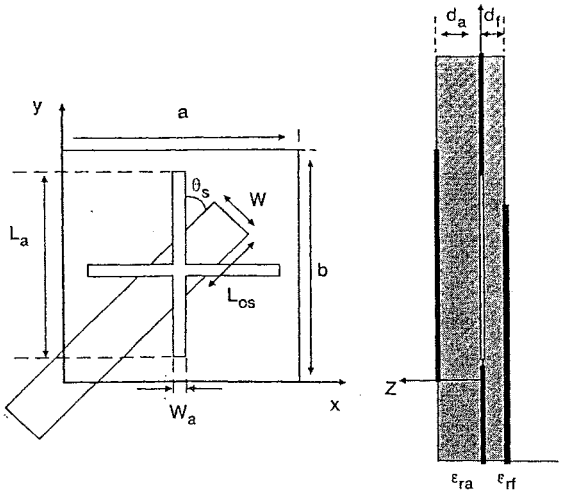

Fig. 1 *Design parameters of cross-aperture coupled microstrip antenna*
$a = 32.1$mm, $b = 34.5$mm, $W = 4.724$mm, $L_{os} = 9$mm, $L_a = 18$mm, $W_a = 2$mm, $\varepsilon_{ra} = 2.33$, $\varepsilon_{rf} = 2.33$, $d_a = 3.15$mm, $d_f = 1.575$mm, $\phi_s = \pm 45°$

The cavity models [12] assumes that the tangential magnetic field at the cavity side walls is zero to a good approximation, and, by the equivalence principle [12], the magnetic currents in each of the two apertures just above the ground plane are then given by

$$M_{ax} = -2E_{ay} \tag{3}$$

and

$$M_{ay} = 2E_{ax} \tag{4}$$

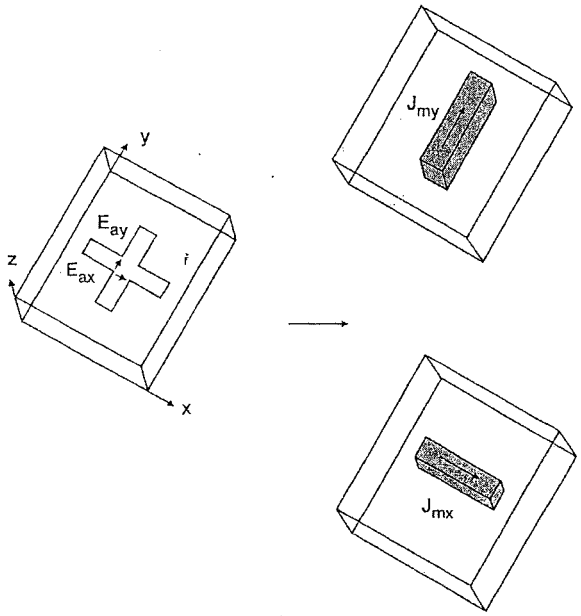

Fig. 2 *Equivalent magnetic currents replacing electric fields in aperture*

The equivalent magnetic current density excitation is assumed to be uniformly distributed in the cavity volume above the slot [13] as shown in Fig. 2. The corresponding current densities J_{mx} and J_{my} in the aperture cavities are therefore given by

$$J_{mx} = \frac{-2V_{0x}}{d_a W_a} \frac{\sin\left[k_a\left(\frac{L_a}{2} - \left|x - \frac{a}{2}\right|\right)\right]}{\sin\left(k_a \frac{L_a}{2}\right)} \quad \begin{matrix} \frac{a-L_a}{2} \le x \le \frac{a+L_a}{2} \\ \frac{b-W_a}{2} \le y \le \frac{b+W_a}{2} \\ 0 \le z \le d_a \end{matrix}$$
$$= 0, \qquad \text{otherwise} \tag{5}$$

and

$$J_{my} = \frac{2V_{0y}}{d_a W_a} \frac{\sin\left[k_a\left(\frac{L_a}{2} - \left|y - \frac{b}{2}\right|\right)\right]}{\sin\left(k_a \frac{L_a}{2}\right)} \quad \begin{matrix} \frac{a-W_a}{2} \le x \le \frac{a+W_a}{2} \\ \frac{b-L_a}{2} \le y \le \frac{b+L_a}{2} \\ 0 \le z \le d_a \end{matrix}$$
$$= 0, \qquad \text{otherwise} \tag{6}$$

The magnetic field H inside the cavity volume due to the magnetic current density J_m is given by Maxwell's equation

$$\nabla \times \nabla \times H - k^2 H = -j\omega\mu_0 J_m \tag{7}$$

For the magnetic fields H_x, H_y which only have x and y components, eqn. 7 reduces to the following two differential equations:

$$\frac{\partial^2 H_y}{\partial x \partial y} - \frac{\partial^2 H_x}{\partial y^2} - k^2 H_x = -j\omega\mu_0 J_{mx} \tag{8}$$

$$\frac{\partial^2 H_x}{\partial x \partial y} - \frac{\partial^2 H_y}{\partial y^2} - k^2 H_y = -j\omega\mu_0 J_{my} \tag{9}$$

The solution of the above differential equations can be expressed in the following eigenfunction expansion form

$$H_x = \sum_m \sum_n B_{x,mn} \Psi_{x,mn} \tag{10}$$

$$H_y = \sum_m \sum_n B_{y,mn} \Psi_{y,mn} \tag{11}$$

where $B_{x,mn}$ and $B_{y,mn}$ are the unknown mode coefficients and $\Psi_{x,mn}$ and $\Psi_{y,mn}$ are the eigenfunction of eqns. 8 and 9. The eigenfunction must satisfy the associated homogenous equations and hence

$$\frac{\partial_2 \Psi_{x,mn}}{\partial x \partial y} - \frac{\partial^2 \Psi_{y,mn}}{\partial y^2} - k_{mn} \Psi_{x,mn} = 0 \tag{12}$$

$$\frac{\partial_2 \Psi_{y,mn}}{\partial x \partial y} - \frac{\partial^2 \Psi_{x,mn}}{\partial y^2} - k_{mn} \Psi_{y,mn} = 0 \tag{13}$$

where k_{mn} are the associated eigenvalues. The boundary conditions on the four magnetic walls are

$$\Psi_{x,mn} = 0 \text{ at } y = 0 \text{ and } y = b$$
$$\Psi_{y,mn} = 0 \text{ at } x = 0 \text{ and } x = a \tag{14}$$

The eigenfunctions are given by

$$\Psi_{x,mn} = A_{mn} . k_n . \cos(k_m x) \sin(k_n y) \tag{15}$$

$$\Psi_{y,mn} = A_{mn} . k_n . \cos(k_n y) \sin(k_m x) \tag{16}$$

with

$$A_{mn} = \sqrt{\frac{\chi_m \chi_n}{ab}}, \text{ where } \chi_p = \begin{cases} 1 & \text{if } p = 0 \\ 2 & \text{if } p \neq 0 \end{cases} \tag{17}$$

and

$$k_m = \frac{m.\pi}{a}, \qquad k_n = \frac{n.\pi}{b} \tag{18}$$

The mode coefficients $B_{x,mn}$ and $B_{y,mn}$ can be found by substituting for H_x and H_y from eqns. 10 and 11 into the non-homogeneous differential eqns. 8 and 9 to give

$$\sum_m \sum_n B_{x,mn}(k_{mn}^2 - k^2)\Psi_{x,mn} = -j\omega\varepsilon J_{mx} \tag{19}$$

and,

$$\sum_m \sum_n B_{y,mn}(k_{mn}^2 - k^2)\Psi_{y,mn} = -j\omega\varepsilon J_{my} \tag{20}$$

Multiplying eqn. 19 with the mode function $\Psi_{x,m'n'}$ and eqn. 20 by $\Psi_{y,m'n'}$ and integrating over the cavity volume o

the patch gives

$$\sum_m \sum_n B_{x,mn}(k_{mn}^2 - k^2) \int_0^a \int_0^b \Psi_{x,mn}\Psi_{x,m'n'}\,dxdy$$

$$= -j\omega\varepsilon \int_0^a \int_0^b J_{mx}\Psi_{x,m'n'}\,dxdy \tag{21}$$

and,

$$\sum_m \sum_n B_{y,mn}(k_{mn}^2 - k^2) \int_0^a \int_0^b \Psi_{y,mn}\Psi_{y,m'n'}\,dxdy$$

$$= -j\omega\varepsilon \int_0^a \int_0^b J_{my}\Psi_{y,m'n'}\,dxdy \tag{22}$$

The orthogonal properties of $\Psi_{x,mn}$ and $\Psi_{y,mn}$ are

$$\int_0^a \int_0^b \Psi_{x,mn}\Psi_{x,m'n'}\,dxdy = \begin{cases} k_n^2 & \text{if } m = m' \text{ and } n = n' \\ 0 & \text{otherwise} \end{cases} \tag{23}$$

$$\int_0^a \int_0^b \Psi_{y,mn}\Psi_{y,m'n'}\,dxdy = \begin{cases} k_m^2 & \text{if } m = m' \text{ and } n = n' \\ 0 & \text{otherwise} \end{cases} \tag{24}$$

hence

$$B_{x,mn} = \frac{j\omega\varepsilon}{(k^2 - k_{mn}^2)\cdot k_n^2} \int_0^a \int_0^b J_{mx}\Psi_{x,mn}\,dxdy \tag{25}$$

$$B_{y,mn} = \frac{j\omega\varepsilon}{(k^2 - k_{mn}^2)\cdot k_m^2} \int_0^a \int_0^b J_{my}\Psi_{y,mn}\,dxdy \tag{26}$$

Substituting for J_{mx}, J_{my}, $\Psi_{x,mn}$ and $\Psi_{y,mn}$ integrating eqns. 25 and 26 gives

$$B_{x,mn} = \frac{-j\omega\varepsilon.A_{mn}V_{0x}}{d_a k_n\cdot(k^2 - k_{mn}^2)} \cdot \frac{4\,\mathrm{sinc}\left(k_n\frac{W_a}{2}\right)\sin\left(\frac{n\pi}{2}\right)\cos\left(\frac{m\pi}{2}\right)}{\sin\left(k_a\frac{L_a}{2}\right)} \cdot \frac{k_a\left[\cos\left(k_m\frac{L_a}{2}\right) - \cos\left(k_a\frac{L_a}{2}\right)\right]}{k_a^2 - k_m^2} \tag{27}$$

$$B_{y,mn} = \frac{-j\omega\varepsilon.A_{mn}V_{0y}}{d_a k_m\cdot(k^2 - k_{mn}^2)} \cdot \frac{4\,\mathrm{sinc}\left(k_m\frac{W_a}{2}\right)\sin\left(\frac{m\pi}{2}\right)\cos\left(\frac{n\pi}{2}\right)}{\sin\left(k_a\frac{L_a}{2}\right)} \cdot \frac{k_a\left[\cos\left(k_n\frac{L_a}{2}\right) - \cos\left(k_a\frac{L_a}{2}\right)\right]}{k_a^2 - k_n^2} \tag{28}$$

With the known mode coefficients the components of the magnetic field in the patch cavity are given by

$$H_x = \sum_m \sum_n A_{mn}B_{x,mn}k_n \cos(k_m x)\sin(k_n y) \tag{29}$$

$$H_y = \sum_m \sum_n A_{mn}B_{y,mn}k_m \sin(k_m x)\cos(k_n y) \tag{30}$$

Finally the electric field E_z can be determined from the Maxwell equation

$$E_{z(x,y)} = \frac{1}{j\omega\varepsilon}\left[\frac{dH_y}{dx} - \frac{dH_x}{dy}\right] \tag{31}$$

giving

$$E_{z(x,y)} = \frac{1}{j\omega\varepsilon}\sum_m \sum_n A_{mn}C_{mn}\cos(k_m x)\cos(k_n y) \tag{32}$$

where

$$C_{mn} = B_{x,mn}k_m^2 - B_{y,mn}k_n^2 \tag{33}$$

Hence, the electromagnetic fields in the volume of the patch are now known and defined by eqns. 29, 30 and 32. The losses in the cavity can also be taken into account by replacing k by an effective wave number [5]

$$k_{eff}^2 = k_0^2\varepsilon_r(1 - j\delta_{eff}) \tag{34}$$

where δ_{eff} is the effective loss tangent, which includes the radiation and copper dielectric losses [14].

3 Input impedance

The admittances of the patch of the two orthogonal apertures can be evaluated using the energy conservation theorem [12] and are given by

$$Y_{x,ant} = \frac{\iiint_V H_x J_{mx}^* dv}{|V_{0x}|^2} \quad \text{and} \quad Y_{y,ant} = \frac{\iiint_V H_y J_{my}^* dv}{|V_{0y}|^2} \tag{35}$$

Substituting the expression for the magnetic field from eqns. 29 and 30 and the magnetic current density from eqns. 5 and 6, and performing the integration, the following analytical formulas are obtained for the admittance values of the antenna at the apertures:

$$Y_{x,ant} = \sum_m \sum_n \frac{16\cdot j\omega\varepsilon\cdot A_{mn}^2}{d_a\left((k^*)^2 - k_{mn}^2\right)} \cdot \left\{\frac{\mathrm{sinc}\left(k_n\frac{W_a}{2}\right)\sin\left(\frac{n\pi}{2}\right)\cos\left(\frac{m\pi}{2}\right)}{\sin\left(k_a\frac{L_a}{2}\right)} \cdot \frac{k_a\left[\cos\left(k_m\frac{L_a}{2}\right) - cos\left(k_a\frac{L_a}{2}\right)\right]}{k_a^2 - k_m^2}\right\}^2 \tag{36}$$

$$Y_{y,ant} = \sum_m \sum_n \frac{16\cdot j\omega\varepsilon\cdot A_{mn}^2}{d_a\left((k^*)^2 - k_{mn}^2\right)} \cdot \left\{\frac{\mathrm{sinc}\left(k_m\frac{W_a}{2}\right)\sin\left(\frac{m\pi}{2}\right)\cos\left(\frac{n\pi}{2}\right)}{\sin\left(k_a\frac{L_a}{2}\right)} \cdot \frac{k_a\left[\cos\left(k_n\frac{L_a}{2}\right) - cos\left(k_a\frac{L_a}{2}\right)\right]}{k_a^2 - k_n^2}\right\}^2 \tag{37}$$

The self-admittance of the aperture is obtained by considering it as two short-circuited slot lines of length $L_a/2$, and, is thus given by

$$Y_{ap} = -\frac{2j}{Z_{ca}} \cot\left(k_a \frac{L_a}{2}\right) \tag{38}$$

Finally, the input impedance of the antenna is given by the following expression:

$$Z_{in} = \frac{n^2}{Y_{x,ant} + Y_{ap}} + \frac{n^2}{Y_{y,ant} + Y_{ap}} - jZ_f \cot(k_f L_{os}) \tag{39}$$

where n is the turns ratio of the microstrip to aperture impedance transformation for the two orthogonal apertures, k_f is the wave number of the feed line [10, 13].

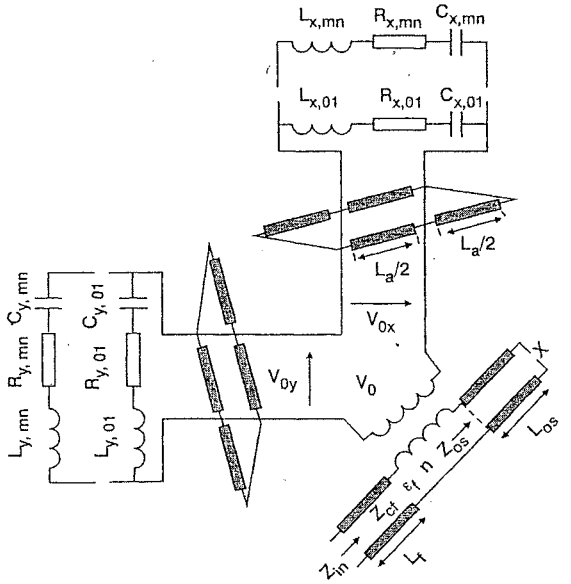

Fig. 3 *Equivalent circuit based on cavity model*

4 Equivalent circuit

Using the developed analytic expressions (see eqns. 36 and 37) for the patch admittances at the apertures, it is possible to draw an equivalent circuit of the cross-aperture coupled CP antenna based on the cavity method as shown in Fig. 3. Eqns. 36 and 37 can be written in the form

$$Y_{x,ant} = \sum_m \sum_n \frac{16 \cdot j\omega\varepsilon \cdot A_{mn}^2}{d_a[\omega^2 - \omega_{mn}^2]\left(1 + j\delta_{eff}\frac{\omega^2}{\omega_{mn}^2}\right)} \cdot \left\{ \frac{\operatorname{sinc}\left(k_n \frac{W_a}{2}\right) \sin\left(\frac{n\pi}{2}\right) \cos\left(\frac{m\pi}{2}\right)}{\sin\left(k_a \frac{L_a}{2}\right)} \cdot \frac{k_a\left[\cos\left(k_m \frac{L_a}{2}\right) - \cos\left(k_a \frac{L_a}{2}\right)\right]}{k_a^2 - k_m^2} \right\}^2 \tag{40}$$

$$Y_{y,ant} = \sum_m \sum_n \frac{16 \cdot j\omega\varepsilon \cdot A_{mn}^2}{d_a[\omega^2 - \omega_{mn}^2]\left(1 + j\delta_{eff}\frac{\omega^2}{\omega_{mn}^2}\right)} \cdot \left\{ \frac{\operatorname{sinc}\left(k_m \frac{W_a}{2}\right) \sin\left(\frac{m\pi}{2}\right) \cos\left(\frac{n\pi}{2}\right)}{\sin\left(k_a \frac{L_a}{2}\right)} \cdot \frac{k_a\left[\cos\left(k_n \frac{L_a}{2}\right) - \cos\left(k_a \frac{L_a}{2}\right)\right]}{k_a^2 - k_n^2} \right\}^2 \tag{41}$$

Each of these formulas corresponds to the expression of the admittance of $m \times n$ series RCL circuits, which are all connected in parallel (see Fig. 3). The equivalent circuit of the patch admittance, as seen by the slot parallel to the y axis, have the following circuit elements:

$$L_{x,mn} = \frac{d_a}{16\varepsilon c^2 A_{mn}^2} \cdot \left\{ \frac{\operatorname{sinc}\left(k_n \frac{W_a}{2}\right) \sin\left(\frac{n\pi}{2}\right) \cos\left(\frac{m\pi}{2}\right)}{\sin\left(k_a \frac{L_a}{2}\right)} \cdot \frac{k_a\left[\cos\left(k_m \frac{L_a}{2}\right) - \cos\left(k_a \frac{L_a}{2}\right)\right]}{k_a^2 - k_m^2} \right\}^2$$

$$C_{x,mn} = L_{x,mn}^{-1} \frac{\varepsilon_{ra} k_{mn}^2}{c^2} \qquad R_{x,mn} = L_{x,mn} k_{mn} c\delta_{eff} \tag{42}$$

Similarly, the equivalent circuit of the patch, as seen by the slot parallel to the x axis, have circuit elements:

$$L_{y,mn} = \frac{d_a}{16\varepsilon c^2 A_{mn}^2} \cdot \left\{ \frac{\operatorname{sinc}\left(k_m \frac{W_a}{2}\right) \sin\left(\frac{m\pi}{2}\right) \cos\left(\frac{n\pi}{2}\right)}{\sin\left(k_a \frac{L_a}{2}\right)} \cdot \frac{k_a\left[\cos\left(k_n \frac{L_a}{2}\right) - \cos\left(k_a \frac{L_a}{2}\right)\right]}{k_a^2 - k_n^2} \right\}^2$$

$$C_{y,mn} = L_{y,mn}^{-1} \frac{\varepsilon_{ra} k_{mn}^2}{c^2} \qquad R_{y,mn} = L_{y,mn} k_{mn} c\delta_{eff} \tag{43}$$

5 Axial ratio

For the calculation of the axial ratio, the far field components of the antenna are first determined in the boresight. This is performed by replacing the electrical field at the edges of the patch by equivalent magnetic currents as given by [15]

$$M = 2d_a \cdot E_{z(x,y)} \cdot z \times n \tag{44}$$

where $\boldsymbol{n}$ is the outward normal unit vector to the magnetic wall at the edges of the patch. Substituting the expression of the electric field from eqn. 32 gives the following values of magnetic currents at the four edges of the patch:

$$M_{x(x,y=0)} = \frac{d_a}{j\omega\varepsilon} \sum_m \sum_n A_{mn} C_{mn} \cos(k_m x) \tag{45}$$

$$M_{x(x,y=b)} = -\frac{d_a}{j\omega\varepsilon} \sum_m \sum_n A_{mn} C_{mn} \cos(k_m x) \cdot (-1)^n \tag{46}$$

$$M_{y(x=0,y)} = \frac{d_a}{j\omega\varepsilon} \sum_m \sum_n A_{mn} C_{mn} \cos(k_n y) \tag{47}$$

$$M_{y(x=a,y)} = -\frac{d_a}{j\omega\varepsilon} \sum_m \sum_n A_{mn} C_{mn} \cos(k_n y) \cdot (-1)^m \tag{48}$$

The electrical field $\boldsymbol{E}(r)$ caused by an infinitesimally smal magnetic current element ($d\boldsymbol{M}$) is obtained as

$$\boldsymbol{E}(r) = \frac{jk_0 e^{-jk_0 r}}{4\pi r} \cdot r \times d\boldsymbol{M} \tag{49}$$

where $\mathbf{r}$ is the unit vector pointing from the magnetic current element to the observation point and r is the distance between the magnetic current and the observation point. The electric field radiated by the patch is obtained by integrating eqn. 49 along the edges of the patch. In the boresight, the components of the electric field are, therefore, given by

$$E_x = \frac{d_a k_0 e^{-jk_0 r}}{4\pi\omega\varepsilon r} \cdot \int_0^b \left(\sum_m \sum_n A_{mn} C_{mn} \cos(k_n y) \cdot (-1)^m - \sum_m \sum_n A_{mn} C_{mn} \cos(k_n y) \right) dy \tag{50}$$

$$E_y = \frac{d_a k_0 e^{-jk_0 r}}{4\pi\omega\varepsilon r} \cdot \int_0^a \left(\sum_m \sum_n A_{mn} C_{mn} \cos(k_m y) - \sum_m \sum_n A_{mn} C_{mn} \cos(k_m y) \cdot (-1)^n \right) dx \tag{51}$$

which simplify to

$$E_x = \frac{d_a k_0 e^{-jk_0 r}}{4\pi\omega\varepsilon r} \cdot \sum_m \sum_n A_{mn} C_{mn} \cdot [(-1)^m - 1] \tag{52}$$

$$E_y = \frac{d_a k_0 e^{-jk_0 r}}{4\pi\omega\varepsilon r} \cdot \sum_m \sum_n A_{mn} C_{mn} \cdot [1 - (-1)^n] \tag{53}$$

where,

$$C_{m0} = \begin{cases} -B_{y,m0} & \text{if } m \text{ odd} \\ 0 & \text{if } m \text{ even} \end{cases} \tag{54}$$

$$C_{0n} = \begin{cases} B_{x,0n} & \text{if } n \text{ odd} \\ 0 & \text{if } n \text{ even} \end{cases} \tag{55}$$

Therefore

$$E_x = \frac{d_a k_0 e^{-jk_0 r}}{4\pi\omega\varepsilon r} \cdot \sum_m A_{m0} B_{y,m0} \tag{56}$$

$$E_y = \frac{d_a k_0 e^{-jk_0 r}}{4\pi\omega\varepsilon r} \cdot \sum_n A_{0n} B_{x,0n} \tag{57}$$

The expressions for $B_{x,0n}$ and $B_{y,m0}$ can be written in the following form:

$$B_{x,0n} = V_{0x} \cdot B'_{x,0n} \tag{58}$$

$$B_{y,m0} = V_{0y} \cdot B'_{y,m0} \tag{59}$$

where

$$B'_{x,0n} = \frac{j\omega\varepsilon . A_{m0}}{d_a k_n \cdot (k^2 - k_n^2)} \cdot \frac{4\,\mathrm{sinc}\left(k_n \frac{W_a}{2}\right) \sin\left(\frac{n\pi}{2}\right)}{\sin\left(k_a \frac{L_a}{2}\right)} \cdot \frac{k_a \left[1 - \cos\left(k_a \frac{L_a}{2}\right)\right]}{k_a^2} \tag{60}$$

$$B'_{y,m0} = \frac{j\omega\varepsilon . A_{0n}}{d_a k_n \cdot (k^2 - k_m^2)} \cdot \frac{4\,\mathrm{sinc}\left(k_m \frac{W_a}{2}\right) \sin\left(\frac{m\pi}{2}\right)}{\sin\left(k_a \frac{L_a}{2}\right)} \cdot \frac{k_a \left[1 - \cos\left(k_a \frac{L_a}{2}\right)\right]}{k_a^2} \tag{61}$$

From the equivalent circuit, the voltages V_{0x} and V_{0y} can be expressed as

$$V_{0x} = V_0 \cdot \frac{(Y_{x,ant} + Y_{ap})^{-1}}{(Y_{x,ant} + Y_{ap})^{-1} + (Y_{y,ant} + Y_{ap})^{-1}} \tag{62}$$

$$V_{0y} = V_0 \cdot \frac{(Y_{y,ant} + Y_{ap})^{-1}}{(Y_{x,ant} + Y_{ap})^{-1} + (Y_{y,ant} + Y_{ap})^{-1}} \tag{63}$$

Substituting these results into the expressions for the electric field components in the boresight gives the computational formulas for the field components E_x and E_y

$$E_x = \frac{V_0 d_a k_0 e^{-jk_0 r}}{2\pi\omega\varepsilon r} \cdot \frac{(Y_{x,ant} + Y_{ap})^{-1}}{(Y_{x,ant} + Y_{ap})^{-1} + (Y_{y,ant} + Y_{ap})^{-1}} \cdot \sum A_{m0} B'_{y,m0} \tag{64}$$

and

$$E_y = \frac{V_0 d_a k_0 e^{-jk_0 r}}{2\pi\omega\varepsilon r} \cdot \frac{(Y_{y,ant} + Y_{ap})^{-1}}{(Y_{x,ant} + Y_{ap})^{-1} + (Y_{y,ant} + Y_{ap})^{-1}} \cdot \sum A_{0n} B'_{x,0n} \tag{65}$$

The amplitude error (Ae) and phase error (ϕ_e) required for the calculation of the axial ratio can be expressed as

$$A_e = \frac{|E_x|}{|E_y|} = \frac{|Y_{y,ant} + Y_{ap}|}{|Y_{x,ant} + Y_{ap}|} \cdot \frac{\left|\sum_m A_{m0} B'_{y,m0}\right|}{\left|\sum_n A_{0n} B'_{x,0n}\right|} \tag{66}$$

$$\phi_e = \angle\left(\frac{E_x}{E_y}\right) = \angle\left(\frac{Y_{y,ant} + Y_{ap}}{Y_{x,ant} + Y_{ap}} \cdot \frac{\sum_m A_{m0} B'_{y,m0}}{\sum_n A_{0n} B'_{x,0n}}\right) \tag{67}$$

Finally, the value of axial ratio is calculated by [12]

$$AR = \sqrt{\frac{1 + A_e^2 + [1 + A_e^4 + 2A_e^2 \cos(2\phi_e)]^{1/2}}{1 + A_e^2 - [1 + A_e^4 + 2A_e^2 \cos(2\phi_e)]^{1/2}}} \tag{68}$$

Eqns. 66 and 67, based on the resonant cavity model, provide a numerical means of determining the axial ratio of the cross-aperture coupled patch antenna at a given frequency when the design parameters shown in Fig. 1 are known.

6 Comparison of cavity method, full wave simulation and experimental results

The input impedance of the antenna with the dimensions in Fig. 1 has been calculated over a frequency range of 2.25–2.7GHz. It can be seen from Fig. 4 that the comparison for the input impedance between cavity model, full wave simulation Ensemble® [16] and experimental results are in good agreement. The impedance loci with the double resonance loop corresponding to the orthogonal modes also demonstrates that good circular polarisation has been achieved. Calculated resonant frequency from the cavity

model of 2.45 GHz is in close agreement with that obtained experimentally and from full-wave simulation.

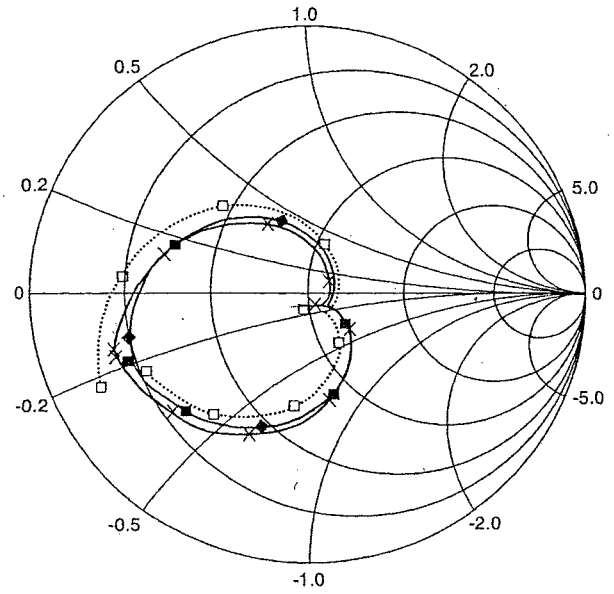

Fig. 4 *Input impedance of cross-aperture coupled antenna Fig. 1*
–□– cavity model
—●— full-wave simulation
—×— experimental results

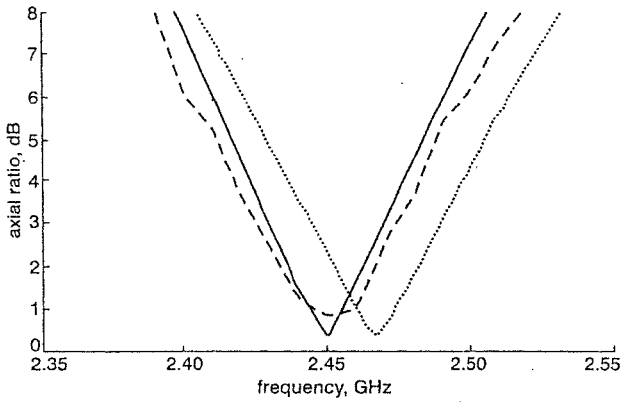

Fig. 5 *Axial ratio of cross-aperture coupled antenna Fig. 1*
····· cavity model
——— full-wave simulation
— — — experimental results

The axial ratio (see Fig. 5) has also been evaluated using the cavity model, simulated using Ensemble and practically measured. The prediction of the frequency for the best axial ratio is accurate to about 2% while that prediction of the axial ratio bandwidth is within the range of 10%, when compared with experimental results.

7 Conclusions

Based on the cavity model of the equal cross-slots structure, this paper has presented a theoretical analysis to determine the modal fields under the patch antenna. Using these fields an equivalent circuit of the antenna has been derived which is then used to determine the input impedance and the axial ratio of the circular polarised antenna. This cavity model has been used successfully to design a circular polarised impedance matched antenna. The results based on the cavity model show a good agreement with full-wave simulation and practical results.

8 References

1 POZAR, D.M.: 'Microstrip antenna Aaperture coupled to a microstrip line', *Electron. Lett.*, 1985, **21**, (2), pp. 49–50
2 TARGONSKI, S.D., and POZAR, D.M.: 'Design of widband circularly polarised aperture-coupled microstrip antennas', *IEEE Trans. Antennas Propag.*, 1993, **41**, (2), pp. 214–220
3 SULLIVAN, P.L., and SCHAUBERT, D.H.: 'Analysis of an aperture coupling microstrip antenna', *IEEE Trans. Antennas Propag.*, 1986, **AP-34**, pp. 977–984
4 POZAR, D.M.: 'A reciprocity method of analysis for printed slot and slot-coupled microstrip antennas', *IEEE Trans. Antennas Propag.*, 1986, **AP-34**, (12), pp. 1439–1446
5 BARLATELY, L., SMITH, H.K., and MOSIG, J.R.: 'Printed radiating structures and transitions in multilayered substrates', *Int. J. Microw. Milimeter-Wave Computer-Aided Engineering*, 1992, **2**, pp. 273–285
6 LO, Y.T., ENGST, B., and LEE, R.Q.: 'Simple design formulas for circularly polarised microstrip antennas', *IEE. Proc.-H*, 1988, **135**, pp. 213–215
7 AKSON, M.I., and CHUANG, S.L.: 'On slot-coupled microstrip antennas and their applications to CP operation-theory and experiment', *IEEE Trans. Antennas Propag.*, 1990, **AP-38**, (8), pp. 1224–1230
8 RICHARDS, W.F., LO, Y.T., and HARRISON, D.D.: 'An improved theory for microstrip antennas and applications', *IEEE Trans. Antennas Propag.*, 1981, **AP-29**, pp. 38–46
9 TASO, C.H., HWANG, Y.M., KILLBURG, F., and DIETRICH, F.: 'Aperture-coupled patch antennas with wide-bandwidth and dual polarisation capabilities', *IEEE Antennas Propag. Symp. Dig.*, 1988, pp. 936–939
10 ALJIBOURI, B., VLASITS, T., KOROLKIEWICZ, E., SCOTT, S., and SAMBELL, A.: 'Transmission line modelling of the crossaperture-coupled circular polarised microstrip patch antenn', *IEE Proc. Microw., Antennas Propag.*, 2000, **147**, (2), pp. 82–86
11 CHON, S.B.: 'Slot line on a dielectric substrate', *IEEE Trans. Microw. Theory Techn.*, 1969, **17**, (10), pp. 786–778
12 BALAJNS, C.A.: 'Antenna theory: analysis and design' (Wiley & sons, 1989)
13 HIMDI, M., DANIEL, J.P., and TERRENT, C.: 'Analysis of aperture-coupled microstrip antenna using cavity method', *Electron. Lett.* 1991, **27**, (5), pp. 455–457
14 THOUROUDDE, D., HIMDI, M., and DANIEL, J.P.: 'Cad-oriented cavity model for rectangular patches', *Electron. Lett.*, 1990, **26** (13), pp. 842–844
15 CARVER, K.R, and MINK, J.W.: 'Microstrip antenna technolog' *IEEE Trans. Antennas Propag.*, 1981, **AP-29**, (1), pp. 2–24
16 ANSOFT Corporation, Ensemble 5.1, 1998

line elements were used with shorting vias to ensure good connectivity between the upper and lower ground planes and prevent the excitation of spurious modes. The return loss at the resonant frequency was measured to be 21dB, with a 2:1 VSWR bandwidth of 2.7%. By comparison, an ordinary probe-fed or microstrip-line fed patch antenna on the same substrate would yield a bandwidth of the order of 1.5%. The impedance bandwidth of this element could be increased by increasing the substrate thickness, as long as the coplanar waveguide line does not become too wide.

Fig. 2 also shows results of modelling this antenna with Momentum, for the case of three vias per side. The resonant frequency and resonant resistance are predicted quite well, although the calculated points do not match the measured data over the entire locus. Nevertheless, considering the complexity of the problem caused by the presence of the vias, the calculations are surprisingly good, and should be more than adequate for design purposes.

The principal plane patterns of the antenna (with three vias per side) is shown in Fig. 3. The measured back radiation in the E-plane is 18dB down, and in the H-plane it is 15dB down. These results are similar to those obtained in [4] for a proximity-coupled circular patch at 5GHz.

Conclusions: A simple structure of a printed antenna fed by slot-coupled GCPW on a single layer substrate is presented. The minimum number of shorting vias required to prevent spurious modes is demonstrated. The measured characteristics of the antenna include the radiation pattern, bandwidth, and front-to-back ratio. Measurements show that the antenna has a good radiation pattern and bandwidth.

10 April 2000
Electronics Letters Online No: 20000776
DOI: 10.1049/el:20000776

S. Hudson and D. Pozar (*ECE Department, University of Massachusetts, Amherst, MA 01003, USA*)

References

1 POZAR, D.M.: 'Microstrip antenna aperture coupled to microstrip line', *Electron. Lett.*, 1985, 21, pp. 49–50
2 MENZEL, W., and GRABHERR, W.: 'A microstrip patch antenna with coplanar feed line', *IEEE Microw. Guided Wave Lett.*, 1991, 1, pp. 340–342
3 SIMONS, R.N., and LEE, R.Q.: 'Coplanar waveguide aperture coupled patch antennas with ground plane/substrate of finite extent', *Electron. Lett.*, 1992, 28, pp. 75–76
4 RAHARDJO, E.T., KITAO, S., and HANEISHI, M.: 'Planar antenna excited by electromagnetically coupled coplanar waveguide', *Electron. Lett.*, 1993, 29, pp. 870–872
5 DUFFY, S.: 'Design and analysis of microwave/millimeter wave active arrays using a multilayered packaging architecture'. PhD thesis, University of Massachusetts, Amherst, 1999

Multiobjective genetic algorithm approach for a dual-feed circular polarised patch antenna design

B. Aljibouri, E.G. Lim, H. Evans and A. Sambell

A design procedure for a dual feed network is presented to produce a circular polarised matched antenna involving eight design parameters with associated constraints. Determination of such design parameters has been made possible by utilising a multiobjective genetic algorithm (MGA) approach. The conditions for circular polarisation and impedance matching were the objective functions employed in the MGA. The associated constraints were the lengths and characteristic impedance values of the feed network. The return loss and axial ratio for a 5.8GHz antenna were investigated and good agreement was obtained between simulated and practical measurements.

Introduction: Microstrip patch antennas are used in a variety of communication systems, especially when the receiver needs to be compact and have a low profile. Further, for applications such as radio frequency identification (RFID) systems in which the receiver may be placed in any orientation, circular polarisation is used. Circular polarisation can be realised by using either a single [1] or a dual feed [2, 3]. In many cases, owing to the simplicity of design and manufacture a dual-feed arrangement is preferred.

An MGA programme has been developed to optimise the design of the dual-feed network, involving eight variables, which are required to meet the conditions for circular polarisation and matching at the feed port. Two constraints on the design parameters have also been applied, one to ensure that the widths of the feed lines are as narrow as possible yet realisable, and the other constraint to ensure that the lengths of the feed lines are sufficient to fit the network around the square patch antenna.

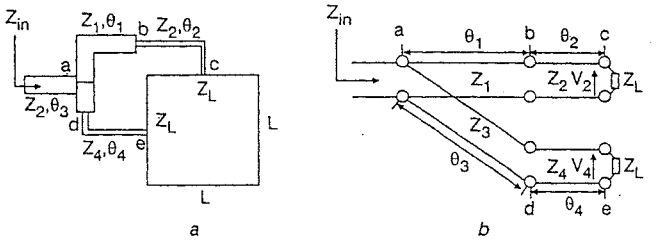

586/1

Fig. 1 *Dual-feed LHCP square patch antenna and equivalent circuit*

Design of feed network using multiobjective genetic algorithm approach: A dual feed network based on a power divider to produce circular polarisation is shown in Fig. 1*a* and its transmission line model in Fig. 1*b*.

It is possible, using a transmission line approach, to match a complex load impedance to a complex source impedance by relaxing the constraint length of a traditional $\lambda/4$ transformer [4]. Consequently, by varying the impedance and lengths of the transmission lines of the feed network, both matching and circular polarisation conditions can be satisfied. For the structure shown in Fig. 1 the design variables' parameters (characteristic impedances and element lengths of the feed network) are Z_1, θ_1, Z_2, θ_2, Z_3, θ_3, Z_4, θ_4 and constitute the parameter set in the MGA. The two objective functions employed in the MGA are given by eqns. 1 and 2 below and give the conditions required for circular polarisation and impedance matching, respectively. For circular polarisation

$$\frac{V_2}{V_4} = \frac{e^{-j(\theta_1+\theta_2)}[1+\Gamma_1][1+\Gamma_2]}{[1+\Gamma_1 e^{-2j\theta_1}][1+\Gamma_2 e^{-2j\theta_2}]} \times \frac{[1+\Gamma_3 e^{-2j\theta_3}][1+\Gamma_4 e^{-2j\theta_4}]}{e^{-j(\theta_3+\theta_4)}[1+\Gamma_3][1+\Gamma_4]} = \mp j \qquad (1)$$

where Γ_1, Γ_2, Γ_3 and Γ_4 are the reflection coefficients at junctions b, c, d, and e, respectively (see Fig. 1).

For the impedance matching

$$\Gamma_{in} = \frac{Z_{in} - Z_0}{Z_{in} + Z_0} = 0 \qquad (2)$$

where Γ_{in} is the input reflection coefficient at junction 'a'.

For microstrip realisation, search intervals between 120Ω and 140Ω were used for the parameters Z_1, Z_2, Z_3, Z_4. The 120Ω impedance was chosen to reduce the coupling between the feed lines and the antenna and also to minimise the step discontinuities at the feed lines junctions, thereby reducing spurious radiation. The 140Ω impedance represents the maximum impedance that can be realised. To fit the feed network around the antenna, the lengths θ_1, θ_2, θ_3, θ_4 were constrained to an interval between $\pi/4$ and π.

The tolerance for $|V_2/V_4|$ was 1 ± 0.1 and for $\arg(V_2/V_4)$ was $90° \pm 4°$, so as to ensure good circular polarisation, while the tolerance for Γ_{in} was ± 0.02 in order to produce good matching conditions.

Results and discussion: The MGA approach, based on a nondominating sorting genetic algorithm [4], was developed to produce sets of feasible solutions. Selection was made from these solutions, using additional factors, such as a preference for similar characteristic impedance values of the feed line network.

The operating frequency of the patch antenna was 5.8GHz, and

the feed network was optimised to produce left- and right-hand circular polarisation (LHCP and RHCP) with a 50Ω matched input impedance condition. The two sets of solutions for the optimised feed network are shown in Table 1.

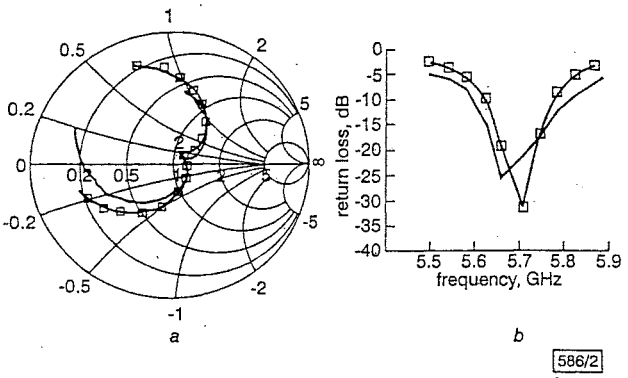

Fig. 2 *Simulated and practical results of dual-feed square microstrip patch antenna*

——— practical
—□— simulated
$h = 0.79$, $\varepsilon_r = 2.33$

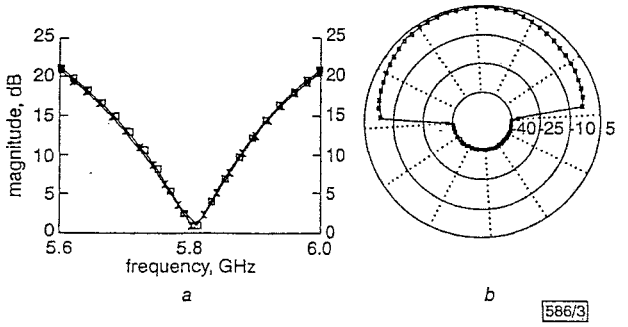

Fig. 3 *Simulated results for LHCP and RHCP designs*

a Axial ratio
b Radiation pattern
—□— LHCP
—×— RHCP

Table 1: Two sets of solutions for optimised feed network

θ_1	Z_1	θ_2	Z_2	θ_3	Z_3	θ_4	Z_4	Z_{in}	$\lvert V_2/V_4\rvert$	$\arg(V_2/V_4)$	CP
2.31	135.0	1.96	132.4	0.8	135.2	1.16	134.3	50–0.5*i*	0.97	86	RH
1.2	137.4	0.74	137.1	2.3	135.7	1.97	138.6	49.5+0.5*i*	1.08	89.7	LH

As can be seen in Table 1, it is possible to use an average value of impedance for all four feed lines as this value is within the design and typical manufacturing tolerances. This makes the design particularly attractive as the effect of the step discontinuity is eliminated and also spurious radiation is reduced.

Practical and simulated (full-wave analysis software) results for the reflection coefficient of the LHCP solution using 137.2Ω are shown in Fig. 2 and indicate that a good matching condition at 5.8GHz has been obtained.

The simulated results of the axial ratio and radiation pattern of the LHCP and RHCP designs are shown in Fig. 3 with a good axial ratio and the expected radiation patterns.

Conclusion: It has been shown that the design of a dual-feed network for a square patch antenna for circular polarisation involves eight variables and that a closed form solution to the problem cannot be obtained. An MGA with specified constraints has been successfully implemented to optimise the design of a dual-feed network. A feed network with single feed impedance has been realised. The practical and simulated results for the return loss, axial ratio and radiation pattern show good agreement and confirm the validity of the approach.

2 March 2000
Electronics Letters Online No: 20000766
DOI: 10.1049/el:20000766

B. Aljibouri, E.G. Lim, H. Evans and A. Sambell (*Communication Systems Research Group, University of Northumbria, United Kingdom*)

References

1 LIM, B., KOROLKIEWICZ, E., and SCOTT, S.: 'Optimised design corner microstrip fed nearly square patch antenna for circ polarisation', *Electron. Lett.*, 1996, 32, pp. 610–612
2 HOWELL, J.Q.: 'Microstrip antennas', *IEEE Trans.*, 1975, AP–23, 90–93
3 SOLIMAN, E.A., BREBELS, S., BEYNE, E., and VANDENBOSCH 'Circularly polarised aperture antenna fed by CPW and buil MCM-D technology', *Electron. Lett.*, 1999, 35, pp. 250–251
4 DAY, P.I.: 'Transmission line transformation between arbitr impedances using the smith chart', *IEEE Trans. Microw. The Tech.*, 1975, pp. 772–773
5 SRINIVAS, N., and KALYANMOY, D.: 'Multiobjective optimizat using nondominating sorting in genetic algorithms', *Evol. Comp* 1995, 2, (3), pp. 221–248

Independent component analysis of saccade-related electroencephalogram waveforms

L. Vigon, R. Saatchi, J. Mayhew, N. Taroyan, J. Frisby, D. Johnston and O. Pascalis

A methodology based on the signal separation technique extended independent component analysis (ICA) is devised analyse saccade-related electroencephalogram (EEG) wavefor The methodology enables saccade-related components to successfully extracted from the EEG mixtures and the bi regions responsible for their generation to be identified.

Introduction: Saccades are rapid changes in the orientation of eyes that are used to realign the visual axes on objects of inter Dysfunction in this system may lead to difficulties in various ual functions such as depth perception and reading. Different n ral signal components are involved in preparation and execut of saccadic eye movements. One of these is described as a pre-s cadic potential related to motor commands for saccade gene tion. Others, such as efferent feedback from saccade generat centres to visual cortex, are believed to provide visual stability the surrounding world across the eye movements. The sacca movement is accompanied by an EEG signal associated with ual information processing called the lambda-wave [1].

The investigation described in this Letter required the obscur ongoing background EEG as well as the electrooculogram (EC signal caused by eye movements to be separated from the sacc components of interest. A popular signal separation techniqu independent component analysis (ICA) [2]. ICA is an extensior principal component analysis (PCA) that deals with higher-or statistical dependencies. It is based on the assumption that the nal sources are statistically independent. The extended version ICA (hereafter referred to as ICA) can handle both super- a sub-Gaussian signals [2]. In this Letter, an analysis of the sacca related EEC waveforms is carried out by applying an ICA-ba procedure. The study provides information about how the br deals with the problem of vision with moving eyes.

Experimental procedure: EEC and EOG data were recorded for healthy human adults using a network of 64 silver-silver chlor electrodes. All electrodes were referred to the vertex. The d were filtered (bandpass frequency range from 0.1 to 100Hz) a digitised with a sampling rate of 250. The subjects were instruc to fixate a red square that appeared randomly on the screen c computer at one of five predefined checkerboard locations: cen left, right, up and down. For each location 50 trials were record The duration of each trial was 2s.

Analysis procedure: The recorded signals were digitally lowpass tered at 45 Hz and their baselines were adjusted to zero. To p serve the saccade-related EEG components, the waveforms in e trial were time synchronised with reference to the EOG signal that trial. The synchronised averaged waveforms were decorrela using PCA and sphered [2]. The EEG waveforms recorded fr the locations close to the international 10-20 system of electr

Application of simulated annealing to design of serial feed sequentially rotated 2 × 2 antenna array

H. Evans, P. Gale, B. Aljibouri, E.G. Lim,
E. Korolkeiwicz and A. Sambell

A 5.8GHz circularly polarised 2 × 2 patch antenna array is presented, employing sequential rotation of dual-feed circularly polarised elements; appropriate phase-shifting and power splitting are achieved via a serial feed arrangement. The feed has been optimised using simulated annealing; the resulting structure has a voltage standing wave ratio 2:1 bandwidth of 9.8%. Results obtained by full wave simulation and practical measurement confirm the integrity of the design.

Introduction: Many modern communication systems use single-layer patch antenna arrays as they are light, low profile and inexpensive. One such system is a two-way digital communication link between a moving vehicle and a roadside beacon for traffic management applications. This array has been used in the roadside unit of a commercial system and also as a sub-array within a 4 × 4 arrangement resulting in a gain of 18.9dBi.

Sequential rotation of radiating elements, with suitable excitation phase-shifting, has been shown to improve the polarisation purity and radiation pattern symmetry over a wide range of frequencies. In addition, owing to the excitation phase-shifting by the feed, off frequency reflections from mismatched elements tend to cancel out at the feed point, leading to improved input impedance over a wider bandwidth [1 – 3]. These applications of sequential rotation all employ some form of corporate feed network.

This Letter presents a design that incorporates sequential rotation using a serial feed to provide appropriate phase-shifting and power splitting between the radiating elements. As it is not possible to obtain closed form expressions, the impedance elements within the feed network have been optimised using a simulated annealing algorithm.

Array description: The antenna configuration is shown in Fig. 1*a*. The radiating elements are dual feed left hand circularly polarised microstrip patches with an input impedance of 50Ω [4], which are sequentially rotated by 90° with respect to each element's immediate neighbour. The serial feed compensates for this physical rotation by shifting the phase of each element's excitation by 90°.

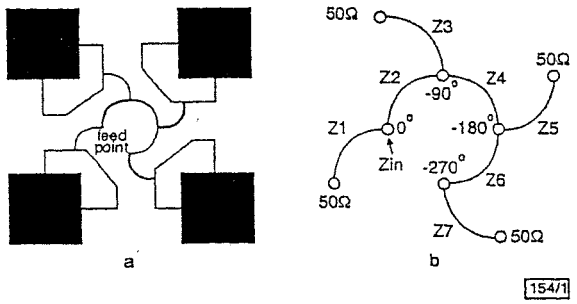

Fig. 1 *Antenna configuration and equivalent circuit*

a 2 × 2 antenna array incorporating sequentially rotated radiating elements excited by serial feed network
b Equivalent circuit for serial feed network

The radiating elements are spaced at 0.74λ as it has been shown that this minimises mutual coupling without substantial degradation of the radiation pattern by side lobes [5]. Smooth bends were used in the feed network as it has been shown that this can reduce feed radiation [6]. The use of high impedance elements in the feed network further reduces coupling and spurious radiation.

At the design frequency, the serial feed ensures that equal power is fed to each element. Off frequency, as the signal propagates along the feed, correct phase-shifting and power splitting progressively deteriorate. Although degradation of accurate power splitting dominates, the use of sequential rotation reduces this problem.

Feed optimisation: The equivalent circuit for the serial feed can be seen in Fig. 1*b*. λ/4 transformers are used to provide the necessary impedance matching and phase delays. The value of Z1 is fixed, as it must both divert a quarter of the power to the first patch while ensuring that the input impedance to the whole structure is 50Ω There is no unique solution to the remaining impedances. However, to ensure Z5 and Z7 are at a maximum impedance, it is necessary to make Z6 the maximum impedance that fabrication constraints will allow, typically between 128 and 145Ω

An adaptation of iterated simulated annealing [7] has been implemented in C++ to optimise the feed network with the following five constraints. The minimum impedance was constrained to 70Ω to reduce coupling and spurious radiation. In this Letter, solutions were found for a maximum impedance of 128 and 145Ω The target impedance was set to the maximum impedance value. The input impedance at the feed point, Z_{in}, was constrained to 50Ω for this array, although it can be changed if the structure were used as a sub-array. The patch input impedance was set to 50Ω for this design.

Results: Two sets of solutions for the feed network can be seen in Table 1. In both cases the optimisation algorithm has ensured that Z6 is at the maximum value, thus ensuring both Z5 and Z7 are also at maximum values; all impedances are within the specified constraints.

Table 1: Feed network solutions with maximum impedance restrained to 125 and 145Ω

Z_{in}	Z1	Z2	Z3	Z4	Z5	Z6	Z7
Ω	Ω	Ω	Ω	Ω	Ω	Ω	Ω
50	100	80	120	96	80	128	80
50	100	90	135	115	85	145	85

The antenna was fabricated on 0.79mm 1/2 oz RT 5870 Duroid (ε_r = 2.33). The integrity of the design has been confirmed using full wave simulation [8] and experimental measurement. The voltage standing wave ratio (VSWR), radiation pattern and axial ratio can be seen in Fig. 2. Practical measurement confirms a VSWR 2:1 bandwidth of 9.8% although the axial ratio is not as wide band. The gain of the main lobe has been measured at 12.4dBi.

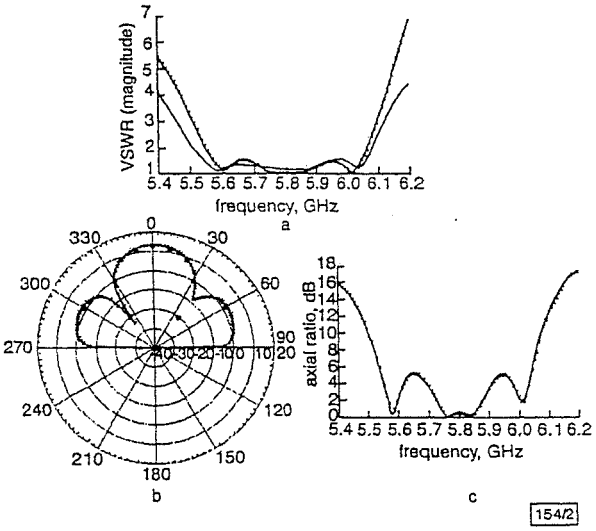

Fig. 2 *VSWR, radiation pattern and axial ratio*

a VSWR
—X— full wave simulation
——— practical measurement
b Radiation pattern
—X— full wave simulation
● practical measurements
c axial ratio
—X— full wave simulation

Conclusion: A sequentially rotated 2 × 2 antenna array with a serial feed has been presented. Simulated annealing successfully optimised the feed network with a minimum of computational resources. The performance of the array has been confirmed both by full wave simulation and experimental measurement confirming a VSWR 2:1 bandwidth of 9.8%.

8 September 2000
Electronics Letters Online No: 20001407
DOI: 10.1049/el:20001407

H. Evans, P. Gale, B. Aljibouri, E.G. Lim, E. Korolkeiwicz and A. Sambell (*School of Engineering, University of Northumbria, Ellison Building, Newcastle Upon Tyne, NE1 8ST, United Kingdom*)

Huw.Evans@unn.ac.uk

References

1 TESHIROGI, T., TANAKA, M., and CHUJO, W.: 'Wideband circularly polarised array antenna with sequential rotation and phase shifts of elements'. Int. Symp. Antennas and Propag., ISAP 85, Tokyo, 1985

2 HALL, P.S.: 'Feed radiation effects in sequentially rotated microstrip arrays', *Electron. Lett.*, 1987, 23, (17), pp. 877–878

3 HALL, P.S., DAHELE, J.S., and JAMES, J.R.: 'Design principles of sequentially fed, wide bandwidth, circularly polarised microstrip patch antennas', *IEE Proc. H*, 1989, 136, (5), pp. 381–389

4 ALJIBOURI, B., LIM, E.G., EVANS, H., and SAMBELL, A.: 'Multiobjective genetic algorithm approach for a dual feed circular polarised patch antenna design', *Electron. Lett.*, 2000, 36, (12), pp. 1005–1006

5 CHAN, T.K.: 'Development of a two way microwave communication system for traffic applications'. PhD thesis, University of Northumbria at Newcastle, June 1994

6 HALL, P.S., and HALL, C.M.: 'Coplanar corporate feed effects on microstrip patch array design', *IEE Proc. H*, 1988, 135, (3), pp. 180–186

7 KIRKPATRICK, S., GELATT, C.D., and VECCHI, M.P.: 'Optimization by simulated annealing', *Science*, 1983, 220, pp. 671–680

8 Ansoft Ensemble® V6. 1 - Method of Moments 2.5D EM field solver

Communications

Efficient Impedance Coupling Formulas for Rectangular Segment in Planar Microstrip Circuits

Eng Gee Lim, E. Korolkiewicz, S. Scott, B. Aljibouri, and Shi-Chang Gao

Abstract—A rectangular patch is one of the most common microstrip segments for which the Green's function is known and is used in the segmentation and desegmentation analysis of complex antenna structures. The coupling impedances between ports on a microstrip segment are derived by integrating the associated Green's function to obtain a result which involves the evaluation of double infinite series. In this paper the double infinite series is replaced by a single term together with a single infinite series to produce a computationally more efficient formula for the coupling impedance. Three coupling port configurations are examined and in each case numerically efficient formulas are derived.

Index Terms—Coupling impedance, Green's function, microstrip rectangular patch antenna.

I. Introduction

Microstrip circuits may be treated as planar two-dimensional circuits [1] with compound planar geometries treated by segmentation [2], [3] and desegmentation methods [4]. This requires the calculation of the impedance coupling between ports on the component segments. The time consuming part in planar circuit computations is the large number of terms required in evaluating the double infinite series form of the coupling impedance formulas.

In this paper the Green's function is expressed in the four modal sets, $(m = 0, n = 0), (m \geq 1, n = 0), (m = 0, n \geq 1), (m \geq 1, n \geq 1)$ and integrated to obtain the impedance coupling formulas in terms of a single term, two single infinite series, and, one double infinite series. The single infinite series are summed to closed form, while the double infinite series is reduced to a single infinite series. The summation formulas derived in the paper are based on Gradshtyn [5].

The new formulation for the coupling impedance between two ports "p" and "q" have been derived for three possible port configurations for a rectangular patch (Fig. 1). The ports all are located along the perimeter of the rectangle.

The initial formulas and their economization procedures are shown in Case A, Case B and Case C below.

II. Computational Analysis

There are three cases to consider as shown in Fig. 1.

The general formula for the coupling impedance given by Okoshi [6] is

$$Z_{pq} = \frac{1}{W_p W_q} \int_{W_p} \int_{W_q} G(s|s_0)\, ds\, ds_0 \tag{1}$$

where, $W_{p,q}$ are the width of the feed lines at ports p and q. $W_{p,q} \ll \lambda$, λ. being the wave length in the substrate. The integrations are taken along the interface between the ports and the antenna patch.

Manuscript received May 31, 2001revised June 11, 2002.

The authors are with the Communication Systems Research Group, School of Engineering, University of Northumbria at Newcastle, Newcastle Upon Tyne, NE1 8ST, U.K. (e-mail: eng.lim@unn.ac.uk).

Digital Object Identifier 10.1109/TAP.2003.814741

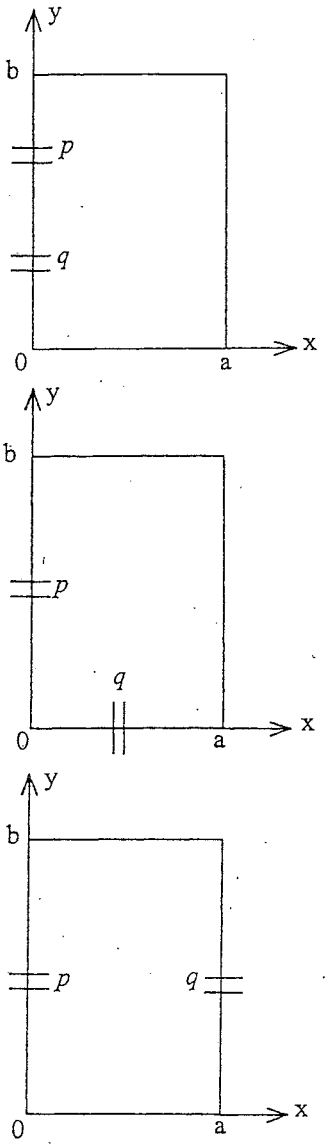

Fig. 1. Three port configurations.

A. Case A: Two Ports on the Same Side

The two ports p, q have centers $(0, y_p)$, $(0, y_q)$ and the Green's function becomes

$$G(0, y_p|0, y_q) = \frac{j\omega\mu h}{ab}\left[-\frac{1}{k^2} + \frac{2a^2}{\pi^2}\sum_{m=1}^{\infty}\frac{1}{m^2 - A^2} + \frac{2b^2}{\pi^2}\sum_{n=1}^{\infty}\frac{\cos\frac{n\pi}{b}y_p \cos\frac{n\pi}{b}y_q}{n^2 - B^2} + \frac{4}{\pi^2}\sum_{m=1}^{\infty}\sum_{n=1}^{\infty} \times \frac{\cos\frac{n\pi}{b}y_p \cos\frac{n\pi}{b}y_q}{\frac{m^2}{a^2} + \frac{n^2}{b^2} - \frac{k^2}{\pi^2}}\right] \tag{2}$$

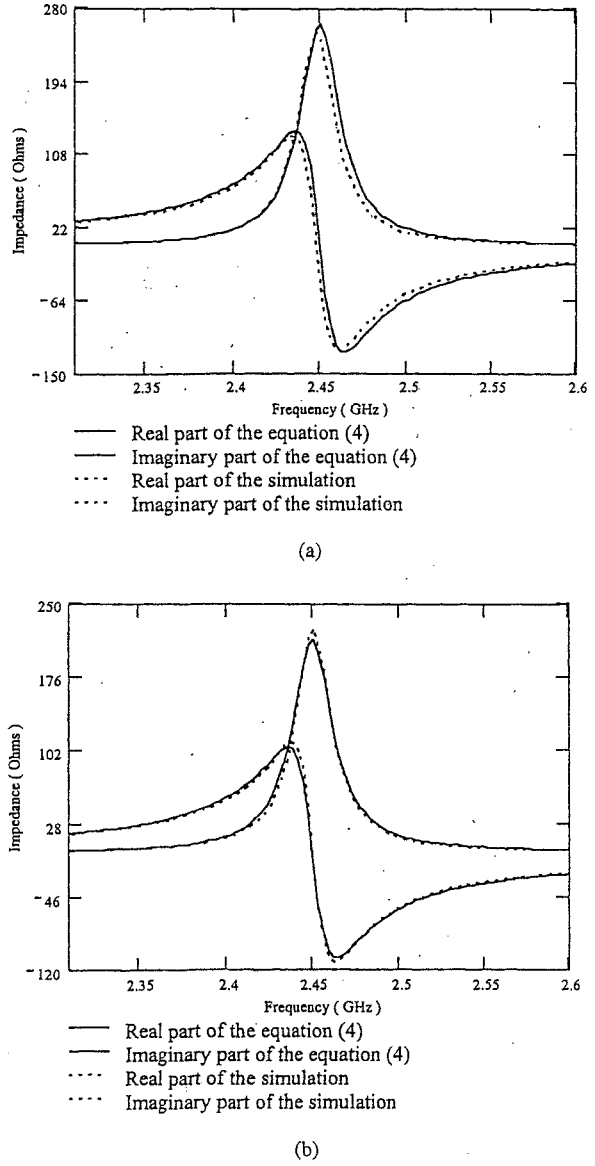

Fig. 2. Coupling impedances of two ports located on the same side at $(0, y_p)$, $(0, y_q)$. (a) Coupling impedances for $y_p = 18$ mm and $y_q = 22$ mm and (b) coupling impedances for $y_p = 14$ mm and $y_q = 26$ mm.

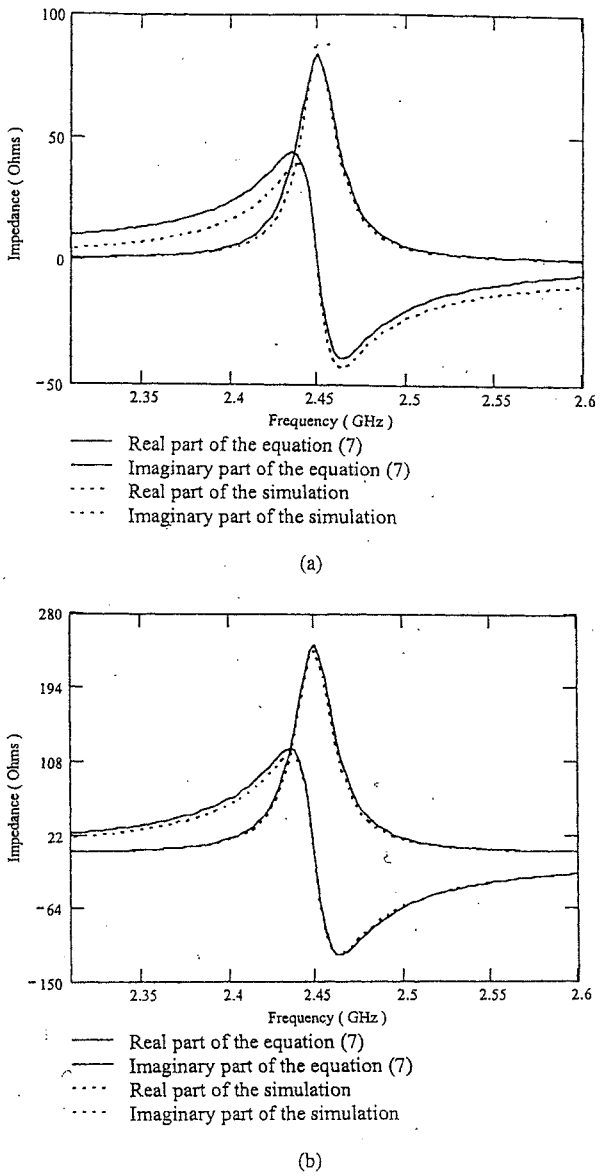

Fig. 3. Coupling impedances of two ports located on adjacent sides at $(0, y_p)$, $(x_q, 0)$. (a) Coupling impedances for $y_p = x_q = 18$ mm and (b) coupling impedances for $y_p = x_q = 14$ mm.

where $A = ak/\pi$, $B = bk/\pi$; h is the dielectric thickness; $k^2 = \omega^2\mu\varepsilon_0\varepsilon_r(1 - j/Q)$ and, Q is the total quality loss factor, which includes, copper (Q_c), dielectric (Q_d), radiation (Q_r) and surface wave (Q_{sw}) losses of the structure where normally the effect Q_{sw} of can be neglected [7].

From (1) and (2), by integration, see (3) at bottom of page, where, $D^2 = (n^2 - B^2)a^2/b^2, \theta_1 = (\pi/b)(y_p - (W_p/2)), \theta_2 = (\pi/b)(y_p + (W_p/2)), \theta_3 = (\pi/b)(y_q - (W_q/2))$, and, $\theta_4 = (\pi/b)(y_q + (W_q/2))$.

Summing the above double series with respect to the inner summation results in total elimination of the second single series. Summing

$$Z_{pq} = \frac{j\omega\mu h}{abW_pW_q}\left[\frac{-W_pW_q}{k^2} + \frac{2a^2W_pW_q}{\pi^2}\sum_{m=1}^{\infty}\frac{1}{m^2 - A^2} + \frac{2b^2}{\pi^4}\sum_{n=1}^{\infty}\frac{(\sin n\theta_1 - \sin n\theta_2)(\sin n\theta_3 - \sin n\theta_4)}{n^2(n^2 - B^2)} + \frac{4a^2b^2}{\pi^4}\sum_{n=1}^{\infty}\sum_{m=1}^{\infty}\frac{(\sin n\theta_1 - \sin n\theta_2)(\sin n\theta_3 - \sin n\theta_4)}{n^2(m^2 + D^2)}\right] \quad (3)$$

the first of the above single series eliminates the $-W_pW_q)/k^2$ term. Total final result of the economization is the new computationally efficient coupling impedance formula

$$Z_{pq} = \frac{j\omega\mu h}{ab}\left[\frac{-a}{k}\cot ka + \frac{2a^2b^2}{W_pW_q\pi^3} \times \sum_{n=1}^{\infty}\frac{(\sin n\theta_1 - \sin n\theta_2)(\sin n\theta_3 - \sin n\theta_4)}{n^2 D} \times \coth D\pi\right] \quad (4)$$

B. Case B: Two Ports on Adjacent Sides

The two ports p, q have centers $(0,y_p)$, $(x_q,0)$ and the Green's function becomes

$$G(0,y_p|x_q,0) = \frac{j\omega\mu h}{ab}\left[-\frac{1}{k^2} + \frac{2a^2}{\pi^2}\sum_{m=1}^{\infty}\frac{\cos\frac{m\pi}{a}x_q}{m^2-A^2} + \frac{2b^2}{\pi^2} \times \sum_{n=1}^{\infty}\frac{\cos\frac{n\pi}{b}y_p}{n^2-B^2} + \frac{4}{\pi^2} \times \sum_{m=1}^{\infty}\sum_{n=1}^{\infty}\frac{\cos\frac{m\pi}{a}x_q\cos\frac{n\pi}{b}y_p}{\frac{m^2}{a^2}+\frac{n^2}{b^2}-\frac{k^2}{\pi^2}}\right]. \quad (5)$$

From (1) and (5), by integration

$$Z_{pq} = \frac{j\omega\mu h}{abW_pW_q} \times \left[\frac{W_pW_q}{k^2} - \frac{2a^3W_p}{\pi^3}\sum_{m=1}^{\infty}\frac{(\sin m\theta_1 - \sin m\theta_2)}{m\,(m^2-A^2)} - \frac{2a^3W_q}{\pi^3} \times \sum_{n=1}^{\infty}\frac{(\sin n\theta_3 - \sin n\theta_4)}{n^2(n^2-B^2)} - \frac{4ab^3}{\pi^4}\sum_{m=1}^{\infty} \times \sum_{n=1}^{\infty}\frac{(\sin n\theta_3 - \sin n\theta_4)(\sin m\theta_1 - \sin m\theta_2}{mn^2(n^2+C^2)}\right] \quad (6)$$

where, $C^2 = (m^2 - A^2)b^2/a^2$; $\theta_1 := (\pi/a)(x_q + (W_q/2))$, $\theta_2 = (\pi/a)(y_q - (W_q/2))$, $\theta_3 = (\pi/a)(x_p - (W_{p/2}))$, and, $\theta_4 = (\pi/a)(y_p + (W_p/2))$.

Summing the above double series with respect to the inner summation results in total elimination of the first single series. Summing the second of the above single series eliminates the $(W_pW_q)/k^2$ term. Total final result of the economization is the new computationally efficient coupling impedance formula, see (7) shown at the bottom of the page.

C. Case C: Two Ports on Opposite Edges

The two ports p, q have centers $(0, y_p)$, (a, y_q) and the Green's function becomes

$$G(0,y_p|a,y_q) = \frac{j\omega\mu h}{ab}\left[-\frac{1}{k^2} + \frac{2a^2}{\pi^2}\sum_{m=1}^{\infty}\frac{(-1)^m}{m^2-A^2} + \frac{2b^2}{\pi^2} \times \sum_{n=1}^{\infty}\frac{\cos\frac{n\pi}{b}y_p\cos\frac{n\pi}{b}y_q}{n^2-B^2} + \frac{4}{\pi^2}\sum_{m=1}^{\infty} \times \sum_{n=1}^{\infty}\frac{(-1)^m\cos\frac{n\pi}{b}y_p\cos\frac{n\pi}{b}y_q}{\frac{m^2}{a^2}+\frac{n^2}{b^2}-\frac{k^2}{\pi^2}}\right]. \quad (8)$$

From (1) and (8), by integration (see (9) at bottom of page) where, D, θ_1, θ_2, θ_3, θ_4 are as defined in case A.

Summing the above double series with respect to the inner summation results in total elimination of the second single series. Summing the first of the above single series eliminates the $(W_pW_q)/k^2$ term. Total final result of the economization is the new computationally efficient coupling impedance formula

$$Z_{pq} = \frac{j\omega\mu h}{bW_pW_q}\left[\frac{W_pW_q}{k\sin ka} - \frac{2ab^2}{\pi^3} \times \sum_{n=1}^{\infty}\frac{(\sin n\theta_1 - \sin n\theta_2)(\sin n\theta_3 - \sin n\theta_4)}{D\sinh D\pi}\right]. \quad (10)$$

III. Results

The derived equations for the coupling impedances were evaluated for a square patch of length $a = 40$ mm at a frequency of 2.45 GHz on

$$Z_{pq} = \frac{j\omega\mu h}{W_pW_q}\left[\frac{W_q\,[\sin B(\pi-\theta_4) - \sin B(\pi-\theta_3)]}{ak^2\sin kb} + \frac{2a^2}{\pi^3}\sum_{m=1}^{\infty}\frac{(\sin m\theta_1 - \sin m\theta_2)\,[\sinh C(\pi-\theta_4) - \sinh C(\pi-\theta_3)]}{m(m^2-A^2)\sinh C\pi}\right] \quad (7)$$

$$Z_{pq} = \frac{j\omega\mu h}{ab}\left[\frac{W_pW_q}{k^2} - \frac{2a^2W_pW_q}{\pi^2}\sum_{m=1}^{\infty}\frac{(-1)^m}{m^2-A^2} - \frac{2b^4}{\pi^4} \times \sum_{n=1}^{\infty}\frac{(\sin n\theta_1 - \sin n\theta_2)(\sin n\theta_3 - \sin n\theta_4)}{n^2(n^2-B^2)} - \frac{4a^2b^2}{\pi^4} \times \sum_{n=1}^{\infty}\sum_{m=1}^{\infty}\frac{(-1)^m(\sin n\theta_1 - \sin n\theta_2)(\sin n\theta_3 - \sin n\theta_4)}{n^2(m^2+D^2)}\right] \quad (9)$$

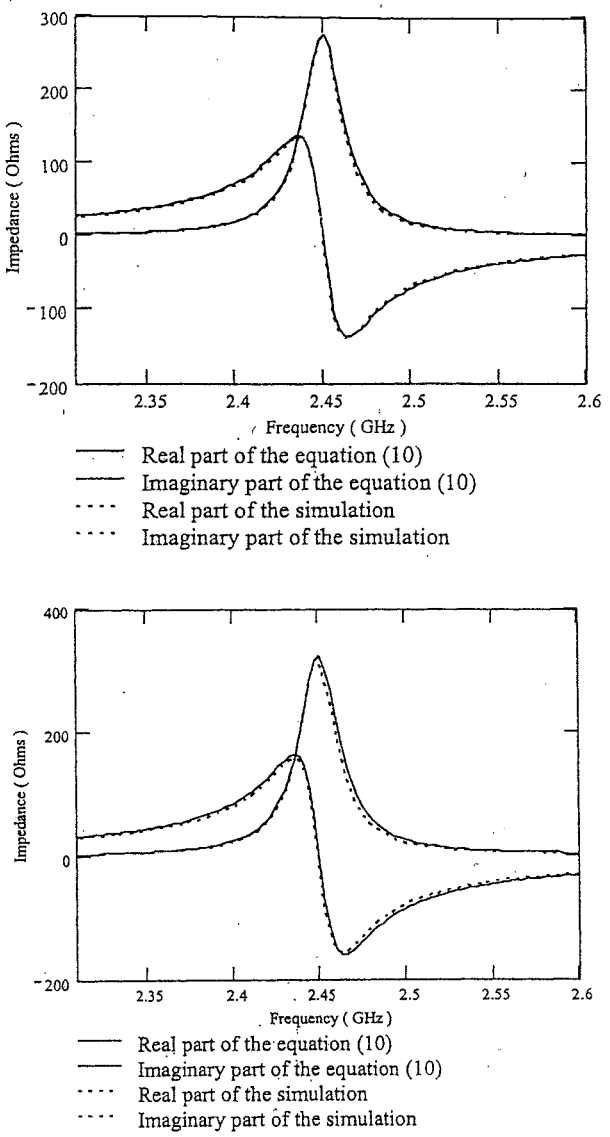

Fig. 4. Coupling impedances of two ports located on opposite sides at $(0, y_p)$, (a, y_q). (a) Coupling impedances for $y_p = 18$ mm and $y_q = 22$ mm and (b) coupling impedances for $y_p = 14$ mm $y_q = 26$ mm.

a substrate (Duroid 5870) where $\varepsilon r = 2.33$, thickness $h = 0.79$ mm and the loss tangent of 0.0012.

A square patch was chosen as this geometry produces a variation of coupling impedance depending on the separation between the two ports in contrast to the rectangular patch case when the coupling impedance is essentially independent of the separation. The quality factor Q of 87 was used which takes into account copper, dielectric and radiation losses.

Results for two different separations between the two ports were obtained for the three cases and compared with those predicted by a full wave analysis software (Ensemble). These results are shown in graphs 2, 3 and 4.

As can be seen in Fig. 2(a) and (b) for case A, the coupling impedances decrease with separation of the two ports. Fig. 3(a) and (b) show the comparison of results for case B and as expected the mutual impedance increase as the two ports are brought closer together. Finally Fig. 4(a) and (b) shows the results for case C. For all three cases there is an excellent agreement between the results obtained from the efficient computational formulas with that predicted by the ensemble.

Numerical trials using the new formula have shown that in all ca considered only one term of the series is required to give converge to three significant figures. In the worst case convergence to five sig icant figures requires at most 4 terms of the series, and, for converge to seven significant figures 10 terms at most are required.

IV. Conclusion

In this paper an efficient computational formula for each of the th possible rectangular patch coupling impedances configurations, l been obtained. Good agreement between results from the new form lation and Ensemble is obtained.

References

[1] G. Kompa and R. Mehran, "Planar waveguide model for calculating crostrip components," *Electron. Lett.*, vol. 11, pp. 459–460, Sept. 19
[2] T. Okoshi, Y. Uehara, and T. Takeuchi, "Segmentation method—an proach to the analysis of microwave planar circuits," *IEEE Trans. crowave Theory Tech.*, vol. MTT-24, pp. 662–668, Oct. 1976.
[3] R. Chadha and K. C. Gupta, "Segmentation method using impeda matrices for analysis of planar microwave circuits," *IEEE Trans. crowave Theory Tech.*, vol. MTT-29, pp. 71–74, Oct. 1981.
[4] P. C. Sharma and K. C. Gupta, "Degmentation method for analysis two-dimensional microwave circuits," *IEEE Trans. Microwave The Tech.*, vol. MTT-29, pp. 1094–1097, 1981.
[5] I. S. Gradshteyn and I. M. Ryzhik, *Table of Integrals, Series, a Product*. New York: Academic Press, 1994.
[6] T. Okoshi, *Planar Circuits for Microwave and Lightwaves*: Spring Verlag, 1985.
[7] J. R. James and P. S. Hall, *Handbook of Mircostrip Antennas*. Lond U.K.: Peregrinus, 1989, vol. 1 and 2.

An Efficient Formula for the Input Impedance of a Microstrip Right-Angled Isosceles Triangular Patch Antenna

E. G. Lim, E. Korolkiewicz, S. Scott, A. Sambell, and B. Aljibouri

Abstract—**Input impedance formulas for feed positions first, on the vertical side and second, on the hypotenuse, are obtained from coplanar microstrip circuit analysis. The formulas that involve both single and double infinite series are economized by introducing closed forms of the infinite series. These new formulas are verified by comparison with practical results and a simulation based on full wave analysis.**

Index Terms—**Efficient formula, input impedance, right-angled triangular patch antenna.**

I. Introduction

In recent years, microstrip antennas have aroused great interest in both theoretical research and engineering application due to their low profile, light weight, low cost, reliability, conformal structure, and ease in fabrication and integration with solid-state devices [1]–[3]. However, the majority of the studies proposed in this area have been concentrated on rectangular and circular microstrip antennas. It is known that the right-angled isosceles triangular patch antenna has radiation properties similar to that of the rectangular patch antenna, with the advantage of being physically smaller.

Using the cavity model a general formula for the input impedance of a single-feed microstrip antenna of any geometry has been derived by Okoshi using the Green's function solution of the wave equation [4]. Included are the effects of radiation, copper, and dielectric losses [1] and also the fringe-filed extensions. This formula involves the double integration of the associated Green's function. The Green's function for a right-angled isosceles triangle has been obtained by Chada and Gupta [5]. They have derived the Green's function by constructing a set of specially selected line sources, the potential from which is expanded in an infinite series to obtained expansion functions satisfying the associated homogeneous wave equation boundary value problem. These functions then applied to the nonhomogeneous wave equation to determine the required Green's function expansion coefficients.

From [4] and [5], impedance formulas are obtained in terms of the feed position and frequency for the geometries shown in Figs. 1 and 2. These initial formulas are economized by the introducing closed forms for the infinite series [6].

Manuscript received December 5, 2001; revised February 13, 2002.

The authors are with the Communication Systems Research Group, University of Northumbria at Newcastle, Newcastle Upon Tyne NE1 8ST, U.K. (e-mail: eng.lim@unn.ac.uk).

Digital Object Identifier 10.1109/LAWP.2002.805125

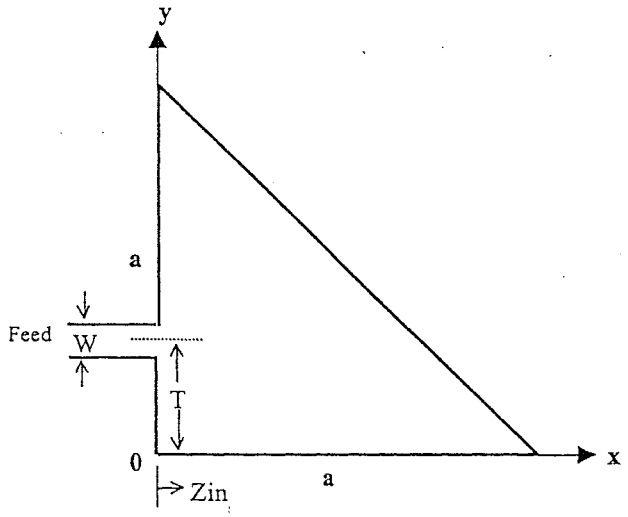

Fig. 1. Patch with feed on vertical side.

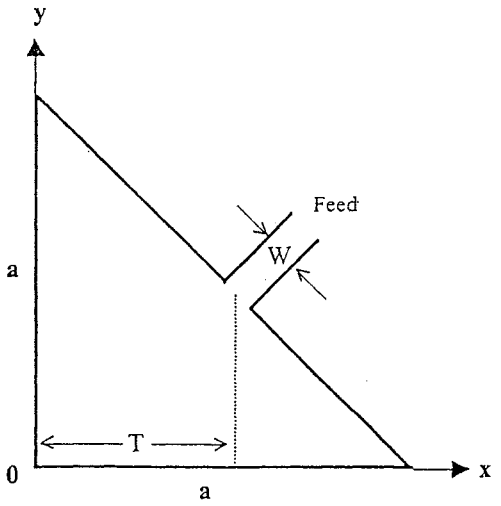

Fig. 2. Patch with feed on hypotenuse.

For the feed on the vertical side the formula involves three single infinite series and two double infinite series in terms of the resonant mode contributions (m, n). Introducing closed forms results in the total elimination of two of the three single infinite series while the closed form applied to the remaining single series eliminates the contribution of the (0, 0) mode. Closed forms of the inner summations of each of the two double infinite series reduces each to a single infinite series.

For the feed on the hypotenuse the initial formula consists of one single infinite series and one double series. The single series reduces to a closed form but the double series cannot be reduced to closed form. Some economization is obtained by extracting the diagonal modes ($m \geq 1$, $n = m$), which take the form of three single infinite series, two of which reduce to closed form. Application of economization to the third series involves eight single infinite series each one reducing to one of four possible closed forms related to convergence conditions. In terms of computational efficiency, it is preferable to directly sum the third series. The remaining double sum, by symmetry, reduces to a semi-infinite double series for the summation indexes $m \geq 1, n = m+1$.

The initial formulas and their economization procedures are shown in Sections II-A and B.

II. Computational Analysis

The general formula for the input impedance given by Okoshi [4] is

$$Zin = \frac{1}{W^2} \int_{W_s} \int_{W_s} G(s|s_0)\, ds\, ds_0 \tag{1}$$

where $W \ll \lambda$, λ being the wavelength in the substrate. The integrations are taken along the interface between the microstrip feed and the antenna patch.

A. Patch With Feed on Vertical Side

For the feed geometry shown in Fig. 1 the Green's function $G(0, y|0, y_0)$ can be arranged in the form shown in (2), at the bottom of the page, where $A = ka/\pi$; h is the dielectric thickness, $k^2 = \omega^2 \mu \varepsilon_0 \varepsilon_r (1 - j/Q)$, and Q is the total quality loss factor [1].

From (1) and (2), by integration

$$\begin{aligned} Zin = & \frac{j2\omega h\mu}{W^2} \left\{ -\frac{W^2}{k^2 a^2} + \frac{W^2}{\pi^2} \sum_{m=1}^{\infty} \frac{1}{m^2 - A^2} \right. \\ & + \frac{2aW}{\pi^3} \sum_{m=1}^{\infty} \frac{(-1)^m (\sin m\theta_1 - \sin m\theta_2)}{m(m^2 - A^2)} \\ & + \frac{a^2}{\pi^4} \sum_{m=1}^{\infty} \frac{(\sin m\theta_1 - \sin m\theta_2)^2}{m^2(m^2 - A^2)} \\ & + \frac{2a^2}{\pi^4} \sum_{m=1}^{\infty} \sum_{n=1}^{\infty} \frac{(\sin m\theta_1 - \sin m\theta_2)^2}{m^2(m^2 + n^2 - A^2)} + \frac{2a^2}{\pi^4} \sum_{m=1}^{\infty} \sum_{n=1}^{\infty} \\ & \left. \frac{(-1)^{m+n} (\sin m\theta_1 - \sin m\theta_2)(\sin n\theta_1 - \sin n\theta_2)}{mn(m^2 + n^2 - A^2)} \right\} \end{aligned} \tag{3}$$

where $\theta_1 = (\pi/a)(T + (W/2))$; $\theta_2 = (\pi/a)(T - (W/2))$.

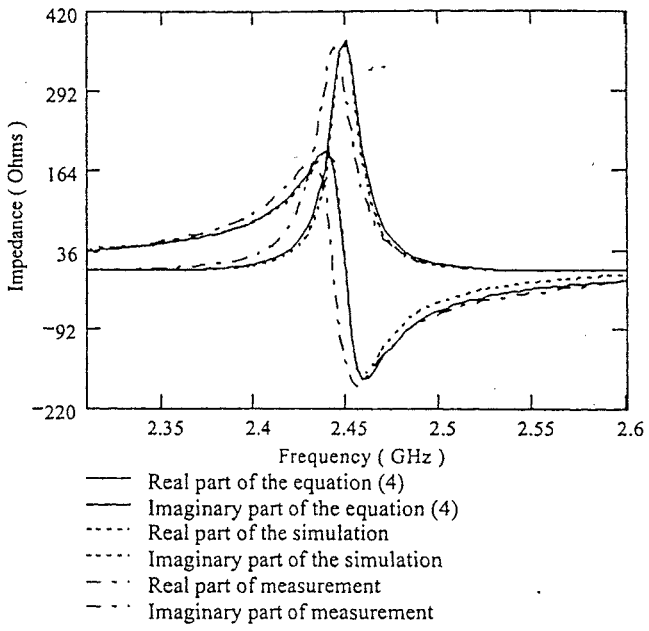

Fig. 3. Feed on vertical side of isosceles triangular patch antenna. (a) Input impedance of center feed position ($T = 20$ mm). (b) Input impedance of offset feed position ($T = 24$ mm).

Summing the first of the above double series with respect to the inner summation results in the total elimination of the third single series. Summing the second double infinite series eliminates the

$$\begin{aligned} G(0, y|0, y_0) = & j2\omega h\mu \left\{ -\frac{1}{k^2 a^2} + \frac{1}{\pi^2} \sum_{m=1}^{\infty} \frac{\left(1 + (-1)^m \cos\frac{m\pi}{a} y\right)\left(1 + (-1)^m \cos\frac{m\pi}{a} y_0\right)}{(m^2 - A^2)} \right. \\ & \left. + \frac{1}{\pi^2} \sum_{m=1}^{\infty} \sum_{n=1}^{\infty} \frac{\left(\cos\frac{n\pi}{a} y + (-1)^m \cos\frac{m\pi}{a} y\right)\left(\cos\frac{n\pi}{a} y_0 + (-1)^m \cos\frac{m\pi}{a} y_0\right)}{(m^2 + n^2 - A^2)} \right\} \end{aligned} \tag{2}$$

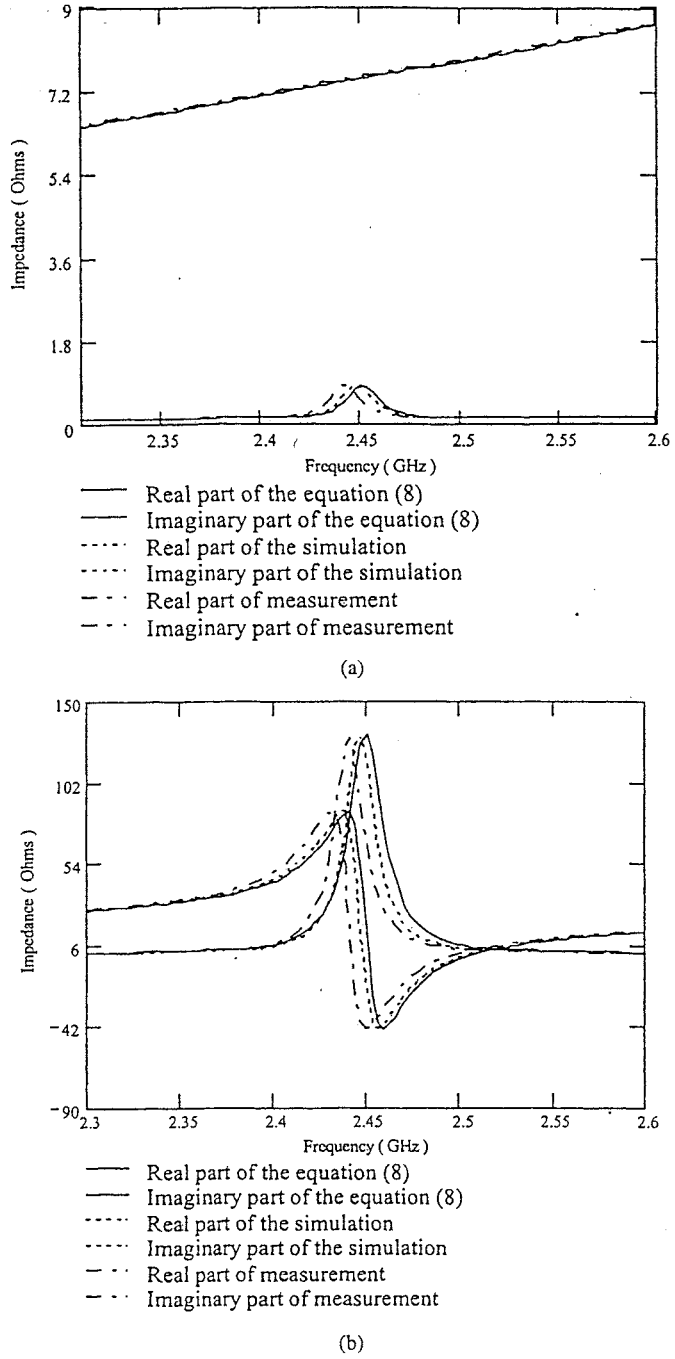

Fig. 4. Feed on the hypotenuse of isosceles triangular patch antenna. (a) Input impedance of center feed position ($T = 20$ mm). (b) Input impedance of offset feed position ($T = 24$ mm).

second of the above single series. Summing the first of the above single series eliminates the $-W^2/k^2a^2$ term. The final result of the economization is the new input impedance formula

$$Zin = \frac{j\omega h\mu}{W^2}\left\{-\frac{W^2}{ka}\cot ka - \frac{W(\sin A\theta_1 - \sin A\theta_2)}{k^2 a \sin A\pi} + \frac{2a^2}{\pi^3}\sum_{m=1}^{\infty}\frac{(\sin m\theta_1 - \sin m\theta_2)^2}{m^2 B}\coth B\pi + \frac{2a^2}{\pi^3}\sum_{m=1}^{\infty} \cdot \frac{(-1)^m(\sin m\theta_1 - \sin m\theta_2)(\sinh B\theta_1 - \sinh B\theta_2)}{m(m^2 - A^2)\sinh B\pi}\right\} \quad (4)$$

where $B = \sqrt{m^2 - A^2}$.

From (4), numerical evaluation shows that for a center fe at $T = a/2$, the first term is dominant and gives the inp impedance to four significant figures. That is

$$Z_{in} = \frac{-j\omega\mu h\cot ka}{ka} \quad (5)$$

is a good analytic approximation that can safely be used f practical impedance matching design requirements.

It is also to be observed that for the center feed position, t impedance is virtually independent of the width W of the fe line.

In contrast, numerical calculations show for an offset fe position the impedance has a relatively low value at the rig angled corner but increases rapidly as the offset feed length is increased.

B. Patch With Feed on Hypotenuse

For the feed geometry shown in Fig. 2 the Green's functi $G(x, a - x|x_0, a - x_0)$ can be arranged in the form shown (6) at the top of the next page.

From (1) and (6), by projecting the integration along the h potenuse into the x axis, the following result is obtained:

$$Zin = \frac{j\omega\mu h}{2W^2\pi^2}\left\{-\frac{W^2\pi^2}{k^2a^2} + \frac{8a^2}{\pi^4}\sum_{m=1}^{\infty}\frac{(\sin m\theta_1 - \sin m\theta_2)}{m^2(m^2 - A^2)} + \frac{2a^2}{\pi^4}\sum_{m=1}^{\infty}\sum_{n=1}^{\infty}\frac{1}{(m^2 + n^2 - A^2)} \cdot \left[\frac{(\sin(m+n)\theta_1 - \sin(m+n)\theta_2)}{(m^2 + n^2)} + \frac{(\sin(m-n)\theta_1 - \sin(m-n)\theta_2)}{(m^2 - n^2)}\right]^2\right\} \quad (6)$$

where θ_1, θ_2 are given in (3).

In the above formula, the single series can be summed closed form making a contribution to the $-W^2\pi^2/k^2a^2$ ter The diagonal term $n = m$ from the double sum is extracted a is in the form of three single infinite series, two of which are e pressed in closed form. By symmetry the remaining terms in t double series are expressed in the form of a semi-infinite dout series for the summation indexes $m \geq 1$, $n = m + 1$.

The final result for the input impedance is given in (8) at t top of the next page.

From (8), numerical evaluation shows that for a feed positi on the hypotenuse, the input impedance is a maximum at t ends of the hypotenuse while falling uniformly to near zero the center.

Consequently, there is a feed location on the hypotenu giving an input impedance of 50 Ω, thus allowing for simp matching implementation.

III. Results

Impedance formulas (4) and (8) were verified by applicati to the patch antennas shown in Figs. 1 and 2, having a reson frequency of 2.45 GHz, $a = 40$ mm, $W = 0.67$ mm substr (Duroid 5870) thickness $h = 0.79$ mm, $\varepsilon r = 2.33$, and the lc tangent of 0.0012.

$$G(x, a-x|x_0, a-x_0)$$

$$=j2\omega h\mu\left\{-\frac{1}{k^2a^2}+\frac{1}{\pi^2}\sum_{m=1}^{\infty}\frac{\left(\cos\frac{m\pi}{a}x+(-1)^m\cos\frac{m\pi}{a}(a-x)\right)\left(\cos\frac{m\pi}{a}x_0+(-1)^m\cos\frac{m\pi}{a}(a-x_0)\right)}{(m^2-A^2)}\right.$$

$$+\frac{1}{\pi^2}\sum_{m=1}^{\infty}\sum_{n=1}^{\infty}\frac{\left(\cos\frac{m\pi}{a}x\cos\frac{n\pi}{a}(a-x)+(-1)^{m+n}\cos\frac{n\pi}{a}x\cos\frac{m\pi}{a}(a-x)\right)}{(m^2+n^2-A^2)}$$

$$\left.\cdot\left(\cos\frac{m\pi}{a}x_0\cos\frac{n\pi}{a}(a-x_0)+(-1)^{m+n}\cos\frac{n\pi}{a}x_0\cos\frac{m\pi}{a}(a-x_0)\right)\right\}. \quad (\text{illegible})$$

$$Zin = \frac{j2\omega\mu h}{W^2}\left\{\frac{W\left(5W-4\sqrt{2}\right)}{2k^2a}+\frac{a^2}{4\pi^2}\sum_{m=1}^{\infty}\frac{(\sin 2m\theta_1-\sin 2m\theta_2)^2}{m^2(m^2-A^2/2)}\right.$$

$$-\frac{4(\cos A\pi-\cos A(\pi-\theta_1-\theta_2)\cos A(\theta_2-\theta_1)+2\sin A(\pi-\theta_1)\sin A\theta_2)}{k^3a\sin ka}$$

$$+\frac{W\left(\sin\frac{A}{\sqrt{2}}(\pi-2\theta_1)-\sin\frac{A}{\sqrt{2}}(\pi-2\theta_2)\right)}{\sqrt{2}k^2a\sin ka/\sqrt{2}}-\frac{W^2\sqrt{2}\cot\frac{A}{\sqrt{2}}\pi}{4ka}$$

$$+\frac{4a^2}{\pi^4}\sum_{m=1}^{\infty}\sum_{n=m+1}^{\infty}\left[\frac{1}{(m^2+n^2-A^2)}\right]$$

$$\left.\cdot\left[\frac{(\sin(m+n)\theta_1-\sin(m+n)\theta_2)}{(m^2+n^2)}+\frac{(\sin(m-n)\theta_1-\sin(m-n)\theta_2)}{(m^2-n^2)}\right]\right\}. \quad (\text{illegible})$$

Input impedance results for the first configuration using a center feed show that only the leading term in (4) is required for four significant figure accuracy. For the offset feed position $T = 24$ mm, convergence to five, six, and eight significant figures is obtained with the upper sum limits $m = 2, 5$, and 24, respectively.

For the second configuration, similar results are obtained. Using a center feed only, the leading term in (8) is required for four significant figure accuracy. For the offset feed position $T = 24$ mm, convergence to five, six, and eight significant figures is obtained with the upper sum limits $m = 2, 5$, and 35, respectively.

Graphs of the impedance values for two feed positions using the new formulas (4) and (8), Ensemble™, and practical measurement, are shown in Fig. 3(a) and (b) and Fig. 4(a) and (b).

In all the above cases the graphs show good agreement between the new formulas, practical measurement and Ensemble results.

IV. Conclusion

In this paper an efficient computational formula for each of two possible right-angled isosceles triangular patch input impedance configurations, using the Green's function a proach, have been obtained. The number of terms in the seri for a required accuracy is given. Good agreement betwe results from new formulas, Ensemble™, and practical me surement is obtained.

References

[1] I. J. Bahl and P. Bhartis, *Microstrip Antennas*. Norwood, MA: Arte House, 1980.

[2] J. Lu, "Dual-frequency operation of single-feed triangular microstrip a tennas," in *Proc. IEEE Antennas and Propagation Society Int. Sym* vol. 3, 1999, pp. 1656–1661.

[3] Y. X. Guo, K. M. Luk, and K. F. Lee, "Small wideband triangular pat antenna with an L-probe feeding," *Microwave Opt. Technol. Lett.*, pt. vol. 30, pp. 218–220, 2001.

[4] T. Okoshi, *Planar Circuits for Microwave and Lightwaves*. New Yo Springer-Verlag, 1985.

[5] R. Chada and K. C. Gupta, "Green's function for triangular segments planar microwave circuits," *IEEE Trans. Microwave Theory Tech.*, v MTT-28, pp. 1139–1143, Oct. 1980.

[6] I. S. Gradshteyn and I. M. Ryzhik, *Table of Integrals, Series, a Product*. New York: Academic Press, 1994.